University of Massachusetts Amherst

Structural Dynamics, Stability And Control Of High Aspect Ratio Wind Turbines

Item Type	article;article
Authors	Stoddard, Forrest S.
Download date	2024-11-24 23:11:30
Link to Item	https://hdl.handle.net/20.500.14394/50485

PF67025F
UC-60
UM-WF-TR-78-11

STRUCTURAL DYNAMICS, STABILITY AND CONTROL OF HIGH ASPECT RATIO WIND TURBINES

TECHNICAL REPORT

by

Forrest S. Stoddard

Energy Alternatives Program

University of Massachusetts

Amherst, Massachusetts 01002

December 1978

Prepared for the United States Department of Energy and Rockwell International, Rocky Flats Plant Under Contract Number PF 67025F.

INTRODUCTION

Dynamics and aeroelastic studies of systems can be thought of as comprising a triangle of interdependent forces:

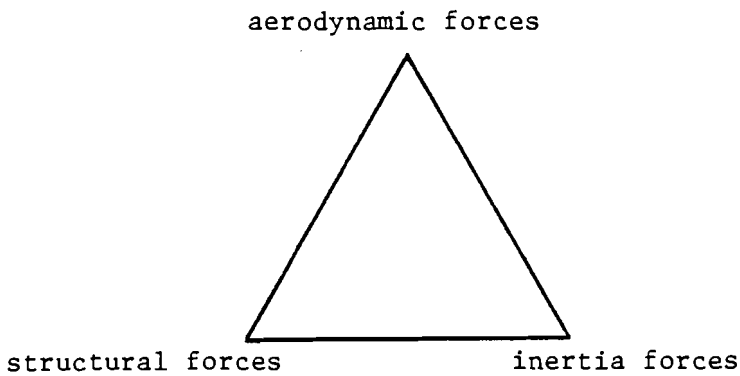

The aerodynamic forces are the most difficult to visualize and to test; they are unsteady and non-linear and are further stigmatized by a random input process. The structural forces are the elastic restraints which we relate to deflections. And the inertia forces make us separate dynamics from statics by the introduction of mass, motion, and gravity. We have three major tools at our disposal in these studies: analytical tools, testing at subscale, and testing at full scale. We cannot subordinate any one of these a priori; we are usually in need of so much knowledge that we have to get it continually and efficiently from analytical and computer studies, from small scale quick-answer wind tunnel tests, and ultimately, from the real thing--the full scale machine in the operating environment.

Those of us engaged in wind power systems are lucky to be more like civil engineers than our aeronautical engineer cousins. Our

structures are complex and vibratory, and must be made safe and reliable, but they are tethered to the ground and rely ultimately on their cost-effective practicality. We are less constrained by weight, and more constrained by dollars. Specifically, our "new anemometers called wind turbines" must have blades that are constructed with attention to the traditional design parameters: torsional stiffness, bending stiffness, mass distribution and polar moment of inertia, control axis placement (to assess control moments and control-induced instabilities), mass axis placement (mass balancing), and the stiffnesses of the hub/windshaft/system. Additionally, we wind turbine designers have discovered new significance of other mature parameters: blade planforms and twist for east of fabrication, material and labor cost, weathering and fatigue life estimation, operation while unattended (e.g., wet strength, ultraviolet effect, foreign object damage, ice, lightning), and gust-induced accelerations and transient dynamic response. This last effect may be ultimately tied to study of the viscous microaerodynamics at the blade airfoil; nevertheless, it is easy to test and hard to theorize.

This dissertation comprises a walk through the fundamental dynamics and vibration of a wind turbine generator rotor with slender blades. It is an evolution, an escalation of thought and understanding to increase the technical fertility of the thoughtful reader. It does not attempt to be the last word in wind turbine rotors, only a first step. It is hoped that you will be struck by its broadness and simplicity, and so on the one hand will find it a useful textbook for

teaching and on the other, a convenient reference for calculations. Further, it is hoped that enough specific design criteria can be learned from this to allow the wind turbine designer to be confident of his preliminary design, the first tool in the study of the aero-elastic triangle.

This report was prepared to document work sponsored by the United States Government. Neither the United States nor its agent the Department of Energy, nor any Federal employees, nor any of their contractors, subcontractors, or their employees, make any warranty, express or implied, or assume any legal liability or responsibility for the accuracy, completeness, or usefulness of any information, apparatus, product or process disclosed, or represent that its use would not infringe private owned rights."

ABSTRACT

Structural Dynamics, Stability and Control
of High Aspect Ratio Wind Turbine Generators

The blade dynamics and vibration of wind turbine generators with high aspect ratio (slender) blades are developed. Equations of motion are derived, and blade motions and forces are found, for degrees of freedom in flapping, lead-lag and feathering subject to gravity, cross-wind, yaw rate, and axisymmetric aerodynamic forces. Tower degrees of freedom are added to assess tower loads and vibration. Significant mechanical and aeroeleastic instabilities which may occur are predicted and discussed. Methods are developed, and quantitative computer programs are given, for the structural and vibration analysis of twisted, tapered, composite shell blades. The University of Massachusetts Wind Furnace I, which is the impetus of this study, is described.

A textbook approach is taken to insure intuitive freedom; results and observations are written for the student and for the designer, and are kept as fundamental as possible.

TABLE OF CONTENTS

TABLE OF CONTENTS (CONTINUED)

TABLE OF CONTENTS (CONTINUED)

LIST OF TABLES

LIST OF FIGURES

LIST OF FIGURES (CONTINUED)

LIST OF FIGURES (CONTINUED)

LIST OF FIGURES (CONTINUED)

LIST OF FIGURES (CONTINUED)

LIST OF SYMBOLS

A	axisymmetric flow term = $(\frac{\mu_o}{3} - \frac{\lambda_i}{3} - \frac{\vartheta_o}{20} - \frac{\vartheta_p}{4})$
A_2	axisymmetric flow term = $\lambda_i - \mu_o$
A_T	total cross sectional area
B	gravity term = $\frac{g\ M_b\ X_g\ R}{2I_b\Omega^2} = \frac{G}{2\Omega^2}$
b	number of blades
C_P	power coefficient = $\frac{P}{\frac{1}{2}\rho A V_o^3}$
C	section lift coefficient
C_D	section drag coefficient
C	lift curve slope = $\frac{dC_\ell}{d\alpha}$
c	blade chord
dm	differential mass element
E	Young's Modulus
EI	section stiffness
EI_{xp}, EI_{yp}	section principal axes stiffness
e	flapping hinge offset
e_2	lead-lag hinge offset
G	gravity term = $\frac{g\ M_b\ X_g\ R}{I_b}$
G	torsional modulus (Chapter VII)
GJ	torsional stiffness

LIST OF SYMBOLS (CONTINUED)

g	acceleration due to gravity
I	moment of inertia
I_b	blade flapping mass moment of inertia
I_f	blade feathering mass moment of inertia
I_t	tower mass moment of inertia
I_x, I_y	blade section moments of inertia
I_{xy}	blade section product of inertia
$I_1, I_2 \ldots I_5$	mass integrals
J	torsional modulus
K	non-dimensional flapping frequency $= (\frac{\omega_\beta}{\Omega})^2 = 1 + \varepsilon + \frac{K_\beta}{I_b \Omega^2}$
K_2	non-dimensional lead-lag frequency $= (\frac{\omega_\zeta}{\Omega})^2 = \varepsilon_2 + \frac{K_\zeta}{I_b \Omega^2}$
K_3	non-dimensional featheirng frequency $= (\frac{\omega_\theta}{\Omega})^2 = 1 + \frac{K_\theta}{(I_f + I_I)\Omega^2}$
K_β	flapping hinge spring
K_ζ	lead-lag hinge spring
K_θ	feathering hinge spring
k	normal mode coefficient
L_β	aerodynamic lift in flapping direction
L_ζ	aerodynamic lift in lead-lag direction
ℓ	lift per unit span
M	bending moment
M_β	flapping bending moment

LIST OF SYMBOLS (CONTINUED)

M	lead-lag bending moment
M_b	mass of blade
n	harmonic index
P	power
p	eigenvalue = $\nu + \eta i$
Q	hub pitching angular velocity
q	nacelle yaw angular velocity
$\bar{q}$	non-dimensional yaw angular velocity = $\frac{q}{\Omega}$
q_L	tower lateral deflection
R	blade radius
r_x, r_y	section principal radius of gyration
r_g	radius to center of mass of blade
S	shear force
S_ζ	flapping shear
S_ξ	lead-lag shear
T	blade tension
T_b	kinetic energy of blade
T_t	kinetic energy of tower
TSR	rotor tip speed ratio = $\frac{\Omega R}{V_o}$
U	potential energy
U_o	crosswind velocity
$\bar{U}_o$	non-dimensional crosswind velocity = $\frac{U_o}{\Omega R}$
U_T	stream velocity tangential to blade element

LIST OF SYMBOLS (CONTINUED)

U_p	stream velocity perpendicular to blade element
V_o	free stream velocity
V_R	resultant stream velocity at blade element
v_i	induced velocity at blade element
X_g	non-dimensional radius to center of mass $= \frac{r_g}{R}$
X_β'	flapping velocity coefficient $= 2\beta + \gamma\ [\frac{A_2}{3} + \sin\psi\ (\frac{\bar{q}}{4} + \frac{\bar{U}_{o\beta}}{3}) + \frac{\theta_o}{4} + \frac{\theta_p}{8}]$
$\bar{x}_c, \bar{y}_c$	blade section centroid
χ	non-dimensional span station $= \frac{\chi}{R}$
Y_I	chordwise distance from elastic axis to mass axis
Y_A	chordwise distance from elastic axis to aerodynamic axis
α	blade section angle of attack
α	Mathieu's equation solution coefficient (Chapter II)
β	blade flapping angle
β_o	blade coning angle (collective flapping)
β_{ic}	cyclic flapping angle (forward tilt of rotor plane)
β_{is}	cyclic flapping angle (lateral tilt of rotor plane)
γ	Lock number $= \frac{\rho\ C_{\ell_\alpha}\ c\ R^4}{I_b}$
$\gamma_1, \gamma_2, \ldots \gamma_6$	aerodynamic flapping coefficients
Δ	determinant of coefficients
δ	Mathieu's equation solution coefficient (Chapter II)

LIST OF SYMBOLS (CONTINUED)

ε	flapping hinge offset term $= \frac{M_b\ e\ X_g\ R^2}{I_b} = \frac{3e}{2(1-e)}$
ε_2	lead-lag hinge offset term $= \frac{M_b\ e_2\ X_g\ R^2}{I_b} = \frac{3e_2}{2(1-e_2)}$
ζ	blade lead-lag angle
ζ_o	collective lead-lag angle
ζ_{ic}	cyclic lead-lag angle (vertical blade scissoring)
ζ_{is}	cyclic lead-lag angle (horizontal blade scissoring)
η	non-dimensional span station $= \frac{r}{R}$
θ	blade feathering angle
θ_o	blade linear twist angle
θ_p	blade pitch angle
λ_i	non-dimensional induced velocity $= \frac{v_i}{\Omega R}$
μ_o	rotor advance ratio (reciprocal of tip speed ratio) $= \frac{V_o}{\Omega R}$
ξ	damping ratio
ρ	density
σ	stress
τ	torque
ϕ	blade element angle
ϕ	angle to principal axes (Chapter VII)
$X_1, X_2, \ldots X_4$	aerodynamic moment mode shapes
ψ	blade azimuth angle (zero vertically downward)
Ω	rotor angular velocity
ω	frequency of vibration

LIST OF SYMBOLS (CONTINUED)

ω_N	frequency of vibration of non-rotating blade
ω_R	frequency of vibration of rotating blade
ω_β	frequency of vibration in flapping
ω_ζ	frequency of vibration in lead-lag
ω_θ	frequency of vibration in feathering

Coordinate Systems (Figure 6)

xyz	blade coordinate system
$\hat{X}\hat{Y}\hat{Z}$	hub coordinate system
X'Y'Z'	bedplate coordinate system

Subscripts

o	relative to blade hinge
β	relative to flapping direction
ζ	relative to lead-lag direction
θ	relative to feathering
p	relative to principal axes
c	relative to centroid

Superscripts

$\cdot$	first derivative with respect to time (d/dt)
$\cdot\cdot$	second derivative with respect to time (d^2/dt^2)
$'$	first derivative with respect to azimuth ($d/d\psi$)
$''$	second derivative with respect to azimuth ($d^2/d\psi^2$)

CHAPTER I

WIND TURBINE GENERATOR SYSTEM: IDENTIFICATION AND IDEALIZATION

Wind turbine generators, or windmills, of every conceivable level of sophistication exist today. Their use is rapidly increasing; and their usefulness is not entirely for practical energy, nor for political reasons, or for social reasons, but for a whole range of emerging needs. The role of the engineer involved in wind turbine design is complex, but his primary function is to increase the chances of success of any preliminary design through adequate modelling of the system and prediction of problems likely to be encountered while using the system. Critical to this endeavor, and really to all engineering, is the beginning step--the reduction of the complex first concept to a set of simply understood subsystems. The temptation to over-complicate the model is strong at first; experience can show on the one hand the hopelessness of accurate models due to incomplete knowledge, and on the other, a resulting superfluity of decimal places when only two would have been sufficient to make a knowledgeable decision. I find wind turbines a fascinating study because the order of significance of the traditional rotor modelling assumptions has not been proven by long experiment. Therefore, we are on our own; we must represent our systems as simply as possible to allow time and resources for the broad studies we must do, and as complex as necessary to predict the new behavior we observe in our models. This chapter sets the stage for the analyses and evolution to follow. Here, the incredible variety of

windmills is reduced to a set of subsystems, to be analyzed and studied separately and in union. Also, the specific experimental system which generated this research (the University of Massachusetts Wind Furnace) is described and the model is further simplified.

A. Idealized Wind Turbine System Concept

A wind turbine generator system is a network of interconnected dynamic subsystems, each of which has a number of degrees of freedom and resultant "natural" frequencies. Additionally, coupling between the subsystems will exist when the boundary deflections are large enough to cause reaction or inertial forces, and vice versa. The subsystem "boundaries" are straightforward to visualize. The important subsystems are the rotor, or momentum exchange device, the torsional mechanical drive, and the (elastic) tower. A control system with suitable servo capability over performance variables (thus providing stability and control capability and adding extra degrees of freedom) can also be included as a separate subsystem. These are diagrammed in Figure 1.

The designer is interested in the loads and deflections in each subsystem; if he can predict these, he can design an efficient, cost effective machine. Steady loads are straightforward, and all are direct or indirect results of wind force on the blades. Performance studies are concerned with steady loads; a computer program for this can be found in Appendix I. However, the true grit of engineering design lies in the structural dynamics: the response to an external

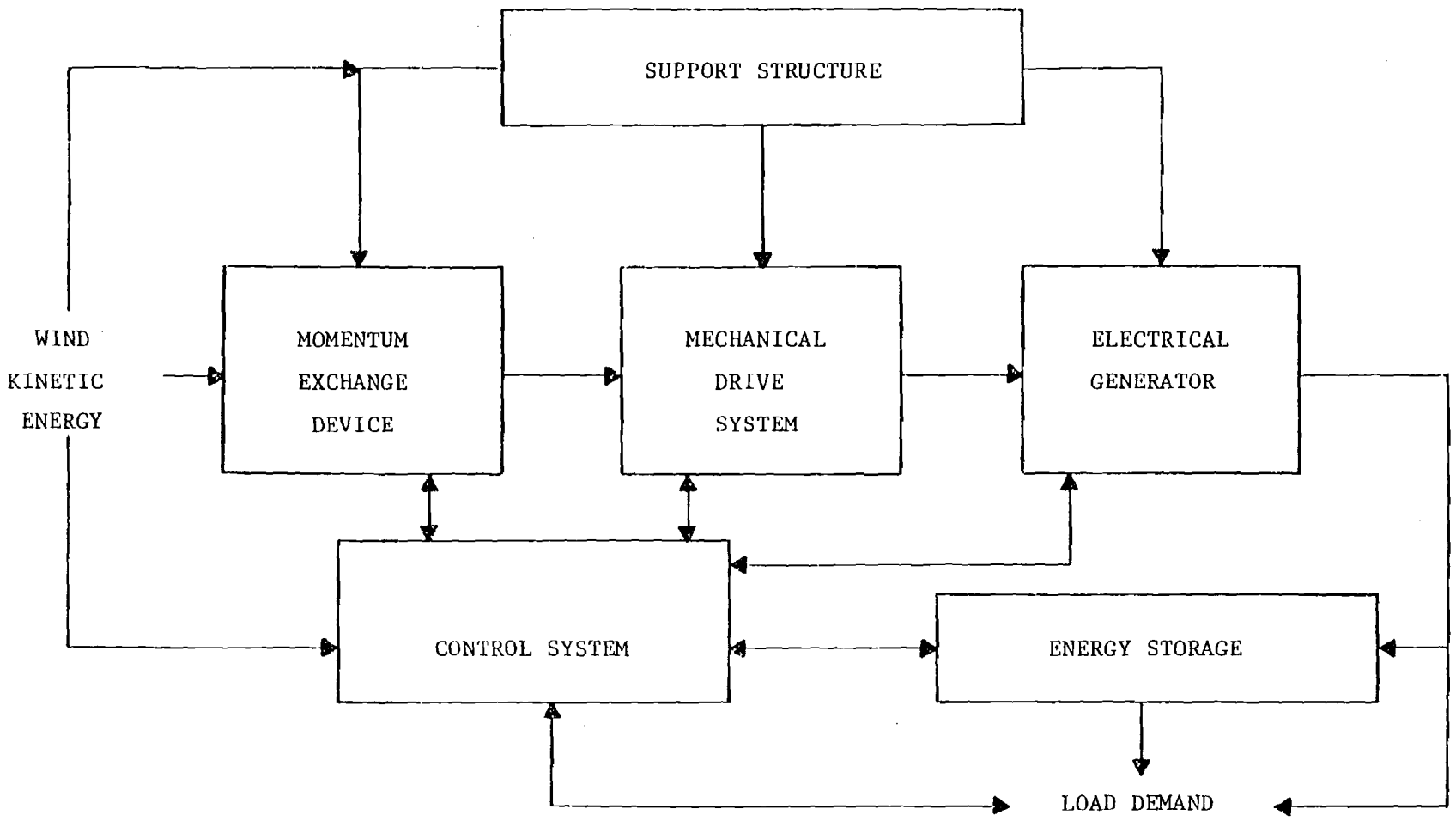

Figure 1. Wind Generator System

forcing function, and the possible mechanical instabilities or self-excited oscillations inherent in any complex system.

The oscillatory response of the wind turbine generator (WTG) to a given forcing function is dependent on the isolated response of each subsystem through its "transfer function," and on the coupling functions. Historically, the most significant subsystem to overall vibratory response is the rotor. That is, the dominant transient and steady state response frequencies of the system are the rotor frequencies, and the most complex dynamical response occurs in the rotor. More degrees of freedom exist for the rotor, thus the possibility of mechanical instability is also greater.

The rotor system is also more difficult to analyze since the main forcing function and the damping are due to aerodynamic loading, which is highly non-linear and aperiodic; in the case of wind turbines operating freely, the rotational speed and the aerodynamic loading are never constant. The dynamics of the helicopter rotors and propellers has been well studied, but new assumptions concerning the aerodynamic loading are warranted for wind generators.

Also, the mass, stiffness, and geometric parameters of wind turbine generator rotor systems are sufficiently different from rotors to dictate a reexamination and redevelopment of the basic system response.

The kinematical model has been simplified to a horizontal wind turbine generator in a uniform profile free stream V_o. The rotor, hub, torsional drive, generator, supports, and tower are diagrammed in Figure 2.

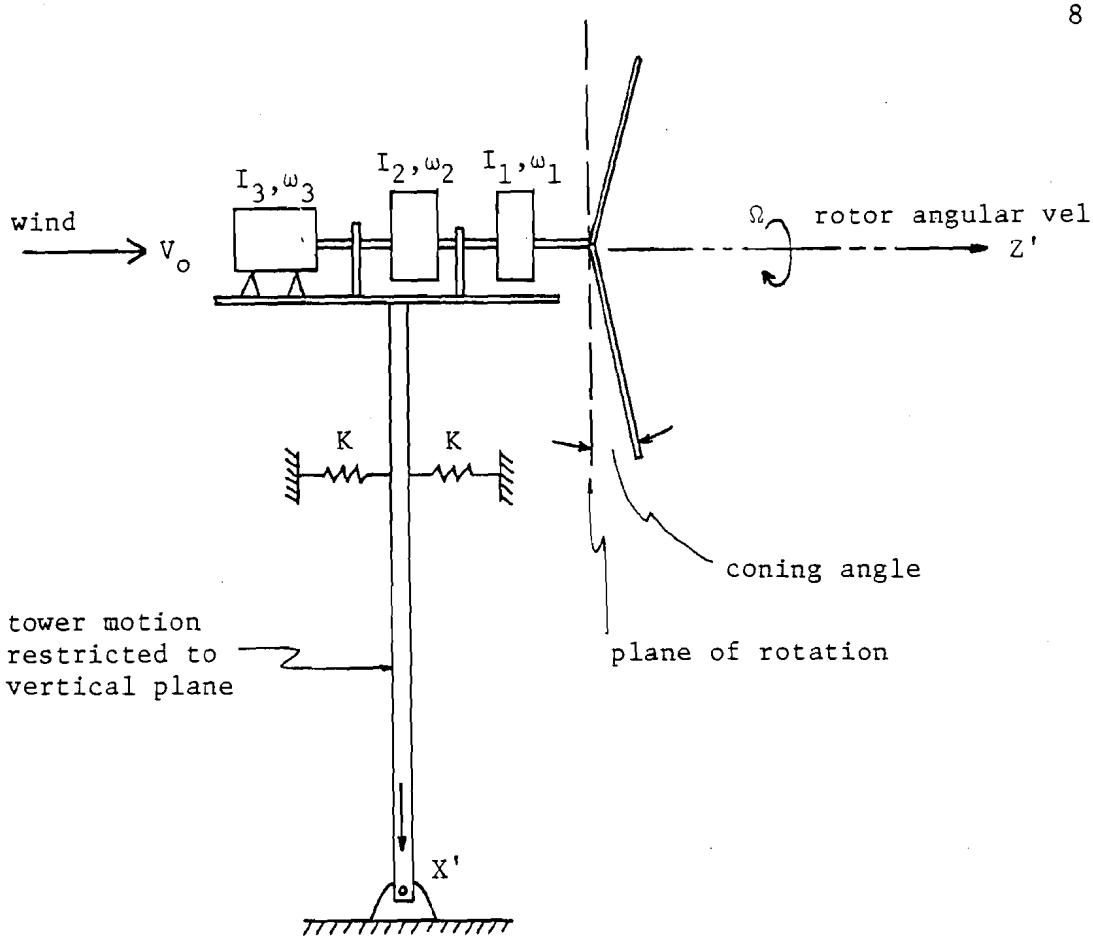

Figure 2. Overall Coupled System

The torsional drive subsystem can be treated as an elastic torsional system, and consists of the horizontal rotor shaft (windshaft) with moment of inertia I_1 and angular velocity Ω, the speedup mechanism with I_2 and ω_2, and the generator rotor, with I_3 and ω_3. The generator torque can be applied to the bedplate in either of two perpendicular vertical planes (e.g., a fore and aft plane X'Z', or as shown in the X'Y' plane in Figure 3). The applied forces and moments from the rotor are:

S_H = the sum of all the hub shears (downwind or Z' direction)

τ_H = the applied rotor shaft torque

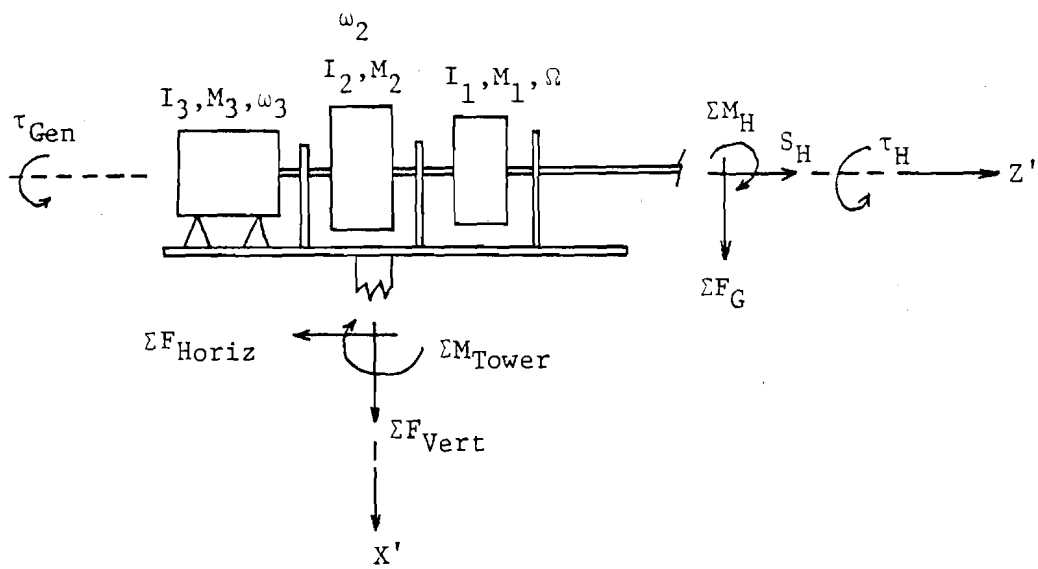

Figure 3. Mechanical Drive System

ΣF_G = the resultant of all hub vertical forces

ΣM_H = the sum of all hub moments (the Y' component alone is shown)

The reactions at the tower-bedplate attachment are:

$\Sigma F_{vertical}$ = the sum of all vertical forces

ΣF_{horiz} = the sum of all horizontal forces (or thrust)

ΣM_{tower} = the sum of all tower moments

The torsional system (mechanical drive) will have its own (torsional) degrees of freedom and natural frequencies. The major forcing frequencies for this system are the applied rotor shaft torque, τ_H, which will contain periodic components, and the applied generator torque, τ_{GEN}, which also can contain periodic components (e.g., alternating current electric field control). The bedplate and internal supports can be assumed to be rigid, thereby transmitting the weights

and rotor reactions without deflection to the tower attachment. The mechanical drive/bedplate system has two important moments of inertia:

$I_{Y'}$ = pitching moment of inertia

$I_{Z'}$ = rolling moment of inertia

A stayed pole mast tower system can be treated as an elastic beam with the spring restraint shown in Figure 4. Motion in the diagram has been restricted to translation in the X'Z' plane, and the origin has been moved to the base pin. A self-supporting tower would be a simple vertical cantilever, with no guy wire restraints. An additional moment would exist at the base. A combination tower would contain all the reactions.

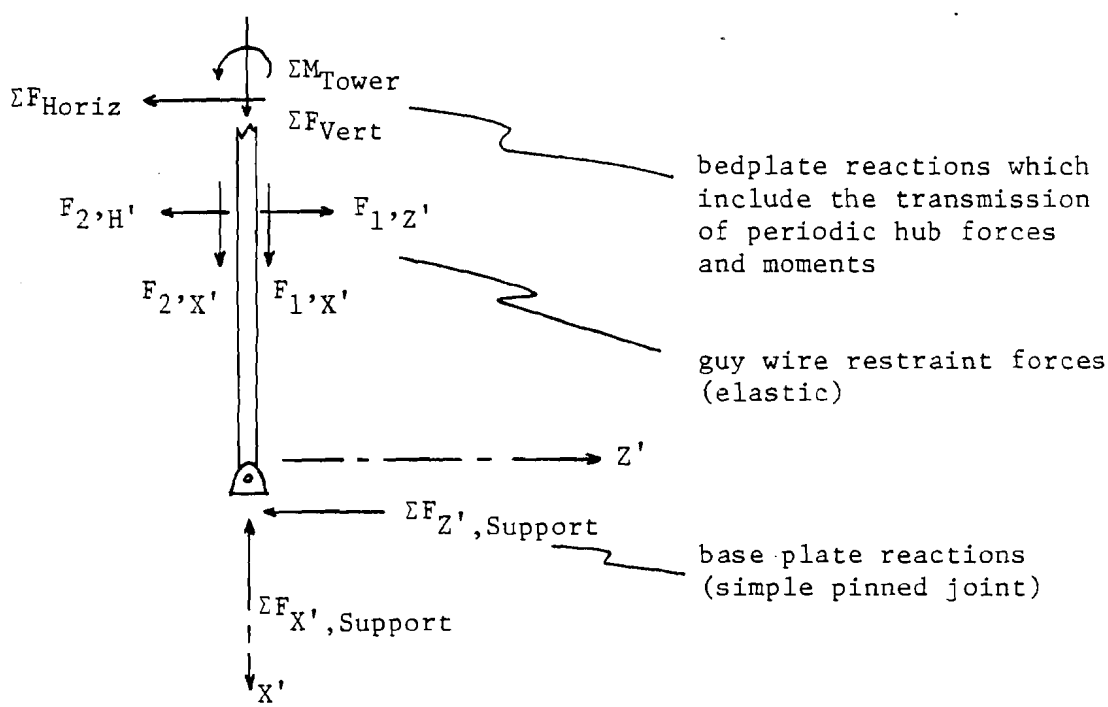

Figure 4. Tower System

The rotor system (as shown in detail in Chapter VII-E) can be simplified to a rigid hub and shaft with rotating elastic blades, as shown in Figure 5. The blades can be modelled as rigid members offset ε with spring restraint K_β. The rotor blade can be isolated in the rotating coordinate system (xyz system), and the forces and moments determined. All the coordinate systems are shown in Figure 6.

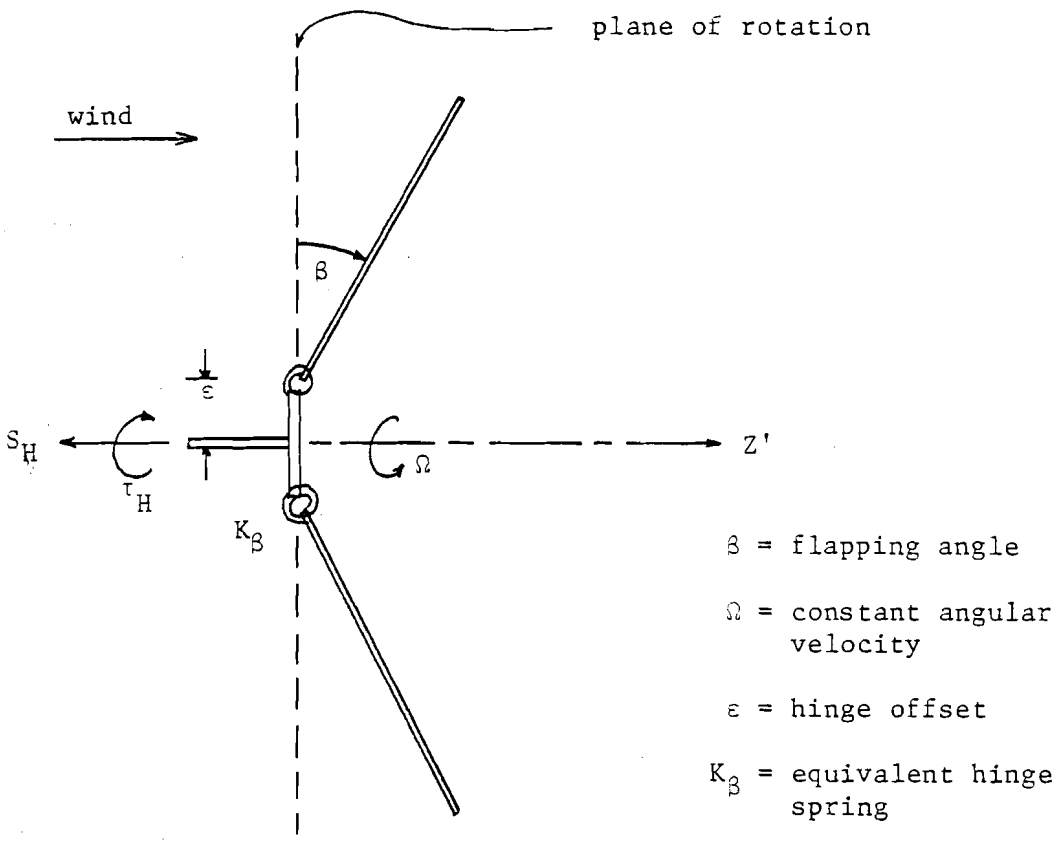

Figure 5. Rotor System

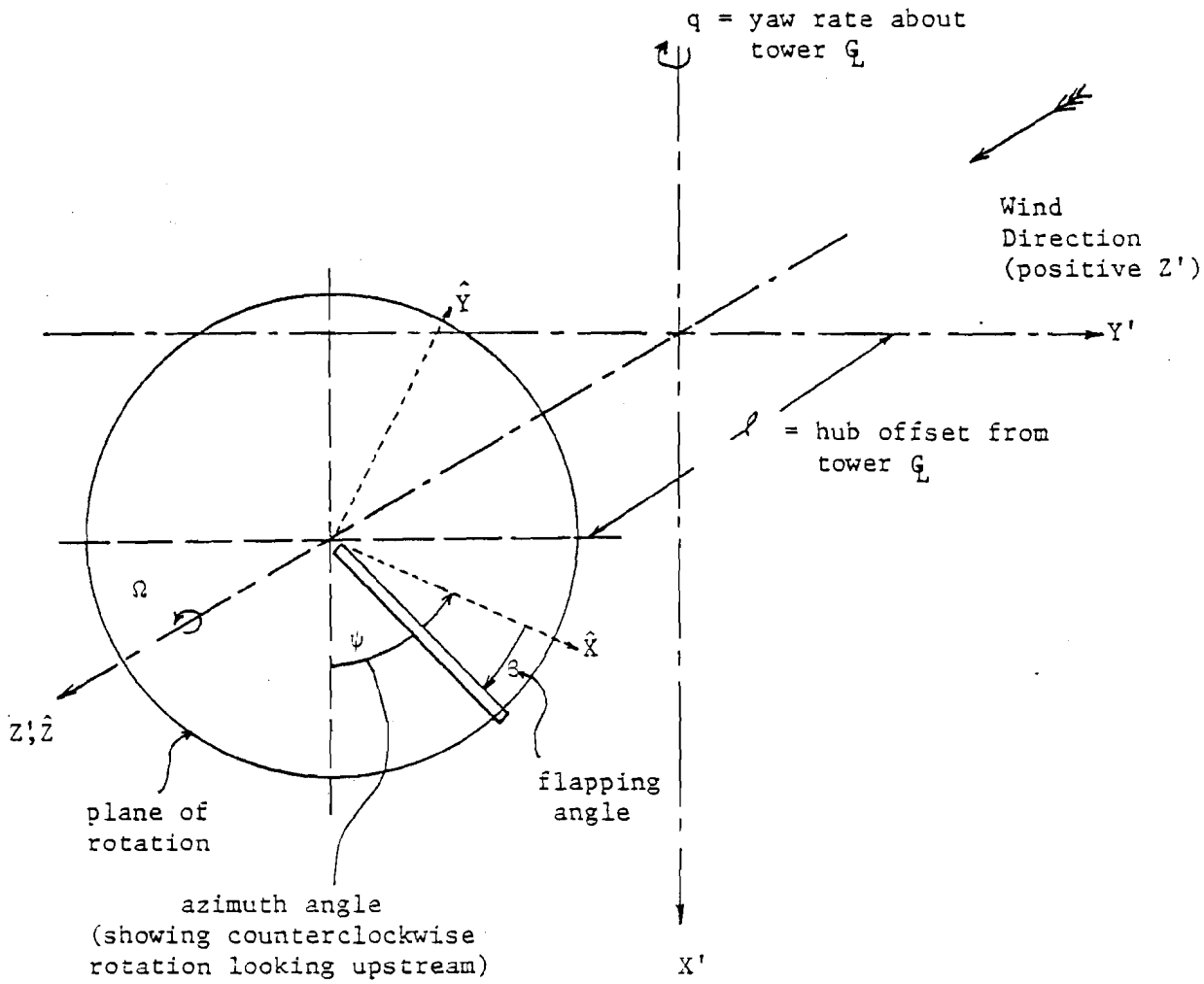

ψ = blade azimuth in X'Y'Z' system

Ω = rotor angular velocity = $\frac{d\psi}{dt}$

X'Y'Z' system: bedplate coordinate system (e.g., if wind direction is changing, yaw angular velocity q is the rotation of X'Y'Z' about fixed tower axis X')

$\hat{X}\ \hat{Y}\ \hat{Z}$ system: rotor hub coordinate system, it rotates around the Z' axis at constant speed Ω

XYZ system: fixed to the blade, and inclined to the $\hat{X}\hat{Y}\hat{Z}$ system by Euler angle $-\beta$ (it is not shown)

Figure 6. Coordinate Systems

The coupled response of the total wind turbine generator system could in theory be determined by deriving the set of coupled equations of motion relating motions and forces in each of these subsystems. The equations could be linearized (e.g., higher order terms discarded) and the transient and steady state dynamic response could be determined from the set of differential equations through various computational techniques, including stability derivatives and analog computer studies. A pragmatic engineering approach also could be taken. The vibratory response of the system could be inferred from an examination of the natural frequencies of each of the subsystems, and the aerodynamic forcing frequencies expected. This dissertation concentrates exclusively on the rotor subsystem for its complexity and significance, and includes the coupling ability of the other subsystems when a destructive instability seems likely.

B. Structural and Dynamic Parameters of the University of Massachusetts Wind Furnace I

This section briefly describes the University of Massachusetts Wind Furnace I wind turbine generator. It was built over the period September 1973 to its erection in November 1976 at the University of Massachusetts by a group of faculty, students, and technicians. Further information on the project and the performance of the system can be found in the numerous technical reports published by the University under the sponsorship of the Department of Energy (References 1-4).

The on-site arrangement of the wind turbine generator (WTG) on its stayed pole mast can be seen in Figure 7. The rotor is 32.5 feet in

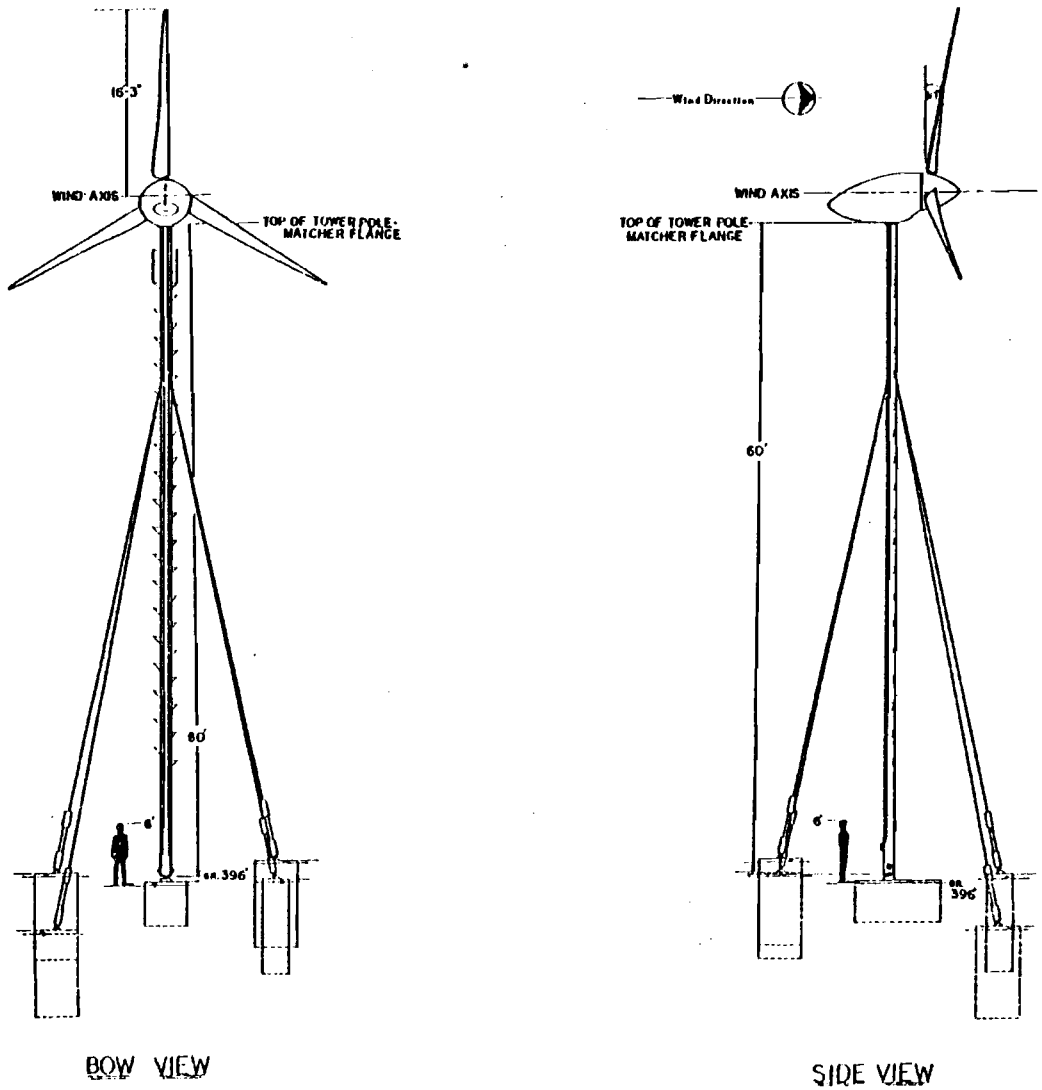

Figure 7. On-Site Arrangement

diameter (10 meters) and is comprised of three fiberglass composite blades in a cantilevered hub. The cutaway assembly can be seen in the next two figures; the hub and pitching arrangement can be seen in Figure 8, the left side, and the two stage mechanical stepup (truck rear end plus enclosed silent chain drive) and the 25 kilowatt (31.3kVa) generator can be seen in Figure 9, the right side. The overall nacelle length is 13.5 feet, height 5.0 feet, and width 5.0 feet; the total aloft weight is about 2,500 pounds, and the tower plus guy wire weight is 2,600 pounds. The tower is 10-inch diameter, 3/8-inch wall thickness standard pipe, with welded fittings.

The hub assembly is a weldment from standard steel shapes, and can be seen in Figure 10. The pitch actuation is achieved by linear motion of a ball screw actuator driven by a servo motor/reducer combination. Linear actuator position in the hub is transformed to pitch angle via a chain-idler sprocket-blade sprocket arrangement, which can be seen in Figure 11.

Pitch control philosophy is an attempt to utilize the high performance capability of the aerodynamically optimum blades by running at constant tip speed ratio ($\Omega R/V_o$) for most of the time, specifically, between cut-in wind speed (6 mph) and rated wind speed (26.1 mph). This is called Region 2 pitch control, and the various regions are depicted in Figure 12. Region 1 is cut in, where blade angle is reduced to achieve high static torque for starting the rotor; Region 2 is constant tip speed ratio (constant pitch angle) operation; Region 3 is the constant power region (pitch angle is reduced to maintain

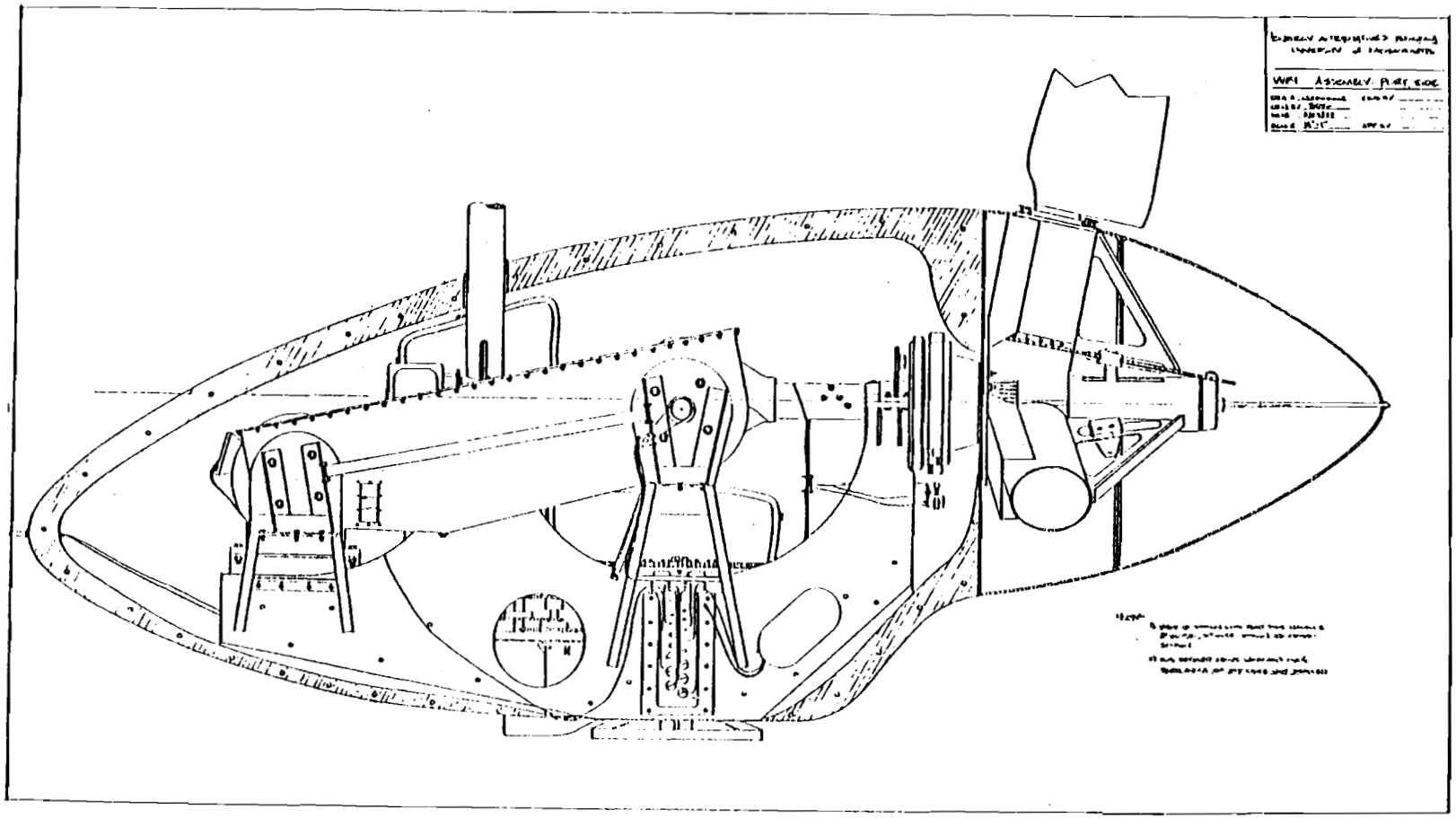

Figure 8. Left Side Cutaway

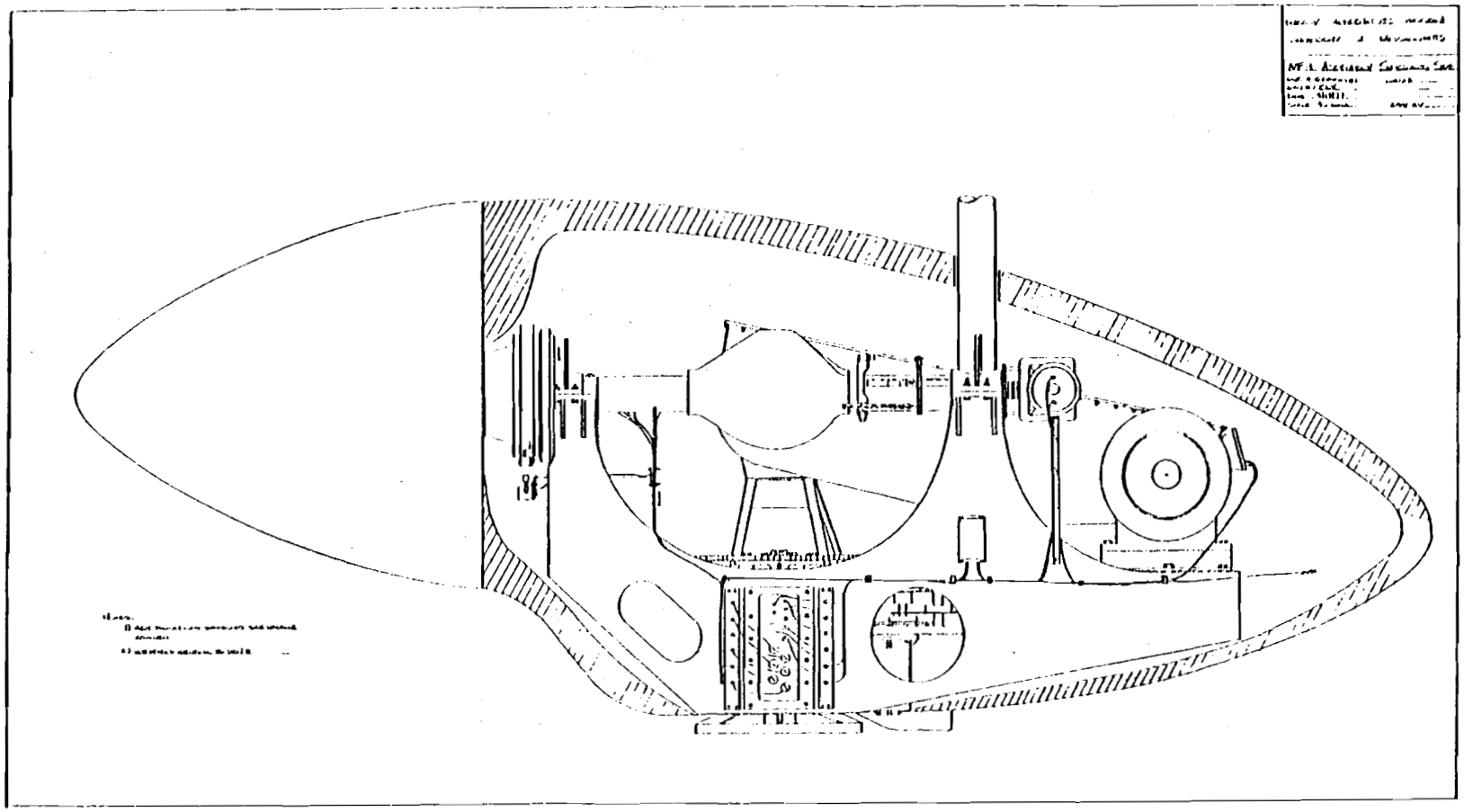

Figure 9. Right Side Cutaway

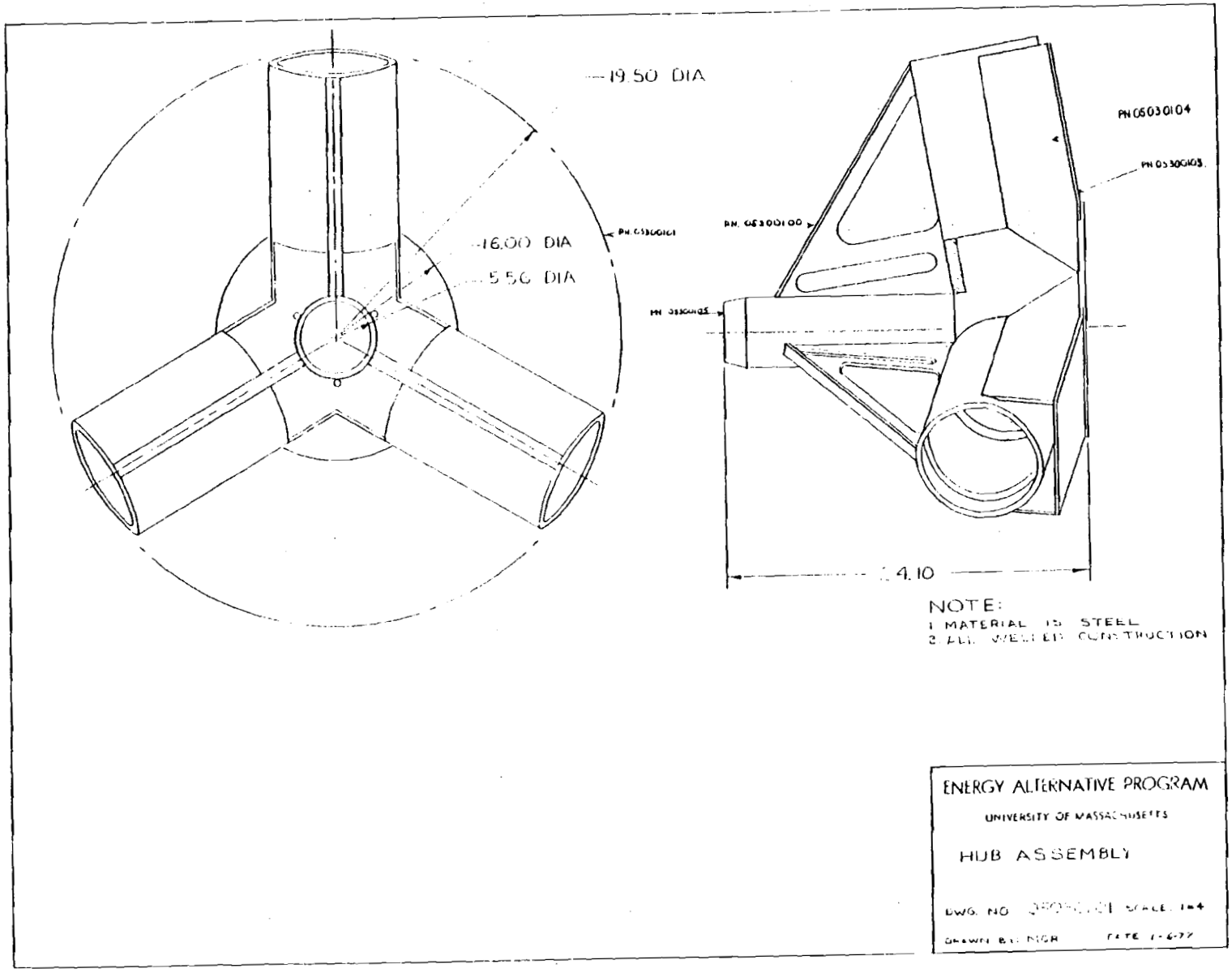

Figure 10. Hub Assembly

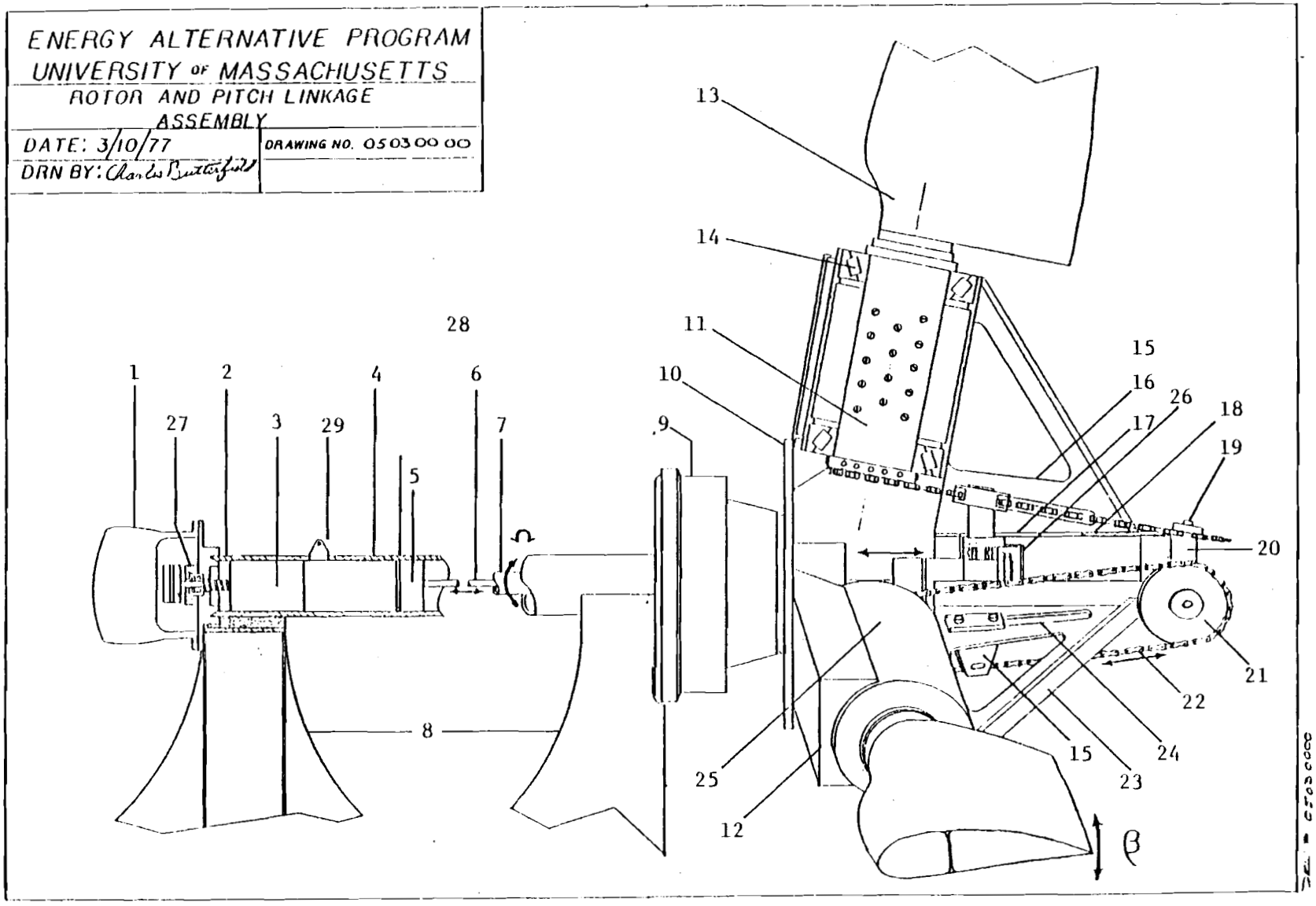

Figure 11. Pitch Assembly

1	Motor and Reducer
2	Ball Screw
3	Ball Nut
4	Truck Rear End Torque Tube
5	Conical Wedge Cup Retainer
6	Control Rod
7	Wind Shaft
8	Main Frame
9	Truck Rear End Brake Drum
10	Base Plate
11	Steel Blade Sleeve HUB
12	Box Beam
13	Blade
14	Blade Bearings
15	Chain Traveler
16	Slide Bar
17	Control Rod Bearings
18	Stand Pipe HUB
19	Idler Sprocket Shaft and Chain Adjuster
20	Coarse Chain Adjuster
21	Idler Sprocket
22	Pitching Chain
23	Compression Strut and Web HUB
24	Chain Traveler Track
25	Blade Shaft Housing
26	Slide Bar Clamp and Bearing Housing
27	Ball Screw Support Bearing
28	Pitch Feedback Linkage
29	Rack and Pinion Arm

Figure 11. Pitch Assembly Key

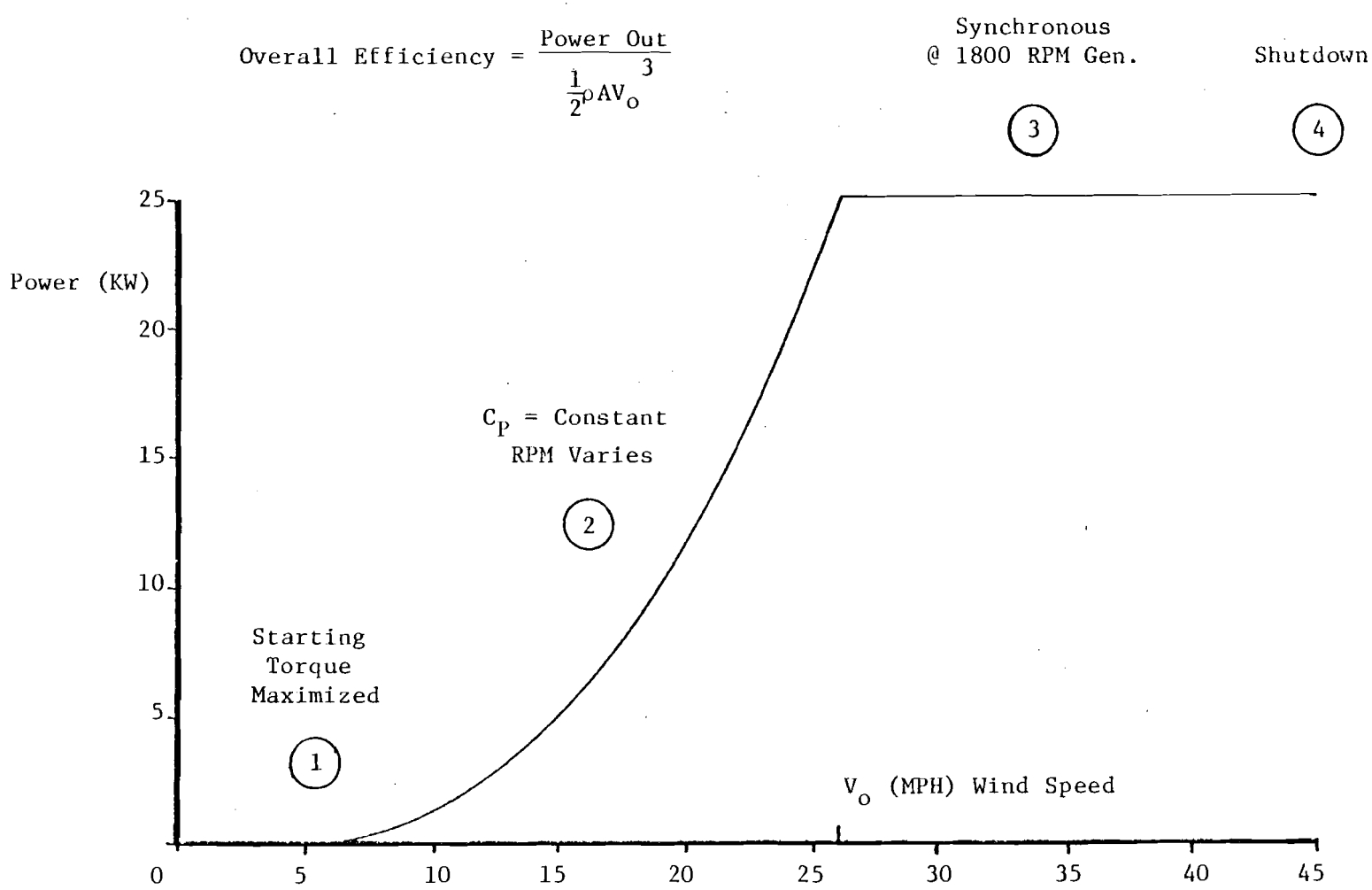

Figure 12. Pitch Control Regions

synchronous generator speed and constant power of 25 kilowatts); and Region 4 is rotor shutdown in high winds.

The performance of the rotor system has been roughly as expected, achieving a higher efficiency than predicted. Output power as a function of shaft speed and a pitch angle of -2° is shown in Figure 13;[1] and constant tip speed ratio operation is seen in Figure 14 for tip speed ratios between 5 and 9.[2]

The blades were originally modelled after the very fine Brace Research Institute, McGill University, Canada, design of the late 1960's,[5] shown in Figure 15. The blade root was modified to accept a steel sleeve (Figure 16) to provide bearing support and moment reactions in the 6-inch tapered roller bearings of the hub retention. The blade sections were kept at NACA 4415 airfoil shape (Figure 17),[6] and the major bending stiffness and strength were provided by a monolithic glass composite D-spar (Figure 18). A high quality glass composite skin forms the exterior shape, and the trailing edge was joined (secondary bond) with a glass roving bundle. A complete blade view can be seen in Figure 19 and Table 1. The schedules of cloth reinforcement for the skin and spar laminates are in Figures 20 and 21.

The final blade design parameters can be seen in Table 2. The experimentally-derived moduli of elasticity and torsion, and densities are also given. The resulting weight distribution is given in Figure 22. The beamwise stiffness distributions are in Figure 23, and the measured static deflection curve is in Figure 24.[7]

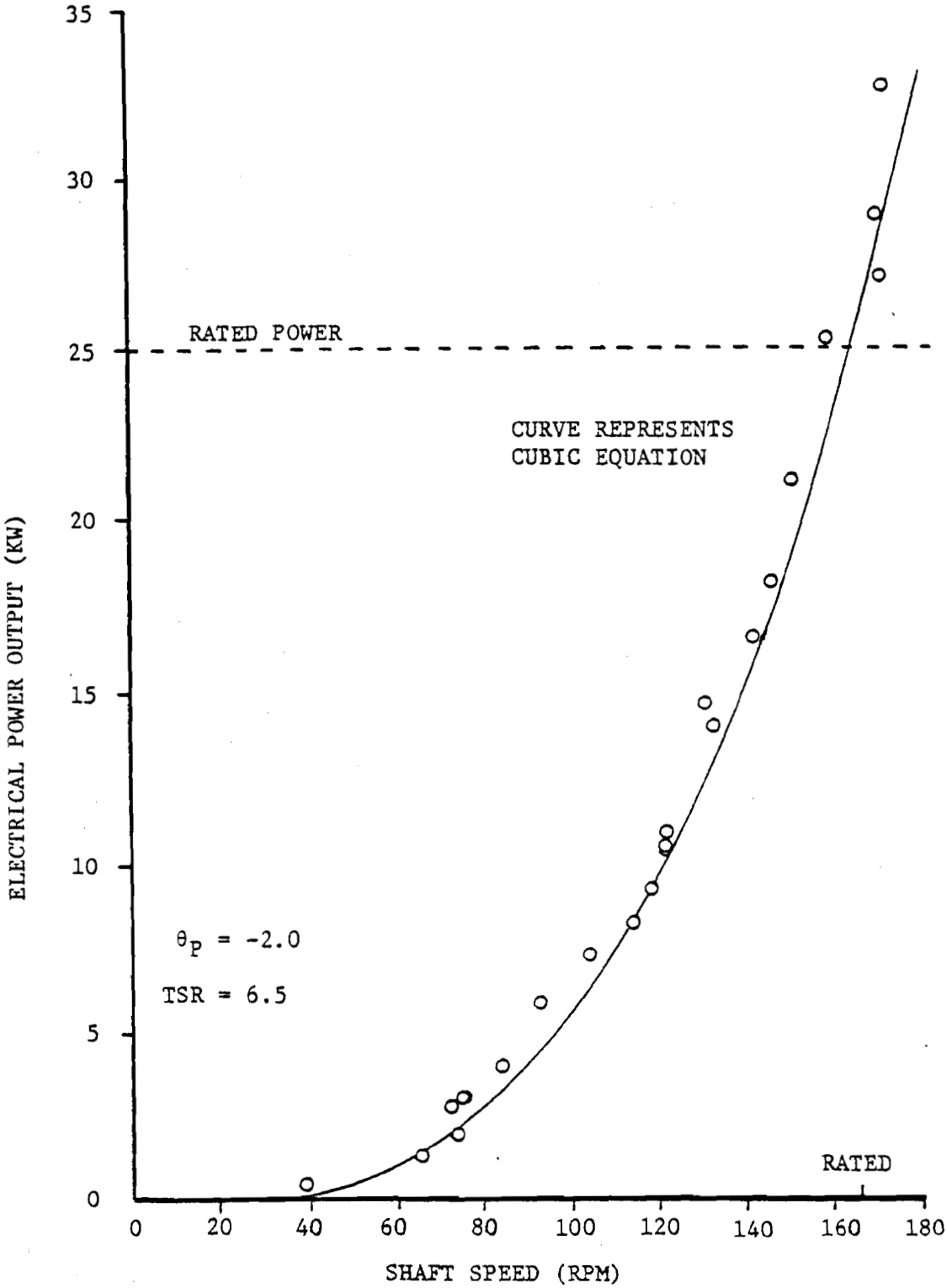

Figure 13. Power Versus Shaft Speed ($\theta_p = -2.0°$)

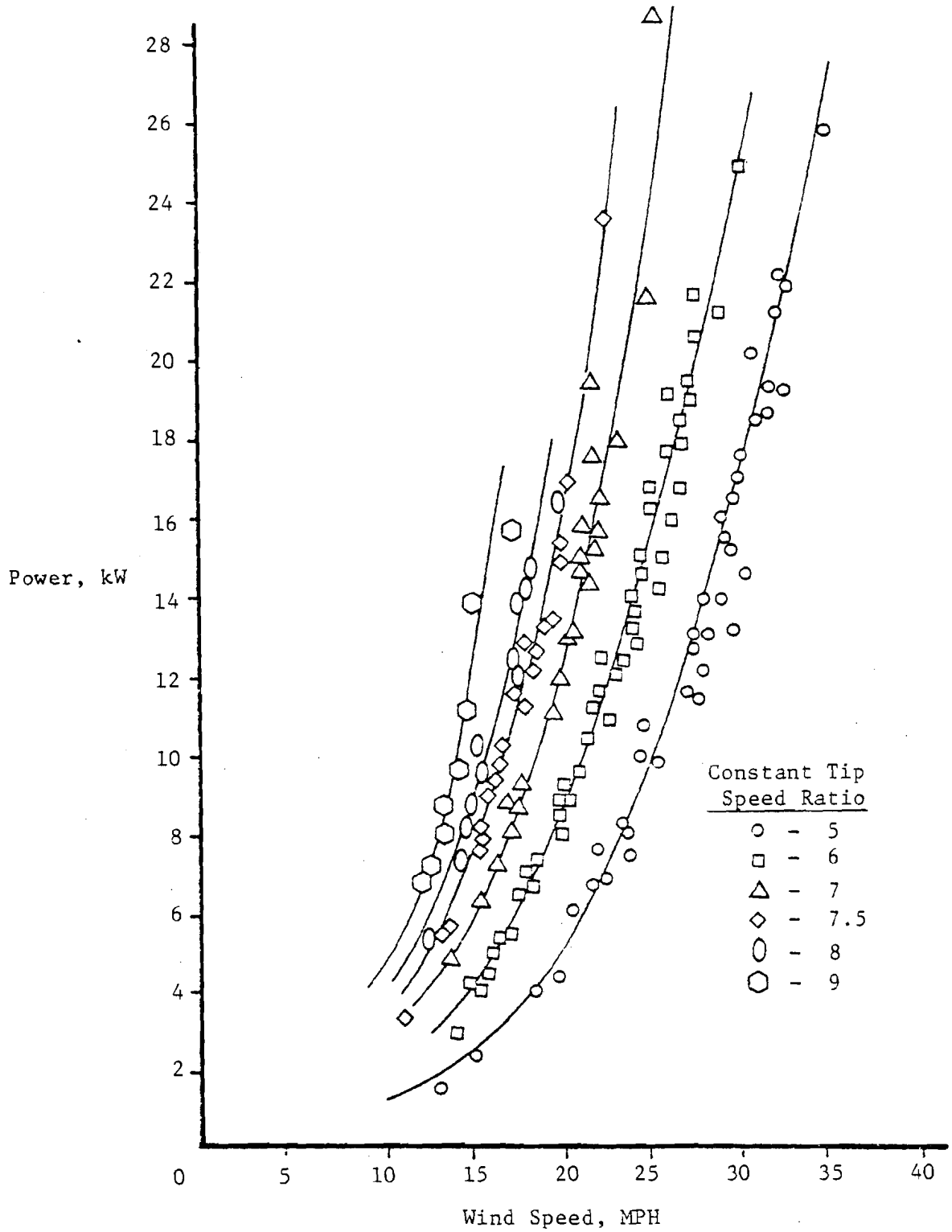

Figure 14. Power Versus Wind Speed for Constant Tip-Speed-Ratio

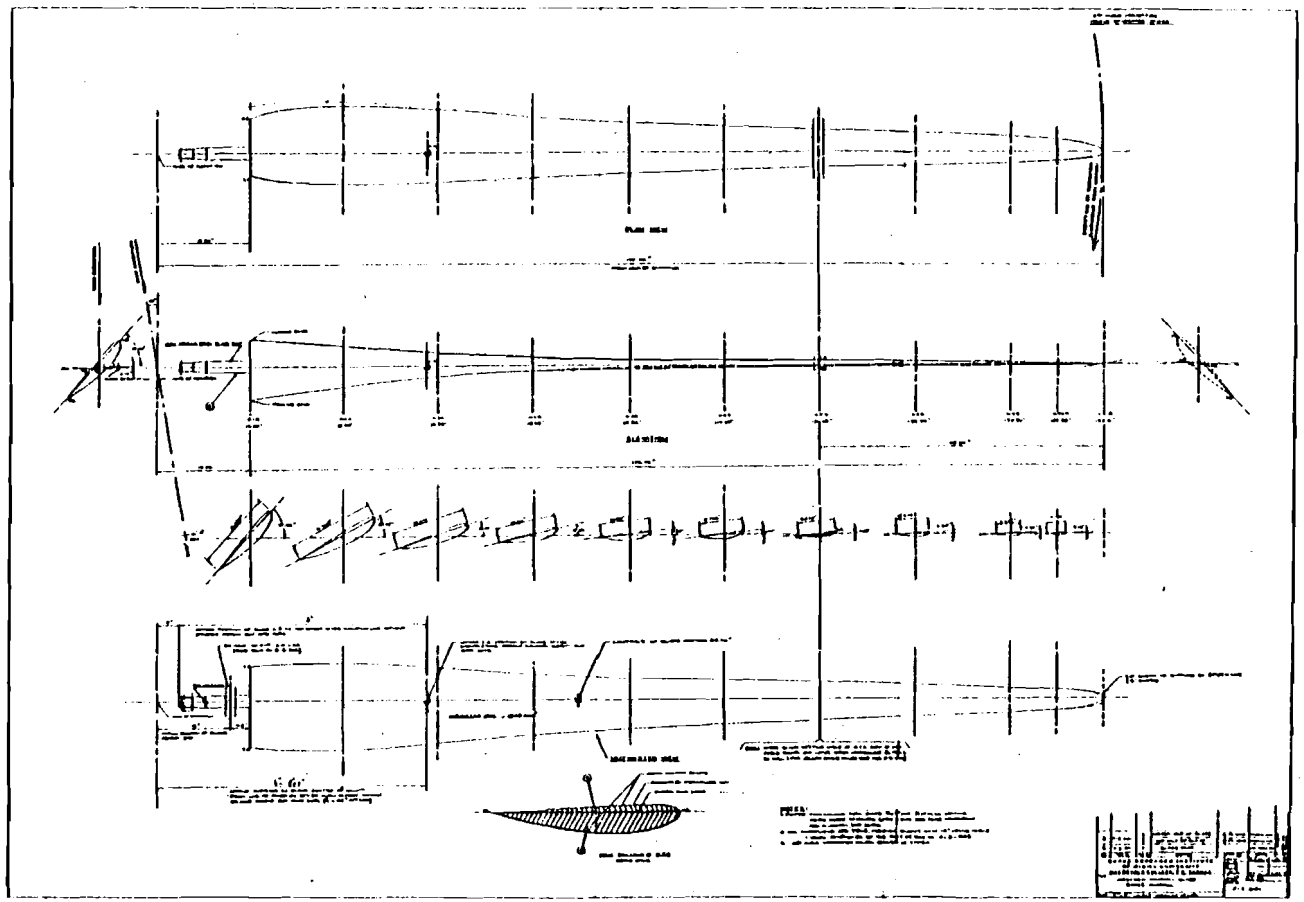

Figure 15. Brace Institute Airscrew Windmill Blade

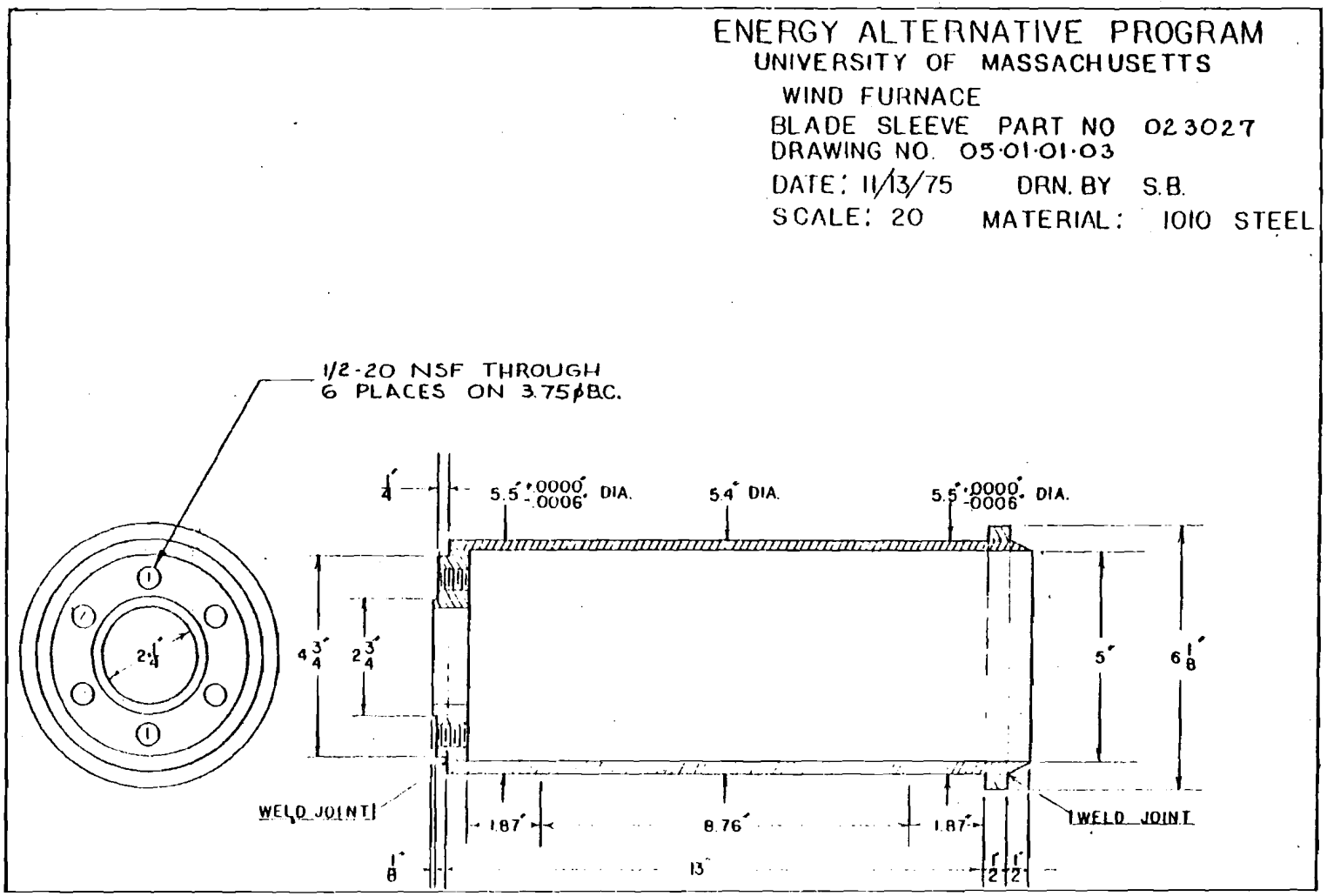

Figure 16. Blade Root Sleeve

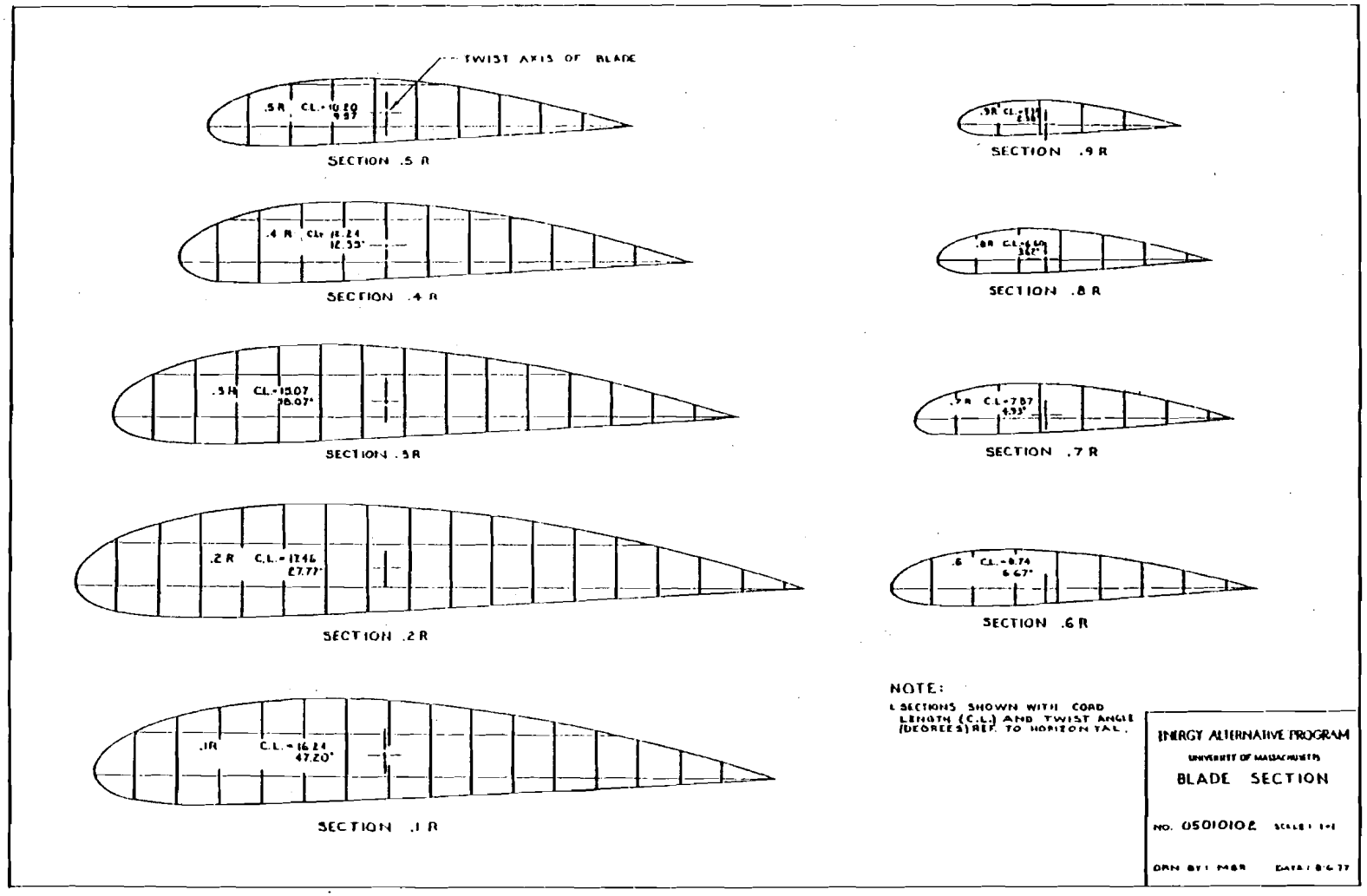

Figure 17. Blade Sections

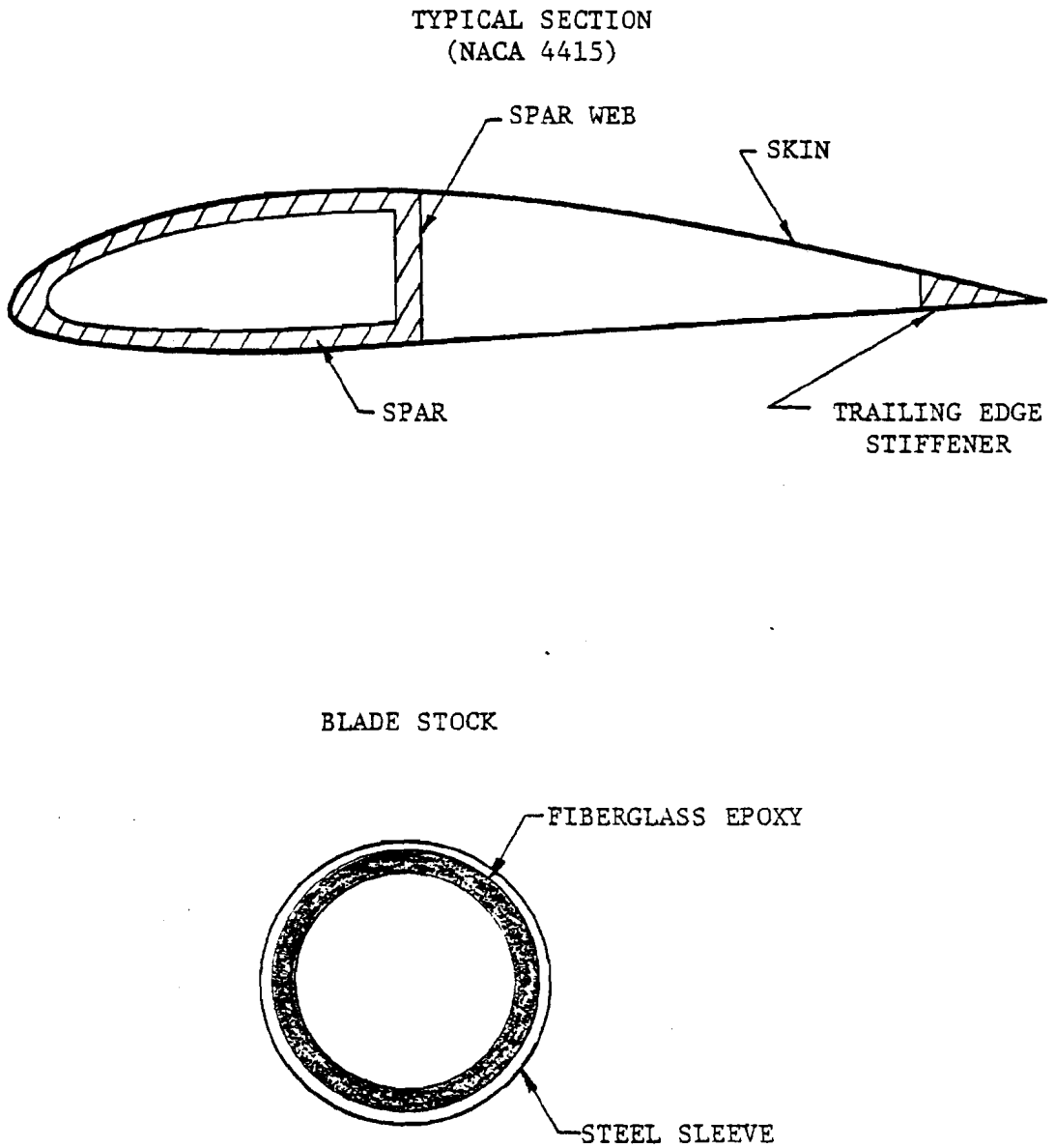

Figure 18. Description of Blade Components

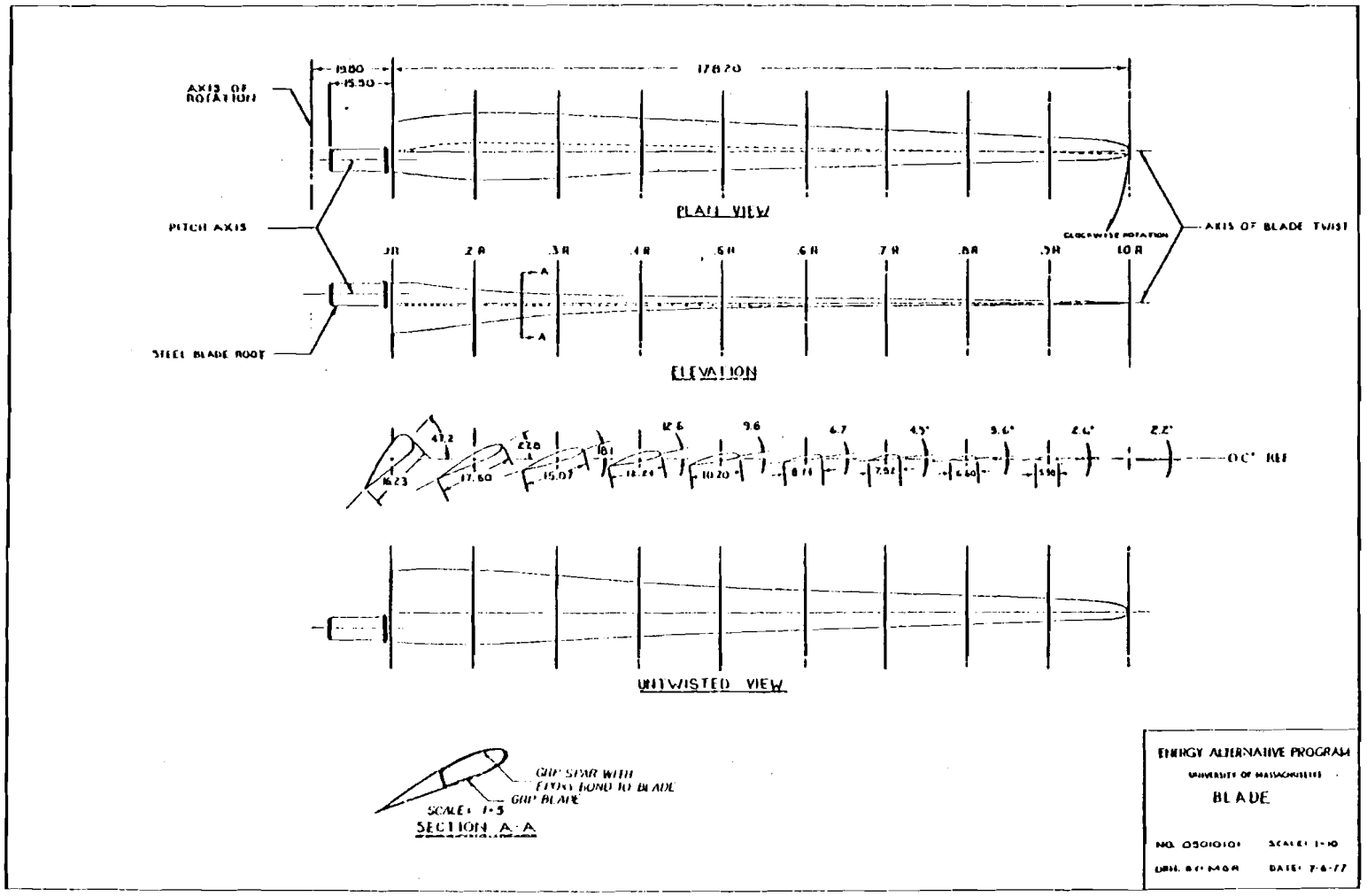

Figure 19. Complete Blade, Wind Furnace I

Table 1. Wind Furnace-1 Planform and Twist

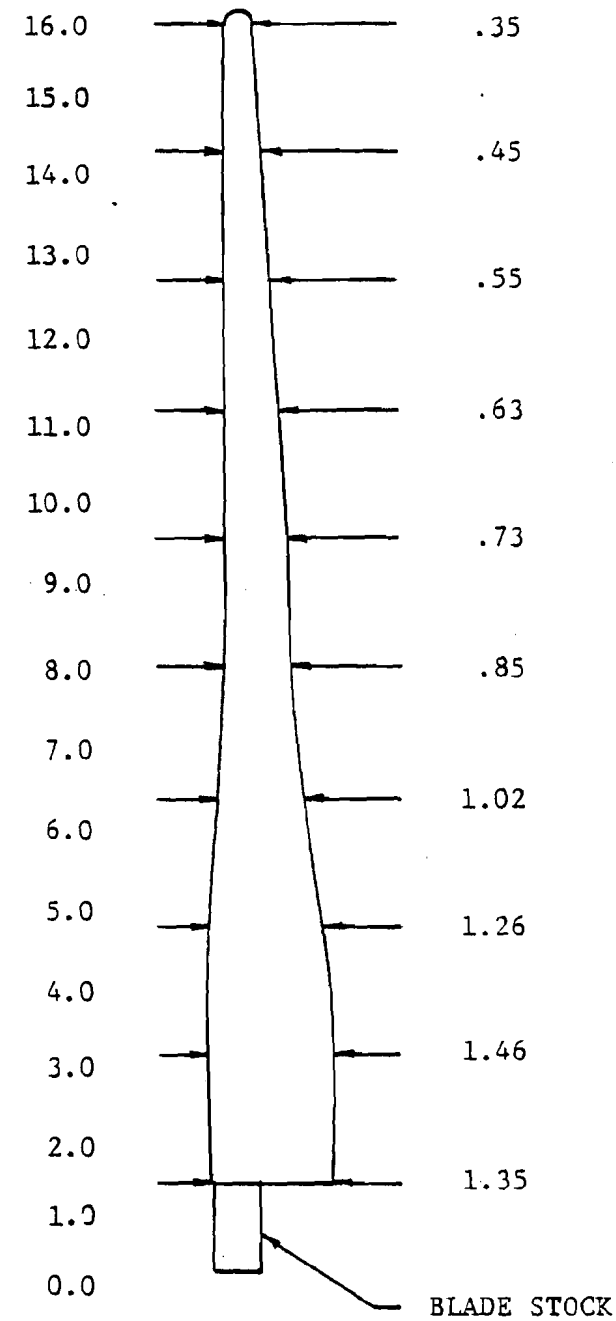

RADIUS ft.	CHORD ft.	TWIST degrees
16.0	.35	0
15.0		
14.0	.45	.4
13.0	.55	1.4
12.0		
11.0	.63	2.7
10.0	.73	4.5
9.0		
8.0	.85	7.4
7.0		
6.0	1.02	10.4
5.0	1.26	15.7
4.0		
3.0	1.46	25.6
2.0		
1.0	1.35	45.0
0.0		

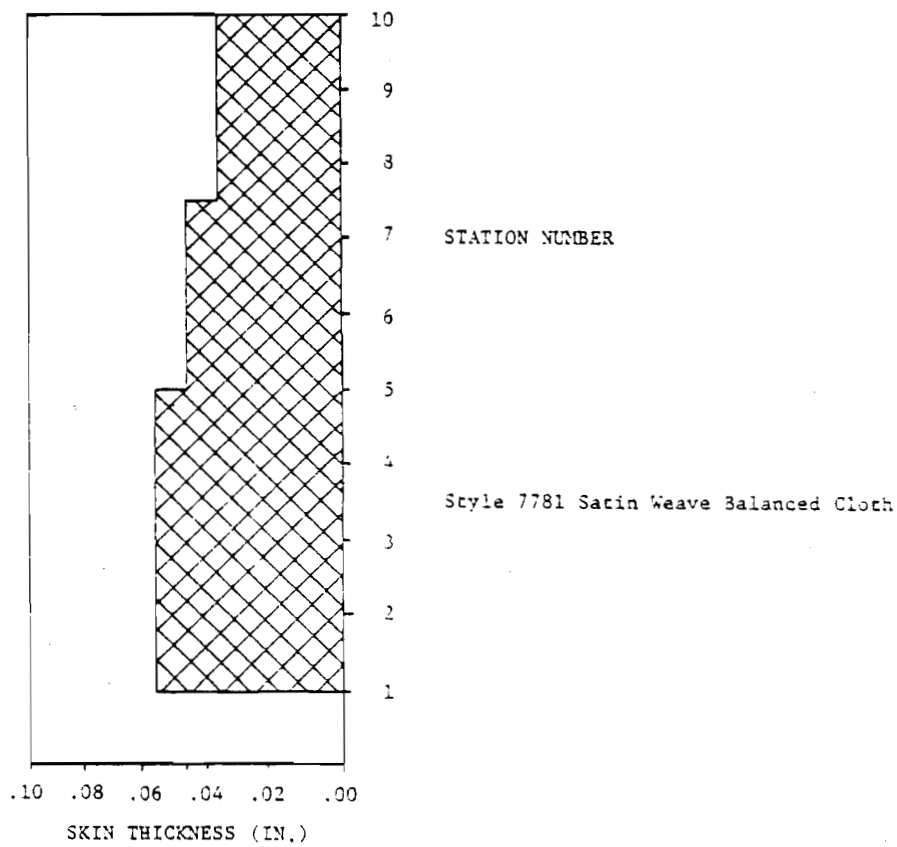

Figure 20. Skin Laminate Schedule

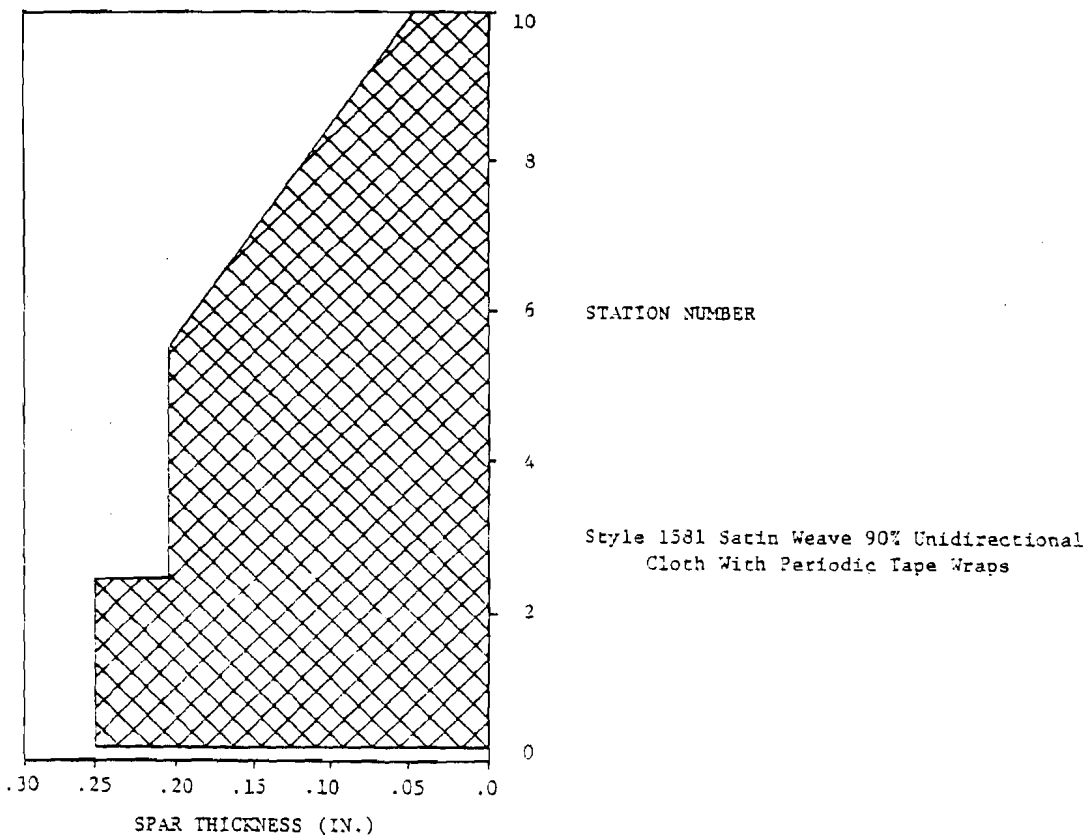

Figure 21. Spar Laminate Schedule

Table 2. Blade Design Parameters

r/Radius (Station/10)	Radius (ft.)	Chord (ft.)	Twist (degrees)	Leading Edge to Spar Web	Skin Layers (7781)	Skin Thickness (in.)	Spar Layers (1543)	Spar Thickness (in.)	Spar Web Thickness (in.)
.05					4	.036	25	.288	.238
.10	1.625	1.35	45.0	.540	4	.036	25	.288	.238
.15					4	.036	25	.288	.238
.20	3.250	1.46	25.6	.584	4	.036	25	.288	.238
.25					4	.036	25	.288	.238
.30	4.875	1.26	15.9	.504	4	.036	21	.250	.220
.35					4	.036	21	.250	.200
.40	6.500	1.02	10.4	.410	4	.036	21	.250	.150
.45					4	.036	21	.250	.100
.50	8.125	.85	7.4	.340	4	.036	21	.250	.050
.55					3	.027	21	.250	.050
.60	9.750	.73	4.5	.292	3	.027	21	.231	.050
.65					3	.027	17	.212	.050
.70	11.375	.63	2.7	.252	3	.027	15	.193	.050
.75					3	.027	13	.174	.050
.80	13.000	.55	1.4	.220	2	.018	11	.165	.050
.85					2	.018	9	.136	.050
.90	14.625	.45	0.4	.180	2	.018	7	.117	.050
.95					2	.018	6	.107	.050
1.00	16.250	.35	0.0	.140	2	.018	5	.098	.050

$E_{skin} = 2.2 \times 10^6 psi$ $\quad G_{skin} = 0.5 \times 10^6 psi$ $\quad \rho_{skin} = .0555 \frac{lb}{in^3}$

$E_{spar} = 4.4 \times 10^6 psi$ $\quad G_{spar} = 0.3 \times 10^6 psi$ $\quad \rho_{spar} = .0501 \frac{lb}{in^3}$

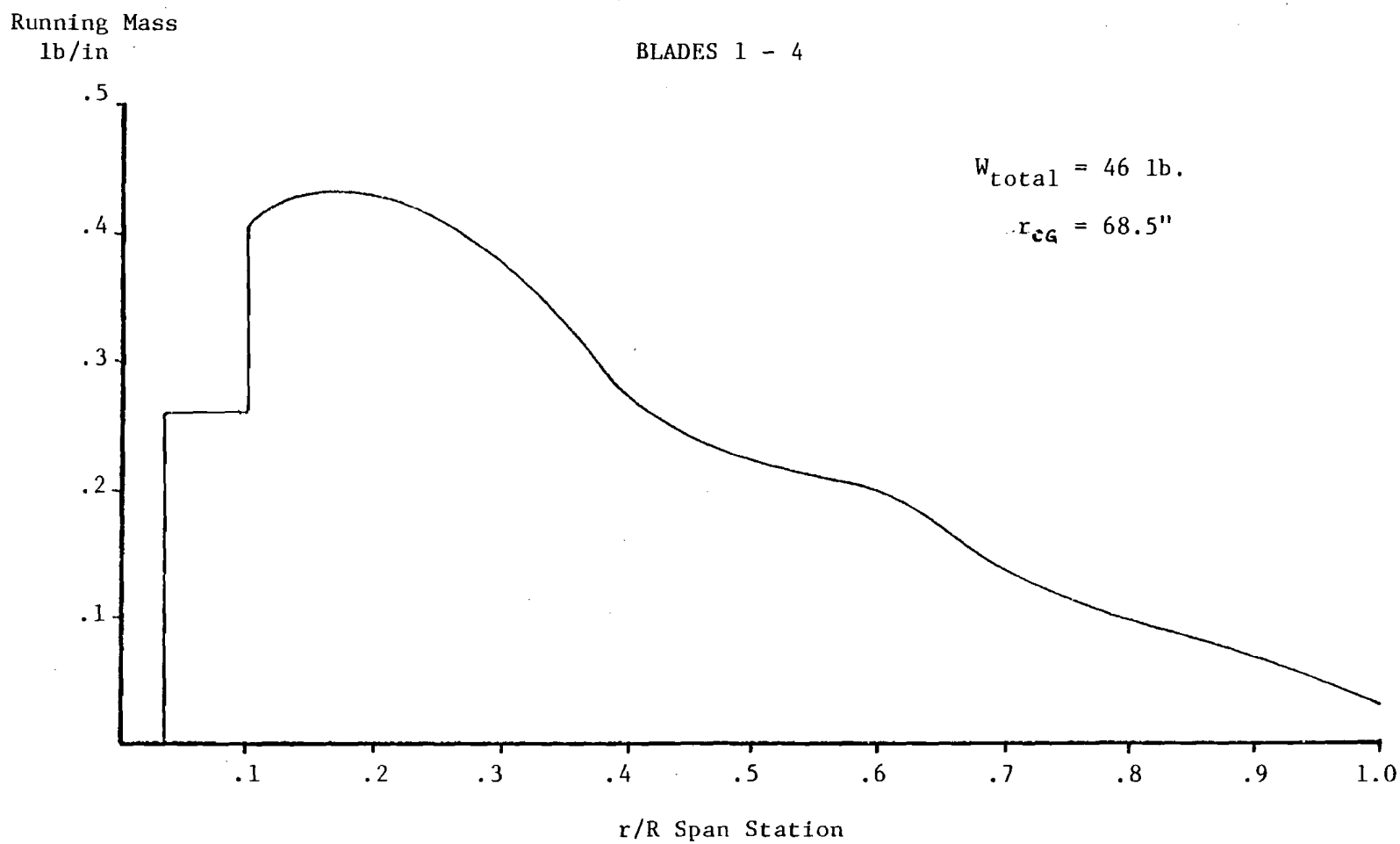

Figure 22. Blade Weight Distribution

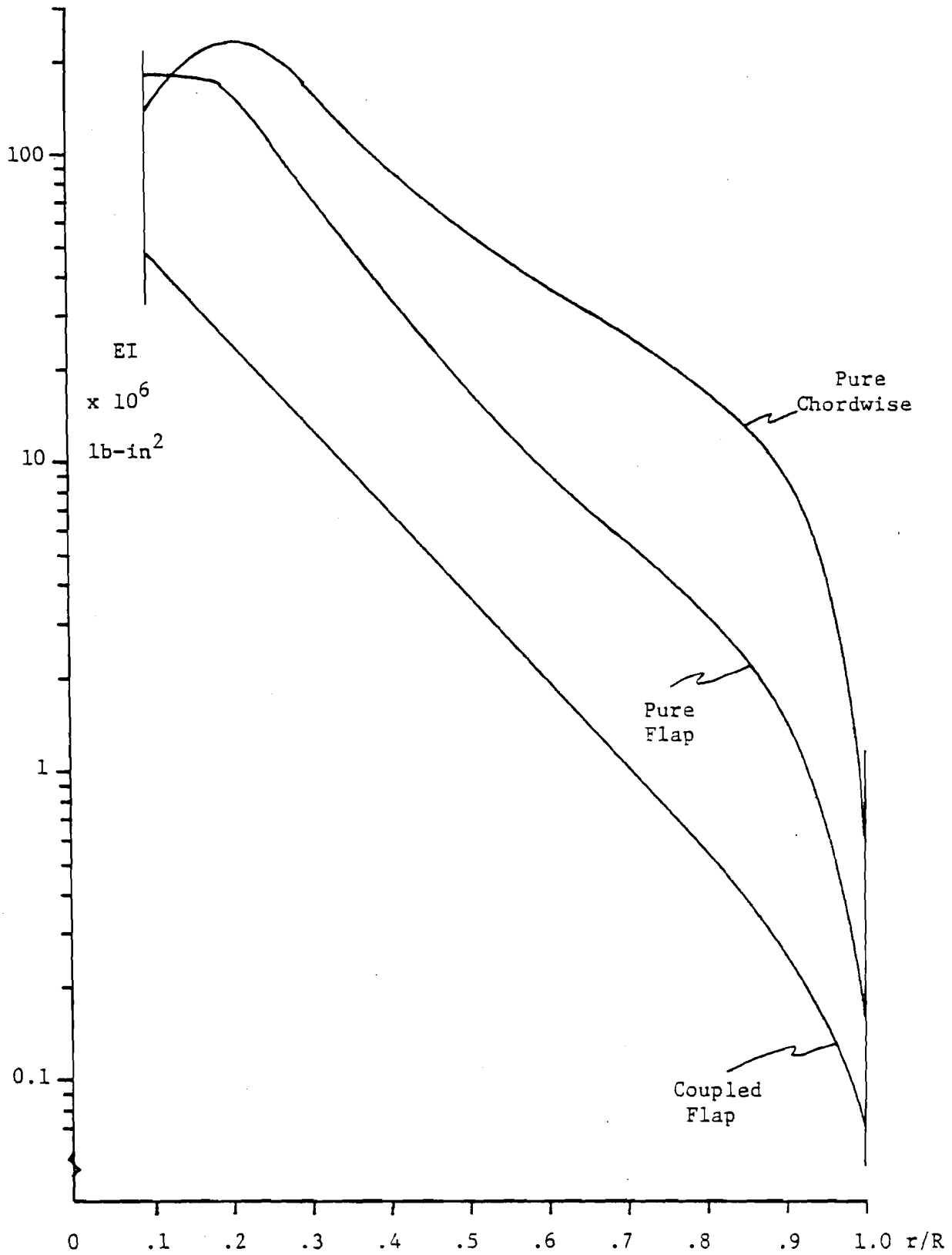

Figure 23. Beamwise Stiffness Distributions

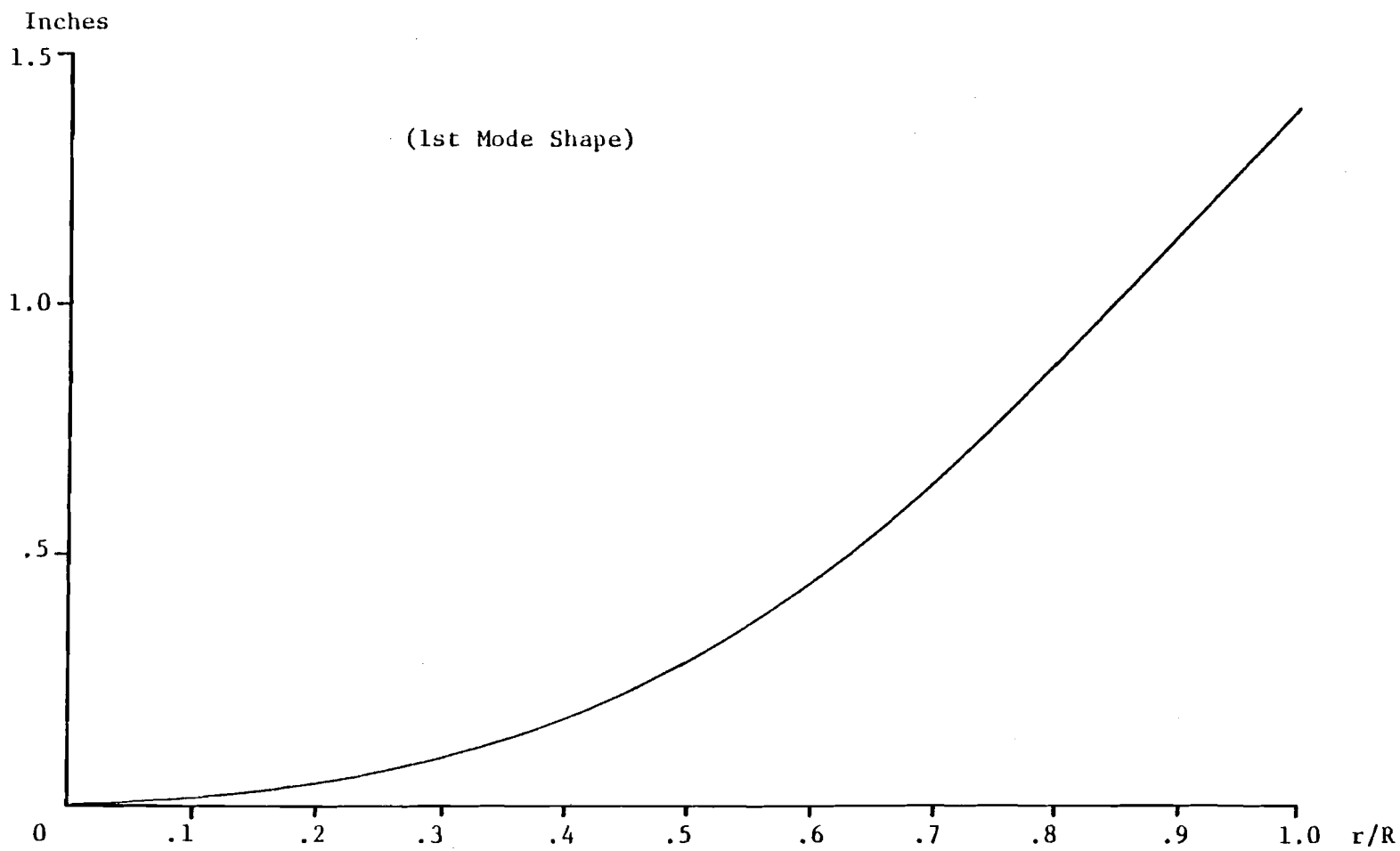

Figure 24. Static Deflection Curve

CHAPTER II

ISOLATED BLADE EQUATIONS OF MOTION

A. Single Blade Equations of Motion

The offset hinge-spring equivalent blade is assumed to be isolated and rotating at constant angular frequency, Ω about the Z' ($\hat{Z}$) axis. The x, y, z ($\bar{i}$, $\bar{j}$, $\bar{k}$) axis system rides with the blades: the x-axis spanwise, and the y-axis forward inplane, as shown in Figure 25; the blade is shown at flapping angle β. As described in Section I-A (Idealized Wind Turbine System), the rotor hub is stationary and the blade is comprised of rigid, uniform parts.

In the interest of clarity, and to isolate the fundamental blade dynamics, these derivations are kept as simple as possible. The aerodynamic terms are dealt with separately in Section II-D. The blade degrees of freedom are uncoupled. A detailed dynamic analysis including the three coupled motions, deflections and degrees of freedom (flapping, lead-lag, feathering) is given in Reference 8. For preliminary design of WTG's (wind turbine generators) we are more interested in the "uncluttered" effects of gravity, yaw rate and crossflow in our dynamics and stability analyses. Hence, these effects are considered separately and cumulatively.

1. Blade flapping equation of motion. The non-aerodynamic forces acting on the elemental mass, dm, at radius r from flapping hinge, are due to centrifugal force (xyz system), gravity, and hinge spring

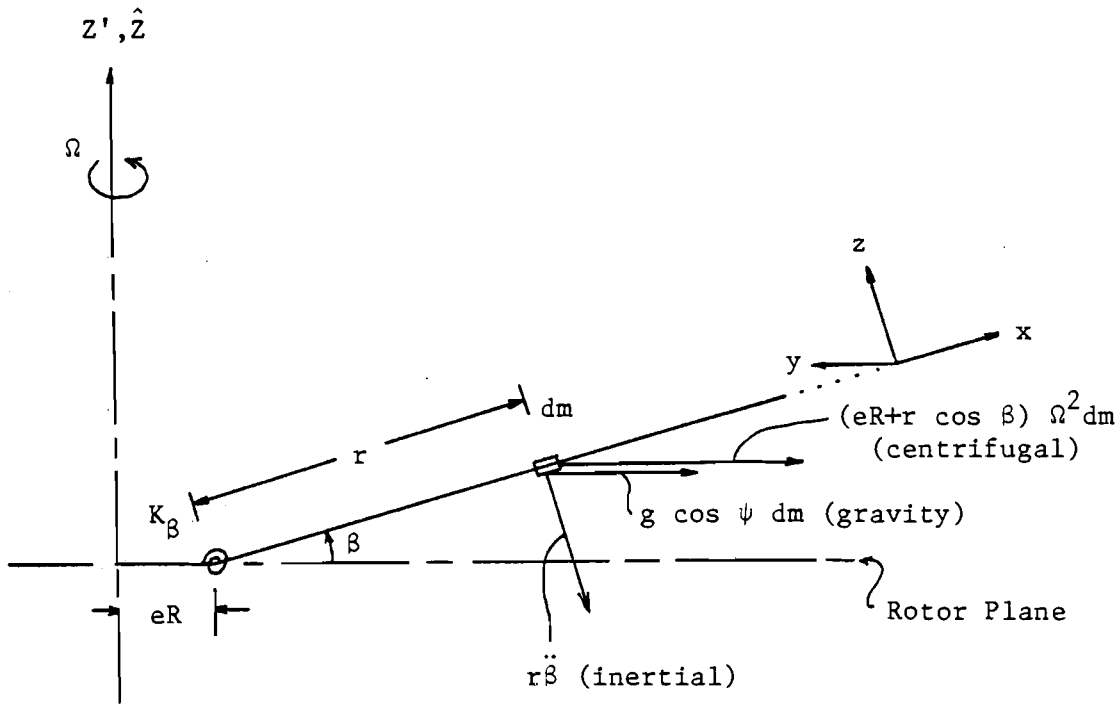

Figure 25. Blade Flapping Mode

restraint; these vectors are shown in Figure 25. The angle ψ is the blade azimuth angle, $\psi = 0$ being vertical downward. As shown in Section VII-E (derivation of the dynamic blade model), the integration along the blade starts at the hinge, although the radius arm, r, is measured from the hub in a usual blade.

Taking moments about the flapping hinge:

$$\Sigma M = \int_{o}^{R(1-e)} r^2 \ddot{\beta} dm + \int_{R_o}^{R(1-e)} (eR + r \cos \beta)\, r\, \Omega^2\, dm \sin \beta$$

$$+ \int_{o}^{R(1-e)} g \cos \psi \sin \beta \, dm + K_\beta \beta = 0 \qquad \text{(II-1)}$$

The blade mass moment of inertia (sometimes ambiguously called polar moment of inertia) is:

$$I_b = \int_o^R r^2 dm, \text{ or for our hinged blade, } I_b = \int_o^{R(1-e)} r^2 dm$$

This gives:

$$I_b \ddot{\beta} + e\ R^2 \Omega^2 X_g\ M_b \sin\beta + I_b \cos\beta\ \Omega^2 \sin\beta$$

$$+ g \cos\psi \sin\beta\ M_b\ X_g\ R + K_\beta \beta = 0 \qquad \text{(II-2)}$$

where:

M_b = mass of the blade

$X_g = \frac{r_g}{R}$ = non-dimensional c.g. of blade

The assumption is made that the flapping angle, β is small; this gives:

$$I_b \ddot{\beta} + [\ eR^2 \Omega^2\ X_g\ M_b + g \cos\psi\ M_b X_g R + I_b \Omega^2\ ]\ \beta + K_\beta \beta = 0 \qquad \text{(II-3)}$$

Now since the blade has a uniform mass distribution, a new term can be defined:[9]

$$\varepsilon = \frac{M_b\ e\ X_g\ R^2}{I_b} = \frac{3\ e}{2(1+e)}$$

And:

$$\boxed{\ddot{\beta} + \Omega^2\ [\ 1 + \varepsilon + \frac{G}{\Omega^2} \cos\psi\ ]\ \beta + \frac{K_\beta}{I_b}\ \beta = 0} \qquad \text{(II-4)}$$

Blade Flapping Equation of Motion

where $G = \frac{g\ M_b\ X_g\ R}{I_b}$

2. Blade lagging equation of motion. The prominent inplane force is due to rotation: centrifugal force. The motion in lead-lag will be derived first including only this force, since the geometry is complex. The blade is shown in Figure 26, looking at the plane of rotation, with the blade at a deflected inplane angle, ζ. Again, the integration will begin at the hinge, so the radius arm, r, is measured from that point.

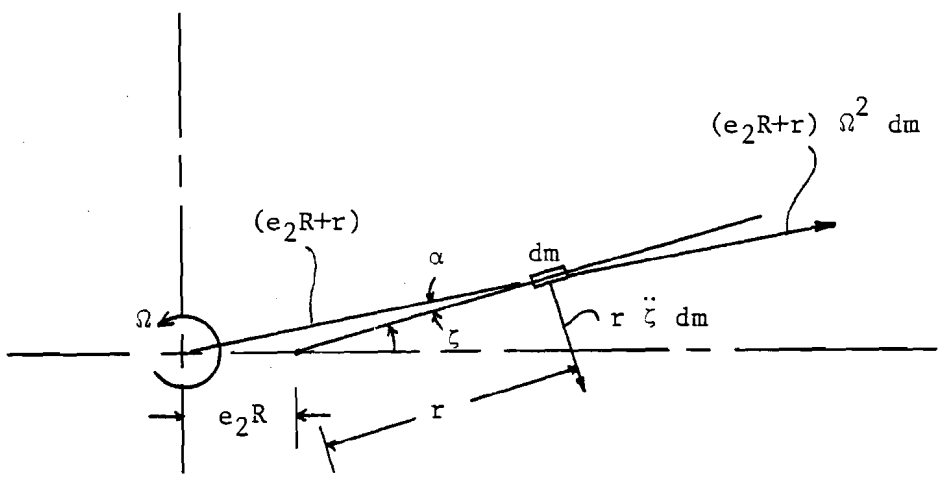

Figure 26. Blade Lead-Lag Mode

For small ζ, the rotation arm to dm is $(e_2R + r)$, and the centrifugal force on dm is:

$$dF = (e_2R + r)\ \Omega^2\ dm$$

The component which produces a moment about the hinge is:

$$dF_\zeta = (e_2R + r)\ \Omega^2 \sin\alpha\ dm$$

where α is the small angle between the blade and the centrifugal moment arm. The angle is found from the following figure.

From geometry of the figure:

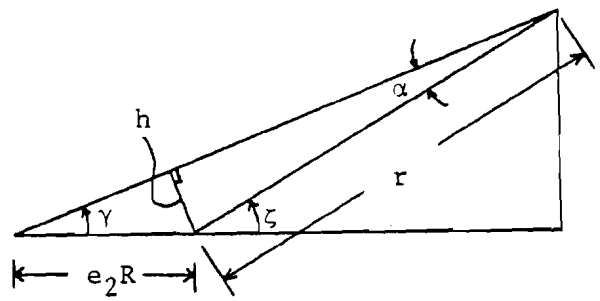

$$\zeta = \gamma + \alpha$$

$$h = e_2R \sin \gamma = r \sin \alpha$$

or

$$\sin \alpha = \frac{e_2R}{r} \sin \gamma$$

For small angles:

$$\sin \alpha \simeq \alpha = \frac{e_2R}{r} \gamma = \frac{e_2R}{r} (\zeta - \alpha)$$

Thus:

$$\sin \alpha = [\frac{e_2R}{r + e_2R}] \sin \zeta \qquad \text{(II-5)}$$

Taking moments about the lag hinge:

$$\Sigma dM_\zeta = r^2 \ddot{\zeta} \, dm + r \, \Omega^2 dm \, (e_2R + r)(\frac{e_2R}{r + e_2R}) \sin \zeta = 0$$

Thus:

$$I_b\ddot{\zeta} + \Omega^2 \, e_2R \sin \zeta \, M_b \, X_g \, R = 0$$

or

$$I_b\ddot{\zeta} + e_2 \, M_b \, X_g \, \Omega^2 \, R^2 \sin \zeta = 0 \qquad \text{(II-6)}$$

With, as before:

$$\varepsilon_2 = \frac{M_b \, e_2 \, X_g \, R^2}{I_b} = \frac{3e_2}{2(1 - e_2)}$$

$$\boxed{I_b\ddot{\zeta} + \varepsilon_2 I_b \, \Omega^2 \sin \zeta = 0} \qquad \text{(II-7)}$$

Blade Lag Equation (for centrifugal force only)

The final forces on the elemental mass are shown in Figure 27. The lead-lag offset, e_2R, and lead-lag spring, K_ζ, are derived from consideration of beam flexibilities as eR and K_β were for the flapping

mode (see Section VII-E). A Coriolis acceleration due to flapping motion, $\dot{\beta}$, is included. Other non-aerodynamic forces are centrifugal, gravity and hinge spring.

Taking moments about the lag hinge:

$$\Sigma dM_\zeta = r^2\ddot{\zeta}\ dm + r\Omega^2\ dm\ \left(\frac{e_2R}{e_2R+r}\right)\ \sin\zeta\ (e_2R + r)$$

(inertial) (centrifugal)

$$- 2r^2\ dm\ \Omega\dot{\beta}\ \sin\beta + r\ dm\ g\ \sin(\psi + \zeta) + K_\zeta\ \zeta = 0 \qquad \text{(II-8)}$$

(Coriolis) (gravity) (hinge spring)

Integrating:

$$I_b\ \ddot{\zeta} + e_2\ M_bX_g\ \Omega^2\ R^2\ \sin\zeta - 2\ I_b\Omega\dot{\beta}\ \sin\beta + g\ \sin(\psi + \zeta)\ M_bX_g\ R + K_\zeta\ \zeta = 0$$

Again with:

$$G = \frac{g\ M_b\ X_g\ R}{I_b} \qquad \text{and } \sin(\psi + \zeta) = \sin\psi + \zeta\cos\psi$$

$$\varepsilon_2 = \frac{M_b\ e_2\ X_g\ R^2}{I_b}$$

$$\boxed{\ddot{\zeta} + \left[\varepsilon_2\ \Omega^2 + G\cos\psi + \frac{K_\zeta}{I_b}\right]\zeta - 2\ \Omega\ \dot{\beta}\ \beta + G\sin\psi = 0} \qquad \text{(11-9)}$$

Blade Lagging Equation (including gravity, hinge offset and spring, flapping velocity $\dot{\beta}$)

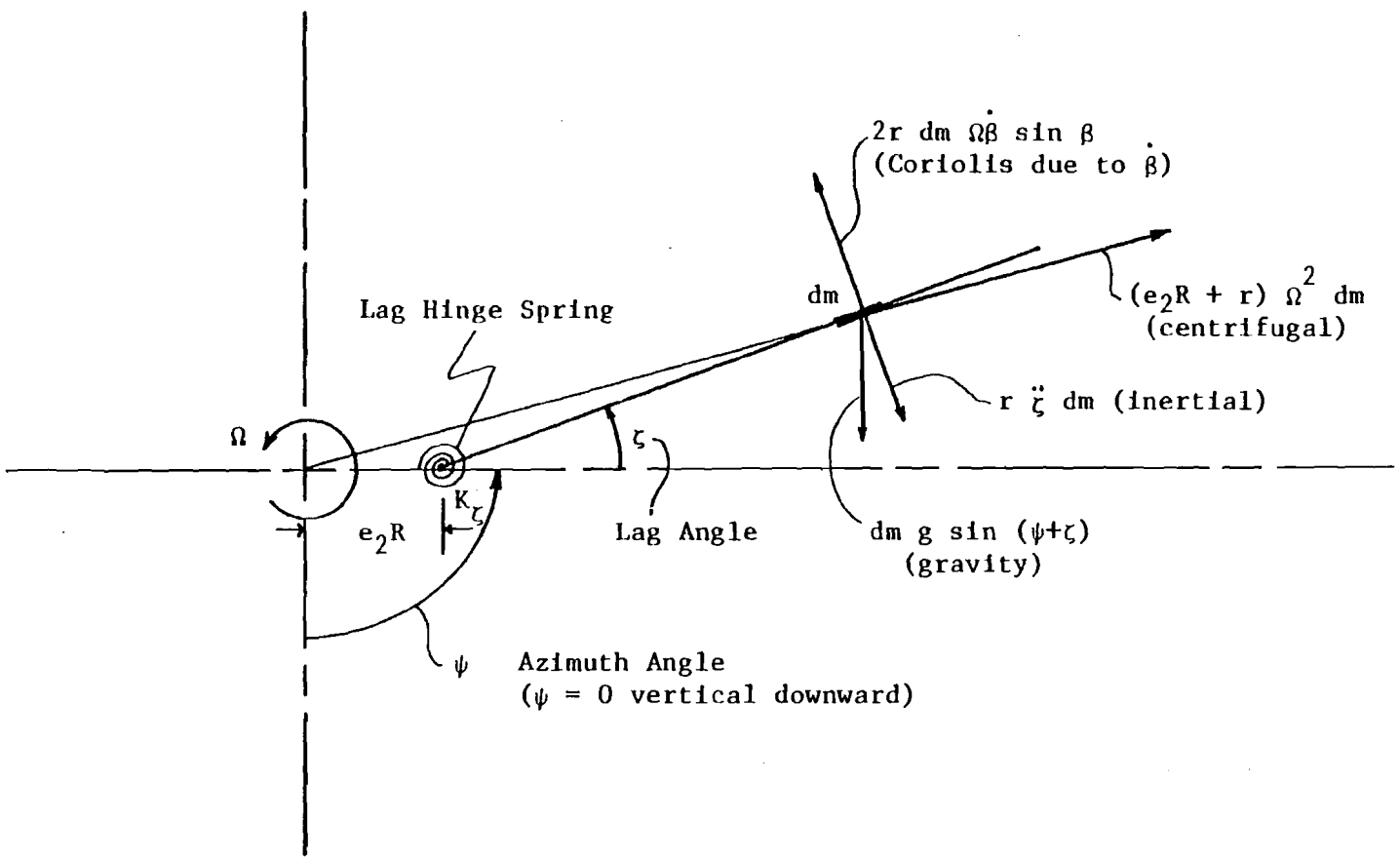

Figure 27. Blade Lead-Lag Mode, Final Forces

3. Blade feathering equation of motion. The figure shows a section of the blade with a torsional (feathering) deflection θ, away from some preset or constant pitch angle. The torsional spring is K_θ, and the feathering (mass) moment of inertia is I_f.

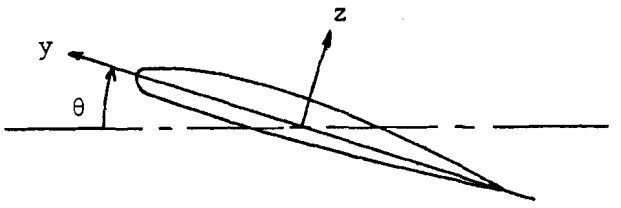

Since the xyz system is rotating at constant Ω, the Euler angular velocities are:[10]

$$\omega_y = \Omega \sin \theta$$

$$\omega_z = \Omega \cos \theta$$

Neglecting all other coupled effects, the simple feathering oscillator is derived:

$$I_f \ddot{\theta} + I_f \Omega^2 \sin \theta \cos \theta + K_\theta \theta = 0 \qquad \text{(II-10)}$$

Or if small θ:

$$\boxed{\ddot{\theta} + [\, \Omega^2 + \frac{K_\theta}{I_f} \,] \theta = 0} \qquad \text{(II-11)}$$

Blade Feathering Equation

B. Elementary Dynamic Motions

Equations II-4, II-9, and II-11 have been derived for the simple hinge equivalent blade with a spring at the hinge for lead-lag and flapping freedom. The second order equations describe the fundamental motion of the blade in the absence of aerodynamic forces (i.e., in a vacuum). Much can be learned from a qualitative look at the dynamic system represented by these equations.

1. Simple flapping response. The flapping equation is:

$$\ddot{\beta} + [\,\Omega^2\,(1 + \varepsilon) + G \cos\psi + \frac{K_\beta}{I_b}\,]\,\beta = 0 \qquad \text{(II-12)}$$

For no gravity, hinge offset or hinge spring ($G = \varepsilon = K_\beta = 0$) the blade oscillates at a natural frequency Ω to an impulsive input, with no dissipation.

Adding first the hinge offset ε, we find the new natural frequency is:

$$\omega^2 = \Omega^2(1+\varepsilon) \qquad \text{(II-13)}$$

The natural frequency of the motion is increased, and the new flapping oscillation will be out of phase with the blade azimuth ψ. In helicopter rotors the hinge factor ε is on the order of 0.06, giving a flap frequency about 3% higher than shaft frequency.[9] Hinged wind turbine blades, or even cantilevered blades with soft flapping stiffness and non-linear mass distribution, will have higher equivalent hinge offsets than rotors.

It is a task of the designer to separate the flap response (frequency) from forcing inputs which may be precisely at rotational frequency Ω, e.g., tower wake. In a hinged (or articulated) rotor, the flapping hinge offset gives the designer a way to further separate flapping frequency from forcing frequencies.

Adding hinge spring K_β greatly increases the flap natural frequency:

$$\omega^2 = \Omega^2 + \frac{K_\beta}{I_b} \qquad \text{(II-14)}$$

This is precisely the relationship used in Section VII-E to equate the non-linear cantilever first bending mode, to the hinge equivalent blade.

It represents the natural bending frequency of a simple beam with hinge stiffness K_β, and mass moment of inertia I_b. In this it models the first bending mode only of the more complex cantilevered blade which it represents.

Adding the hinge offset gives the complete equation:

$$\boxed{\omega_\beta{}^2 = \Omega^2 (1 + \varepsilon) + \frac{K_\beta}{I_b}} \qquad \text{(II-15)}$$

Inertial Flapping Frequency

The problem of choosing flapping frequency reduces to this equation if the designer has a blade material which gives him the latitude to vary K_β and ε. Neglecting for the moment the other structural blade considerations (ultimate strength, fatigue, endurance, etc.), the vibratory dynamic response of the blade in flapping is largely determined by this equation, (II-15). For example, using GRP (glass reinforced plastic) design, the flapping frequency can be located at any desired percentage of rotational speed, for a given Ω. Thus, a synchronous WTG, that is, running at constant Ω to deliver 60 Hz grid power, can easily be designed to have a flapping frequency well separated from all other periodic inputs (inertial, gravitational, aerodynamic, and generator excitation).

The gravity-excited system will be covered in Section II-C.

2. Simple lead-lag response. The lead lag equation is:

$$\ddot{\zeta} + [\ \varepsilon_2\Omega^2 + G \cos \psi + \frac{K_\zeta}{I_b}\ ]\ \zeta - 2\Omega\dot{\beta}\ \beta + G \sin \psi = 0 \qquad \text{(II-16)}$$

The last two terms give a "steady" baseline value of ζ caused by flapping velocity (Coriolis) and gravity. They will both be periodic, one at frequency Ω and the other at the natural frequency of flapping motion, but both these terms are small. More importantly, they can be considered outside the dynamic system of interest here, since oscillations which may be unstable occur in spite of these terms.

Looking then at the natural frequency terms we find the lead-lag frequency in the absence of gravity and hinge spring to be:

$$\omega_\zeta{}^2 = \Omega^2 \varepsilon_2 \tag{II-17}$$

The lead lag frequency is much lower than the rotational frequency, typically 25% Ω. [Note: for zero hinge offset, the dynamic model derived here is not applicable (it is no longer an oscillator) and the next inplane cantilever mode must be included.] In practical installations with no lag hinge the offset refers to the derived quantity from flexibility modeling (Section VII-E). Including the lag spring gives:

$$\boxed{\omega_\zeta{}^2 = \Omega^2 \varepsilon_2 + \frac{K_\zeta}{I_b}} \tag{II-18}$$

Inertial Lead-Lag Frequency

The lead-lag spring increases lag frequency; the "softer" dependency of lag stiffness with increasing Ω is seen here. In the flapping case "centrifugal stiffening" appears as $(1 + \varepsilon)$, whereas in the lag case stiffening is greatly attenuated by geometry, and appears as (ε_2).

The significance of the gravity effect is covered in Section II-C.

3. Simple feathering response. The feathering equation of motion is:

$$\ddot{\theta} + [\ \Omega^2 + \frac{K_\theta}{I_f}\ ]\ \theta = 0 \qquad \text{(II-19)}$$

In the absence of torsional stiffness at the hinge (i.e., $K_\theta = 0$), the blade oscillates at frequency Ω. This means simply that the feathering motion is exactly one cycle per revolution; this gives a feathering moment which must be resisted by the pitch mechanism. The significance of this appears in the aerodynamic terms (Section II-D). This "feathering moment" can be explained by looking at the centrifugal force couple on a blade section:

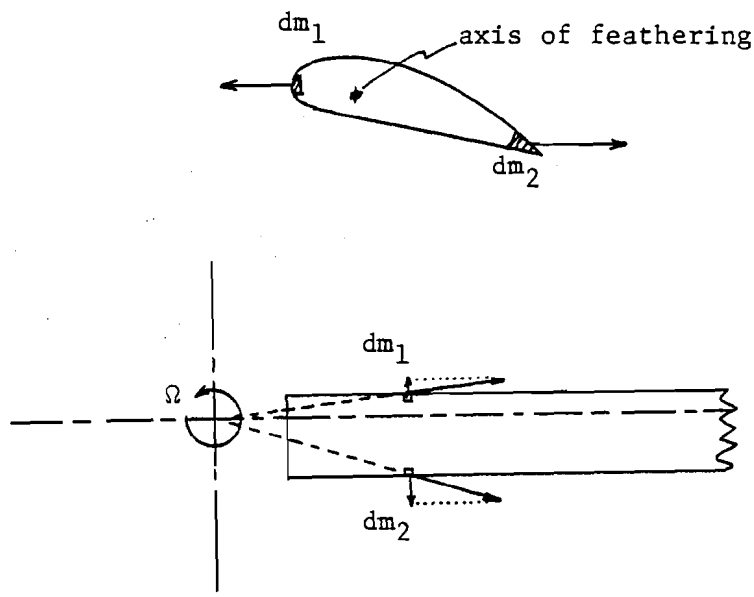

Figure 28. Blade Feathering Moment

When the blade is pitched through θ, the couple due to centrifugal force tends to reduce pitch (see Figure 28). As with flapping, the centrifugal force thus provides a spring with natural frequency exactly equal to Ω.

When the torsional spring, K_θ, is added, the natural frequency in feathering is greatly increased. Usually K_θ is very high and I_f is on the order of one percent of I_b, so the elastic frequency of torsional oscillation is usually orders of magnitude higher than either flapping or lead-lag motion for wind turbines. In the event of a loss of K_θ, the equation would describe (as above) the dynamics of the pitch link system, and the aerodynamic terms (see Chapter III) including blade pitching moment, become very significant.

C. Gravity and Yaw Induced Effects

The gravity forces have been included in the foregoing derivations; they are significant in the flapping and lead-lag oscillators. Yaw rate effects will be included in Section II-C-2. The flapping and lead-lag equations from Section II-A are:

$$\boxed{\ddot{\beta} + \Omega^2 \left[1 + \varepsilon + \frac{K_\beta}{I_b \Omega^2} + \frac{G}{\Omega^2} \cos \psi \right] \beta = 0} \qquad \text{(II-4)}$$

Flapping Equation of Motion

$$\boxed{\ddot{\zeta} + \left[\varepsilon_2 \Omega^2 + G \cos \psi + \frac{K_\zeta}{I_b} \right] \zeta - 2\Omega\dot{\beta}\beta + G \sin \psi = 0} \qquad \text{(II-9)}$$

Lead Lag Equation of Motion

1. Effects of gravity. The gravity term in the flap equation complicates the response by adding a periodic coefficient. Neglecting ε and K_β:

$$\ddot{\beta} + \left[\Omega^2 + G \cos \psi \right] \beta = 0 \qquad \text{(II-20)}$$

Substituting:

$$\frac{d}{dt} = \frac{d}{d\psi}\frac{d\psi}{dt} = \frac{d}{d\psi}\,\Omega$$

We get:

$$\boxed{\frac{d^2\beta}{d\psi^2} + \left[\,1 + \frac{G}{\Omega^2}\cos\psi\,\right]\beta = 0} \qquad \text{(II-21)}$$

This is a linear differential equation, a form of the classical Mathieu's equation which describes a physical system with a periodic change of stiffness, that can lead to special stability problems.[11] Instead of assuming linearly independent solutions to II-21 and writing the Wronskian to solve for the coefficients,[12] we will examine the stability of II-21 since it is more germaine to this development. [Note: the closed form solution of II-21 will yield two natural frequencies, which may or may not be stable as the following will show.] For II-21, assume a periodic solution:

$$\beta = \beta_o + \sum_{n=1}^{\infty}\left[\,\beta_{cn}\cos n\,\psi + \beta_{sn}\sin n\psi\,\right] \qquad \text{(II-22)}$$

After substituting and equating like harmonics, we obtain Hill's Determinant; and neglecting higher order terms, we get the classical solution to pendular stability. Standard form of Mathieu's equation is:[11]

$$\frac{d^2x}{dz^2} + \left[\,\delta + \alpha\cos z\,\right]x = 0 \qquad \text{(II-23)}$$

From Hill's Determinant:

$$\delta^2 - \delta - \frac{\alpha^2}{4} = 0 \qquad \text{(II-24)}$$

Solutions to this are shown in Figure 29. For the simple case with hinge offset and spring equal to zero, the Mathieu's coefficients are $\delta = 1$, $\alpha = \frac{G}{\Omega^2}$, and the system is unstable for all $\alpha \geq 0.1$, that is, for all values of gravity and Ω. However, if we include the entire coefficient from II-21 we get:

$$\boxed{\begin{aligned} \delta &= 1 + \varepsilon + \frac{K_\beta}{I_b \Omega^2} \\ \alpha &= \frac{G}{\Omega^2} \end{aligned}}$$

Flapping Pendular Stability Parameters (II-25)

The instability is simply a growth in flapping (pendulum) angle with time due to gravity input. As the effect of gravity increases (i.e., α increases), the instability region grows, and the limits on δ decrease. For example,

$$\frac{G}{\Omega^2} = 0.5 = \frac{g\ M_b\ X_g\ R}{I_b \Omega^2} = \frac{3g\ M_b\ X_g\ R}{M_b\ R^2\ \Omega^2} = \frac{3g\ X_g}{R\Omega^2}$$

for uniform blade. Then, according to Figure 29, the instability boundary occurs at:

$$\delta = 1.10 = 1 + \varepsilon + \frac{K_\beta}{I_b \Omega^2}$$

Thus the designer must respect the conditions:

$$\varepsilon + \frac{K_\beta}{I_b \Omega^2} \geq 0.10 \qquad \text{(II-26)}$$

As one would expect, increasing rotational speed Ω increases stability limits as does decreasing center of gravity X_g.

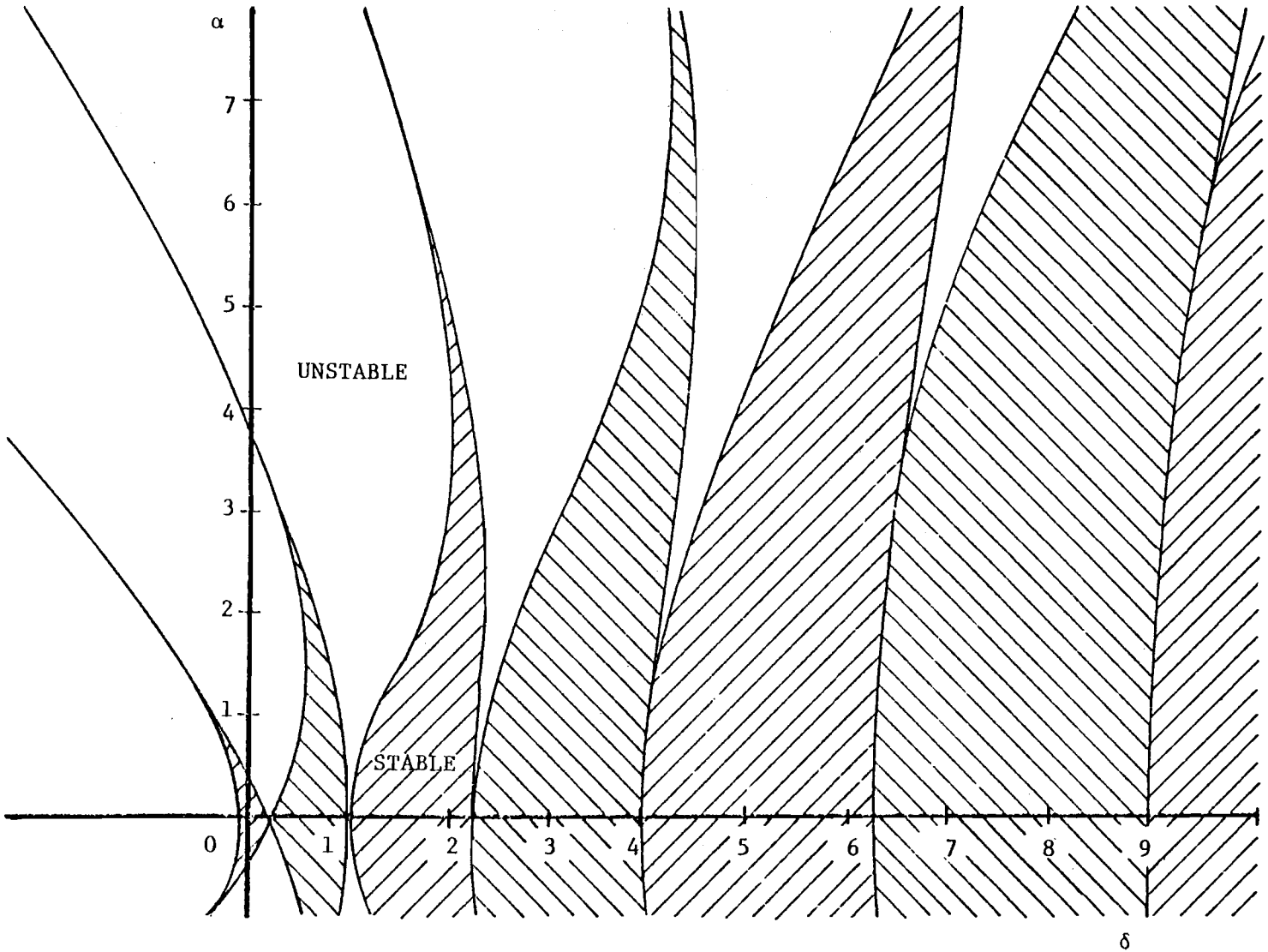

Figure 29. Solutions to Mathieu's Equation

For a numerical example, assume a uniform articulated blade with the following characteristics:

$R = 25'$

$X_g = 12.5'$

$\varepsilon = 0.08$

$$I_b = \frac{MR^2}{3} = \frac{150}{(32.2)} \frac{(25)^2}{3} = 970.5 \text{ slug ft}^2$$

$$\Omega = 100 \text{ RPM} = 10.47 \frac{\text{radians}}{\text{sec}}$$

$K_\beta = 0$ (articulated blade)

Then:

$$\alpha = \frac{G}{\Omega^2} = \frac{3(32.2)}{(10.47)^2} \frac{(12.5)}{(25)} = 0.441$$

$$\delta = 1 + 0.08 + \frac{0}{(970.5)(10.47)^2} = 1.08$$

And the blade is just inside the stability boundary indicated in the figure ($\delta_{min} = 0.08$). Should the rotational speed be reduced to 95 RPM = 9.85 rad/sec, then the system would be unstable: $\alpha = 0.489$, $\delta = 108$, $\delta_{min} = 1.12$. The designer must add flapping restraint with spring rate:

$$K_\beta = I_b\ \Omega^2(.03) = (.03)(970.5)(9.95)^2 = 2882.5 \text{ ft-lb/rad}$$

or

$K_\beta = 50.3$ ft-lb/degree of flapping.

In existing systems the pendular instability is not a problem since there are no articulated wind turbines with large X_g and small hinge offset. Also, the damping effect of aerodynamics has been neglected here and the stabilizing flapping moments due to $\dot{\beta}$ which also arise from aerodynamics, are effective dissipators.

For the blade lag equation, we get:

$$\ddot{\zeta} + [\ \varepsilon_2\Omega^2 + \frac{K_\zeta}{I_b} G \cos\psi\ ]\ \zeta = 0 \qquad \text{(II-27)}$$

or

$$\frac{d^2\zeta}{d\psi^2} + [\ \varepsilon_2 + \frac{K_\zeta}{I_b\Omega^2} + \frac{G}{\Omega^2}\cos\psi\ ]\ \zeta = 0 \qquad \text{(II-28)}$$

Again we have the special form of Mathieu's equation. However, this time in the solution space of Figure 29, δ is changed:

$$\boxed{\begin{aligned} \delta &= \varepsilon_2 + \frac{K_\zeta}{I_b\Omega^2} \\ \alpha &= \frac{G}{\Omega^2} \end{aligned}} \qquad \text{Lead-Lag Pendular Stability Parameters} \qquad \text{(II-29)}$$

With ε_2 very small (and lag frequency very high) the pendular stability boundary changes rapidly with variation in δ. For instance at $\delta = 1/4$, the system is neutrally stable for any value of α (gravity). Likewise for all the x-intercepts:

$$\alpha_{critical} = 1/4,\ 1/2,\ 9/4,\ 4,\ 25/4,\ \ldots$$

or

$$(\alpha_{critical})^2 = n^2/4 \qquad \text{(II-30)}$$

Since K_ζ is much more variable than K_β (given a lag hinge) then critical values of K_ζ/I_b should be identified and avoided. Another important factor not yet discussed is the lack of aerodynamic damping to lead-lag motion. Historically, lag instabilities are more numerous and destructive in helicopters since aerodynamic damping is on the order of two to five percent of critical (flapping damping is usually close to critical).[13] This is because lag damping originates with only the small

changes of drag on a blade as the blade oscillates, while flap damping sees the much larger lift changes on the blade. Therefore it is critical for the designer to identify the lag frequency (or equivalent frequency) and to employ lag damping to avoid or attenuate the gravity induced instabilities defined by II-30.

2. Effects of yaw angular velocity. We will now consider the effect caused by a steady yaw angular velocity, q, about the tower axis, X'. Aerodynamic forces due to yaw rate are important also, and are derived in the next section; the present discussion deals only with the (gyroscopic) inertial effects on the blade.

The coordinate systems are given in Figure 6, and are reproduced here:

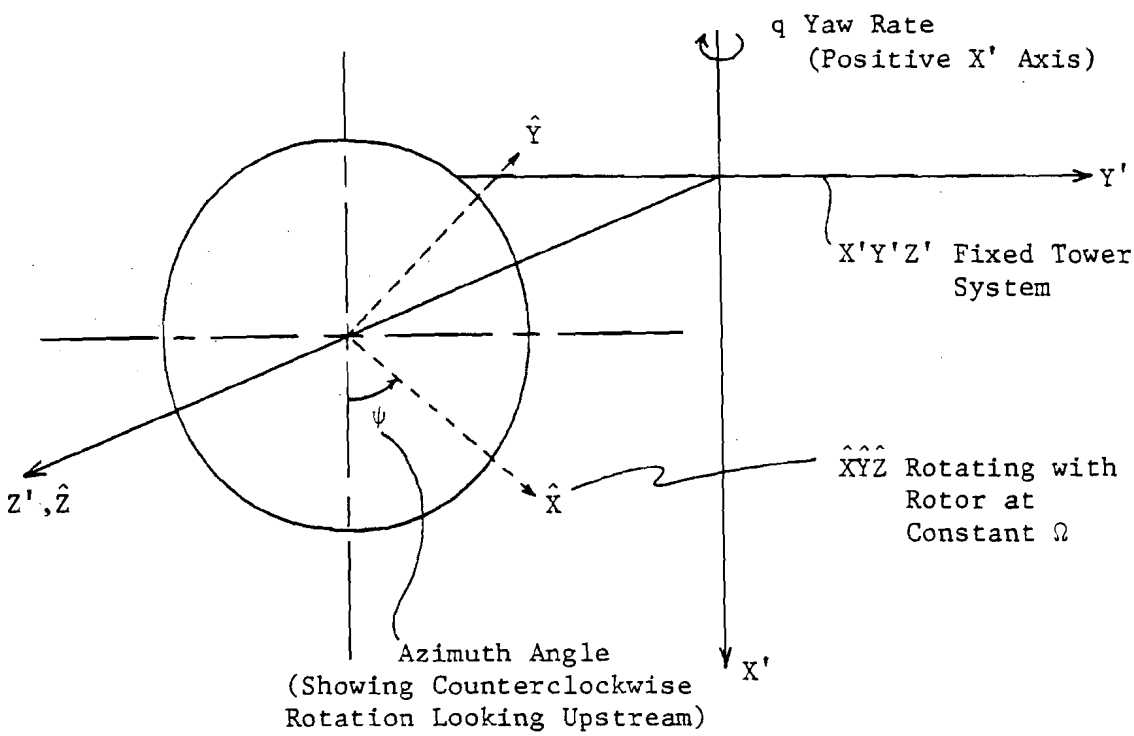

[Note: the xyz system is fixed to the blade, and is inclined to the $\hat{X}\hat{Y}\hat{Z}$ system by (Euler angle) $\phi = -\beta$; it is not shown.]

The only moments (or forces) are caused by accelerations due to rotation; if the yaw rate q is constant, the translations of the blades (i.e., their translations around the pole axis X') will not contribute to the gyroscopic forces. However, the translational velocities will affect the relative wind, hence the angles of attack, on the blade and will thus cause aerodynamic forces. For the moment, flapping angle β is ignored. We have in the xyz (or $\hat{X}\hat{Y}\hat{Z}$) system:

$I_x = I_f$ feathering mass moment of inertia

I_y = flapping mass moment of inertia

I_z = lead-lag mass moment of inertia (II-31)

The angular velocity components of the blade are:

$$\omega_x = \omega_{\hat{x}} = q \cos \psi$$

$$\omega_y = \omega_{\hat{y}} = -q \sin \psi$$

$$\omega_z = \omega_{\hat{z}} = \Omega \qquad \text{(II-32)}$$

Euler's dynamical equation appear in the following form if there are no axes of symmetry of the body, and the primary (xyz) axis system therefore is fixed to, and rotates with, the body.[10]

$$M_{xe} = I_x \frac{d\omega_x}{dt} - [\, I_y - I_z \,]\, \omega_y\, \omega_z$$

$$M_{ye} = I_y \frac{d\omega_y}{dt} - [\, I_z - I_x \,]\, \omega_z\, \omega_x \qquad \text{Euler's Dynamical Equations}$$

$$M_{ze} = I_z \frac{d\omega_z}{dt} - [\, I_x - I_y \,]\, \omega_x\, \omega_y \qquad \text{(II-33)}$$

where M_{xe}, M_{ye}, M_{ze} are the external moments in the torsional, (negative) flapping, and lead-lag directions, respectively. This gives:

$$M_{xe} = I_x \frac{d}{dt} [\, q \cos \psi \,] - [\, I_y - I_z \,] (-q \sin \psi) (\Omega)$$

$$M_{ye} = I_y \frac{d}{dt} [\, -q \sin \psi \,] - [\, I_z - I_x \,] (\Omega) (q \cos \psi)$$

$$M_{ze} = I_z \frac{d}{dt} [\Omega] - [\, I_x - I_y \,] (q \cos \psi) (-q \sin \psi)$$

or

$$\boxed{\begin{aligned} M_{xe} &= q\, \Omega \sin \psi \,[\, I_y - I_z - I_x \,] \\ M_{ye} &= -q\, \Omega \cos \psi \,[\, I_y + I_z - I_x \,] \\ M_{ze} &= q^2 \cos \psi \sin \psi \,[\, I_x - I_y \,] \end{aligned}} \qquad \text{(II-34)}$$

These are the external (gyroscopic) moments on the blade caused by a constant yaw rate q. These gyroscopic moments, as shown in Chapter V, give rise to a vibratory input to the hub and tower; for the case of a single or a two-bladed WTG, the forcing frequency is twice the rotational speed Ω. This is also the source of the "yawing roughness" often observed with high speed, two-bladed WTG's. A complete description of this is found in Section V-A.

Equation II-34 can be reduced to simpler form if approximations are made. The flapping and lead-lag mass moments of inertia are not strictly equal; they would be exactly so for an x-axis of symmetry. However, they are close enough to be considered equal (= I_b); also, the value of I_b is much greater than I_f, the feathering moment of inertia. Thus:

$$\begin{aligned} I_x &= I_f \\ I_y &\simeq I_b \\ I_z &\simeq I_b \end{aligned} \qquad \text{(II-35)}$$

The moments now become:

$$M_{xe} = -M_{\Theta} \simeq -q\ \Omega \sin \psi\ I_f$$

$$M_{ye} = -M_{\beta} \simeq -2q\ \Omega \cos \psi\ I_b$$

$$M_{ze} = M_{\zeta} \simeq -q^2 \cos \psi \sin \psi\ I_b \qquad \text{(II-36)}$$

Going back to the original angular velocity components, II-32, a flapping deflection β is now introduced:

$$\omega_x = \omega_{\hat{x}} \cos \beta + \omega_{\hat{z}} \sin \beta = q \cos \psi \cos \beta + \Omega \sin \beta$$

$$\omega_y = \omega_{\hat{y}} = -q \sin \psi$$

$$\omega_z = \omega_{\hat{z}} \cos \beta - \omega_{\hat{x}} \sin \beta = \Omega \cos \beta - q \cos \psi \sin \beta \qquad \text{(II-37)}$$

Going back through the Euler analysis again, the final values for gyroscopic moments are obtained,[9] after taking the small angle assumption on β, and neglecting terms containing q^2.

$$\boxed{\begin{aligned} M_{\theta} &= I_f\ q\ \Omega \sin \psi \\ M_{\beta} &= 2I_b\ q\ \Omega \cos \psi \\ M_{\zeta} &= 0 \end{aligned}} \qquad \text{(II-38)}$$

The blade equations of motion thus affected are the torsional and flapping equations:

$$\boxed{\ddot{\beta} + \Omega^2 \left[1 + \varepsilon + \frac{K_{\beta}}{I_b \Omega^2} + \frac{G}{\Omega^2} \cos \psi \right] \beta = -2q\ \Omega \cos \psi} \qquad \text{(II-39)}$$

Flapping Equation of Motion

$$\boxed{\ddot{\theta} + \Omega^2 \left[1 + \frac{K_{\theta}}{I_f \Omega^2} \right] \theta = -q\ \Omega \sin \psi} \qquad \text{(II-40)}$$

Torsion Equation of Motion

The effect of yaw rate on the blade is thus to introduce a periodic moment with frequency Ω, proportional to the yaw rate q, in both the

flapping and the torsional degrees of freedom. Since no damping exists in these (non-aerodynamic) equations, dynamic instability would result when the national frequency of motion is exactly Ω. This would be the case of a free hinge with no offset, and no gravity, for the flapping equation; and would also occur for free hinge in feathering (a purely academic example). Theoretically, then, a rotating blade with no hinge spring or offset, in the absence of gravity and aerodynamic forces, would be excited at its natural frequency in flapping with no chance of damping. Fortunately this case could not exist for an Earth-bound system. However, a spacecraft (which has been designed by the Jet Propulsion Laboratory, Pasadena, California) with a propulsion system consisting of long, flexible, slender blades rotating under the extremely diffuse pressure of the solar wind, does fit this description. The spacecraft will experience large flapping amplitudes if caused to yaw at a constant rate q.

D. Aerodynamic Forces and Moments

1. Derivation of lift function. To derive the aerodynamic forces, we isolate a blade element dr at radius r, and draw a vector diagram of the velocities perpendicular and tangential to the rotor plane; this is shown in Figure 30. [Note: here the effect of the hinge offset is neglected since it makes no difference in the aerodynamic force on the blade.] The axis of rotation is the $\hat{Z}$ axis, and the blade is inclined at flapping angle β.

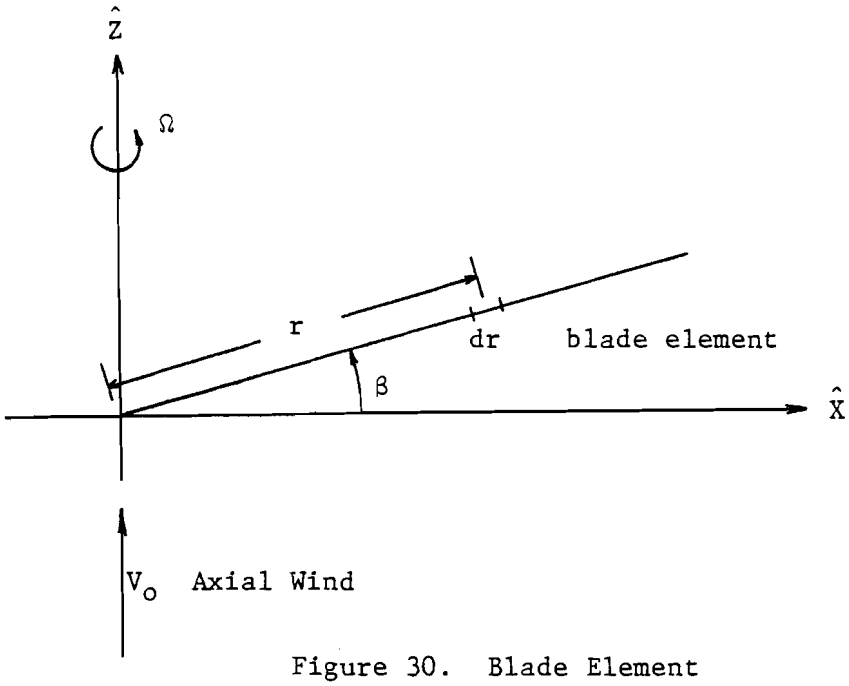

Figure 30. Blade Element

Looking at the blade element down the $\hat{X}$ axis:

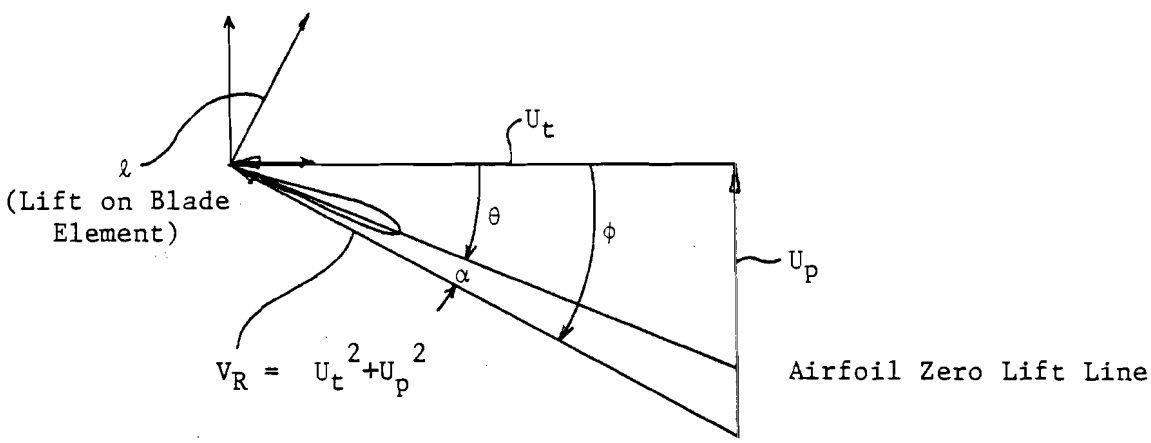

Figure 31. Blade Element Diagram

[Note: increasing θ decreases α, and also lift; this convention is exactly opposite helicopter and propeller literature which has θ increasing in the direction of increasing lift, or thrust.]

where:

U_p = velocity perpendicular to the rotor plane ($\hat{Z}$ direction)

U_t = velocity tangential to the blade element ($\hat{Y}$ direction)

(This velocity is primarily due to rotation Ωr)

$V_R = \sqrt{U_t^2 + U_p^2}$ = resultant total velocity at blade element

ϕ = blade element angle = $\tan^{-1} \frac{U_p}{U_t}$

θ = blade element pitch angle

α = blade element angle of attack

ℓ = lift force per unit span

lift is then:

$$\ell = \frac{1}{2} \rho \, C_{\ell_\alpha} \, c \, V_R^2 \, \alpha \qquad \text{(II-41)}$$

where:

ρ = air density

$C_{\ell_\alpha} = \frac{dC_\ell}{d\alpha}$ = slope of lift curve

c = chord

α = angle of attack

The drag, which would appear in the V_R direction, is discarded for now since it is small compared to lift. The significant aerodynamic perturbations will depend on changes in angle of attack α, so V_R will be allowed to remain constant. A further assumption is made, saying the magnitude of V_R is roughly the same as U_t. The effect of these assumptions will be to decrease the sensitivity of the aerodynamic forces to magnitude changes in velocity, and to increase the relative significance of angle of attack changes, which are retained.[14]

Assume $U_p << U_t$, this gives $V_R^2 \simeq U_t^2 \simeq (\Omega r)^2$.

Lift is now

$$\ell = \frac{1}{2} \rho C_{\ell_\alpha} c (\Omega r)^2 \alpha$$

And:

$$\alpha = \tan^{-1} (\phi - \theta) \simeq \phi - \theta = \frac{U_p}{U_t} - \theta$$

This gives:

$$\ell = \frac{1}{2} \rho C_{\ell_\alpha} c (\Omega r)^2 \left[\frac{U_p}{U_t} - \theta \right] \qquad \text{(II-42)}$$

We now assume linear twist along the blade, so total pitch is:

$$\theta = \theta_o [1 - r/R] + \theta_p$$

with

θ_o = blade twist

θ_p = pitch setting at tip

This is a good assumption for most wind turbine generators.

$$\boxed{\ell = \frac{1}{2} \rho C_{\ell_\alpha} c (\Omega r)^2 \left[\frac{U_p}{U_t} - \theta_o(1 - \frac{r}{R}) - \theta_p \right]} \qquad \text{(II-43)}$$

Lift Per Unit Length for a Linearly-Twisted WTG Blade at Constant Ω

The velocities can be written:

$U_t \simeq \Omega r$

U_p = axial velocity perpendicular to blade = $[V_o - v_i] \cos \beta - r\dot{\beta}$

where:

V_o = constant free stream (axial wind)

v_i = axial induced velocity (due to lift on the blade)

$r\dot{\beta}$ = contribution of flapping velocity to U_p

Writing λ_i = nondimensional induced velocity = $\frac{v_i}{\Omega R}$ [Note: this assumes the induced velocity is constant for $0 \leq r \leq R$, or over the entire rotor disc.] gives:

$$U_p = V_o \; [\; 1 - \lambda_i \;] \cos \beta - r\dot{\beta} \qquad \text{(II-44)}$$

$$U_t = \Omega r$$

2. Effects of crosswind and yaw rate on function. If the wind has a component parallel to the rotor plane (crosswind), U_o, the delta in the blade element velocity vector is shown in Figure 32. The crosswind is along the Y' axis.

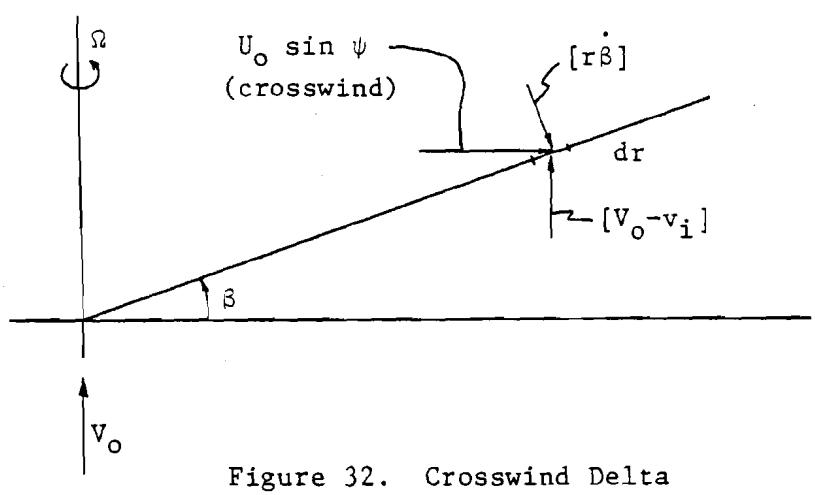

Figure 32. Crosswind Delta

The delta in U_p due to crosswind is: $\Delta U_p = - U_o \sin \beta \sin \psi$. The velocity perpendicular to the blade is now:

$$U_p = [\; V_o - v_i \;] \cos \beta - r\dot{\beta} - U_o \sin \beta \sin \psi$$

where ψ is the azimuthal angle, $\psi = 0$ being vertical. Likewise, the tangential velocity can be represented:

$$\Delta U_t = - U_o \cos \psi$$

A yaw motion (q rad/sec) about the X' (tower) axis likewise produces harmonic velocity deltas at the blade element:

$$\Delta U_p = - rq \sin \psi$$

$$\Delta U_t = - rq \cos \psi \sin \beta$$

Finally, the complete equations for U_p and U_t are:

$$U_p = [V_o - v_i] \cos \beta - r\dot{\beta} - U_o \sin \beta \sin \psi - rq \sin \psi$$

$$U_t = \Omega r - U_o \cos \psi - rq \cos \psi \sin \beta \qquad \text{(II-45)}$$

Assuming small β and retaining harmonic ψ:

$$\boxed{\begin{aligned} U_p &= [V_o - v_i] - r\dot{\beta} - [U_o \beta + rq] \sin \psi \\ U_t &= \Omega r - [U_o + rq \beta] \cos \psi \end{aligned}} \qquad \text{(II-46)}$$

Blade Element Velocities

3. Effect of wind shear on function. Wind shear is the variation with height of velocities U_o and V_o. Its effects are not considered important for small WTG's, on the order of 50' diameter or less. But in the interest of completeness, a method is developed for inclusion of wind shear effects in the U_p, U_t velocity components.[15]

Assuming U_o and V_o vary linearly with height across the rotor disc:

$$V_o = V [1 - rk_1 \cos \beta \cos \psi]$$

$$U_o = U [1 - rK_2 \cos \beta \cos \psi] \qquad \text{(II-47)}$$

where V, U are axial wind and crosswind at the rotor hub, and K_1, K_2 are gradients of U and V across rotor disc. To include wind shear in the aerodynamic force function, one has to include the above expressions in the already-derived expressions for U_p and U_t at the blade element.

4. Blade element lift function. Lift from before II-43 can be written:

$$\ell = \frac{1}{2} \rho \, C_{\ell_\alpha} \, c \, (\Omega r)^2 \left[\frac{U_p}{U_t} - \theta_o(1 - \frac{r}{R}) - \theta_p \right]$$

Our original assumption was that the inplane velocity, U_t, could be approximated by the local Ωr at each station. This assumption allows us to retain azimuthal variation in angle of attack in the above expression, but keeping the velocity terms constant with no azimuthal variation. Hence:

$$\text{Angle of attack} = \alpha = \left[\frac{U_p}{U_t} - \theta_o(1 - \frac{r}{R} + \frac{\theta_p}{\theta_o}) \right] = \frac{1}{U_t} \left[U_p - \theta_o \, U_t(1 - \frac{r}{R} \frac{\theta_p}{\theta_o}) \right]$$

$$\approx \frac{1}{\Omega r} \left[U_p - \theta_o \, \Omega r \, (1 - \frac{r}{R} + \frac{\theta_p}{\theta_o}) \right] \qquad \text{(II-48)}$$

[Note: the effect of yaw rate and crosswind on the tangential velocity is averaged out by assumption. But, the effect of yaw rate and crosswind on α is retained.]

The values of U_p and U_t were found in Section II-D-2; substituting in the lift equation gives:

$$\ell = \frac{1}{2} \rho \, C_{\ell_\alpha} \, c \, \Omega r \left[U_p - \Omega r \, \theta_o(1 - \frac{r}{R} + \frac{\theta_p}{\theta_o}) \right] \qquad \text{(II-49)}$$

$$\ell = \frac{1}{2} \gamma I_b \frac{\Omega r}{R^4} \left[V_o - v_i - r\beta - (rq - U_o\beta) \sin \psi - r\Omega \, \theta_o(1 + \frac{\theta_p}{\theta_o}) + \frac{r^2}{R} \theta_o \right]$$

(II-50)

or nondimensionally:

$$\boxed{\ell = \frac{1}{2} \gamma \, I_b \, \Omega^2 (\frac{1}{R^2}) \left[\mu_o \eta - \lambda_i \eta - \eta^2 \beta' - (\eta \bar{q} + \bar{U}_o \beta) \, \eta \sin \psi - \eta^2 \theta_o(1 + \frac{\theta_p}{\theta_o}) + \eta^3 \theta_o \right]} \qquad \text{(II-51)}$$

Lift on Blade Element

where non-dimensional quantities are:

$$\mu_o = \frac{V_o}{\Omega R} = \frac{1}{\text{tip speed ratio}}$$

$$\lambda_i = \frac{v_i}{R} = \text{non-dimensional induced velocity (assumed constant over disc)}$$

$$\eta = \frac{r}{R} = \text{span station}$$

$$\bar{q} = \frac{q}{\Omega} = \text{non-dimensional yaw rate}$$

$$\bar{U}_o = \frac{U_o}{\Omega R} = \text{non-dimensional crossflow}$$

$$\gamma = \frac{\rho C_{\ell_\alpha} c R^4}{I_b} = \text{Lock Number = ratio of aerodynamic forces to inertial forces}$$

$$\beta' = \frac{d\beta}{d\psi} = \frac{\dot{\beta}}{\Omega}$$

5. Aerodynamic forces and moments. With the derived expression for lift (II-50, 51), the aerodynamic forces in the axial (flapping) direction and the inplane (lead-lag) direction can be found by integration. Likewise the moments about these two hinges and the blade tension can be found.

The force component in the axial ($\hat{Z}$) direction is $\ell \cos \phi \cos \beta$. In the inplane (lead-lag) direction the force is $\ell \sin \phi$, which produces the shaft torque and inplane moments at the hub.

Oscillatory components introduced in the velocities and angles of attack will result in oscillatory thrust, moments and shaft torque. This derivation has suppressed variation in the velocities in the interest of simplicity, but has retained terms that affect angle of attack. This approach seems justifiable for frequency information and stability calculations, but less suitable for detailed studies of

the lift distribution and rotor performance.[16] In parametric performance studies, a more exact approach, which simulates the actual velocities at each span station, is used. This practical approach is called strip theory and the forces and moments derived from such a detailed computer program could also be used in these dynamic studies, by employing the familiar quasi-steady force assumption.[17] However, the frequency information and overall dynamic behavior is retained by the present, more "physical" approach. A strip theory has been written for WTG's and is used for detailed blade loading and performance tradeoffs based on blade geometry and flight condition (Appendix I).

The hub shear in the flapping direction (vertical shear at the hinge) is given by:

$$S_\beta = \int_0^R \ell \cos\phi \cos\beta \, dr \simeq \int_0^1 \ell R \, d\eta \qquad \text{(II-52)}$$

The hub shear in the lead-lag direction is:

$$S_\zeta = \int_0^R \ell \sin\phi \, dr \simeq \int_0^1 \ell R \frac{U_p}{U_t} \, d\eta \qquad \text{(II-53)}$$

The flapping moment due to aerodynamics is:

$$M_{\beta \text{ aerodynamic}} = \int_0^R \ell \cos\phi \cos\beta \, r \, dr \simeq \int_0^1 \ell R^2 \eta \, d\eta \qquad \text{(II-54)}$$

And the lead-lag moment is:

$$M_{\zeta \text{ aerodynamic}} = \int_0^R \ell \sin\phi \, r dr \simeq \int_0^1 \ell R^2 \frac{U_p}{U_t} \eta \, d\eta \qquad \text{(II-55)}$$

After substitution and manipulation the final aerodynamic hinge forces and moments are:

$$\boxed{S_\beta = \frac{1}{2}\gamma I_b \frac{\Omega^2}{R} \frac{\mu_o}{2} - \frac{\lambda_i}{2} - \frac{\beta'}{3} - \sin\psi \left(\frac{\bar{q}}{3} + \frac{\bar{U}_o\beta}{2}\right) - \frac{\theta_p}{3} - \frac{\theta_o}{12}} \qquad \text{(II-56)}$$

Vertical Aerodynamic Shear

$$\boxed{M_{\beta aero} = \frac{1}{2}\gamma I_b \Omega^2 \frac{\mu_o}{3} - \frac{\lambda_i}{3} - \frac{\beta'}{4} - \sin\psi \left(\frac{\bar{q}}{4} + \frac{\bar{U}_o\beta}{3}\right) - \frac{\theta_p}{4} - \frac{\theta_o}{20}} \qquad \text{(II-57)}$$

Aerodynamic Flapping Moment

$$\boxed{\begin{aligned} S_\zeta = \frac{1}{2}\gamma I_b \frac{\Omega^2}{R} & (\lambda_i - \mu_o)(\lambda_i - \mu_o + \beta') \\ & + 2\sin\psi \left[\frac{\bar{q}}{2}\left(\lambda_i + \frac{2}{3}\beta' - \mu_o + \frac{\theta_p}{3} + \frac{\theta_o}{12}\right) \right. \\ & \left. + \bar{U}_o\beta\left(\lambda_i + \frac{\beta'}{2} - \mu_o + \frac{\theta_p}{4} + \frac{\theta_o}{12}\right) \right] \\ & + \frac{\theta_o}{6}\left[\lambda_i + \frac{\beta'}{2} - \mu_o\right] + \frac{\theta_p}{2}\left[\lambda_i + \frac{2\beta'}{3} - \mu_o\right] \end{aligned}} \qquad \text{(II-58)}$$

Inplane Aerodynamic Shear

$$\boxed{\begin{aligned} M_{\zeta aero} = \frac{1}{4}\gamma I_b \Omega^2 & (\lambda_i - \mu_o)(\lambda_i - \mu_o + \frac{4}{3}\beta') \\ & + 4\sin\psi \left[\frac{\bar{q}}{3}\left(\lambda_i + \frac{3\beta'}{4} - \mu_o + \frac{3}{8}\theta_p + \frac{3}{40}\theta_o\right) \right. \\ & \left. + \frac{\bar{U}_o\beta}{2}\left(\lambda_i + \frac{2\beta'}{3} - \mu_o + \frac{\theta_p}{3} + \frac{\theta_o}{12}\right) \right] \\ & + \frac{\theta_o}{6}\left[\lambda_i + \frac{3\beta'}{5} - \mu_o\right] + \frac{2\theta_p}{3}\left[\lambda_i + \frac{3\beta'}{4} - \mu_o\right] \end{aligned}} \qquad \text{(II-59)}$$

Aerodynamic Lead-Lag Moment

CHAPTER III

BLADE MOTIONS/DEFLECTION SOLUTIONS

In Chapter II, the isolated blade equations of motion in flapping, lead-lag, and torsion, were developed and discussed. The inertial effects discussed did not include aerodynamic forces, which are complex. This section will use the aerodynamic forcing function derived in Section II-D to complete the flapping and lead-lag equations, and then the blade motions can be determined. A similar derivation of blade motions for wind turbines can be found in the excellent paper by Ormiston (Reference 15).

In order to make use of varying flexibilities and stiffnesses in rotating systems, especially rotors, designers must be able to predict the excursions caused by forcing functions. In the case of wind turbine generators (WTG's), the maximum blade tip deflections often size the supporting tower guy wires and the yaw arm to the rotor plane. There is a clear cost trade off between increased yaw arm and tower stiffness, and increased blade stiffness to avoid blade-tower interaction. Additionally, some rotor loads are dependent on coupled deflections and velocities; these loads are among the most damaging, fatigue-wise, since they are unavoidable, periodic, and difficult to predict.

A. Flapping and Lead-Lag Equations of Motion

The complete flapping and lead-lag equations of motion are obtained from II-4 and II-9 by including the aerodynamic hinge moments in the

summation:

$$\boxed{\frac{\ddot{\beta}}{\Omega^2} + \left[1 + \varepsilon + \frac{G}{\Omega^2} \cos\psi + \frac{K_\beta}{I_b\ \Omega^2} \right] \beta = \frac{M_{\beta_{aero}}}{I_b\ \Omega^2} - 2\ \bar{q} \cos\psi} \qquad \text{(III-I)}$$

Flapping Equation

$$\boxed{\frac{\ddot{\zeta}}{\Omega^2} + \left[\varepsilon_2 + \frac{G}{\Omega^2} \cos\psi + \frac{K_\zeta}{I_b\ \Omega^2} \right] \zeta = \frac{2\dot{\beta}\beta}{\Omega} - \frac{G}{\Omega^2} \sin\psi + \frac{M_{\beta_{aero}}}{I_b\ \Omega^2}}$$

Lead-Lag Equation (III-2)

where the aerodynamic hinge moments are:

$$\frac{M_{\beta_{aero}}}{I_b\ \Omega^2} = \frac{\gamma}{2} \left[\frac{\mu o}{3} - \frac{\lambda i}{3} - \frac{1}{4}\frac{d\beta}{d\psi} - \sin\psi \left(\frac{\bar{q}}{4} + \frac{\bar{U}_o\beta}{3}\right) - \frac{\theta_o}{20} - \frac{\theta_p}{4} \right] \qquad \text{(III-3)}$$

$$\begin{aligned}\frac{M_{\zeta_{aero}}}{I_b\ \Omega^2} = \frac{\gamma}{4} & (\lambda_i - \mu_o) \left[\lambda_i + \frac{4}{3}\frac{d\beta}{d\psi} - \mu_o \right] \\ & + 4 \sin\psi \left[\frac{\bar{q}}{3} \left(\lambda_i + \frac{3}{4}\frac{d\beta}{d\psi} - \mu_o + \frac{3}{8}\theta_p + \frac{3}{40}\theta_o\right) \right. \\ & + \frac{\bar{U}_o\beta}{2} \left(\lambda_i + \frac{2}{3}\frac{d\beta}{d\psi} - \mu_o + \frac{\theta_p}{3} + \frac{\theta_o}{12}\right) \Big] \\ & + \frac{\theta_o}{6} \left[\lambda_i + \frac{3}{5}\frac{d\beta}{d\psi} - \mu_o \right] + \frac{2\theta_p}{3} \left[\lambda_i + \frac{3}{4}\frac{d\beta}{d\psi} - \mu_o \right]\end{aligned} \qquad \text{(III-4)}$$

The time coordinate is changed to azimuthal coordinate ψ:

$$\frac{d}{dt} = \frac{d}{d\psi}\frac{d\psi}{dt} = \Omega \frac{d}{d\psi}$$

Or:

$$\ddot{\beta} = \Omega^2 \frac{d^2\beta}{d\psi^2} = \Omega^2\ \beta''$$

$$\dot{\beta} = \Omega \frac{d\beta}{d\psi} = \Omega\ \beta' \qquad \text{(III-5)}$$

The flapping equation becomes:

$$\beta'' + \left[1 + \varepsilon + \frac{G}{\Omega^2} \cos \psi + \frac{K_\beta}{I_b \Omega^2} \right] \beta = \frac{M_{\beta aero}}{I_b \ \Omega^2} - 2 \ \overline{q} \cos \psi$$

Collecting terms, we get the complete equation of motion including aerodynamic forces:

$$\boxed{\begin{aligned} &\beta'' + \frac{\gamma}{8} \beta' + \left[1 + \varepsilon + \frac{G}{\Omega^2} \cos \psi + \frac{K_\beta}{I_b \ \Omega^2} + \frac{\gamma}{6} \overline{U}_o \sin \psi \right] \beta \\ &\quad = \frac{\gamma}{2} \left[\frac{\mu_o}{3} - \frac{\lambda_i}{3} - \frac{\overline{q}}{4} \sin \psi - \frac{\theta_o}{20} - \frac{\theta_p}{4} \right] - 2 \ \overline{q} \cos \psi \end{aligned}} \qquad \text{(III-6)}$$

Flapping Equation of Motion

Likewise the lead-lag equation is:

$$\zeta'' + \left[\varepsilon_2 + \frac{G}{\Omega^2} \cos \psi + \frac{K_\zeta}{I_b \ \Omega^2} \right] \zeta = 2\beta\beta' - \frac{G}{\Omega^2} \sin \psi + \frac{M_\zeta}{I_b \ \Omega^2}$$

Collecting terms, we get the complete equation of motion including aerodynamic forces:

$$\boxed{\begin{aligned} &\zeta'' + \left[\varepsilon_2 + \frac{G}{\Omega^2} \cos \psi + \frac{K_\zeta}{I_b \ \Omega^2} \right] \zeta - \ 2\beta + \gamma \left[\frac{1}{3}(\lambda_i - \mu_o) \right. \\ &+ \sin \psi \left(\frac{\overline{q}}{4} + \frac{\overline{U}_o \beta}{3} \right) + \frac{\theta_p}{8} + \left. \frac{\theta_o}{40} \right] \quad \beta' = - \frac{G}{\Omega^2} \sin \psi \\ &+ \frac{\gamma}{4} \ (\lambda_i - \mu_o) \left[\lambda_i - \mu_o + \frac{\theta_o}{6} + \frac{2\theta_p}{3} \right] \\ &+ \sin \psi \left(\lambda_i - \mu_o + \frac{\theta_p}{3} + \frac{\theta_o}{15} \right) \left[\frac{4}{3} \overline{q} + 2 \ \overline{U}_o \beta \right] \end{aligned}} \qquad \text{(III-7)}$$

Lead-Lag Equation of Motion

B. Harmonic Series Solution

Since it has been straightforward to express the differential equations in the azimuthal domain, it is logical to assume a Fourier

series solution for β and ζ, and solve for the coefficients, viz:

$$\beta = \beta_o + \beta_{1c} \cos \psi + \beta_{1s} \sin \psi + \beta_{2c} \cos 2 \psi + \beta_{2s} \sin 2 \psi + \ldots \qquad \text{(III-8)}$$

In this development, the blade flexibilities have been reduced to single fundamental mode vibration; only the fundamental bending modes, in flapping and in lead-lag, have been used in the dynamic model. A blade oscillating in flapping, then, will always trace a circular tip path; this locus of points defines the tip path plane. The terms in the above series representation of β then take on a physical meaning: the first term is the constant coning angle resulting from axisymmetric equilibrium, and the next two terms represent tilting of this tip path plane vertically forward and yawing to the left (β_{1c} and β_{1s}, respectively). The next higher order terms would represent the higher modes of vibration of the blades, for which we have made no provision. In the case of a rigid blade, freely hinged at the rotor axis, the first three terms completely and uniquely describe the transient and equilibrium motion of the blade.[9] In the case of blades with higher stiffness, these terms represent the most significant motions experienced by the blade, and constitute a good engineering approximation.[14] When calculating bending moments, however, the approximation is less valid, and the higher order terms are usually included in standard helicopter practice.

Hence the series is truncated to three terms:

$$\beta = \beta_o + \beta_{1c} \cos \psi + \beta_{1s} \sin \psi$$

and

$$\beta' = - \beta_{1c} \sin \psi + \beta_{1s} \cos \psi$$

$$\beta'' = -\beta_{1c}\cos\psi - \beta_{1s}\sin\psi \qquad \text{(III-9)}$$

The solution is found by substituting the above expressions into the equation of motion. The resulting equation will contain a system of three linear equations, obtained by simply equating the harmonic coefficients to zero. Thus:

$$f_1(\beta_o, \beta_{1c}, \beta_{1s})\cos\psi + f_2(\beta_o, \beta_{1c}, \beta_{1s})\sin\psi$$

$$+ f_3(\beta_o, \beta_{1c}, \beta_{1s})\cos(0)\psi = 0$$

Therefore:

$$f_1(\beta_o, \beta_{1c}, \beta_{1s}) = 0$$

$$f_2(\beta_o, \beta_{1c}, \beta_{1s}) = 0$$

$$f_3(\beta_o, \beta_{1c}, \beta_{1s}) = 0 \qquad \text{(III-10)}$$

And the Fourier coefficients can be found from the resulting system of linear equations:

$$[A_{i_j}]\begin{Bmatrix}\beta_o\\ \beta_{1c}\\ \beta_{1s}\end{Bmatrix} = \begin{Bmatrix}B_{i_j}\end{Bmatrix} \qquad \text{(III-11)}$$

C. Flapping Behavior

1. Flapping dynamics. The flapping equation is:

$$\boxed{\begin{aligned}&\beta'' + \frac{\gamma}{8}\beta' + [\,K + 2B\cos\psi + \frac{\gamma}{6}\overline{U}_o\sin\psi\,]\,\beta\\ &= \frac{\gamma}{2}[\,A - \frac{\overline{q}}{4}\sin\psi\,] - 2\,\overline{q}\cos\psi\end{aligned}} \qquad \text{(III-12)}$$

where:

$$K = [\,1 + \varepsilon + \frac{K_\beta}{I_b\,\Omega^2}\,] = (\frac{\omega_\beta}{\Omega})^2$$

$$A = [\,\frac{\mu_o}{3} - \frac{\lambda_i}{3} - \frac{\theta_o}{20} - \frac{\theta_p}{4}\,]\,; \qquad B = \frac{G}{2\Omega^2}$$

This describes a damped oscillator, with a steady and periodic forcing function. Recalling the inertial results of Section II-B, it can be seen that aerodynamic terms will produce all the flap damping, and will modify the free natural frequency.

The damping ratio is always positive, and is given by (where ω_o is the natural frequency)

$$\text{flapping damping ratio} = \frac{\gamma}{16}\frac{1}{(\omega/\Omega)} \qquad \text{(III-13)}$$

Flexible cantilever rotors and articulated rotors have flapping natural frequencies close to Ω; stiffer rotors have frequencies a factor or two or three higher. Thus, the damping will range from $\frac{\gamma}{16}$ (for fully articulated) to about $\frac{\gamma}{48}$ (for a very stiff blade). Typical values of γ are 5-10, giving a range of damping of 0.5 to 0.16.[18] These are reasonably high values; hence it would not usually be necessary for the designer to add damping to the flapping degree of freedom, unless a resonance was present. If a rotor needed to have critical damping, the necessary values of γ could be calculated from the following expression, derived from fundamental free oscillator theory:

$$\left(\frac{\gamma_{critical}}{8}\right) = 2\Omega\sqrt{K} = 2\Omega\left(\frac{\omega_\beta}{\Omega}\right) \qquad \text{(III-14)}$$

The natural frequency in flapping is affected by aerodynamic forces due to crosswind, $\overline{U}_o$. This input will change the instability poles of the Mathieu's equation solution; that is, in the presence of a crosswind, the pendular instabilities in flapping will be altered from their initial values (see Section II-C). The new values of K and γ necessary to avoid Mathieu instability could be calculated from III-12. In practice this would not be necessary in view of the large damping and

the small magnitudes of the coefficients of (cos ψ) and (sin ψ). [Note: a much more significant case for pendular instability exists for lead-lag motion, where damping is practically nil and the K term is much smaller. See Section D.]

It is also interesting to note the right hand side of the equation. The steady term:

$$\frac{\gamma}{2}\left[\frac{\mu_o}{3} - \frac{\lambda_i}{3} - \frac{\theta_o}{20} - \frac{\theta_p}{4}\right] \qquad \text{(III-15)}$$

gives rise to the steady-state coning angle caused by (axisymmetric) aerodynamic thrust (Note: as shown in detail in the next section, the magnitude of the coning can be obtained by dividing III-15 by the actual ω^2, obtained from the left hand side).

The other term is:

$$-\bar{q}\left[\frac{\gamma}{8}\sin\psi + 2\cos\psi\right]$$

The yaw rate, $\bar{q}$, appears as a periodic forcing function. The term in the brackets denotes a function with frequency Ω, and amplitude $\sqrt{\gamma^2/64 + 4}$. This function lags the blade by the phase angle $-\tan^{-1}(\gamma/16)$. This term is significant (as we will see in Section 5). The purely inertial effect of gyroscopic moment is the cosine component, and the aerodynamic effect is the sine component. A blade with high mass and low C_ℓ (thus low γ) will be dominated by an inertial gyroscopic response with little phase lag. A high activity blade (high γ) will have a much larger "gyroscopic" response, containing both inertial and aerodynamic components, and will lag the blade motion by roughly 45°.

2. Flapping motion. Using, as in Section III-B, the first three terms of a harmonic series, substitution is made in the flapping equation,

III-12. Equating coefficients to zero:

$$K\beta_o + B\,\beta_{1c} + \frac{\gamma}{12}\,\overline{U}_o\,\beta_{1s} = \frac{\gamma}{2}\,A$$

$$\beta_{1c}\,(K-1) + 2B\,\beta_o + \frac{\gamma}{8}\,\beta_{1s} = -\,2\,\overline{q}$$

$$\beta_{1s}\,(K-1) + \frac{\gamma}{6}\,\overline{U}_o\,\beta_o - \frac{\gamma}{8}\,\beta_{1c} = -\,\frac{\gamma}{8}\,\overline{q} \qquad \text{(III-16)}$$

or:

$$\boxed{\begin{bmatrix} K & B & \frac{\gamma}{12}\,\overline{U}_o \\ 2B & (K-1) & \frac{\gamma}{8} \\ \frac{\gamma}{b}\,\overline{U}_o & -\,\frac{\gamma}{8} & (K-1) \end{bmatrix} \begin{Bmatrix} \beta_o \\ \beta_{1c} \\ \beta_{1s} \end{Bmatrix} = \begin{Bmatrix} \frac{\gamma}{2}\,A \\ -\,2\,\overline{q} \\ -\,\frac{\gamma}{8}\,\overline{q} \end{Bmatrix}} \qquad \text{(III-17)}$$

Flapping Matrix

where:

$$K = \left[\,1 + \varepsilon + \frac{K_\beta}{I_b\,\Omega^2}\,\right] = \left(\frac{\omega_\beta}{\Omega}\right)^2 = \text{(square of) "inertial" natural frequency}$$

$$A = \left[\,\frac{\mu_o}{3} - \frac{\lambda_i}{3} - \frac{\theta_o}{20} - \frac{\theta_p}{4}\,\right] = \text{axisymmetric flow term}$$

$$B = \frac{G}{2\Omega^2} = \frac{g\,M_b\,X_g\,R}{2I_b\,\Omega^2} = \text{gravity term}$$

$$\gamma = \frac{\rho\,C_{\ell_\alpha}\,c\,R^4}{I_b} = \text{Lock Number} = \text{ratio of aerodynamic to inertial forces}$$

$$\overline{U}_o = \frac{U_o}{\Omega R} = \text{non-dimensional cross flow}$$

$$\overline{q} = \frac{q}{\Omega} = \text{non-dimensional yaw rate}$$

Since the blade has been assumed to be uniform for dynamic simulitude, the gravity term can be simplified, using the hinge offset e:

$$G = \frac{g\,M_b\,X_g\,R}{I_b} = \left(\frac{\varepsilon}{e}\right)\frac{g}{R} = \frac{3g}{2R(1-e)} \qquad \text{(III-18)}$$

A good approach to the solution of III-17 is to assume a "design range" of values of variables under consideration, and plug in and solve the matrix for each value of q, U_o and G of interest.[15] By computer this process could be mechanized, giving plots of flapping coefficients ($\beta_o, \beta_{1c}, \beta_{1s}$) versus abscissas of yaw rate, crosswind, etc., for every combination of blade values of interest (I_b, e, $\frac{dC_\ell}{d\alpha}$, θ_o, θ_p, etc.). In preliminary design it is much more valuable to investigate the general stability -- the "physical" characteristics -- of III-17 first, and then to solve for detailed behavior for the narrow variable ranges that come out. It remains a common practice in industry to blindly reduce systems like III-17 to the parametric graph form to evaluate stability; it is often more rewarding and interesting to use the present approach. In this development analytical complication has been suppressed and approximations have been made specifically for this purpose; if the parametric simulation approach were being used, the equations could (and should) be more complicated and exact, and include more terms in the assumed harmonic series.

For the simplest case, where gravity, crosswind and yaw rate are zero, with no hinge offset or hinge spring (i.e., articulated at the root, simple axisymmetric flow), the matrix is:

$$\begin{bmatrix} 1 & 0 & 0 \\ 0 & 0 & \frac{\gamma}{8} \\ 0 & -\frac{\gamma}{8} & 0 \end{bmatrix} \begin{Bmatrix} \beta_o \\ \beta_{1c} \\ \beta_{1s} \end{Bmatrix} = \begin{Bmatrix} \frac{\gamma}{2} A \\ 0 \\ 0 \end{Bmatrix} \qquad \text{(III-19)}$$

which gives the solution:

$$\boxed{\begin{aligned} \beta_o &= \frac{\gamma}{2} A \\ \beta_{1s} &= \beta_{1c} = 0 \end{aligned}}$$ Simple Axisymmetric Flow Solution (III-20)

In this case β_o is the aerodynamic coning, the equilibirum between aerodynamic thrust and centrifugal force.

With hinge spring and offset, the solution is:

$$\boxed{\begin{aligned} \beta_o &= \left(\frac{1}{K}\right) \frac{\gamma}{2} A \\ \beta_{1s} &= \beta_{1c} = 0 \end{aligned}} \qquad \text{(III-21)}$$

where $K = \left(1 + \varepsilon + \dfrac{K_\beta}{I_b\ \Omega^2}\right) = \left(\dfrac{\omega_\beta}{\Omega}\right)^2$

And as one would expect, the coning angle is modified by the stiffness, or the ratio of "inertial" natural frequency in flapping to rotational speed.

3. <u>Effect of gravity on flapping.</u> Adding the gravity terms, the equations become:

$$\begin{bmatrix} K & B & 0 \\ 2B & (K-1) & \frac{\gamma}{8} \\ 0 & -\frac{\gamma}{8} & (K-1) \end{bmatrix} \begin{Bmatrix} \beta_o \\ \beta_{1c} \\ \beta_{1s} \end{Bmatrix} = \begin{Bmatrix} \frac{\gamma}{2} A \\ 0 \\ 0 \end{Bmatrix} \qquad \text{(III-22)}$$

The determinant of the coefficients is called Δ:

$$\Delta = |\text{coefficients}| = K\ [\ (K-1)^2 + \left(\frac{\gamma}{8}\right)^2\ ] - 2B^2\ (K-1) \qquad \text{(III-23)}$$

Then:

$$\beta_o = \frac{1}{\Delta} \begin{vmatrix} \frac{\gamma A}{2} & B & 0 \\ 0 & (K-1) & \frac{\gamma}{8} \\ 0 & -\frac{\gamma}{8} & (K-1) \end{vmatrix} = \frac{}{\Delta} \left[\frac{\gamma A}{2} (K-1)^2 + (\frac{\gamma}{8})^2 \right]$$

$$\beta_{1c} = \frac{1}{\Delta} \begin{vmatrix} K & \frac{\gamma A}{2} & 0 \\ 2B & 0 & \frac{\gamma}{8} \\ 0 & 0 & (K-1) \end{vmatrix} = -\frac{1}{\Delta} \left[\gamma\ B(K-1)A \right]$$

$$\beta_{1s} = \frac{1}{\Delta} \begin{vmatrix} K & B & \frac{\gamma A}{2} \\ 2B & (K-1) & 0 \\ 0 & -\frac{\gamma}{8} & 0 \end{vmatrix} = -\frac{1}{\Delta} \left[(\frac{\gamma}{2})^2 \frac{B}{2} A \right]$$

Then the final solution is:

$$\beta_o = \frac{\gamma\ A}{2} \left\{ \frac{\left[(K-1)^2 - (\frac{\gamma}{8})^2 \right]}{K \left[(K-1)^2 - (\frac{\gamma}{8})^2 \right] - 2B^2(K-1)} \right\} \qquad \text{(III-24)}$$

$$\beta_{1c} = - \left\{ \frac{\gamma\ B\ (K-1)\ A}{K \left[(K-1)^2 - (\frac{\gamma}{8})^2 \right] - 2B^2(K-1)} \right\} \qquad \text{(III-25)}$$

$$\beta_{1s} = - \left\{ \frac{(\gamma^2/8)\ B\ A}{K \left[(K-1)^2 - (\frac{\gamma}{8})^2 \right] - 2B^2(K-1)} \right\} \qquad \text{(III-26)}$$

Flapping Due to Gravity and Axisymmetric Flow

As a first check, with B = 0 (gravity = 0) these reduce to the simple coning result from before. Gravity first causes a small increase in β_o

by decreasing the denominator. It also gives rise to a tilting of the rotor disc, both vertically backward (β_{1c}) and yawing to the right (β_{1s}). The tilting and yawing are related:

$$\beta_{1s} = \frac{\gamma}{8(K-1)} \beta_{1c} \qquad \text{(III-27)}$$

This expresses the effect of hinge spring on the proportion of tilt between β_{1c} and β_{1s}. That is, for a very stiff cantilever, (K-1) is on the order of 10, giving $\beta_{1s} \approx 10\% \ \beta_{1c}$; this means the rotor will experience mostly vertical tilting and very little yawing. If the blade is soft in flapping, (K-1) is on the order of 0.5 (or even lower for articulated blade), giving $\beta_{1s} \approx 200\% \ \beta_{1c}$; this would yield mostly yaw tilting and much less vertical tilt.

Another effect is the Lock number term, $\gamma/8$. If the blade has a low mass and a high design C_ℓ, it has a high γ ($\approx$ 10-15 for helicopters); if it has high mass and low radius, it has a low γ ($\approx$ 4.5 for original Jacob's blade).[19] A high γ blade will have a tendency to yaw in response to gravity excitation, while a low γ blade will tilt vertically (thus causing tower vibration). A classical way of looking at this describes the phase lag of a blade's response to a forcing input. Actually the phase is dependent on both the γ term and the K term, but in general, this phase is around 90° for hinged blades, and it decreases with increasing flapping stiffness (cantilevered blades). For each specific case of interest, Equations III-24, 25, 26 should be solved and investigated.

The flapping equations show the pendular instability of the Mathieu's equation in the denominator. The blade is unstable in

flapping (β_o increases without limit) for:

$$K\left[(K-1)^2 - \left(\frac{\gamma}{8}\right)^2\right] - 2B^2(K-1) = 0$$

or

$$\boxed{K^3 - 2K^2 + K\left[1 - \left(\frac{\gamma}{8}\right)^2 - 2B\right] + 2B^2 = 0} \qquad \text{(III-28)}$$

Taking typical values for a numerical example we have:

$\gamma = 8$

$e = 0.15$

$R = 25'$

and $G = \dfrac{3g}{2R(1-e)} = 2.273$

Since $B = \dfrac{G}{2\Omega^2}$, we substitute the above values in III-28 and solve for a pair of values, K and Ω; these will constitute an unstable point. We find:

$$K_{critical} = 2.1$$

$$\Omega_{critical} = 1.593\ \frac{rad}{sec} = 15.21\ RPM \qquad \text{(III-29)}$$

The equation is solved, and the system is unstable in flapping. This is a reasonable value of K; however, it is unlikely a 25' rotor would be operated at a frequency of 1.593, a more likely value being 7.5 - 12. Investigating further, for values of $K < 2.1$ the roots of III-28 are imaginary and the system is therefore stable.

The designer thus has the task of solving III-28 for the set of structural parameters of interest in order to determine the (K, Ω) critical point.

Going back to the expressions for β_o, β_{1c}, β_{1s} (III-24, 25, 26), it can also be seen that flapping angle is directly proportional to

the aerodynamic term, A:

$$A = [\ \frac{\mu_o}{3} - \frac{\lambda_i}{3} - \frac{\theta_o}{20} - \frac{\theta_p}{4}\ ] \qquad \text{(III-30)}$$

As the tip speed ratio $(\frac{\Omega R}{V_o})$ increases, μ_o decreases and coning decreases. Likewise, as θ_p is reduced (increasing C_ℓ and thrust) flapping is increased.

4. Effect of crosswind on flapping. Including the crosswind $(\overline{U}_o)$ terms, the system becomes:

$$\begin{bmatrix} K & B & \frac{\gamma}{12}\overline{U}_o \\ 2B & (K-1) & \frac{\gamma}{8} \\ \frac{\gamma}{6}\overline{U}_o & -\frac{\gamma}{8} & (K-1) \end{bmatrix} \begin{Bmatrix} \beta_o \\ \beta_{1c} \\ \beta_{1s} \end{Bmatrix} = \begin{Bmatrix} \frac{\gamma A}{2} \\ 0 \\ 0 \end{Bmatrix} \qquad \text{(III-31)}$$

And the determinant of the coefficient is:

$$\Delta = \underbrace{K\ [\ (K-1)^2 + (\frac{\gamma}{8})^2\ ]}_{\text{natural frequency term}} - \underbrace{2B^2(K-1)}_{\text{gravity term}} - \underbrace{(\frac{\gamma}{2})^2(\frac{\overline{U}_o^2}{3})\ \frac{(K-1)}{2}}_{\text{crosswind term}} \qquad \text{(III-32)}$$

The same remarks of Section III-B-3 apply; including crosswind thus changes the critical values of B, γ, and K. In practice this requirement could be important if the operating conditions dictated operation at a constant yaw (or crosswind) angle. For instance, if a crosswind is produced nearby by, say, another WTG, or some other structure.

Solving again for the flapping response, we get:

$$\beta_o = \frac{\gamma A}{2\Delta} \left[(K-1)^2 + \left(\frac{\gamma}{8}\right)^2 \right] \tag{III-33}$$

$$\beta_{1c} = -\frac{1}{\Delta} \left[\gamma B (K-1) A - \left(\frac{\gamma}{2}\right)^3 \frac{A}{12} \bar{U}_o \right] \tag{III-34}$$

$$\beta_{1s} = -\frac{1}{\Delta} \left[\frac{\gamma^2}{8} BA + \left(\frac{\gamma}{2}\right)^2 \frac{A\bar{U}_o}{3} (K-1) \right] \tag{III-35}$$

Flapping Due to Gravity and Crosswind

As might be expected, crosswind does not affect β_o, but does modify rotor tilt angles β_{1c} and β_{1s}. It's also interesting to note that the proportion of rotor tilt shared by the sine and cosine components is just reversed for crosswind. That is:

$$\Delta\beta_{1s}\Big|_{\substack{\text{due to}\\ \text{gravity}}} = \frac{\gamma}{8(K-1)} \Delta\beta_{1c}\Big|_{\text{gravity}} \tag{III-27}$$

But:

$$\Delta\beta_{1s}\Big|_{\substack{\text{due to}\\ \text{crosswind}}} = \frac{8(K-1)}{\gamma} \Delta\beta_{1c}\Big|_{\text{crosswind}} \tag{III-36}$$

Thus, for any set of values of rotor parameters, there must exist a crosswind (or steady yaw angle) for which the rotor vertical tilt can be made zero; but the yaw tilting would be increased because of the signs being additive in III-35, and the increase in yaw tilting would be of magnitude identically equal to the loss in vertical tilt.

5. Effect of yaw rate on flapping. Including the yaw rate term, $\bar{q}$, the system is:

$$\begin{bmatrix} K & B & \frac{\gamma}{12}\bar{U}_o \\ 2B & (K-1) & \frac{\gamma}{8} \\ \frac{\gamma}{6}\bar{U}_o & -\frac{\gamma}{8} & (K-1) \end{bmatrix} \begin{Bmatrix} \beta_o \\ \beta_{1c} \\ \beta_{1s} \end{Bmatrix} = \begin{Bmatrix} \frac{\gamma A}{2} \\ -2\bar{q} \\ -\frac{\gamma\bar{q}}{8} \end{Bmatrix} \qquad \text{(III-37)}$$

And the determinant of the coefficients is the same as before (with the same instabilities as for the last case).

The flapping solution is:

$$\beta_o = \frac{1}{\Delta}\left\{\frac{\gamma A}{2}\left[(K-1)^2 + \left(\frac{\gamma}{8}\right)^2\right] + B\bar{q}\left[2(K-1) - \left(\frac{\gamma}{8}\right)^2\right] + \left(\frac{\gamma}{8}\right)^2(K+1)\,\bar{q}\bar{U}_o\right\} \qquad \text{(III-38)}$$

$$\beta_{1c} = -\frac{1}{\Delta}\left\{\gamma B(K-1)A - \left(\frac{\gamma}{2}\right)^3\frac{A}{12}\bar{U}_o - \left(\frac{\gamma}{8}\right)^2 K\bar{q} + \frac{\gamma^2}{48}B\bar{q}\bar{U}_o + 2\bar{q}K(K-1) - \left(\frac{\gamma}{6}\right)^2\bar{U}_o^{\,2}\bar{q}\right\} \qquad \text{(III-39)}$$

$$\beta_{1s} = -\frac{1}{\Delta}\left\{\frac{\gamma^2}{8}BA + \left(\frac{\gamma}{2}\right)^2\frac{\bar{U}_o}{3}A(K-1) + \frac{\gamma}{3}B\bar{q}\bar{U}_o + \frac{\gamma}{8}K(K+1)\bar{q} - \frac{\gamma}{4}B^2\bar{q}\right\} \qquad \text{(III-40)}$$

Isolating the new terms due to $\bar{q}$, we have:

$$\Delta\beta_o\Big|_{\text{due to }\bar{q}} = \frac{1}{\Delta}\left\{B\bar{q}\left[2(K-1) - \left(\frac{\gamma}{8}\right)^2\right] + \left(\frac{\gamma}{8}\right)^2(K+1)\,\bar{q}\bar{U}_o\right\} \qquad \text{(III-41)}$$

$$\Delta\beta_{1c}\Big|_{\text{due to }\bar{q}} = \frac{1}{\Delta}\left\{\left(\frac{\gamma}{8}\right)^2 K\bar{q} - \left(\frac{\gamma}{4}\right)^2\frac{\bar{U}_o}{3}B\bar{q} - 2\bar{q}K(K-1) + \left(\frac{\gamma}{6}\right)^2\bar{U}_o^{\,2}\bar{q}\right\} \qquad \text{(III-42)}$$

$$\Delta\beta_{1s}\Big|_{\text{due to }\bar{q}} = \frac{1}{\Delta}\left\{\frac{\gamma}{4}B^2\bar{q} - \frac{\gamma}{8}K(K+1)\bar{q} - \frac{\gamma}{3}B\bar{q}\bar{U}_o\right\} \qquad \text{(III-43)}$$

In the β_o equation (III-41), two new terms are added which can appreciably affect the coning angle. They are both coupling terms, the

first gravity coupled with yaw, and the second, crosswind, stiffness and yaw. In the first term the inertial effect [2(K-1)] is separated from the aerodynamic effect $[(\frac{\gamma}{8})^2]$; in the second these effects are coupled.

The tilting equations, $\Delta\beta_{1c}$ and $\Delta\beta_{1s}$, each contain a pure yaw-driven aerodynamic term: the vertical tilting, β_{1c}, increasing $[(\frac{\gamma}{8})^2 K\bar{q}]$, and the horizontal tilting, β_{1s}, to the right $[-\frac{\gamma}{8} K(K+1)\bar{q}]$. These terms are related as before, but the inertial effect of the gyroscopic motion changes the familiar amplitude ratio, (K-1) now appears as (K+1):

$$\Delta\beta_{1s}\Big|_{\bar{q}} = -\frac{(K+1)}{\gamma/8}\,\Delta\beta_{1c}\Big|_{\bar{q}}$$

A large inertial gyroscopic term, which is independent of aerodynamics, dominates the vertical tilting: $-2\bar{q}K(K-1)$. Recalling the discussion of Section I, the forcing function in the flapping equation of motion (III-12) has two periodic components, one aerodynamic and the other gyroscopic, with roughly equal magnitudes and acting at frequency Ω and lagging the blade. Thus a quick check on gyroscopic-induced deflections due to yaw rate can be gained from this inertial term alone. The remaining coupling terms in the equation are not likely to be significant.

6. Summary. These solutions are the approximate blade trajectories for equilibrium. That is, these equations represent the blade motion when transients have died out, and the long term particular motion solution takes over. This is why the motions are conveniently expressed in terms

of ψ and Ω, since the dominant forcing functions are occuring at $\frac{d\psi}{dt} = \Omega$. Therefore, the stable equilibrium condition is also at frequency Ω, even though the blade natural frequency may be quite different from Ω. The transient response in flapping is determined from the homogeneous equations, or more precisely, from the characteristic equation derived by setting the coefficient matrix to zero. When solving in this way for transient motion it is usually necessary to include more terms in the harmonic series (III-8). Transient blade motion can be solved by substituting structural and flight parameters in the matrix, and solving for the eigenvectors, which determine the damped, transient response. For this development, it has been sufficient to explore the frequency characteristics in general, and to seek possible instabilities lurking in the general system. For detailed design, though, maximum transient blade excursions should be found in order to avoid unwanted interactions.

D. Lead-Lag Behavior

1. Lead-lag dynamics. The lead-lag equation is (after combining terms and making appropriate approximations):

$$\boxed{\begin{aligned} &\zeta'' + [\, 2B \cos\psi + K_2 \,]\, \zeta - X_{\beta'}\, \beta' = -\, 2B \sin\psi \\ &\quad + \frac{\gamma}{4} \quad A_2 \left(A_2 + \frac{\theta_o}{6} + \frac{2\theta_p}{3}\right) + \frac{4}{3}\bar{q} \sin\psi \left(A_2 + \frac{\theta_p}{3} + \frac{\theta_o}{15}\right) + 2\, \bar{U}_o \beta \end{aligned}}$$

(III-44)

where

$$B = \frac{G}{2\Omega^2} = \frac{g\, M_b\, X_g\, R}{2 I_b\, \Omega^2}$$

$$K_2 = \varepsilon_2 + \frac{K_\zeta}{I_b\ \Omega^2} = (\frac{\omega_\zeta}{\Omega})$$

$$A_2 = [\ \lambda_i - \mu_o\ ]$$

$$X_{\beta'} = 2\beta + \gamma\ [\ \frac{A_2}{3} + \sin\psi\ (\frac{\overline{q}}{4} + \frac{\overline{U}_o\beta}{3}) + \frac{\theta_o}{40} + \frac{\theta_p}{8}\ ] \qquad \text{(III-45)}$$

If the β' coupling term is ignored for the moment, the equation has the form of a simple undamped oscillator. Some damping due to aerodynamic drag changes does occur, but it is extremely small, and drag has been neglected in this treatment. In helicopter systems, damping is usually added to the lag hinge.[13] Again, the natural frequency in lead-lag is given by:

$$(\frac{\omega_\zeta}{\Omega})^2 = K_2 \qquad \text{(III-46)}$$

The Mathieu's instabilities in lead-lag from Section II-C-1 are unchanged since aerodynamic terms do not affect the transient oscillator. Thus, pendular instability will exist for certain values of K_2 and B (see Section II-C-1).

For steady motion (no dynamic terms) the right hand side gives the "steady" lead-lag angles; these values are changed from those in Chapter II, by addition of aerodynamic forces. The forcing function contains both periodic and steady terms, to be investigated later. It is also interesting to note that the aerodynamic forcing term due to crosswind is also dependent on steady flapping angle β (coning angle).

When the flap coupling term is added (III-45), lag angle becomes dependent on flapping motion through Coriolis forces. The existence of

a lag hinge (or inplane flexibility) offers a means for accommodating this large inplane moment. However, mechanical damping is usually needed since lag motion is undissipated. For blade motion solutions, the coupled motion can be solved by first solving for the flapping coefficients, β_o, β_{1c}, β_{1s}, and substituting them into the lag equation. Instability can also arise; flap-lag coupling is described in Chapter VI.

2. Lead-lag motion. Again using the first three terms of a harmonic series solution for ζ, and equating coefficients to zero, gives the following system for lead-lag motion:

$$\zeta = \zeta_o + \zeta_{1c} \cos \psi + \zeta_{1s} \sin \psi \tag{III-47}$$

And

$$2B\ \zeta_o + (K_2-1)\ \zeta_{1c} = 0$$

$$(K_2-1)\ \zeta_{1s} = \frac{\gamma}{4}\left(A_2 + \frac{\theta_p}{3} + \frac{\theta_o}{15}\right)\left(\frac{4}{3}\bar{q} + 2\bar{U}_o\beta\right) - 2B$$

$$K_2\ \zeta_o + B\ \zeta_{1c} = \frac{\gamma}{4} A_2\left(A_2 + \frac{\theta_o}{6} + 2\frac{\theta_p}{3}\right) \tag{III-48}$$

Or:

$$\begin{bmatrix} 2B & (K_2-1) & 0 \\ 0 & 0 & (K_2-1) \\ K_2 & B & 0 \end{bmatrix} \begin{Bmatrix} \zeta_o \\ \zeta_{1c} \\ \zeta_{1s} \end{Bmatrix} = \begin{Bmatrix} 0 \\ \frac{\gamma}{4}\left(A_2 + \frac{\theta_p}{3} + \frac{\theta_o}{15}\right)\left(\frac{4}{3}\bar{q} + 2\bar{U}_o\beta\right) - 2B \\ \frac{\gamma}{4}A_2\left(A_2 + \frac{\theta_o}{6} + \frac{2\theta_p}{3}\right. \end{Bmatrix} \tag{III-49}$$

The motion solution decouples:

$$\boxed{\zeta_{1s} = \frac{1}{K_2-1}\ \frac{\gamma}{4}\left(A_2 + \frac{\theta_p}{3} + \frac{\theta_o}{15}\right)\left(\frac{4}{3}\bar{q} + 2U_o\beta\right) - 2B} \tag{III-50}$$

Also:

$$\boxed{\begin{aligned} \zeta_o &= \left\{\frac{1-K_2}{K_2(1-K_2) + 2B^2}\right\} \frac{\gamma}{4} A_2 \left(A_2 + \frac{\theta_o}{6} + \frac{2\theta_p}{3}\right) && \text{(III-51)} \\ \zeta_{1c} &= \left\{\frac{2B}{K_2(1-K_2) + 2B^2}\right\} \frac{\gamma}{4} A_2 \left(A_2 + \frac{\theta_o}{6} + \frac{2\theta_p}{3}\right) && \text{(III-52)} \end{aligned}}$$

Looking first at the steady lag angle ζ_o (III-51), the pendular instability is given by:

$$K_2(1-K_2) + 2B^2 = 0 \qquad \text{(III-53)}$$

or when:

$$\boxed{K_2 = \frac{1}{2} + \frac{1}{2}\sqrt{8B^2 + 1}} \qquad \text{(III-54)}$$

This equation constitutes the critical stiffness-frequency combination which yields lead-lag pendular instability. This form of the instability equation is much easier for design purposes than the general development of Section II-C-1.

The lead-lag equation (III-44) also shows the natural frequency in the absence of gravity to be $K_2\Omega^2$. This is reiterated in expression III-54, and cautions the designer to avoid K_2's around 1.0 where the system would be forced at its natural frequency in lead lag.

Ignoring the gravity term, steady lead-lag angle is positive--power is coming out of the system. As θ_p is increased, less thrust is produced since angle-of-attack decreases, hence, within the aerodynamic performance range modeled here, lag angle increases. In general, steady lag angle will be zero only if no power (or shaft torque) is being taken out of the system (as in a wind turbine) or being put into the system

(lifting rotor). It is also interesting to note that steady lag is unaffected by yaw rate or crosswind.

The cosine component ("vertical scissoring") is also unaffected by crosswind or yaw rate, but is a direct result of gravity:

$$\zeta_{1c} = \left(\frac{2B}{1-K_2}\right) \zeta_o \tag{III-56}$$

Isolating the gravity portion of the sine component ("horizontal scissoring") we get:

$$\Delta\zeta_{1s}\Big|_{\substack{\text{due to}\\ \text{gravity}}} = -\frac{2B}{K_2-1} = \frac{2B}{1-K_2} \tag{III-57}$$

Thus:

$$\zeta_{1c} = \zeta_o \, \Delta\zeta_{1s}\Big|_{\substack{\text{due to}\\ \text{gravity}}} \tag{III-58}$$

And the cosine response ("vertical scissoring") is exclusively an inertial, coupled effect--the gravity inertial force acting through the steady lag angle ζ_o.

The asymmetrical aerodynamics due to crosswind and yaw rate show up in the other sine portion:

$$\Delta\zeta_{1s}\Big|_{\substack{\text{due to}\\ \text{aerodynamics}}} = \frac{1}{K_2-1}\left\{\frac{\gamma}{4}\left(A_2 + \frac{\theta_p}{3} + \frac{\theta_o}{15}\right)\left(\frac{4}{3}q + 2U_o\beta\right)\right\} \tag{III-59}$$

In the absence of aerodynamics, A = 0, and the only lead-lag component is ζ_{1s}. This is the mode which grows without limit for pendular instability.

E. Torsional (Feathering) Behavior

Torsional motion of interest to rotor designers centers around flutter. A rotor blade can experience divergence or flutter as a classical slender wing.[20] Also flutter due to coupled torsional and flapping motion $\dot{\beta}$ can be experienced.[9] These instabilities are addressed in Chapter VI. For present purposes, a simplified equation of motion in feathering is derived, with no attempt to solve for the aerodynamic-induced instabilities, which are complex. The present equation of motion will be sufficient to calculate steady values of blade torsional moment, and to point the way for preliminary structural design considerations.

Looking more closely at the blade, we have in general, four non-coincident axes: the mass axis, elastic axis, control axis, and aerodynamic axis. The elastic axis is the spanwise locus of points about which no section torsional deflection is incurred with bending deflection. The control axis is simply the axis of mechanical feathering, determined by the blade retention and pitching mechanism. The aerodynamic axis, for a conventional airfoil shape within the "linear" performance limits ($\frac{dc_\ell}{d\alpha}$ assumed constant, as in this paper), is at the quarter chord (25% chord). Thus, our idealized, uniform blade is:

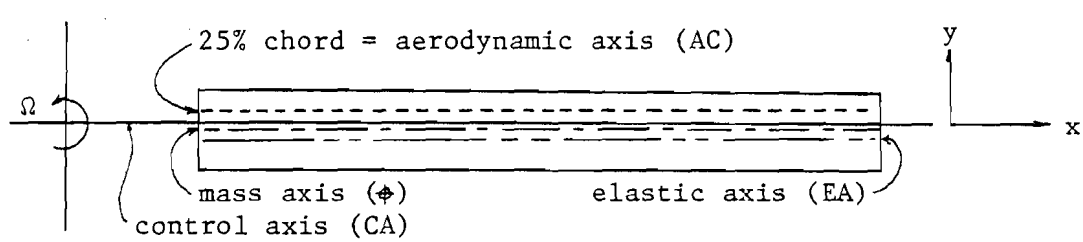

Figure 33. Blade Spanwise Axes

A blade section, with the elemental forces and moments drawn is:

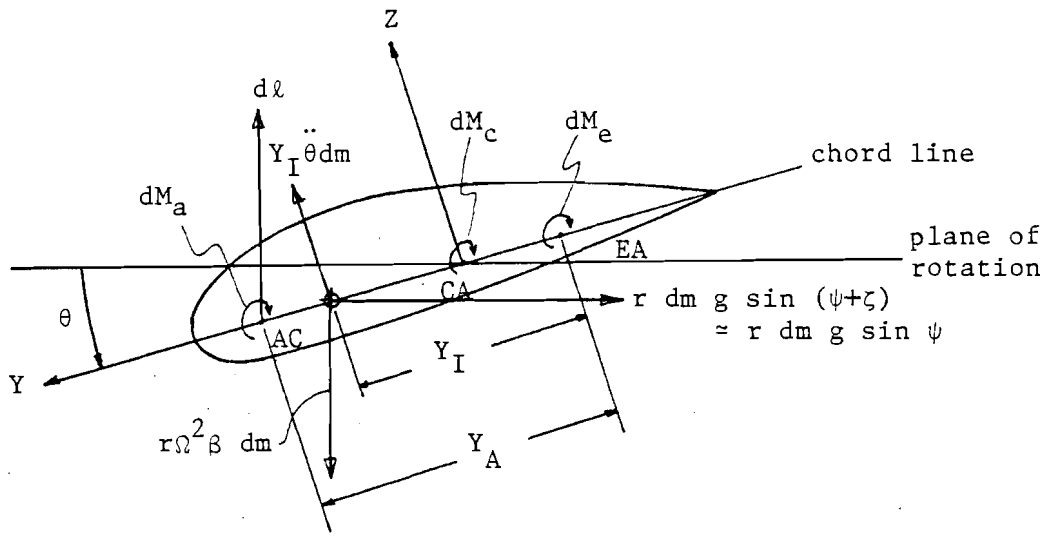

Figure 34. Blade Flutter Section

where: dM_a = aerodynamic pitching moment about aerodynamic center (tending to increase angle of attack)

dM_e = blade elastic moment

$d\ell$ = elemental lift

dM = control system elastic moment

Y_I = distance from elastic axis (shear center of blade) to center of mass

Y_A = distance from elastic axis to aerodynamic center.

For the idealized blade, with all torsional elasticity concentrated at the root, the elastic axis and control axis become coincident, and the restoring blade elastic moment is combined with the control system elastic moment:

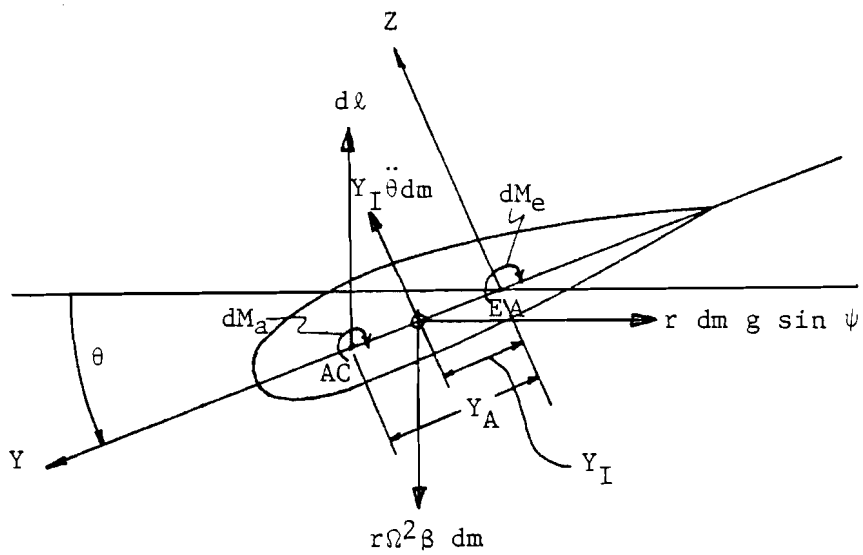

Figure 35. Idealized Blade Section

The moments on the element are dM_a, the aerodynamic pitching moment about the aerodynamic center (independent of C_ℓ) and dM_e, the elastic spring moment. The lift force is $d\ell$, acting at Y_A from the elastic axis. The centrifugal force is taken in two parts. First, the familiar $r\Omega^2$ dm spanwise term (see Section II-A-1) has a vertical component perpendicular to the plane of rotation, acting at the center of mass. Also, there is a horizontal term due to the vertical distribution of mass around the elastic axis at the section, viz.:

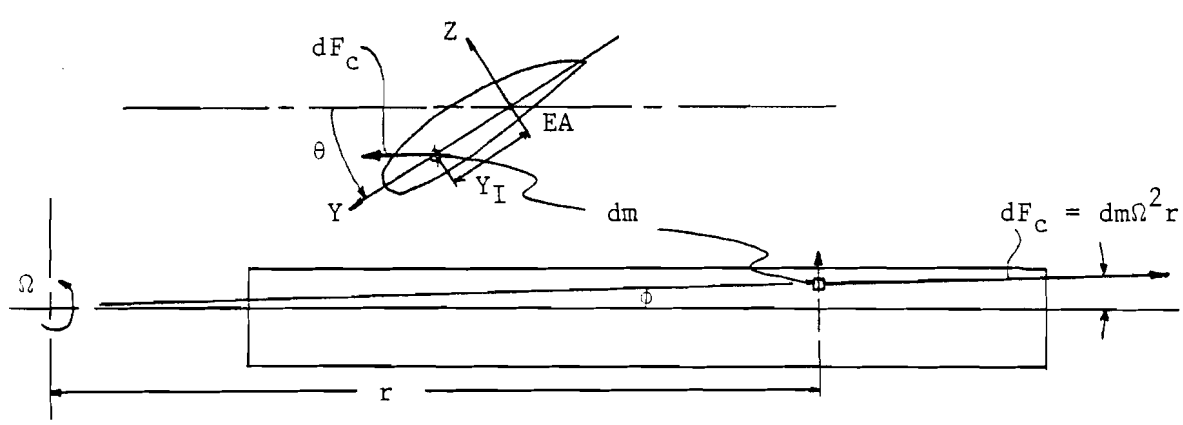

Figure 36. Centrifugal Force Components

The horizontal component perpendicular to the elastic axis is:

$$dF_c \sin \phi \simeq dF_c \phi = r\Omega^2 \, dm \left(\frac{Y_I}{r}\right)$$

$$= Y_I \Omega^2 \, dm$$

The elemental moment is then:

$$dM_c = Y_I{}^2 \, \theta \, \Omega^2 \, dm \qquad \text{(III-60)}$$

To this must be added the standard $I_f \Omega^2 \theta$ moment about the center of mass (Section III-A-3). Now moments are taken about the elastic axis:

$$dM_{aero} + dM_{elastic} + dM_{centrifugal} + dM_{inertial} + dM_{gravity} = 0 \qquad \text{(III-61)}$$

or:

$$-dM_a - d\ell \, Y_a - d(K_\theta)\theta + r\Omega^2 \beta \, dm^{Y_I} - Y_I{}^2 \theta \, \Omega^2 \, dm - d(I_f)\Omega^2 \theta$$

$$+ r \, dm \, g \sin \psi \, Y_I \sin \theta - Y_I{}^2 \, \ddot{\theta} dm - d(I_f)\ddot{\theta} = 0 \qquad \text{(III-62)}$$

Integration along the blade gives:

$$-M_a - Y_A \int_o^R d\ell - K_\theta \theta + \beta\Omega^2 I_R - \theta\Omega^2 I_I - I_I \ddot{\theta} - I_f \ddot{\theta}$$

$$- \theta\Omega^2 I_f + I_R \, g \sin \psi \, \theta = 0 \qquad \text{(III-63)}$$

where:

$$I_R = \int_o^R Y_I \, r \, dm = Y_I \frac{M_b R}{2}$$

$$I_I = \int_o^R Y_I{}^2 \, dm = Y_I{}^2 \, M_b$$

$$I_R g = G I_b \left(\frac{Y_I}{R}\right)$$

Or:

$$\boxed{\begin{aligned}(I_f + I_I)\ddot{\theta} + (I_f + I_I)\Omega^2\theta + K_\theta\theta - I_R\,\beta\Omega^2 + GI_b(\frac{Y_I}{R})\sin\psi\,\theta \\ + \bar{q}\,(I_f + I_I)\Omega^2\sin\psi = -M_a - (\frac{Y_A}{R})\ \frac{\gamma}{2}\,I_b\Omega^2\ [\ \frac{\mu_o}{2} - \frac{\lambda_i}{2} \\ - \frac{\beta'}{3} - \sin\psi\ (\frac{\bar{q}}{3} + \frac{\bar{U}_o\beta}{2}) - \frac{\theta_o}{12} - \frac{\theta_p}{3}\ ]\end{aligned}}$$

Single Degree of Freedom Feathering Equation (III-64)

As a first check, the equation reduces to the simple oscillator of Chapter II (II-11) when aerodynamic forces, yaw rate, and mass offset are zero:

$$\ddot{\theta} + [\ \Omega^2 + \frac{K_\theta}{I_f}\ ]\ \theta = 0 \qquad \text{(II-11)}$$

The added inertial integral I_I in III-64 is simply a manifestation of the parallel axis theorem; and the aerodynamic forcing function appears as a constant moment (which is independent of lift, by design), and a lift offset component (dependent on Y_A/R).

The torsional behavior is dependent on flapping behavior. This simple derivation has included β coupling only in the lift term, which is very small, mainly because Y_A is usually small. Retaining the forces due to flapping, the free body diagram picks up a $\ddot{\beta}Y_I$ dm term, which gives a new coupled equation in feathering:

$$(I_f + I_I)\ddot{\theta} + [\ (I_f + I_I)\Omega^2 + GI_b(\frac{Y_I}{R})\sin\psi + K_\theta\ ]\ \theta - I_R\ddot{\beta} - I_R\Omega^2\beta$$

$$= \text{aerodynamic terms} \qquad \text{(III-65)}$$

Flutter analysis combines this equation with the flapping equation of motion (now including the coupled θ terms) in order to derive solutions to coupled β, θ motion and to search for instabilities.

Harmonic content in the aerodynamic terms includes the simple $\beta\bar{U}_o \sin \psi$ crosswind term and the $\frac{dB}{d\psi}$ varying inflow term, both seen in this analysis. Other important harmonic terms in the right-hand side occur because of viscous wake effects, not modelled here. The effects are germaine to a discussion of flutter and pitch-flap coupling instability; discussion of this can be found in Chapter VI.

The simple feathering equation then becomes:

$$\boxed{\begin{aligned} &\theta'' + \left[K_3 + 2B\left(\frac{I_b}{I_f+I_I}\right)\left(\frac{Y_I}{R}\right) \sin \psi \right] \theta \\ &= -\frac{M_a}{(I_f+I_I)\Omega^2} + \left(\frac{I_R}{I_f+I_I}\right)\beta - \bar{q} \sin \psi \\ &+ \left(\frac{I_b}{I_f+I_I}\right)\left(\frac{Y_A}{R}\right) \frac{\gamma}{4} \left[A_2 + \frac{2}{3}\beta' + \sin \psi \left(\frac{2\bar{q}}{3} + \bar{U}_o\beta\right) + \frac{\theta_o}{6} + \frac{2\theta_p}{3} \right] \end{aligned}} \qquad \text{(III-66)}$$

where

$$K_3 = 1 + \frac{K_\theta}{(I_f+I_I)\Omega^2} = \left(\frac{\omega_\theta}{\Omega}\right)^2$$

$$B = \frac{G}{2\Omega^2}$$

$$A_2 = \lambda_i - \mu_o$$

The gravity term is very small compared to torsional frequency $\frac{K_\theta}{I\Omega^2}$; hence the torsional pendular stability is not a problem. The natural frequency of the oscillator is affected by the parallel axis theorem through I_I, but this is also a small effect.

The right-hand side contains the forcing function. The major one is pitching moment due to aerodynamic center offset Y_A. The steady

aerodynamic pitching moment M_a is very small and tends to reduce torsional deflection, thereby is stabilizing. A mass coupling term due to coning (flapping) is an appreciable destabilizing moment dependent exclusively on mass axis offset and flapping angle β. Periodic terms appear in the aerodynamic lift, due to yaw rate $\overline{q}$ and crosswind; again, the effects of these are greatly attenuated by reduction of Y_A, or judicious placement of control axis versus aerodynamic center axis.

The designer's task is to assess the effects of mass axis offset (Y_I) and aerodynamic axis offset (Y_A) on the cyclic terms in this equation. The major design criteria are: high enough torsional stiffness K_θ to withstand flutter (Chapter VI), and high enough torsional strength to withstand steady and cyclic pitching moments (Chapter IV).

CHAPTER IV

BLADE AND HUB LOADS

A companion problem to calculating blade deflections and excursions, to the designer, is to estimate loading on the blade due to expected conditions. The structural designer of the blade has two tasks, in general: appropriate stiffness to avoid instabilities, and sufficient strength to withstand loads. "Strength design" parameters can consist of large loads expected rarely, such as hurricanes, which must be within a factor of safety and elastic limits; continuous loads due to operation, which may have different factors of safety;[21] and periodic, or vibratory loads, which must lie within material endurance limits.[22] In the absence of long term experimental results on wind turbines, each loading category must be addressed and studied with high priority; the operating conditions therefore are site dependent as are the expected loads during the life of the machine. This chapter will develop practical expressions for the loading magnitudes and distributions for the simple blade model assumed in Chapter II. Maximum bending moments, shears, and tensions will be calculated and presented.

A. Hub Loads

For a single blade, the blade root bending moment is simply the elastic moment at the assumed hinge spring:

Σ(Moments about hinge) = 0 for equilibrium

or:

Elastic hinge moment = inertial moments + aerodynamic moments
+ gravity moments + crosswind moments
+ ...

For the straight blade, hinge spring - offset model, the elastic hinge moment is simply $K_\beta \beta$, where K_β is the assumed spring. In other words, the blade root moments, in flapping, lead-lag, and feathering, are given by the angular deflections calculated in Chapter III, times the value of the corresponding hinge spring:

$$M_{\beta_o}(\psi) = K_\beta \left[\beta_o + \beta_{1c} \cos \psi + \beta_{1s} \sin \psi \right]$$

$$M_{\zeta_o}(\psi) = K_\zeta \left[\zeta_o + \zeta_{1c} \cos \psi + \zeta_{1s} \sin \psi \right]$$

$$M_{\theta_o}(\psi) = K_\theta \left[\theta_o + \theta_{1c} \cos \psi + \theta_{1s} \sin \psi \right] \qquad \text{(IV-1)}$$

Single Blade Root Moments

Thus the single blade hub retention must resist these moments. The torsional moment is best expressed as a steady moment due to θ_o, leaving the periodic torsional deflection and motions to a more complete flutter analysis (Chapter VI). As shown here, only the first harmonics are used; as discussed in Chapter III, the higher harmonics should also be used when more detailed loading information is needed. Typically, the first five harmonics are used for preliminary design in industry (i.e., sin 5ψ, cos 5ψ). However, the first harmonics are sufficient for most calculations, and for our purposes here. In addition to these moments (IV-1), single blade hub shears and blade tension at the hub

must be calculated. But a check on the root moments is a good preliminary design approach to structural tradeoffs.

The loads transmitted by the hub to the windshaft, and eventually the tower, are the vector sums of the loads from each single blade. The loads are very dependent on hub configuration and geometry. For a fully articulated blade the flapping and lead-lag hinges are free, so no moments are transmitted to the hub, only shears and tension. A gimballed, or teetering rotor has its blades rigidly attached to the hub, which is in turn, hinged to the windshaft. The tower moments also depend on the number of blades. The tower moments are calculated in Chapter V.

B. Aerodynamic Loads

From Chapter II, the differential forces on a blade element dm are, in flapping and lead-lag:

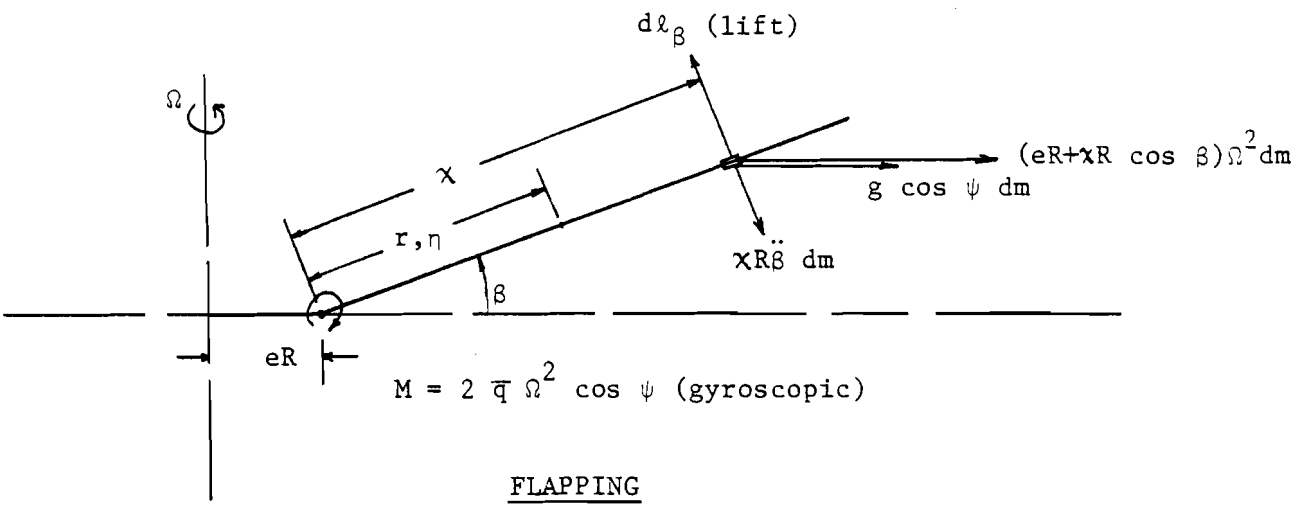

FLAPPING

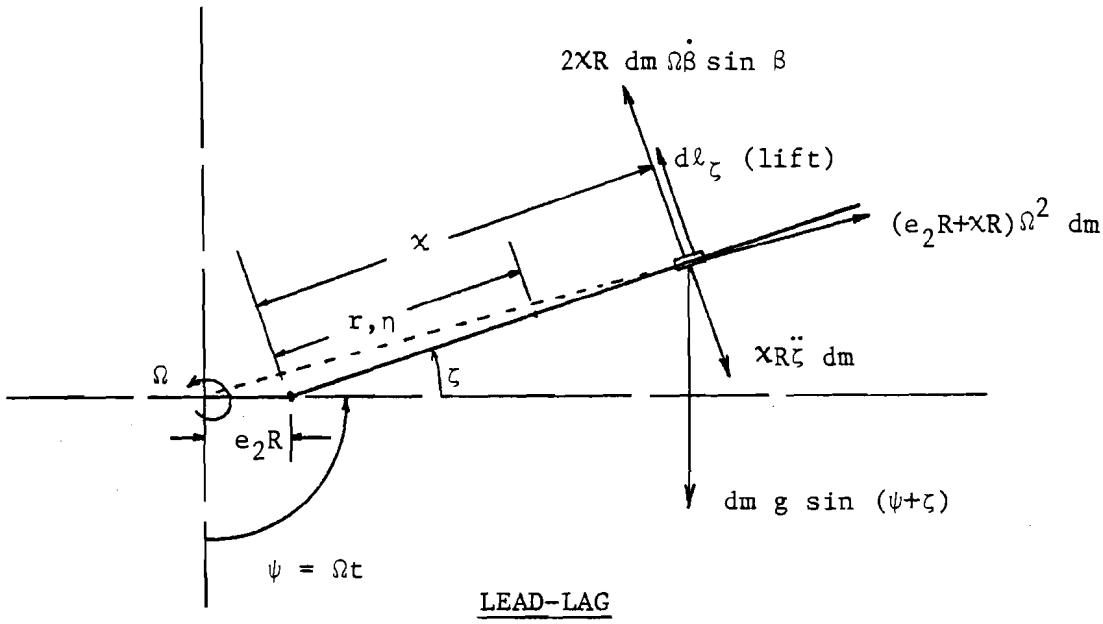

Figure 37. Differential Forces on a Blade Element

The moments at $\eta = \frac{r}{R}$ due to the single aerodynamic differential force are:

$$M_\beta(\eta) = \int_\eta^1 \ell\ R^2\ (x-\eta)\ dx \tag{IV-2}$$

$$M_\zeta(\eta) = \int_\eta^1 \ell\ \left(\frac{U_p}{U_t}\right)\ R^2\ (x-\eta)\ dx \tag{IV-3}$$

The shears at $\eta = \frac{r}{R}$ are

$$S_\beta(\eta) = \int_\eta^1 \ell\ R\ dx \tag{IV-4}$$

$$S_\zeta(\eta) = \int_\eta^1 \ell\ R\ \left(\frac{U_p}{U_t}\right)\ dx \tag{IV-5}$$

where $x = \frac{x}{R}$ is taken as a dummy variable for the integration, and (U_p/U_t) and $\ell(\eta)$ are from II-46 and II-51. In Chapter II, the integrals

(IV-2 to 5) were taken from 0 to 1 over η, since the root moments were needed. Here the distribution is needed, hence the integration must be done for the general case.

From before:

$$\ell \frac{U_p}{U_t} = \frac{1}{2} \gamma I_b \frac{\Omega^2}{R^2} \Big\{ \mu_o^2 - 2\mu_o\lambda_i + \lambda_i^2 + 2\beta' \eta [\lambda_i - \mu_o]$$

$$+ 2 \sin \psi [(\lambda_i + \eta\beta' - \mu_o)(\eta\bar{q} + \bar{U}_o\beta)]$$

$$+ \eta\theta_o [(1 - \eta + \frac{\theta_p}{\theta_o})(\lambda_i + \eta\beta' - \mu_o)]$$

$$+ \eta\theta_o \sin \psi [(\eta\bar{q} + \bar{U}_o\beta)(1 + \frac{\theta_p}{\theta_o} - \eta)] \Big\} \qquad \text{(IV-6)}$$

Integrated to get inplane shear, we have:

$$S_\zeta = \int_\eta^1 \ell (\frac{U_p}{U_t}) R \, dx = \frac{1}{2} \gamma I_b \frac{\Omega^2}{R} \Big\{ (\mu_o - \lambda_i)^2(1-\eta) - (\mu_o - \lambda_i)\beta'(1-\eta^2)$$

$$+ 2 \sin \psi \Big\{ \bar{q}(\frac{\lambda_i}{2} [1-\eta^2] + \frac{\beta'}{3} [1-\eta^3] - \frac{\mu_o}{2} [1-\eta^2] + \frac{\theta_o}{24} [1+3\eta^4-4\eta^3]$$

$$+ \frac{\theta_p}{6} [1-\eta^3]) + \bar{U}_o\beta(\lambda_i[1-\eta] + \frac{\beta'}{2} [1-\eta^2] - \mu_o [1-\eta]$$

$$+ \frac{\theta_o}{12} [1+2\eta^3-3\eta^2] + \frac{\theta_p}{4} [1-\eta^2]) \Big\}$$

$$+ \theta_o [\frac{\lambda_i}{6} (1-3\eta^2+2\eta^3) + \frac{\beta'}{12} (1-4\eta^3+3\eta^4) - \frac{\mu_o}{6} (1-3\eta^2+2\eta^3)]$$

$$+ \theta_p [\frac{\lambda_i}{2} (1-\eta^2) + \frac{\beta'}{3} (1-\eta^3) - \frac{\mu_o}{2} (1-\eta^2)] \Big\} \qquad \text{(IV-7)}$$

Likewise, the flapping shear is:

$$S_\beta = \int_\eta^1 \ell\, R\, dx = \frac{1}{2}\gamma I_b \frac{\Omega^2}{R}\left\{\frac{1}{2}(\mu_o - \lambda_i)(1-\eta^2) - \frac{\beta'}{3}(1-\eta^3)\right.$$

$$- \sin\psi\left[\frac{\bar{q}}{3}(1-\eta^3) + \frac{\bar{U}_o\beta}{2}(1-\eta^2)\right] - \frac{\theta_o}{12}(1-4\eta^3+3\eta^4)$$

$$\left. - \frac{\theta_p}{3}(1-\eta^3)\right\} \qquad \text{(IV-8)}$$

When $\eta = 0$, the root shears are found to be the same as before in expressions II-56 and II-58.

The flapping and lead-lag moments are found to be:

$$M_\beta = \int_\eta^1 \ell\, R^2\,(x-\eta)\, dx$$

$$= \frac{1}{2}\gamma I_b \Omega^2 \left\{\left[\frac{1}{3} + \frac{1}{6}\eta(\eta^2-3)\right]\left[\mu_o - \lambda_i - \bar{U}_o\beta\sin\psi\right]\right.$$

$$- \left[\frac{1}{4} + \frac{1}{12}\eta(\eta^3-4)\right]\left[\beta' + \bar{q}\sin\psi + \theta_o + \theta_p\right]$$

$$\left. + \left[\frac{1}{5} + \frac{1}{20}\eta(\eta^4-5)\right]\theta_o\right\} \qquad \text{(IV-9)}$$

$$M_\zeta = \int_\eta^1 \ell\left(\frac{U_p}{U_t}\right) R^2\,(x-\eta)\, dx$$

$$= \frac{1}{2}\gamma I_b \Omega^2 \left\{\eta(\eta-1)\,\gamma_o + \frac{(1-\eta^2)}{2}\left[\gamma_o - \gamma_1\eta\right]\right.$$

$$+ \frac{(1-\eta^3)}{3}\left[\gamma_1 - \gamma_2\eta\right] + \frac{(1-\eta^4)}{4}\left[\gamma_2 - \gamma_3\eta\right]$$

$$\left. - \frac{(1-\eta^5)}{5}\gamma_3\right\} \qquad \text{(IV-10)}$$

Where the aerodynamic coefficients are:

$$\gamma_o = (\mu_o - \lambda_i)^2 + 2\overline{U}_o\beta \sin\psi\,(\lambda_i - \mu_o)$$

$$\gamma_1 = (\lambda_i - \mu_o)[2\beta' + \theta_o + \theta_p] + \sin\psi[2\overline{q}(\lambda_i - \mu_o) + \overline{U}_o\beta(2\beta' + \theta_o + \theta_p)]$$

$$\gamma_2 = \theta_o(\mu_o - \lambda_i) + \beta'(\theta_o + \theta_p) + \sin\psi[\overline{q}(2\beta' + \theta_o + \theta_p) - \overline{U}_o\beta\theta_o]$$

$$\gamma_3 = \theta_o(\beta' + \overline{q}\sin\psi) \qquad \text{(IV-11)}$$

Lead-Lag Coefficients

Again when $\eta = 0$, the root moments are found to be identical to II-57 and III-59 from before.

Rearrangement and manipulation of expressions IV-9 and IV-10 give surprisingly simple expressions for the moment distributions in flapping and lead-lag aerodynamic lift:

$$M_\zeta = \frac{1}{2}\gamma I_b \Omega^2[\gamma_o\,\chi_1 + \gamma_1\,\chi_2 + \gamma_2\,\chi_3 + \gamma_3 + \dot{\chi}_4] \qquad \text{(IV-12)}$$

$$M_\beta = \frac{1}{2}\gamma I_b \Omega^2[\gamma_4\,\chi_2 + \gamma_5\,\chi_3 + \gamma_6\,\chi_4] \qquad \text{(IV-13)}$$

The γ's are aerodynamic coefficients, collections of terms, coupled and uncoupled, and the χ's are mode shapes entirely dependent on spanwise station η. Hence, the parametric effects of each variable can be assessed by looking at a linear combination of nondimensional mode shapes. Coefficients γ_o through γ_3 are given in IV-11. Other values are:

$$\gamma_4 = \mu_o - \lambda_i - \overline{U}_o\beta\sin\psi$$

$$\gamma_5 = -\beta' - \overline{q}\sin\psi - \theta_o - \theta_p$$

$$\gamma_6 = \theta_o \qquad \text{(IV-14)}$$

Flapping Coefficients

The mode shapes are:

$$\boxed{\begin{aligned} X_1 &= \frac{1}{2}(\eta - 1)^2 \\ X_2 &= \frac{1}{3}(\eta + 2)\ X_1 \\ X_3 &= \frac{1}{6}(\eta^2 + 2\eta + 3)\ X_1 \\ X_4 &= \frac{1}{10}(\eta^3 + 2\eta^2 + 3\eta + 4)\ X_1 \end{aligned}}$$

Aerodynamic Moment Mode Shapes

(IV-15)

For this case, where analytical expressions are obtained for moment distribution, the shear and loading distributions can be obtained by integration. Thus:

$$M_\zeta = \frac{1}{2}\ \gamma I_b \Omega^2\ [\ \gamma_o\ X_1 + \gamma_1\ X_2 + \gamma_2\ X_3 + \gamma_3\ X_4\ ]$$

$$S_\zeta = \frac{1}{2}\ \gamma I_b\ \frac{\Omega^2}{R}\ [\ \gamma_o \frac{dX_1}{d\eta} + \gamma_1 \frac{dX_2}{d\eta} + \gamma_2 \frac{dX_3}{d\eta} + \gamma_3 \frac{dX_4}{d\eta}\ ]$$

$$L_\zeta = \frac{1}{2}\ \gamma I_b\ \frac{\Omega^2}{R^2}\ [\ \gamma_o \frac{d^2X_1}{d\eta^2} + \gamma_1 \frac{d^2X_2}{d\eta^2} + \gamma_2 \frac{d^2X_3}{d\eta^2} + \gamma_3 \frac{d^2X_4}{d\eta^2}\ ] \qquad \text{(IV-16)}$$

And:

$$M_\beta = \frac{1}{2}\ \gamma I_b \Omega^2\ [\ \gamma_4\ X_2 + \gamma_5\ X_3 + \gamma_6\ X_4\ ]$$

$$S_\beta = \frac{1}{2}\ \gamma I_b\ \frac{\Omega^2}{R}\ [\ \gamma_4 \frac{dX_2}{d\eta} + \gamma_5 \frac{dX_3}{d\eta} + \gamma_6 \frac{dX_4}{d\eta}\ ]$$

$$L_\beta = \frac{1}{2}\ \gamma I_b\ \frac{\Omega^2}{R^2}\ [\ \gamma_4 \frac{d^2X_2}{d\eta^2} + \gamma_5 \frac{d^2X_3}{d\eta^2} + \gamma_6 \frac{d^2X_4}{d\eta^2}\ ] \qquad \text{(IV-17)}$$

The various mode shapes are:

$$
\begin{array}{lll}
\chi_1 = \frac{1}{2}(\eta-1)^2 & \chi_1' = (\eta-1) & \chi_1'' = 1 \\
\chi_2 = \frac{1}{3}(\eta+2)\chi_1 & \chi_2' = \frac{1}{2}(\eta^2-1) & \chi_2'' = \eta \\
\chi_3 = \frac{1}{6}(\eta^2+2\eta+3)\chi_1 & \chi_3' = \frac{1}{3}(\eta^3-1) & \chi_3'' = \eta^2 \\
\chi_4 = \frac{1}{10}(\eta^3+2\eta^2+3\eta+4)\chi_1 & \chi_4' = \frac{1}{4}(\eta^4-1) & \chi_4'' = \eta^3 \\
\text{Moment} & \text{Shear} & \text{Load}
\end{array}
\qquad \text{(IV-18)}
$$

The aerodynamic moment, shear, and loading distributions along the blade can thus be expressed simply as a linear combination of the mode shapes above. The design task is to assess the values of the aerodynamic coefficients, the γ's, (IV-11, 14) and simply add up the modes in the correct proportion. The mode shapes for loading and moment along the blade are given in Figure 38.

Looking at the load distribution modes, and the flapping coefficients, IV-14, it can be seen that inflow ratio λ_i and μ_o (1/tip speed ratio) result in a triangular airload distribution on the blade, χ_2''. The simplified aerodynamic model used here assumes uniform induced velocity, v_i, across the rotor disc.[18] Inclusion of annular effects, wake vorticity, axial velocity in the wake, and unsteady effects will all modify this assumption. The first level of wake and induced velocity sophistication is to allow radial variation in induced velocity (annular momentum theory), account for a cylindrical vortex trailing wake, and make provision for a loss of airload at the tip.[23] In order to make this calculation, a numerically iterative computer simulation (strip theory) is done.[24] For detailed performance studies such as

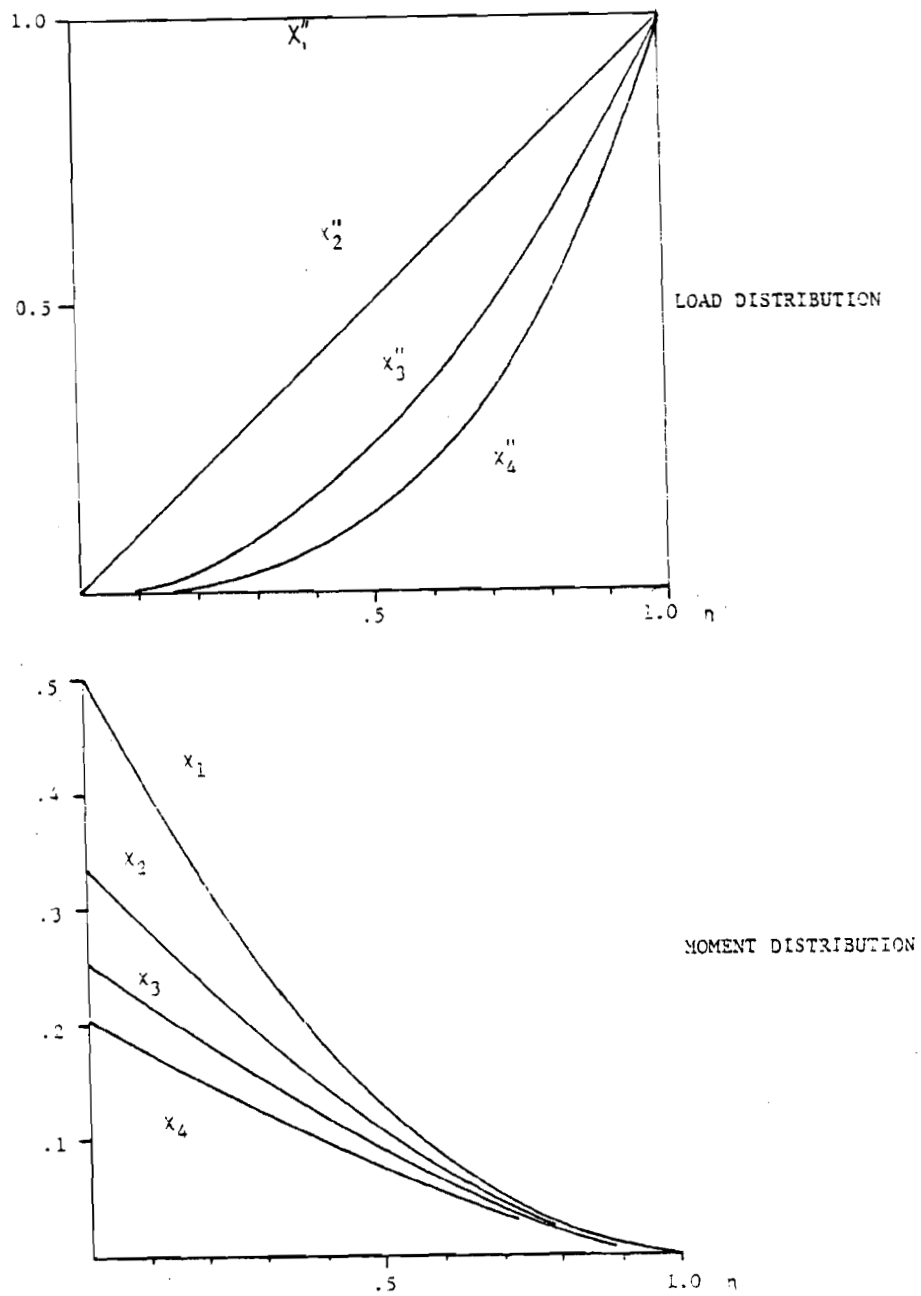

Figure 38. Aerodynamic Load and Moment Distribution Modes

geometric tradeoffs (e.g., twist, taper, airfoil), this simulation is essential; a strip theory as described, can be found in Appendix I. For non-aerodynamic loads, and for the fundamental effects of other flow phenomena such as crossflow and yaw rate, the simple terms in the above aerodynamic coefficients and their corresponding mode shapes, are valuable and sufficient.[15]

Looking again at the flapping loading modes IV-14, it can be seen that periodic loads are introduced by crosswind, $\overline{U}_o\beta$ and yaw rate, $\overline{q}$, over the triangular and the quadratic modes χ_2'' and χ_3''. This indicates the yaw rate may be a more stringent load requirement since its effect is localized nearer the blade tip. Also, the effect of twist angle, θ_o, is a cubic distribution, χ_4''. Not surprisingly, also, the moments are maximum at the blade root. However, the stress due to bending at each section along the blade must be determined from the local value of total moment (of which the aerodynamic moment is a part).

The inplane load and moment magnitude are not so important in preliminary design since they are much less than flapping moments. A more critical design consideration is loading frequency; the inplane stiffness is usually high enough to avoid resonance, except in some special cases, or for coupled motion. However, it is interesting to note that the mean inflow term $(\mu_o - \lambda_i)$ appears as a constant load along the beam. Also, periodicity occurs in all four modes for the inplane case; and twist effect, θ_o, is dependent on flapping velocity β'.

C. Dynamic Loads

Other forces acting on the blade element are due to inertial, gyroscopic, gravity, Coriolis, and centrifugal effects. In the rotating system, these forces act on the blade element of mass, dm, as before:

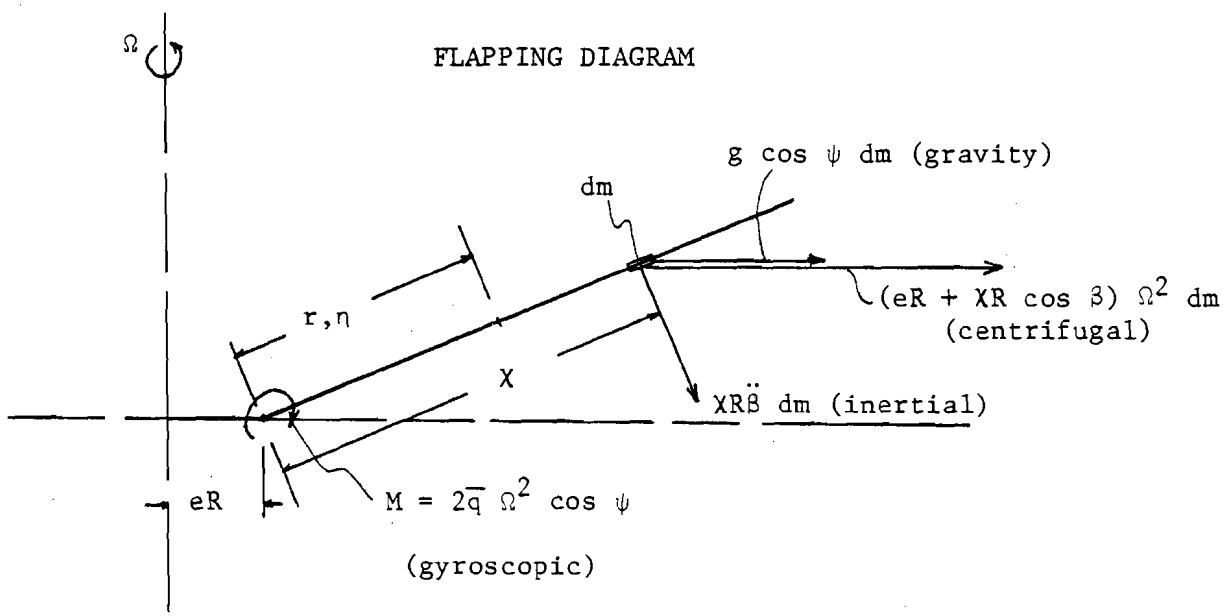

Figure 39. Blade Element Forces

When deriving the aerodynamic moment along the blade in the last section, the deflected blade shape was not as important a factor as relative blade element velocities. The straight section - hinge offset model is only an approximation of the actual blade shape which might be a combination of many bending modes and quite complex:

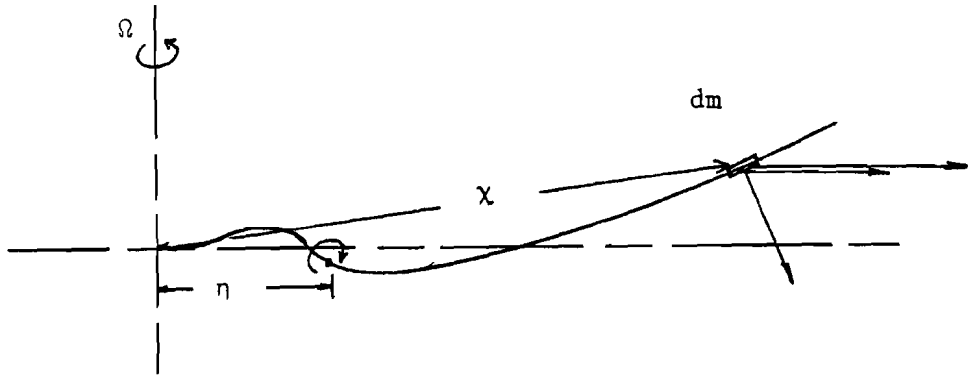

Figure 40. Elastic Blade

The geometry is more important in the calculation of mass and inertial loads; again a more exact method of solution would solve the blade motion as a combination of harmonic modes, establish the instantaneous blade shape, and calculate mass integrals to get the loading and iterate.[9] This present analysis approximates the complex geometry with the simple segmented blade. This approach allows an analytical solution, which is then investigated to gain insight and preliminary loads, rather than detailed design.

When the integration along the blade is performed as before, dynamic (time dependent) terms, $\dot{\beta}$, $\ddot{\beta}$, will appear. These are a result of the inertial loads and (coupled) loads due to velocity (Coriolis). Therefore, the moments cannot be calculated unless a function $\beta(t)$ is known; or in this analysis, β_o, β_{1s}, and β_{1c}, where time dependency has been reduced to azimuthal dependency. If a motion solution is known, as in Chapter III, then these terms can be calculated, and time varying values of loading and moment distributions will be found. For present purposes, a "static" solution, which sets all dynamic terms to zero,

will be sought. Again, the justification for this step is to look for modal simplicity, as in the case of the airloads and to gain insight. It is a straightforward task to add the motion solution as described. Also, if only the root moments are calculated, as in Section A, the moments are automatically azimuth (time) dependent. Before continuing with the "static" solution, the classical method of handling dynamic loads will be described.

One valuable engineering approach to the estimation of dynamic loads is to calculate a "dynamic load magnification factor." Briefly, this approximate method separates the blade deflection into normal modes, expressed analytically or in tabular form.[14] The elastic blade bending equation in flapping is (neglecting all but aerodynamic and inertial forces):

$$\frac{d^2}{dr^2}\left[EI \frac{d^2\hat{Z}}{dr^2} \right] - P(r) \frac{d^2\hat{Z}}{dr^2} + mr\Omega^2 \frac{dZ}{dr} + m\ddot{Z} + D\dot{Z} = \frac{d\ell(r)}{dr} \qquad \text{(IV-19)}$$

where:

$\hat{Z}$ = axial (flapping) coordinate

$P(r) = \int_r^R \eta\Omega^2 \, m d\eta$ = centrifugal force term

$\ell(r)$ = aerodynamic lift force

$D = \Delta$ angle of attack term extracted from the lift term

(Note: this term constitutes all the damping in the system, and is due to aerodynamics.)

This equation appears in slightly different form in many textbooks, and in the rotor literature; but the intent of this argument is to illustrate an alternative method of solution to that of this dissertation. Going

on, in IV-19, the lift, $\ell(r)$, can be expressed in any convenient way, with consistent simplifications, as is done in this dissertation.

The final form of IV-19 is then:

$$m\ddot{Z} + D\dot{Z} + \phi(Z) = \frac{d\ell(r,t)}{dr} \qquad \text{(IV-20)}$$

$$\phi(Z) = \frac{d^2}{dr^2}\left[EI \frac{d^2Z}{dr^2} \right] - P(r) \frac{d^2Z}{dr^2} + rm\Omega^2 \frac{dZ}{dr} \qquad \text{(IV-21)}$$

The "static bending" equation, IV-21, is solved in the classical way, by assuming normal modes, $\eta_k(r)$:

$$Z = \sum_{k=1}^{\infty} \eta_k(r)\, g_k(t) \qquad \text{(IV-22)}$$

Simple harmonic motion is assumed, and the integration is performed as follows, either analytically or numerically; we now have:

$$\int_o^R \eta_k{}^2(r)m(r)dr \left[\ddot{g}_k(t) + \left(\frac{\omega k}{\Omega}\right)^2 \Omega^2 g_k(t) \right] = \frac{d\ell(r,t)}{dr} \quad K = 1,2,3, \ldots \qquad \text{(IV-23)}$$

In the investigation of classical flutter on rotor blades, the above equation appears in more complex form in the literature,[14] including the aerodynamic forcing term and the coupled torsional spring term:

$$\int_o^R m(r)\eta_k^2(r) \left[\ddot{g}_k + \nu_k^2\, \Omega^2\, g_k \right] dr - \int_o^R X_I \eta_k m(r) \left[\ddot{\theta} + \Omega^2\theta \right] dr$$

$$- \int_o^R \eta_k \frac{d\ell}{dr}\, dr = 0 \qquad k = 1,2,3, \ldots$$

or:

$$\frac{\ddot{\beta}}{\Omega^2} + \beta - I_f \frac{\ddot{\theta}}{\Omega^2} - I_f\theta - \frac{1}{I_b\Omega^2} \int_o^R \frac{d\ell}{dr}\, rdr = 0$$

if the first mode only is considered on a uniform blade.

When the static equation, IV-21, is solved, the static moment is found from:

$$M_s = EI \frac{d^2Z}{dr^2} \qquad \text{(IV-24)}$$

Engineering procedure is to find an appropriate dynamic magnification factor to multiply IV-24,[26] to account for blade dynamics, or response to a periodic input. Equation IV-20 is generalized:

$$\ddot{g}_k(t) + \sigma_k \dot{g}_k(t) + \omega_k^2 g_k(t) = \sum_{n=1}^{\infty} C_{k_n} e^{in\Omega t} \qquad \text{(IV-25)}$$

And the assumed response of the $k^{\underline{th}}$ bending mode to the $n^{\underline{th}}$ harmonic forcing function is:

$$g_{kn} = \bar{g}_{kn} e^{i[n\Omega t + \phi_{kn}]}$$

where:

$\bar{g}_{kn}$ = amplitude of mode

n = $n^{\underline{th}}$ harmonic forcing function

k = $k^{\underline{th}}$ bending mode

ϕ = phase angle

Substitution gives the straightforward result:

$$A_{kn} = \frac{\text{dynamic amplitude}}{\text{static amplitude}} = \frac{\bar{g}_{kn}}{\bar{g}_{k_{n_s}}} = \frac{\omega_k^2}{\sqrt{(\omega_k^2 - n^2\Omega^2)^2 + n^2\Omega^2\sigma_k^2}}$$

or:

$$A_{kn} = \frac{1}{\sqrt{\left(1 - \frac{n^2}{\nu_k^2}\right)^2 + \frac{n^2\sigma_k^2}{\Omega^2\nu_k^2}}} \qquad \text{Dynamic Magnification Factor}$$

(IV-26)

where:

$$\nu_k = \frac{\omega_k}{\Omega}$$

σ_k = aerodynamic damping term from IV-25

$$= \frac{\int_0^R \eta_k^2 \, D \, dr}{\int_0^R \eta_k^2 \, m \, dr}$$

Equation IV-26 then gives the familiar frequency ratio - amplitude ratio plot showing resonance of a single degree of freedom system, in this case, the $k^{\underline{th}}$ bending mode of the elastic blade:

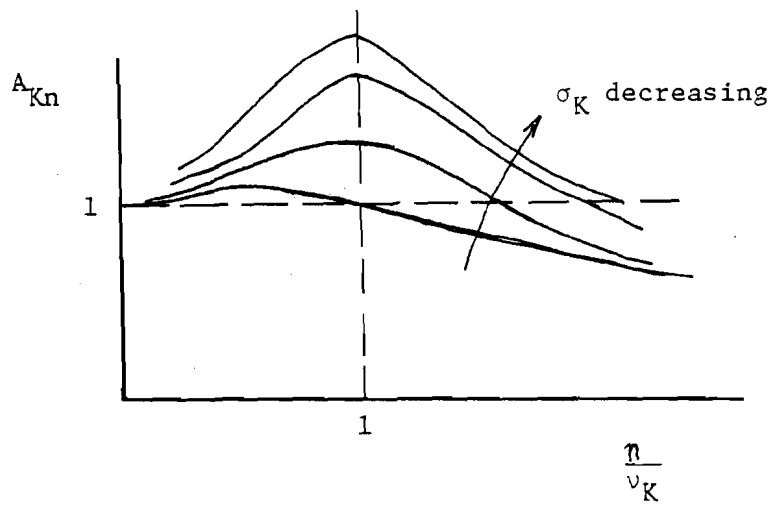

Figure 41. General Frequency Ratio - Amplitude

We have restricted our dynamics to a single flapping (and a single lead-lag) mode. Again, a more complete analysis would assume a number of orthogonal modes, and solve for a dynamic amplification (and phase) for each one, in the manner illustrated here. In general:

$$Z = \sum_{n=1}^{\infty} \eta_k(r)\ g_k(t) \qquad \text{(IV-22)}$$

$$= \eta_1(r)\ g_1(t) + \eta_2(r)\ g_2(t) + \ldots$$

$$= r\beta \qquad\qquad + \eta_2\ g_2 + \ldots$$

and $\eta = r\beta$ for the simple straight blade used here. From equation III-6, the flapping equation of motion:

$$D = \begin{matrix}\text{damping in}\\ \text{flapping}\end{matrix} = \frac{\gamma}{8}\ m\ \Omega$$

Integrating to find σ_1:

$$\sigma_k = \frac{\int_o^R \eta_k^2\ D\ dr}{\int_o^R \eta_k^2\ m\ dr} \quad \frac{\int_o^R r^2(\frac{\gamma}{8}\ m\Omega)\ dr}{\int_o^R r^2\ m\ dr} = \frac{\gamma}{8}\ \Omega = \sigma_1 \qquad \text{(IV-27)}$$

So the amplification factor is:

$$\boxed{A_{1n} = \frac{1}{\left[\ (1 - \frac{n^2}{\nu_1^2})^2 + (\frac{\gamma}{8})^2\ (\frac{n}{\nu_1})^2\ \right]^{1/2}}} \qquad \text{(IV-28)}$$

A_{1n} is plotted in Figure 42 for four values of Lock number, γ. It can be seen that critical damping occurs for a Lock number between 8 and 12. For lower Lock numbers, the dynamic multiplication factor can be very high over a large range of forcing frequency. Thus, with this simple analysis, a magnification of 1.5 to 2.0 on static bending moment must be used for the Jacob's blade ($\gamma \approx 4.1$).[19] This simple approach would not be expected to give very accurate blade loads, but is certainly an indication of magnitudes, and serves as a rule of thumb.

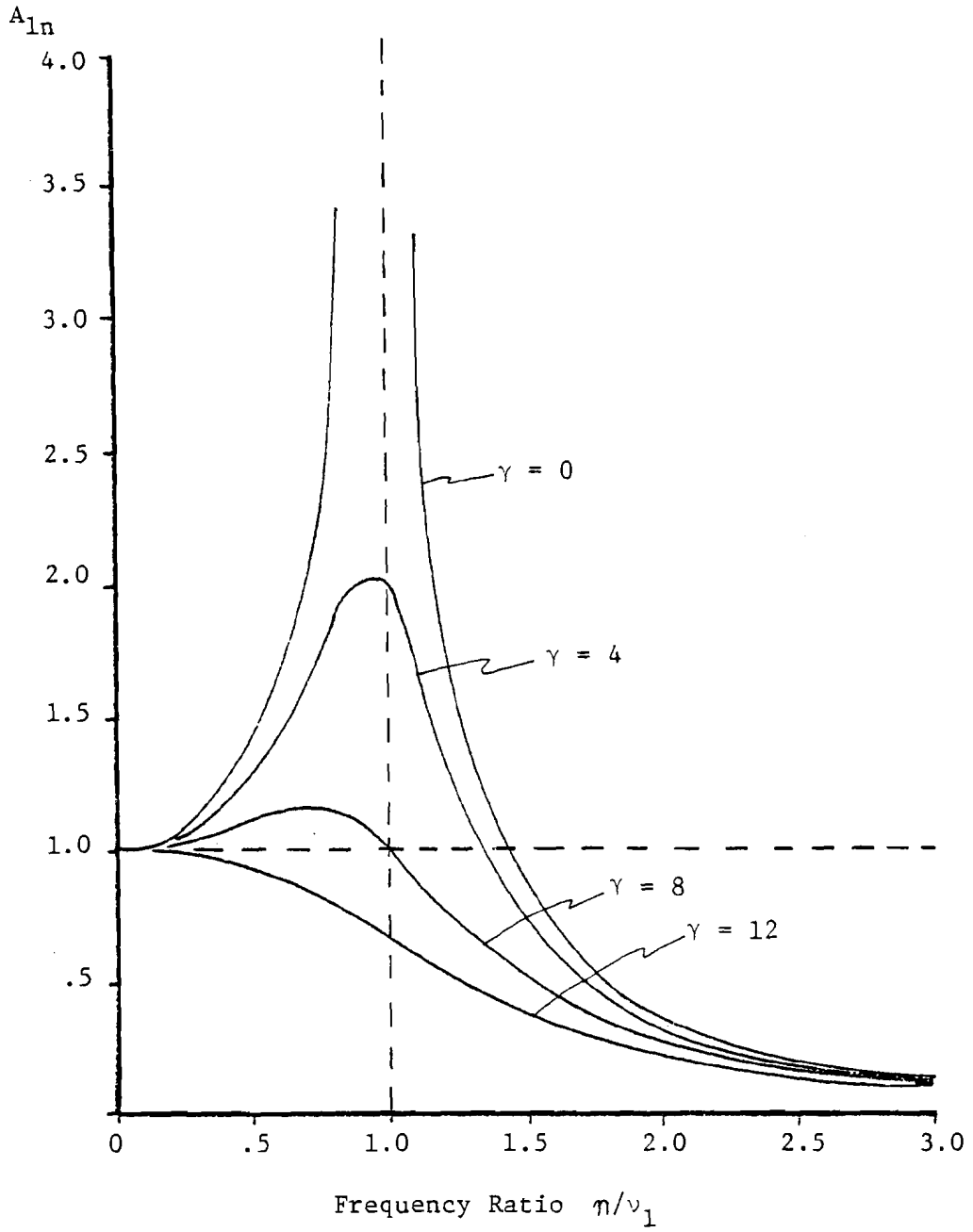

Figure 42. Flapping Dynamic Amplification Factor, First Mode

Should higher blade bending modes be used, amplification factors for them will be calculated in the same way. A problem exists in the summation of dynamic modes. To obtain the dynamic bending moment from the static bending moment, there will be more than one amplification factor. Two methods are commonly used. The Goodyear method assumes the dominant component of the dynamic moment is due to the amplitude of the $k^{\underline{th}}$ mode response, thus:[26]

$$M_n = A_{kn} M_{ns} \qquad \text{Goodyear Method}$$

In Flax's method,[26] the amplification factor is applied only to the static bending moment corresponding to the displacement of the $k^{\underline{th}}$ mode:

$$\Delta M_{ns} = M_{ns} - M_{nk_s}$$

$$\text{then } M_n = \Delta M_{ns} + A_{kn} M_{nk_s} \qquad \text{Flax's Method}$$

Both methods apply the $k^{\underline{th}}$ mode which is closest to resonance with the $n^{\underline{th}}$ harmonic airload (or forcing function) being considered. Multiple dynamic loads will occur for multiple frequency inputs, and all must be added to calculate the "best guess" dynamic bending moment.

D. Inertial Loads

From the last section, the flapping diagram is again:

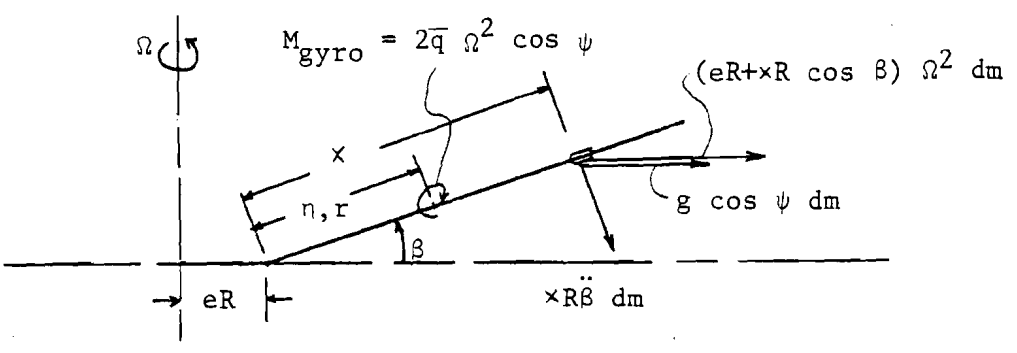

Figure 43. Flapping Diagram

Summing the moments at spanwise station η:

$$\Sigma dM\Big|_{\eta} = xR^2\ddot{\beta}\ (x-\eta)dm + g\ \cos\ \psi\ \sin\ \beta\ R(x-\eta)dm$$
$$+ (e + x\ \cos\ \beta)\ R^2\ \Omega^2(x-\eta)dm + \frac{d}{d\eta}\ [\ 2\overline{q}\Omega^2\ \cos\ \psi\ ] \qquad \text{(IV-29)}$$

The bending moment is obtained by integration along the segment η to 1.0:

$$M_\beta(\eta) = R^3\ddot{\beta}\int_\eta^1 x(x-\eta)m\ dx + g\ \cos\ \psi\ \beta\ \ R^2\int_\eta^1 (x-\eta)m\ dx$$
$$+ \beta\ eR(\Omega R)^2\int^1 (x-\eta)m\ dx + \beta\ R(\Omega R)^2\int^1 x(x-\eta)m\ dx$$
$$+ 2\overline{q}\Omega^2\ \cos\ \psi \qquad \text{(IV-30)}$$

Or:

$$M_\beta = R^3\ \ddot{\beta}\ I_1 - R^3\ \beta\ I_2 + g\ \cos\ \psi\ \beta\ R^2\ I_3 - g\ \cos\ \psi\ \beta\ R^2\ I_4$$
$$+ eR(\Omega R)^2\beta\ I_3 - eR(\Omega R)^2\beta\ I_4$$
$$+ R(\Omega R)^2\beta\ I_1 - R(\Omega R)^2\beta\ I_2 + 2\overline{q}\ \Omega^2\ \cos\ \psi \qquad \text{(IV-31)}$$

Where the mass integrals are:

$$I_1 = \int_\eta^1 m\ x^2\ dx$$

$$I_2 = \int_\eta^1 m\ x\ \eta\ dx$$

$$I_3 = \int_\eta^1 m\ x\ dx$$

$$I_4 = \int_\eta^1 m\ \eta\ dx \qquad \text{(IV-32)}$$

For a uniform blade (m = constant) the integrals are:

$$I_1 = \frac{I_b}{R^3} \; [\; 1-\eta^3 \;]$$

$$I_2 = \frac{3I_b}{2R^3} \; \eta \; [\; 1-\eta^2 \;]$$

$$I_3 = \frac{3I_b}{2R^3} \; [\; 1-\eta^2 \;]$$

$$I_4 = \frac{3I_b}{R^3} \; \eta \; [\; 1-\eta \;]$$

And equation IV-31 reduces to:

$$M_\beta = I_b \; \ddot{\beta} \; [\; \tfrac{1}{2}(\eta-1)^2(\eta+2) \;] + I_b \; \frac{\beta}{R} \; [\; \tfrac{3}{2} \; g \cos \psi \; (\eta-1)^2 \;]$$

$$+ I_b \; \beta \; \Omega^2 \; [\; \tfrac{3}{2} \; e(\eta-1)^2 + \tfrac{1}{2}(\eta-1)^2 \; (\eta+2) \;] + 2\overline{q} \; \Omega^2 \cos \psi \qquad \text{(IV-33)}$$

Using the non-dimensional quantities derived before, we get:

$$\boxed{\begin{aligned} \frac{M_\beta}{I_b \Omega^2} &= \frac{\ddot{\beta}}{\Omega^2} \; [\; \tfrac{1}{2}(\eta-1)^2(n+2) \;] + \frac{2\overline{q}}{I_b} \cos \psi \\ &\quad + \beta \; [\; \frac{G}{\Omega^2} \cos \psi \; (\eta-1)^2 + \varepsilon \; (\eta-1)^2 + \tfrac{1}{2}(\eta-1)^2(\eta+2) \;] \end{aligned}}$$

Flapping Moment (IV-34)

Where:

$$\varepsilon = \frac{M_b \; e \; X_g \; R^2}{I_b} = \frac{3e}{2(1-e)}$$

$$I_b = \frac{MR^2}{3} = \frac{mR^3}{3}$$

$$X_g = \frac{r_g}{R} = \frac{1}{2}$$

$$G = \frac{g \; M_b \; X_g \; R}{I_b}$$

The moment at the root, $\eta = 0$, is:

$$\left.\frac{M_\beta}{I_b\Omega^2}\right|_{\eta=0} = \frac{\ddot{\beta}}{\Omega^2} + \beta\left[\frac{G}{\Omega^2}\cos\psi + \varepsilon + 1\right] + 2\frac{\overline{q}}{I_b}\cos\psi \qquad \text{(IV-35)}$$

This is identical to the result already derived, (II-4), excluding the hinge spring moment and including the gyroscopic moment due to $\overline{q}$.

The bracketed terms in IV-34 again represent mode shapes, or moment distributions, as for the aerodynamic moments in Section A. The mass integrals can be related to these terms as follows:

$$\int_\eta^1 m_x(x-\eta)d\eta = I_1 - I_2 = \frac{M_b}{R}\left[\frac{1}{6}(\eta-1)^2(\eta+2)\right]$$

$$\int_\eta^1 m(x-\eta)d\eta = I_3 - I_4 = \frac{M_b}{R}\frac{(\eta-1)^2}{2} \qquad \text{(IV-36)}$$

For Uniform Blade

Thus, the flapping moment in terms of the mass integrals is now:

$$\frac{M_\beta}{I_b\Omega^2} = \frac{3\ddot{\beta}}{\Omega^2}\frac{R}{M_b}\left[I_1-I_2\right] + \frac{2\overline{q}}{I_b}\cos\psi$$

$$+ \beta\ 2\left(\frac{G\cos\psi}{\Omega^2} + \varepsilon\right)\left(\frac{R}{M_b}\right)\left[I_3-I_4\right] + 3\left(\frac{R}{M_b}\right)\left[I_1-I_2\right] \qquad \text{(IV-37)}$$

As before, the shear and loading can be found by differentiating. We have for the flapping solution:

Moment

$$\frac{M_\beta}{I_b\Omega^2} = \frac{\ddot{\beta}}{\Omega^2}\left[\frac{1}{2}(\eta-1)^2(\eta+2)\right] + \frac{2\bar{q}}{I_b}\cos\psi$$

$$+ \beta\left[\left(\frac{G\cos\psi}{\Omega^2} + \varepsilon\right)(\eta-1)^2 + \frac{1}{2}(\eta-1)^2(\eta+2)\right]$$

Shear

$$\frac{S_\beta}{I_b\Omega^2} = \frac{\ddot{\beta}}{\Omega^2 R}\left[\frac{3}{2}(\eta^2-1)\right] + \frac{\beta}{R}\left[\left(\frac{G\cos\psi}{\Omega^2} + \varepsilon\right)2(\eta-1) + \frac{3}{2}(\eta^2-1)\right]$$

Load

$$\frac{L_\beta}{I_b\Omega^2} = \frac{\ddot{\beta}}{\Omega^2 R^2}\left[3\eta\right] + \frac{\beta}{R^2}\left[\left(\frac{G\cos\psi}{2} + \varepsilon\right)2 + 3\eta\right] \qquad \text{(IV-38)}$$

In terms of the mass integrals the solution is:

Moment

$$\frac{M_\beta}{I_b\Omega^2} = \frac{3\ddot{\beta}}{\Omega^2}\left(\frac{R}{M_b}\right)\left[I_1-I_2\right] + \frac{2\bar{q}}{I_b}\cos\psi$$

$$+ \beta\; 2\left(\frac{G\cos\psi}{\Omega^2} + \varepsilon\right)\left(\frac{R}{M_b}\right)\left[I_3-I_4\right] + 3\left(\frac{R}{M_b}\right)\left[I_1-I_2\right]$$

Shear

$$\frac{S_\beta}{I_b\Omega^2} = \frac{3\ddot{\beta}}{\Omega^2 R}\left(\frac{R}{M_b}\right)\frac{d}{d\eta}\left[I_1-I_2\right]$$

$$+ \frac{\beta}{R}\; 2\left(\frac{G\cos\psi}{\Omega^2} + \varepsilon\right)\left(\frac{R}{M_b}\right)\frac{d}{d\eta}\left[I_3-I_4\right] + 3\left(\frac{R}{M_b}\right)\frac{d}{d\eta}\left[I_1-I_2\right]$$

Load

$$\frac{L_\beta}{Ib\Omega^2} = \frac{3\ddot{\beta}}{\Omega^2 R^2}\left(\frac{R}{M_b}\right)\frac{d^2}{d\eta^2}\left[I_1-I_2\right]$$

$$+ \frac{\beta}{R^2}\; 2\left(\frac{G\cos\psi}{\Omega^2} + \varepsilon\right)\left(\frac{R}{M_b}\right)\frac{d^2}{d\eta^2}\left[I_3-I_4\right] + 3\left(\frac{R}{M_b}\right)\frac{d^2}{d\eta^2}\left[I_1-I_2\right]$$

(IV-39)

The lead-lag diagram is:

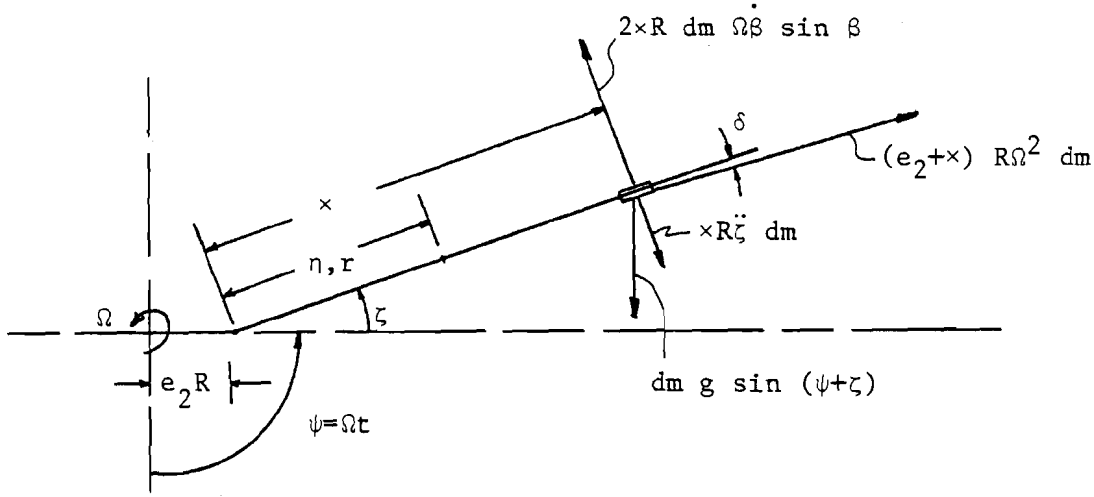

Figure 44. Lead-Lag Diagram

Again, summing moments at η:

$$\Sigma\, dM\Big|_{\eta} = \times R^2\, \ddot{\zeta}(\times-\eta)\, dm + g \sin(\psi + \zeta) R \cos \zeta(\times-\eta)\, dm$$
$$+ (e_2+\times)\, R\Omega^2\, dm \sin \delta(\times-\eta)R - 2\times R^2\Omega\, \dot{\beta} \sin \beta(\times-\eta)\, dm \qquad \text{(IV-40)}$$

The integration is performed:

$$M_\zeta(\eta) = R^3\ddot{\zeta} \int_\eta^1 \times(\times-\eta)m\, d\times + g\,(\sin\psi + \zeta\cos\psi)R^2 \int_\eta^1 (\times-\eta)m\, d\times$$
$$+ e_2R\,\zeta(\Omega R)^2 \int_\eta^1 (\times-\eta)m\, d\times - 2\Omega\dot{\beta}\beta\, R^3 \int_\eta^1 \times(\times-\eta)m\, d\times \qquad \text{(IV-41)}$$

And as before, with a uniform blade, the moment is:

$$\boxed{\begin{aligned}\frac{M_\zeta}{I_b\Omega^2} = \frac{\ddot{\zeta}}{\Omega^2}\left[\frac{1}{2}(\eta+2)(\eta-1)^2\right] + \zeta\left[\frac{G}{\Omega^2}\cos\psi + \varepsilon_2\right](\eta-1)^2 \\ - 2\frac{\dot{\beta}}{\Omega}\beta\left[\frac{1}{2}(\eta-2)(\eta-1)^2\right] + \frac{G}{\Omega^2}\sin\psi\,(\eta-1)^2\end{aligned}} \qquad \text{(IV-42)}$$

Lead-Lag Moment

At the root, the moment checks with exp. II-9:

$$\frac{M_{\zeta_o}}{I_b\Omega^2} = \frac{\ddot{\zeta}}{\Omega^2} + \zeta\left[\frac{G}{\Omega^2}\cos\psi + \varepsilon_2\right] - 2\frac{\dot{\beta}}{\Omega}\beta + \frac{G}{\Omega^2}\sin\psi$$

The shear and loading are found by integration:

$$\frac{S_\zeta}{I_b\Omega^2} = \frac{\ddot{\zeta}}{\Omega^2 R}\left[\frac{3}{2}(\eta^2-1)\right] + \frac{\zeta}{R}\left[\frac{G}{\Omega^2}\cos\psi + \varepsilon_2\right]2(\eta-1)$$

$$- \frac{2\dot{\beta}\beta}{\Omega R}\left[\frac{3}{2}(\eta^2-1)\right] + \frac{G\sin\psi}{\Omega^2 R}\,2(\eta-1) \qquad \text{(IV-43)}$$

$$\frac{L_\zeta}{I_b\Omega^2} = \frac{\ddot{\zeta}}{\Omega^2 R^2}[3\eta] + \frac{\zeta}{R^2}\left[\frac{G}{\Omega^2}\cos\psi + \varepsilon_2\right](2) - \frac{2\dot{\beta}\beta}{\Omega R^2}(3\eta) + \frac{G\sin\psi}{\Omega^2 R^2}(2) \qquad \text{(IV-44)}$$

In terms of the mass integrals I_i:

Moment

$$\frac{M_\zeta}{I_b\Omega^2} = \frac{3\ddot{\zeta}}{\Omega^2}\left(\frac{R}{M_b}\right)[I_1-I_2] + \zeta\left\{2\left(\frac{G}{\Omega^2}\cos\psi + \varepsilon_2\right)\left(\frac{R}{M_b}\right)[I_3-I_4] - \frac{6\dot{\beta}\beta}{\Omega}\left(\frac{R}{M_b}\right)[I_1-I_2] + \frac{2G\sin\psi}{\Omega^2}\left(\frac{R}{M_b}\right)[I_3-I_4]\right\}$$

Shear

$$\frac{S_\zeta}{I_b\Omega^2} = \frac{3\ddot{\zeta}}{R\Omega^2}\left(\frac{R}{M_b}\right)\frac{d}{d\eta}[I_1-I_2] + \frac{\zeta}{R}\left\{2\left(\frac{G}{\Omega^2}\cos\psi + \varepsilon_2\right)\left(\frac{R}{M_b}\right)\frac{d}{d\eta}[I_3-I_4] - \frac{6\dot{\beta}\beta}{\Omega R}\left(\frac{R}{M_b}\right)\frac{d}{d\eta}[I_1-I_2] + \frac{2G\sin\psi}{\Omega^2 R}\left(\frac{R}{M_b}\right)\frac{d}{d\eta}[I_3-I_4]\right\}$$

Load

$$\frac{L_\zeta}{I_b\Omega^2} = \frac{3\ddot{\zeta}}{\Omega^2 R^2}\left(\frac{R}{M_b}\right)\frac{d^2}{d\eta^2}[I_1-I_2] + \frac{\zeta}{R^2}\left\{2\left(\frac{G}{\Omega^2}\cos\psi + \varepsilon_2\right)\left(\frac{R}{M_b}\right)\frac{d^2}{d\eta^2}[I_3-I_4] - \frac{6\dot{\beta}\beta}{\Omega R^2}\left(\frac{R}{M_b}\right)\frac{d^2}{d\eta^2}[I_1-I_2] + \frac{2G\sin\psi}{\Omega^2 R^2}\left(\frac{R}{M_b}\right)\frac{d^2}{d\eta^2}[I_3-I_4]\right\}$$

(IV-45)

In summary, the loading, shear, and moment expressions for the blade have been found for flapping and lead-lag directions. When the d^2/dt^2 terms are set to zero, these are the static loading solutions, and they must be multiplied by the dynamic amplification factor if the dynamic moments are needed. For a uniform blade (or for preliminary design) expressions IV-38 and IV-42, 43, 44 give the mode shapes and coefficients of the loading by setting the time derivative to zero ($\ddot{\beta} = \ddot{\zeta} = 0$).

E. Loading Distributions

The uniform distribution of mass assumption is a good one for conventional rotor blades; but most wind turbines have a variable mass per unit length. Two other mass distributions will be investigated, and the mode shapes of the moment, shear and loading will be calculated in this section.

For a blade with linear mass distribution decreasing to zero at the tip, we have:

$$m(r) = \frac{2\ M_b}{R}\left[1 - \frac{r}{R}\right] = \frac{2\ M_b}{R}\left[1 - \eta\right] \qquad \text{(IV-46)}$$

Linear Mass Distribution

The mass integrals are:

$$I_1 = \int_{\eta}^{1} m\ x^2\ dx = \frac{M_b}{6R}\left[3\eta^4 - 4\eta^3 + 1\right]$$

$$I_2 = \int_{\eta}^{1} m\ \eta\ x\ dx = \frac{M_b}{3R}\ \eta\ \left[2\eta^3 - 3\eta^2 + 1\right]$$

$$I_3 = \int_{\eta}^{1} m \times dx = \frac{M_b}{3R} [2\eta^3 - 3\eta^2 + 1]$$

$$I_4 = \int_{\eta}^{1} m \eta \, dx = \frac{M_b}{R} \eta [\eta^2 - 2\eta + 1] \qquad \text{(IV-47)}$$

The mode terms are then:

$$\boxed{\begin{aligned} I_1 - I_2 &= \int_{\eta}^{1} mx \, (x-\eta) dx = \frac{M_b}{R} [\tfrac{1}{6}(1 - 2\eta + 2\eta^3 - \eta^4)] \\ I_3 - I_4 &= \int_{\eta}^{1} m(x-\eta) \, dx = \frac{M_b}{R} [\tfrac{1}{3}(1 - 3\eta + 3\eta^2 - \eta^3)] \end{aligned}} \qquad \text{(IV-48)}$$

Linear Mass Distribution

For a blade with parabolic mass distribution, decreasing to zero at the tip, we have:

$$m(r) = \frac{3M_b}{R} [1 - \frac{r}{R}]^2 = \frac{3M_b}{R} [1 - \eta]^2 \qquad \text{(IV-49)}$$

Parabolic Mass Distribution

Likewise the mass integrals and mode terms are:

$$I_1 = \frac{M_b}{10R} [1 - 10\eta^3 + 15\eta^4 - 6\eta^5]$$

$$I_2 = \frac{M_b}{4R} \eta [1 - 6\eta^2 + 8\eta^3 - 3\eta^4]$$

$$I_3 = \frac{M_b}{4R} [1 - 6\eta^2 + 8\eta^3 - 3\eta^4]$$

$$I_4 = \frac{M_b}{R} \eta [1 - 3\eta + 3\eta^2 - \eta^3] \qquad \text{(IV-50)}$$

$$\boxed{\begin{aligned} I_1 - I_2 &= \frac{M_b}{R} [\tfrac{1}{20}(2 - 5\eta + 10\eta^3 - 10\eta^4 + 3\eta^5)] \\ I_3 - I_4 &= \frac{M_b}{R} [\tfrac{1}{4}(1 - 4\eta + 6\eta^2 - 4\eta^3 + 4\eta^4)] \end{aligned}} \qquad \text{(IV-51)}$$

Parabolic Mass Distribution

The mode shapes are summarized in Table 3; there are two modes for moment, shear, and loading, for each of the mass distributions of interest: uniform, linear, and parabolic.

The load and moment distribution are plotted in Figures 45 and 46. The mode diagrams are all comparable since they are drawn to the same normalized scale. As would be expected, the loading is highest for the parabolic blade near the root, where mass is concentrated; and the corresponding moments are low since moment arms are smaller. As for all cantilevers, the maximum bending moments occur at the root, and all moment distributions are higher order.

The engineering solution is to calculate the coefficients in the equations and multiply them times their corresponding modes. The aerodynamic modes from Section A must be added, and dynamic amplification factors must be found for the periodic functions at their corresponding frequencies.

F. Blade Tension

The spanwise, or tension force in the blade consists of the centrifugal spanwise component, and the periodic gravity force. The sine components of these forces occur in both the flapping and lead-lag equations; the tension equation includes the cosine components:

$$T(\eta) = \begin{matrix}\text{blade}\\ \text{tension}\end{matrix} = \int_{\eta}^{1} (e + x \cos \beta)\Omega^2 R \, dm + \int_{\eta}^{1} g \cos \psi \, dm \qquad \text{(IV-52)}$$

Integration yields:

$$T(\eta) = e(\Omega R)^2 \int_{\eta}^{1} m \, dx + (\Omega R)^2 \int_{\eta}^{1} m \, x \, dx + g \, R \cos \psi \int_{\eta}^{1} m \, dx$$

Table 3. Summary of Blade Mode Shapes

		Uniform Blade: $m = \frac{M_b}{R}$	Linear Distribution: $m = \frac{2M_b}{R}(1-\eta)$	Parabolic Distribution: $m = \frac{3M_b}{R}(1-\eta)^2$
		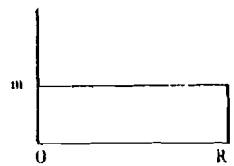	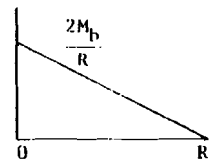	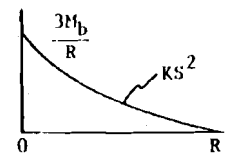
MOMENT	$\int_\eta^1 mx(x-\eta)dx$	$\frac{M_b}{R}\left[\frac{1}{6}(\eta^3-3\eta+2)\right]$	$\frac{M_b}{R}\left[\frac{1}{6}(1-2\eta+2\eta^3-\eta^4)\right]$	$\frac{M_b}{R}\left[\frac{1}{20}(2-5\eta+10\eta^3-10\eta^4+3\eta^5)\right]$
	$\int_\eta^1 m(x-\eta)dx$	$\frac{M_b}{R}\left[\frac{1}{2}(\eta^2-2\eta+1)\right]$	$\frac{M_b}{R}\left[\frac{1}{3}(1-3\eta+3\eta^2-\eta^3)\right]$	$\frac{M_b}{R}\left[\frac{1}{4}(1-4\eta+6\eta^2-4\eta^3+\eta^4)\right]$
SHEAR	$\frac{d}{d\eta}\int_\eta^1 mx(x-\eta)dx$	$\frac{M_b}{R}\left[\frac{1}{2}(\eta^2-1)\right]$	$\frac{M_b}{R}\left[\frac{1}{3}(-1+3\eta^2-2\eta^3)\right]$	$\frac{M_b}{R}\left[\frac{1}{4}(-1+6\eta^2-8\eta^3+3\eta^4)\right]$
	$\frac{d}{d\eta}\int_\eta^1 m(x-\eta)dx$	$\frac{M_b}{R}\left[\eta-1\right]$	$\frac{M_b}{R}\left[-1+2\eta-\eta^2\right]$	$\frac{M_b}{R}\left[-1+3\eta-3\eta^2+\eta^3\right]$
LOADING	$\frac{d^2}{d\eta^2}\int_\eta^1 mx(x-\eta)dx$	$\frac{M_b}{R}\left[\eta\right]$	$\frac{M_b}{R}\left[2\eta(1-\eta)\right]$	$\frac{M_b}{R}\left[3\eta(1-2\eta+\eta^2)\right]$
	$\frac{d^2}{d\eta^2}\int_\eta^1 m(x-\eta)dx$	$\frac{M_b}{R}\left[1\right]$	$\frac{M_b}{R}\left[2(1-\eta)\right]$	$\frac{M_b}{R}\left[3(1-2\eta+\eta^2)\right]$

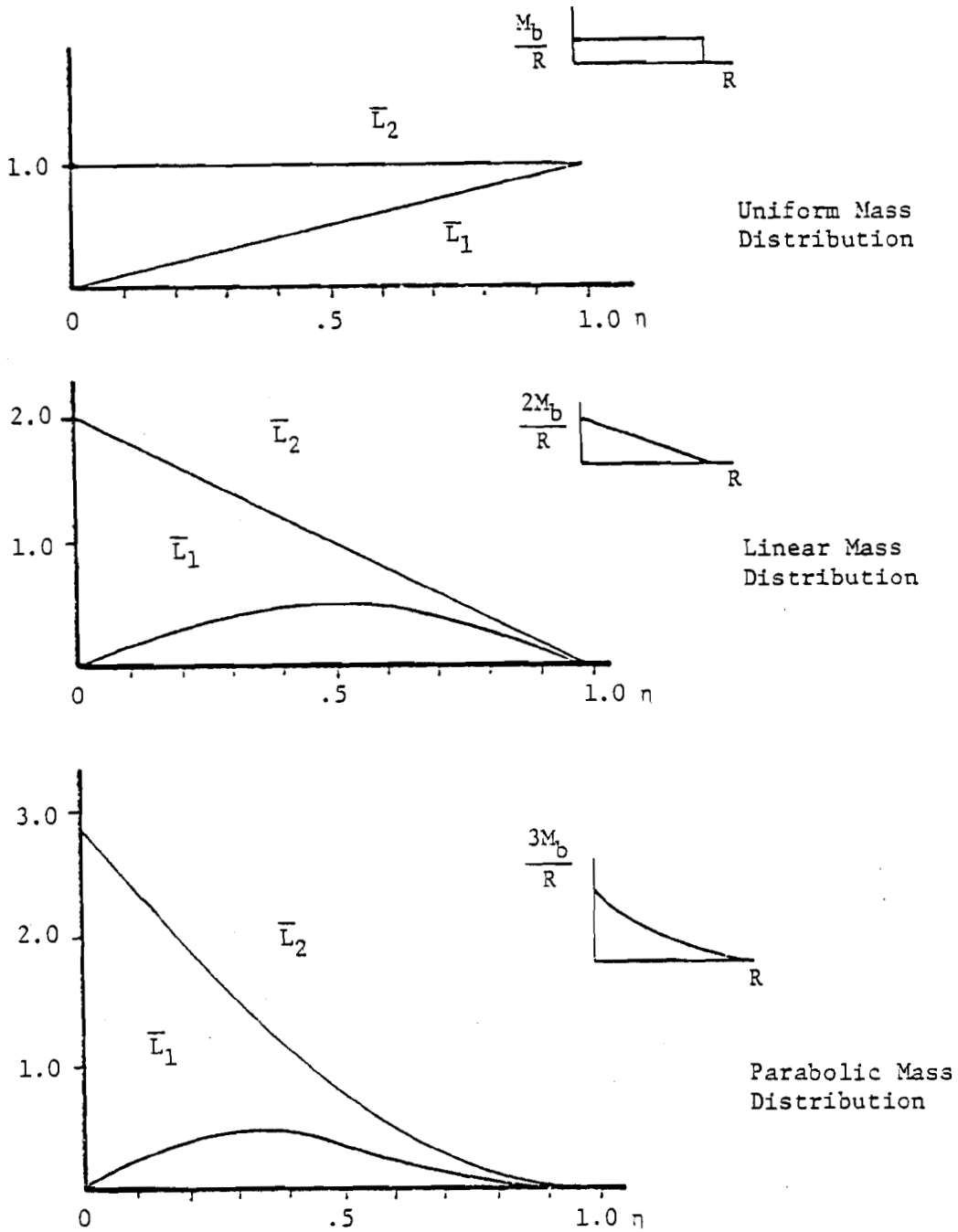

Figure 45. Loading Distributions

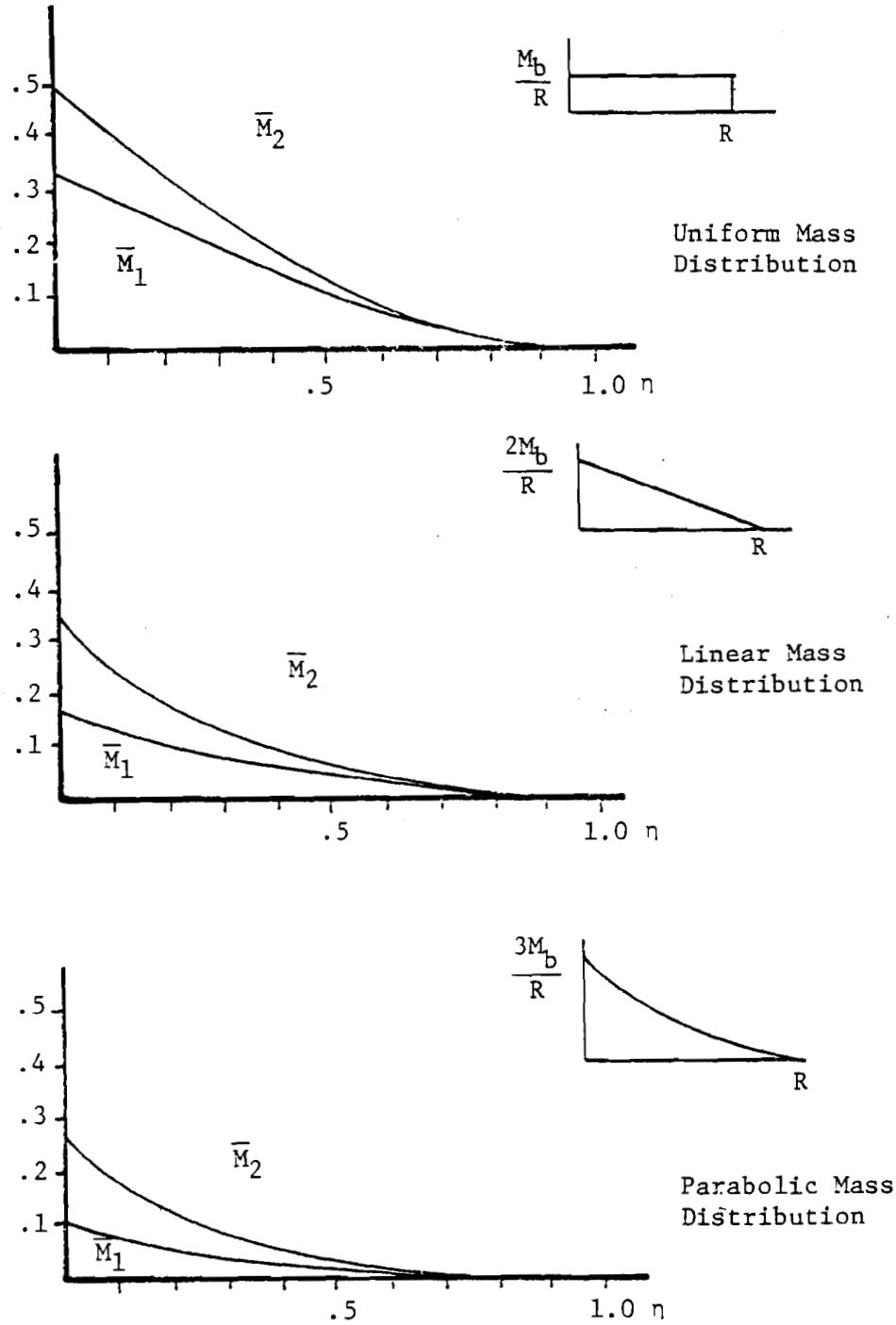

Figure 46. Moment Distributions

Or:

$$\boxed{T = (\Omega R)^2 \, [I_3 + eI_5] + g \, R \cos \psi \, I_5} \qquad \text{(IV-53)}$$

Blade Tension

Where:

$$I_3 = \int_{\eta}^{1} m \times dx \qquad \text{(as before)}$$

$$I_5 = \int_{\eta}^{1} m \, dx$$

The modes for blade tension due to the three mass distributions already considered are shown in Figure 47. Clearly, the periodic gravity term is important to blade root tension, and mass distribution has a major effect on tension distribution along the blade span.

G. Blade Torsion

The torsion along the blade was calculated in Chapter III; the feathering equation of motion is:

$$\boxed{\begin{aligned} &\frac{\ddot{\theta}}{\Omega^2} + [K_3 + 2B \left(\frac{I_b}{I_f+I_I}\right)\left(\frac{Y_I}{R}\right) \sin \psi] \, \theta \\ &= - \frac{M_a}{(I_f+I_I)\Omega^2} + \left(\frac{I_R}{I_f+I_I}\right)\beta + \left(\frac{I_b}{I_f+I_I}\right)\left(\frac{Y_a}{R}\right) \frac{\gamma}{4} \, [A_2 + \frac{2}{3}\beta' \\ &\quad + \sin \psi \left(\frac{2\overline{q}}{3} + \overline{U}_o\beta\right) + \frac{\theta_o}{6} + \frac{2\theta_p}{3}] \end{aligned}} \qquad \text{(III-66)}$$

where:

$$K_3 = 1 + \frac{K_\theta}{(I_f+I_I)\Omega^2} = \left(\frac{\omega_o}{\Omega}\right)^2$$

$$B = \frac{G}{2\Omega^2}$$

$$A_2 = \lambda_i - \mu_o$$

Figure 47. Blade Tension Modes and Distributions

	Uniform Blade $m = \frac{M_b}{R}$	Linear Mass Distribution $m = (\frac{2M_b}{R})[1-\eta]$	Parabolic Mass Distribution $m = (\frac{3M_b}{R})[1-\eta]^2$
$I_3 = \int_\eta^1 mx\,dx$	$\frac{M_b}{2R}[1-\eta^2]$	$\frac{M_b}{3R}[1-3\eta^2+2\eta^3]$	$\frac{M_b}{4R}[1-6\eta^2+8\eta^3-3\eta^4]$
$I_5 = \int_\eta^1 m\,dx$	$\frac{M_b}{R}[1-\eta]$	$\frac{M_b}{R}[1-\eta]^2$	$\frac{M_b}{R}[1-\eta]^3$

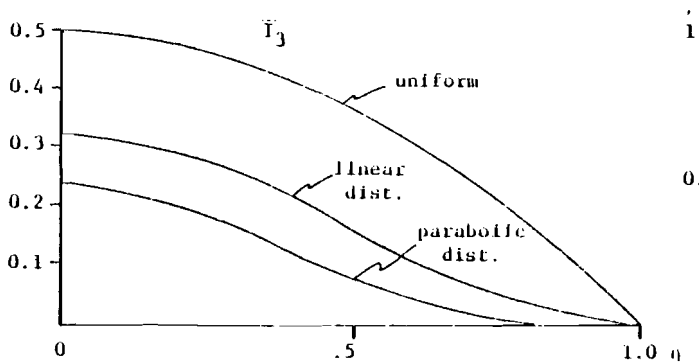

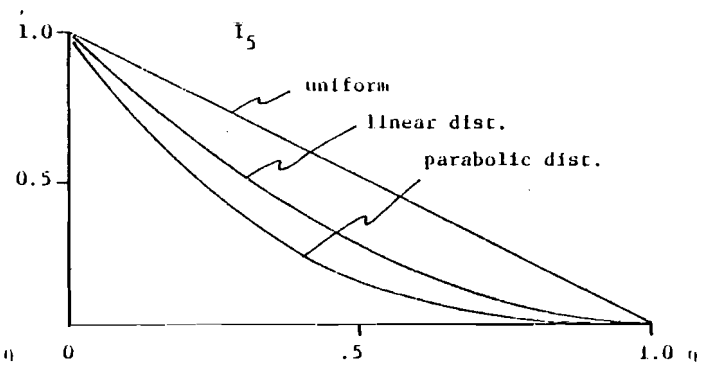

The right-hand side includes the effects of coning angle (steady β_o), aerodynamic center offset $(\frac{Y_a}{R})$, flapping velocity β', yaw rate $\overline{q}$, cross-wind $\overline{U}_o$, and twist. The "static" torsion is obtained by setting the $\ddot{\theta}$ dynamic term to zero, as before. A dynamic amplification factor could be obtained as in Section C for the dynamic load magnitude; in this case there is no torsional damping, so the factor is infinite at resonance. In actual practice, the torsional strength is never a design issue; it is torsional stiffness which dictates the design, in order to avoid the flutter and instabilities in the coupled system. This is discussed in Chapter VI. For the present, the "static" torsion can be calculated from exp. III-66. The torsion consists of steady terms due to pitching moment, coning angle, inflow, pitch and twist angle; it contains periodic terms due to gravity, yaw rate, and cross-wind. The periodic terms all appear at frequency Ω. It can be easily seen that cyclic pitch change could be introduced to nullify the periodic moments; actually, cyclic pitch could be used for rotor thrust direction changes in order to provide yaw moment and directional control.[27] The complexity of a swash plate, however, seems inconsistent with wind turbine goals and uneconomic in the long run.

CHAPTER V

ROTOR-TOWER DYNAMICS

The hub loads (blade root moments, shears and tension) developed in the last chapter are now transferred to the fixed, or tower system, and the individual blades are summed over the rotor. From the design standpoint, magnitudes and frequencies of the rotor forces and moments are critical factors in the tower and supports design. Steady tower loads arise from rotor thrust and torque and weight of the aloft system. However, the strength of the tower and supports must be sufficient to resist the maximum expected transient loading, and the stiffness must be determined to avoid instabilities. The frequencies and magnitudes of the operating loads of interest are developed in this chapter, and instabilities in coupled rotor-tower flapping and lead-lag are investigated.

A. Tower Moments: 1/Rev. Frequencies

A vector $\bar{R}$ rotating with the rotor at frequency $\Omega = \frac{d\psi}{dt}$, is transferred to the non-rotating tower system by:

$$\underset{\substack{X'Y'Z' \\ \text{non-rotating system}}}{\begin{Bmatrix} R_x' \\ R_y' \\ R_z' \end{Bmatrix}} = \begin{bmatrix} \cos\psi & -\sin\psi & 0 \\ \sin\psi & \cos\psi & 0 \\ 0 & 0 & 1 \end{bmatrix} \underset{\substack{\hat{X}\hat{Y}\hat{Z} \\ \text{rotating system}}}{\begin{Bmatrix} R_{\hat{x}} \\ R_{\hat{y}} \\ R_{\hat{z}} \end{Bmatrix}} \qquad \text{(V-1)}$$

The blade root moments consist of the flapping moment, $M_{\beta_o}(\psi)$, the lead-lag moment, $M_{\zeta_o}(\psi)$, and the torsional moment, $M_{\theta_o}(\psi)$ shown in Figure 48. We have in the rotating frame:

$$\begin{Bmatrix} M_{\hat{x}} \\ M_{\hat{y}} \\ M_{\hat{z}} \end{Bmatrix} = \begin{Bmatrix} M_{\theta_o} \\ -M_{\beta_o} \\ M_{\zeta_o} \end{Bmatrix} \tag{V-2}$$

And thus for the non-rotating frame:

$$\begin{Bmatrix} M_x' \\ M_y' \\ M_z' \end{Bmatrix} = \begin{bmatrix} \cos\psi & -\sin\psi & 0 \\ \sin\psi & -\cos\psi & 0 \\ 0 & 0 & 1 \end{bmatrix} \begin{Bmatrix} M_{\theta_o} \\ -M_{\beta_o} \\ M_{\zeta_o} \end{Bmatrix} \tag{V-3}$$

Then:

$$\boxed{\begin{aligned} M_x' &= M_{\theta_o} \cos\psi + M_{\beta_o} \sin\psi \\ M_y' &= M_{\theta_o} \sin\psi - M_{\beta_o} \sin\psi \\ M_z' &= M_{\zeta_o} \end{aligned}} \tag{V-4}$$

Fixed Tower Moments

The x' moment causes yaw of the nacelle (clockwise along x' axis; i.e., in the same direction as positive $\overline{q}$) and is reacted by torsion of the tower. The y' moment is a "pitching moment" on the tower, positive nose up, and is reacted on the pole matcher supports. The z' moment is the rotor windshaft torque reaction on the nacelle and tower.

The moments transmitted from the blades to the hub and tower depend on the type of hub being considered. An articulated hub has free hinges in flapping and lead-lag, and therefore receives no elastic restraint moment from the blade in either flapping or in lead-lag. The feathering moment in this case (for helicopters) is transmitted to the

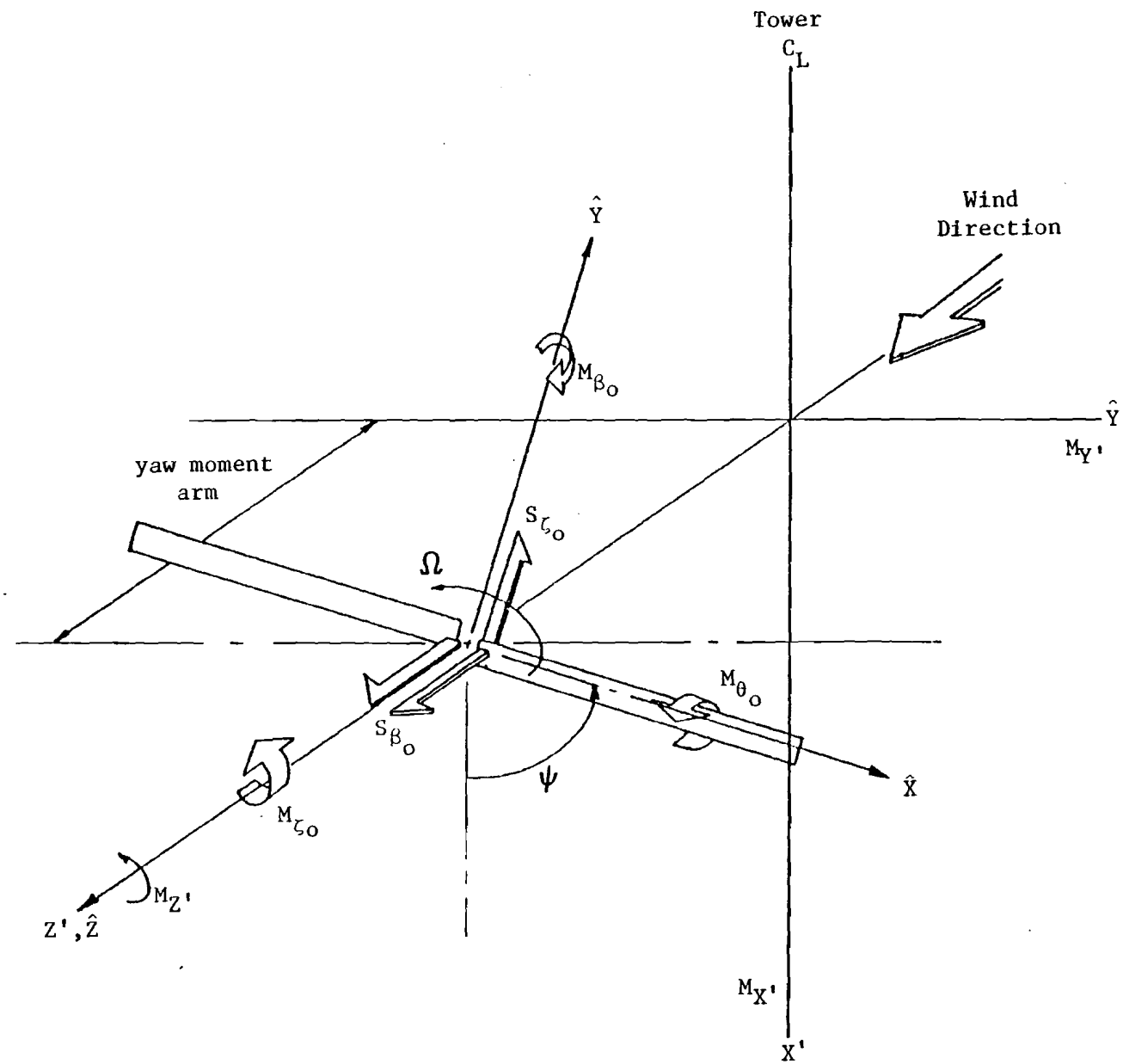

Figure 48. Hub Forces and Moments

rotor swash plate and control system through a mechanical arm linkage called a pitch link which implements pitch change commanded by the swash plate, and restrains the blade in feathering.[9] Few wind turbines have been built with articulation since the complexity of the hinges is costly. A teetering rotor has blades rigidly connected together (usually a two-bladed system) but gimballed to the rotating shaft. Inplane moments only are transmitted. The third and most usual type of configuration for wind turbines is simple cantilevered blades, or a hingeless rotor. All moments and forces are transmitted to the hub and in turn, the tower, as shown in Figure 48.

The most direct approach to get the root moments is to solve for the blade angular deflections, and write the elastic restraining moment as done in the last chapter. This gives:

$$M_{\beta_o} = K_\beta \, [\beta_o + \beta_{1c} \cos \psi + \beta_{1s} \sin \psi]$$

$$M_{\zeta_o} = K_\zeta \, [\zeta_o + \zeta_{1c} \cos \psi + \zeta_{1s} \sin \psi]$$

$$M_{\theta_o} = K_\theta \, [\theta_o + \theta_{1c} \cos \psi + \theta_{1s} \sin \psi] \qquad \text{(V-5)}$$

Blade Root Moments

These root moments, as solved in the last chapter, contain only the equilibrium rotor plane tilt angles. That is, the forcing functions allowed are at most frequency 1Ω, since the equilibrium motion solution is simple tilt of the rotor plane. The forcing functions considered (crosswind, gravity, etc.) are all at frequency 1Ω, so the steady-state solution will be at 1Ω also. All the transients, which occur at natural frequencies of the blades, will have died out. Hence, these moments (V-5) when transformed according to V-4 will determine the equilibrium

tower moments due to crosswind $\overline{U}_o$, yaw rate $\overline{q}$, gravity, mean inflow $(\mu_o - \lambda_i)$, pitch and twist angle, in the same way as did the blade motions in Chapter III. For instance, the flapping moment on the blade consists of delta angles due to the forcing functions:

$$\frac{M_{\beta_o}}{K_\beta} = \frac{\gamma A}{2\Delta}\left[(K-1)^2 + \left(\frac{\gamma}{8}\right)^2 \right] + \Delta\beta_o \Big|_{\text{due to } \overline{q}}$$

$$+ \Delta\beta_{1c}\Big|_{\text{due to gravity}} + \Delta\beta_{1c}\Big|_{\text{due to crosswind}} + \Delta\beta_{1c}\Big|_{\text{due to yaw}} \cos\psi$$

$$+ \Delta\beta_{1s}\Big|_{\text{due to gravity}} + \Delta\beta_{1s}\Big|_{\text{due to crosswind}} + \Delta\beta_{1s}\Big|_{\text{due to yaw}} \sin\psi \qquad \text{(V-6)}$$

Combining V-3, V-4, and V-5:

$$\boxed{\begin{aligned} M_x' &= \frac{1}{2}\left[K_\beta\beta_{1s} + K_\theta\theta_{1c} \right] + K_\beta\beta_o \sin\psi + K_\theta\theta_o \cos\psi \\ &+ \frac{1}{2}\left[K_\beta\beta_{1c} + K_\theta\theta_{1s} \right] \sin 2\psi + \frac{1}{2}\left[K_\theta\theta_{1c} - K_\beta\beta_{1s} \right] \cos 2\psi \end{aligned}} \qquad \text{(V-7)}$$

Tower Yawing Moment due to Single Blade

$$\boxed{\begin{aligned} M_y' &= \frac{1}{2}\left[K_\theta\theta_{1s} - K_\beta\beta_{1c} \right] + K_\theta\theta_o \sin\psi - K_\beta\beta_o \cos\psi \\ &+ \frac{1}{2}\left[K_\theta\theta_{1c} - K_\beta\beta_{1s} \right] \sin 2\psi - \frac{1}{2}\left[K_\theta\theta_{1s} + K_\beta\beta_{1c} \right] \cos 2\psi \end{aligned}} \qquad \text{(V-8)}$$

Tower Pitching Moment due to Single Blade

$$\boxed{M_z' = K_\zeta\zeta_o + K_\zeta\zeta_{1c} \cos\psi + K_\zeta\zeta_{1s} \sin\psi} \qquad \text{(V-9)}$$

Tower Antitorque Moment due to Single Blade

Important observations here are that the <u>single blade</u> 1/Rev. (one per revolution or 1Ω) frequency appears at twice that frequency on the non-rotating tower, and there are constant tower moments resulting from rotor plane tilt (single blade).

The moments from all the blades must be added to obtain the actual tower moments. Also, the blade centrifugal tension on the hub has not been considered in deriving the three root moments; its effect on the stationary tower will be a periodic moment (the periodic force acting through the nacelle yaw arm to the hub). When more than one blade has been summed, it will be seen that the centrifugal tension moment will vanish. For the realistic case, however, of a loss of blade accident, or of blade imbalance (e.g., due to icing), the centrifugal term would appear at frequency Ω, and amplitude equal to the centrifugal force of the unbalanced mass.

Equations V-7 and V-8, the tower moments due to a single blade, are simplified further by noticing that the flapping deflections (and moments) are much greater than the feathering moments; this gives:

$$M_x' \simeq \frac{1}{2} K_\beta \beta_{1s} + K_\beta \beta_o \sin \psi + \frac{1}{2} K_\beta \beta_{1c} \sin 2\psi - \frac{1}{2} K_\beta \beta_{1s} \cos 2\psi$$

Tower Yaw

$$M_y' \simeq - \frac{1}{2} K_\beta \beta_{1c} - K_\beta \beta_o \cos \psi - \frac{1}{2} K_\beta \beta_{1s} \sin 2\psi - \frac{1}{2} K_\beta \beta_{1c} \cos 2\psi \qquad \text{(V-10)}$$

Tower Pitch

Tower Moments, Single Blade

For a two-bladed system the total moment is the sum of the individual blades, phase π apart:

$$\begin{aligned} M_x' &= \sum_{K=1}^{b} M_{x_K}' = M_x'(\psi) + M_x'(\psi-\pi) \\ &= K_\beta \beta_{1s} + K_\beta \beta_o [\sin \psi + \sin(\psi-\pi)] \\ &+ \frac{1}{2} K_\beta \beta_{1c} [\sin 2\psi + \sin(2\psi-2\pi)] \\ &- \frac{1}{2} K_\beta \beta_{1s} [\cos 2\psi + \cos(2\psi-2\pi)] \end{aligned} \qquad \text{(V-11)}$$

The third and fourth terms add, giving:

$$\boxed{\begin{aligned} M_x' &= K_\beta\beta_{1s} + K_\beta\beta_{1c}\sin 2\psi - K_\beta\beta_{1s}\cos 2\psi \\ M_y' &= -K_\beta\beta_{1c} - K_\beta\beta_{1s}\sin 2\psi - K_\beta\beta_{1c}\cos 2\psi \end{aligned}} \qquad \text{(V-12)}$$

Tower Moments, Two Blades

The rotor plane tilt, β_{1c} and β_{1s}, appears as a steady tower moment and as a periodic input at 2/Rev. frequency. Thus, there will always be 2Ω frequencies in a two-bladed system, whether or not the blades are exactly balanced. The steady yaw moment is due to the yaw tilt of the rotor plane, and the pitching moment is due to the fore and aft tilt of the rotor plane. In addition, the two tilt angles cause a 2/Rev. oscillation in yaw direction; this will show up especially on a system free in yaw, that has low yawing inertia (of the nacelle and rotor). In a massive system, or one with damping in yaw, this periodic force will not cause a noticeable movement (i.e., NASA Mod-0; see References 28, 29, and 30). The appearance of the tilt angles in a linear (uncoupled) way like this makes it an easy task to measure β_{1c} and β_{1s} by measuring the 1/Rev. harmonic tower pitching moment. This can easily be done with strain gages, and could even be a fail safe device which would monitor cyclic tilts (cyclic loads) and cause a shutdown command if the values got too high.

For a three-bladed rotor, we have:

$$\begin{aligned} M_x' &= M_x'(\psi) + M_x'(\psi - \tfrac{2\pi}{3}) + M_x'(\psi - \tfrac{4\pi}{3}) \\ &= \tfrac{3}{2} K_\beta\beta_{1s} + K_\beta\beta_o\,[\,\sin(I) + \sin(II) + \sin(III)\,] \\ &+ \tfrac{1}{2} K_\beta\beta_{1c}\,[\,\sin 2(I) + \sin 2(II) + \sin 2(III)\,] \\ &- \tfrac{1}{2} K_\beta\beta_{1s}\,[\,\cos 2(I) + \cos 2(II) + \cos 2(III)\,] \end{aligned} \qquad \text{(V-13)}$$

In this case (and in all others with $b \geq 3$) the second, third, and fourth terms all cancel:

$$\boxed{\begin{aligned} M_x' &= \frac{3}{2} K_\beta \beta_{1s} \\ M_y' &= -\frac{3}{2} K_\beta \beta_{1c} \end{aligned}} \qquad \text{(V-14)}$$

Tower Moments, Three Blades

And for $b \geq 3$:

$$\boxed{\begin{aligned} M_x' &= \frac{b}{2} K_\beta \beta_{1s} \\ M_y' &= -\frac{b}{2} K_\beta \beta_{1c} \end{aligned}} \qquad \text{(V-15)}$$

Tower Moments, b Blades

The method of multiblade coordinates (used in the next section) makes use of this result, which can be generalized as:[31]

$$\boxed{\begin{aligned} \sum_{i=1}^{b} \sin n\,\psi_i &= 0 && n \neq \text{multiple of } b \\ &= b \sin n\psi && n = Sb,\ S = 1, 2, \ldots \\ \sum_{i=1}^{b} \cos n\,\psi_i &= 0 && n \neq \text{multiple of } b \\ &= b \cos n\psi && n = Sb,\ S = 1, 2, \ldots \end{aligned}} \qquad \text{(V-16)}$$

Harmonic Identities

where:

b = number of blades

ψ_i = azimuth phase angle

n = n^{th} harmonic of rotor speed $\Omega = \frac{d\psi}{dt}$

Looking at the multiblade results (V-15), the tower moments for three or more blades are simpler than for two blades. The fore and aft rotor plane tilt, β_{1c}, causes a steady tower pitching moment M_y'. The yaw tilt of the rotor plane is β_{1s}; this gives a steady yawing moment

M_x'. In the absence of any other restoring moment, the rotor would yaw around the tower. A restoring moment is produced, though: as the rotor plane yaws it rotates slightly out of the direct wind direction. This causes a crosswind component $\overline{U}_o$ to be produced; the rotor will yaw until the $\Delta\beta_{1s}$ due to crosswind balances the β_{1s} from other sources. The equation from Chapter III is:

$$\beta_{1s} = -\frac{1}{\Delta}\frac{\gamma^2}{8}BA + \left(\frac{\gamma}{2}\right)^2\frac{A\overline{U}_o}{3}(K-1) + \Delta\beta_{1s}\Big|_{\text{due to } \overline{q}} \qquad \text{(III-40)}$$

where:

$$B = \frac{G}{2\Omega^2} = \text{gravity term}$$

$$A = \left[\frac{\mu_o}{3} - \frac{\lambda_i}{3} - \frac{\theta_o}{20} - \frac{\theta_p}{4}\right] = \text{axisymmetric flow term}$$

$$K = \left[1 + \varepsilon + \frac{K_\beta}{I_b\Omega^2}\right] = \left(\frac{w_n}{\Omega}\right)^2 = \text{"inertial" natural frequency}$$

$$\gamma = \text{Lock number}$$

$$\overline{U}_o = \frac{U_o}{\Omega R} = \text{crosswind term}$$

In the absence of yaw rate $\overline{q}$, the gravity term and crosswind term are present. For steady yaw moment to be zero, according to V-15, β_{1s} must be zero. This gives:

$$\frac{\gamma^2}{8}BA + \frac{\gamma^2}{4}\frac{A\overline{U}_o}{3}(K-1) = 0 \qquad \text{For zero yaw moment}$$

The symmetric flow term A, and Lock number terms cancel, and we get the following expression for the equilibrium crosswind to cancel gravity:

$$\boxed{\overline{U}_o = -\frac{3}{2}\frac{B}{(K-1)}} \qquad \text{Freely Yawing System} \qquad \text{(V-17)}$$

Taking the numerical example from Section III-3, we have:

<u>Example</u>: $R = 25'$ radius

$e = 0.15$ hinge offset

$G = 2.273$ gravity term $\left(= \frac{g\ M_b\ X_g\ R}{I_b}\right)$

$K = 2.1$ (relatively soft rotor)

Range of operation:

$72 \text{ RPM} \leq \Omega \leq 115 \text{ RPM}$

$(7.5 \text{ rad/sec} \leq \Omega \leq 12 \text{ rad/sec})$

This gives the range for $\overline{U}_o$ due to gravity:

$$-0.0276 \leq \overline{U}_o \leq -0.0107 \quad (187.5 \text{ ft/sec} \leq \Omega R \leq 300 \text{ ft/sec})$$

And the range of U_o, crosswind velocity is:

$$\boxed{-5.18 \text{ ft/sec} \leq U_o \leq 3.21 \text{ ft/sec}}$$

This range of crosswind velocities corresponds to an RPM range of 72 to 115 on the rotor. It means that no matter what the free stream wind speed is, the crosswind needed to counteract gravity is 5.18 ft/sec for 72 RPM, and 3.21 ft/sec for 115 RPM. For a typical free stream value of 30 ft/sec (Note: this gives a tip speed ratio range of $\frac{\Omega R}{V_o} = 6.25$ to 10) the steady yaw angle will vary between 9.9° and 6.1° $\left(\frac{5.18}{30} \text{ to } \frac{3.21}{30}\right)$. It can easily be seen from IV-17 that a stiffer rotor (K larger) will have a smaller yaw deflection than a soft rotor. An articulated rotor with $K \approx 1.1$-1.2 will experience large yaw angles; e.g., for this case, the yaw deflections would be 54.5° to 33.6°.

B. Tower Moments: Other Frequencies

Other periodic forces will exist in the rotating system than the 1/Rev. tilting moments discussed in the last section. The most

significant ones are the transient moments due to oscillations of the blades at some natural structural frequency. A source of disturbance is wind gusting, which can act as a step function or impulse, causing blade vibration. We have already seen that flapping transients are highly damped by aerodynamics, but lead-lag transients have very little damping. Also, coupled structural modes may be important if forced at their natural frequencies. The task now is to investigate which frequencies will penetrate the coordinate transformation to tower coordinates and thus could excite a tower-support resonance.

Taking a general form for a blade moment of frequency $\omega_k = k\Omega$:

$$M_\beta = M_{\beta_{sk}} \sin k\psi + M_{\beta_{ck}} \cos k\psi \tag{V-18}$$

or

$$M_\beta = M_{\beta_{sk}} \sin \omega_k t + M_{\beta_{ck}} \cos \omega_k t$$

where:

$k = k^{th}$ harmonic of Ω

$\omega_k = k\Omega$

The transformation gives:

$$M_x' = M_{\beta_{sk}} \sin \omega_k t \sin \Omega t + M_{\beta_{ck}} \cos \omega_k t \cos \Omega t$$

$$M_y' = - M_{\beta_{sk}} \sin \omega_k t \cos \Omega t - M_{\beta_{ck}} \cos \omega_k t \cos \Omega t$$

and

$$M_x' = M_{\beta_{sk}} \sin k\psi \sin \psi + M_{\beta_{ck}} \cos k\psi \cos \psi$$

$$M_y' = M_{\beta_{sk}} \sin k\psi \cos \psi - M_{\beta_{ck}} \cos k\psi \cos \psi \tag{V-19}$$

With the identities:

$$\sin\alpha \sin\beta = \frac{1}{2}\,[\cos(\alpha-\beta) - \cos(\alpha+\beta)]$$

$$\cos\alpha \cos\beta = \frac{1}{2}\,[\cos(\alpha+\beta) + \cos(\alpha-\beta)]$$

$$\sin\alpha \cos\beta = \frac{1}{2}\,[\sin(\alpha+\beta) + \sin(\alpha-\beta)]$$

$$\cos\alpha \sin\beta = \frac{1}{2}\,[\sin(\alpha+\beta) - \sin(\alpha-\beta)]$$

We now have:

$$\boxed{\begin{aligned} M_x' &= \frac{M_{\beta_{sk}}}{2}\,[\cos(k-1)\psi - \cos(k+1)\psi] \\ &\quad + \frac{M_{\beta_{ck}}}{2}\,[\sin(k+1)\psi - \sin(k-1)\psi] \\ M_y' &= \frac{M_{\beta_{sk}}}{2}\,[\sin(k+1)\psi + \sin(k-1)\psi] \\ &\quad - \frac{M_{\beta_{ck}}}{2}\,[\cos(k+1)\psi + \cos(k-1)\psi] \end{aligned}} \qquad \text{(V-20)}$$

Tower Moments, Single Blade, General Harmonic K

Thus, a blade forcing function at frequency $\omega_k = k\Omega$, becomes two forcing functions on the tower, at frequencies $(k+1)\Omega$ and $(k-1)\Omega$. Now the task remains to investigate further which frequencies (now the k+1 and k-1 components we are interested in) will cancel when the blades are summed as before.

From the last section, when summing tower contributions from a rotor with b blades we have:

$$\sum_{i=1}^{b} \begin{Bmatrix} \sin \\ \cos \end{Bmatrix} (n\psi_i) = \begin{cases} 0 & \text{n not a multiple of b} \\ b \begin{Bmatrix} \sin \\ \cos \end{Bmatrix} (n\psi_i) & \text{n an integer multiple of b, } n = Sb,\ S = 1, 2, 3 \ldots \end{cases}$$

(V-16)

This formula says that single blade frequency of order n on the tower,

appears as a moment of order n (and magnitude b) when summed, if the harmonic is a multiple of the number of blades.

For the designer the implication is straightforward; for example, with a three-bladed rotor, a natural frequency of 4Ω will cause tower moments of frequencies 3Ω and 5Ω according to V-20 and the 5Ω moment vanishes according to V-16. Resonance may occur at 3Ω. If the rotor is variable speed, the range of allowable Ω will establish a range of critical multiples (3Ω) which must be predicted and either avoided or damped to prevent tower resonance. Likewise a natural blade frequency of 5Ω yields tower frequencies of 4Ω and 6Ω, and only the 6Ω moment appears.

It is especially useful to investigate the non-integer frequencies, that is, to establish a coefficient equivalent to the sum of V-16, which gives the amplitude of moments transferred to the tower system and then summed over the blades. We already know from V-16 that this coefficient is zero at non-multiple integers and b at integer multiples of the number of blades.

Generalizing, the sum of V-16 is:

$$S = \sum_{m=1}^{N} \cos\,(n\psi_m) \qquad \text{where } \psi_m = \psi - \frac{2\pi m}{N} \tag{V-21}$$

Writing in complex form: $e^{i\theta} = \cos\theta + i\sin\theta$

$$S = \sum_{m=1}^{N} \cos\,[n\psi - \frac{2\pi mn}{N}] = \mathrm{Re} \sum_{m=1}^{N} e^{\,i[n\psi - \frac{2\pi mn}{N}]}$$

Then the complex sum is:

$$\sum_{m=1}^{N} = e^{i[n\psi - \frac{2\pi n}{N}]} + e^{i[n\psi - \frac{4\pi n}{N}]} + e^{i[n\psi - \frac{6\pi n}{N}]} + \ldots$$

$$= e^{in\psi} [e^{-\frac{2\pi n}{N}} + e^{-\frac{4\pi n}{N}} + e^{-\frac{6\pi n}{N}} + \ldots]$$

$$\boxed{\Sigma = e^{in\psi} \sum_{m=1}^{N} e^{-(2\pi\frac{n}{N}m)i}} \qquad \text{(V-22)}$$

The first term of this expression gives the frequency in ψ, and the sinusoidal function. The second term contains a coefficient which is the sum of all the complex vectors representing the blades at their respective phase angles. The task is to evaluate this term for the number of blades of interest (N) over the continuous range of frequency of interest (n); taking the real part:

$$\text{Harmonic Coefficient} = \text{Re} \sum_{m=1}^{N} e^{-(2\pi\frac{n}{N}m)i}$$

$$= \sum_{m=1}^{N} \cos\ (2\pi\frac{n}{N}m) \qquad \text{(V-23)}$$

For two blades it becomes:

$$\Sigma_2 = \cos\ (n\pi) + \cos\ (2n\pi) \qquad \text{(V-24)}$$

For three blades:

$$\Sigma_3 = \cos\ (n\frac{2\pi}{3}) + \cos\ (n\frac{4\pi}{3}) + \cos\ (n2\pi) \qquad \text{(V-25)}$$

These two expressions are plotted in Figures 49 and 50. The results give the coefficient which appears with a given frequency in the tower system after the individual blade contributions have been sorted. The maxima appear at multiples of the number of blades, as before, and zeroes appear at non-multiple integers of rotor speed.

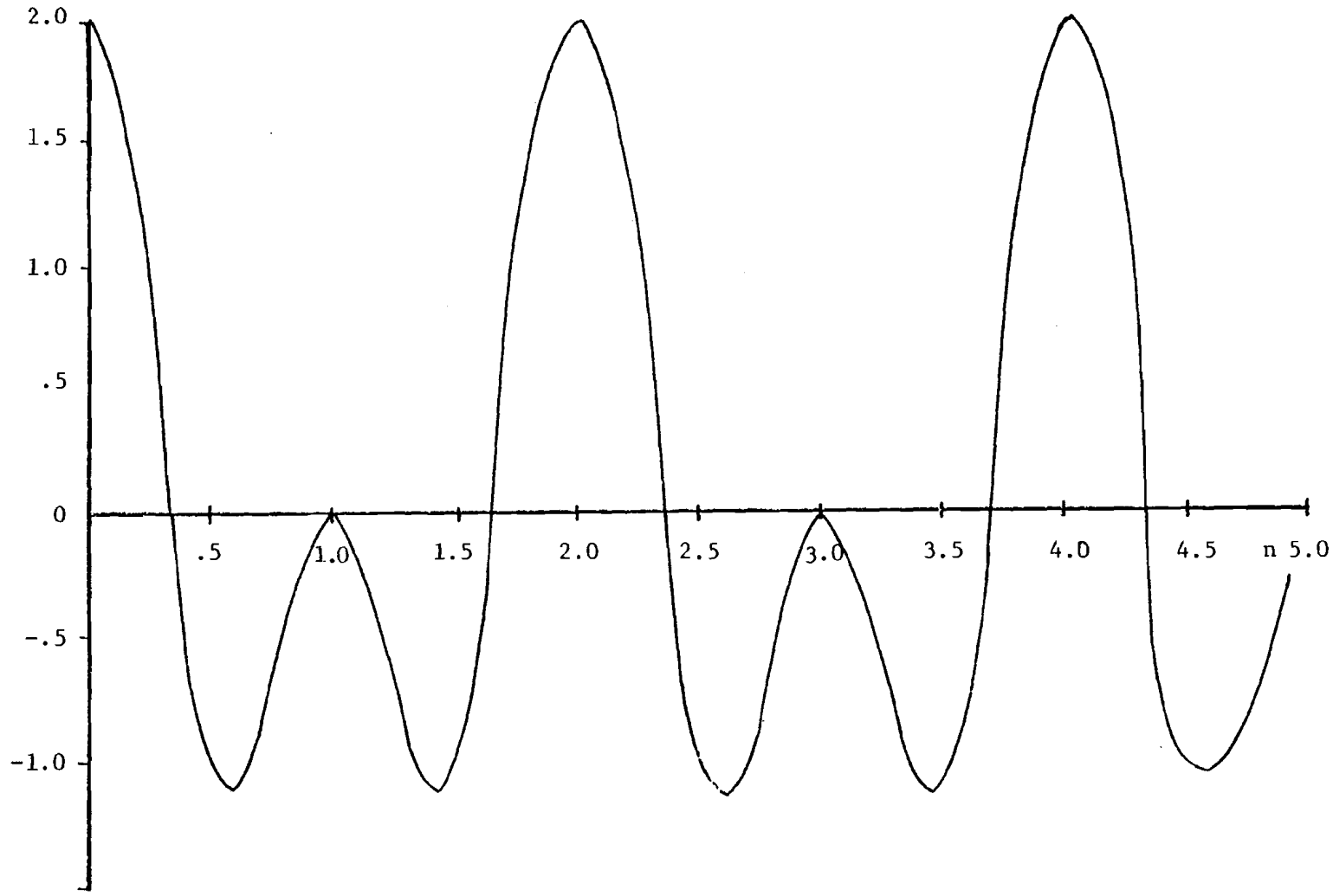

Figure 49. Harmonic Coefficient, Two Blades

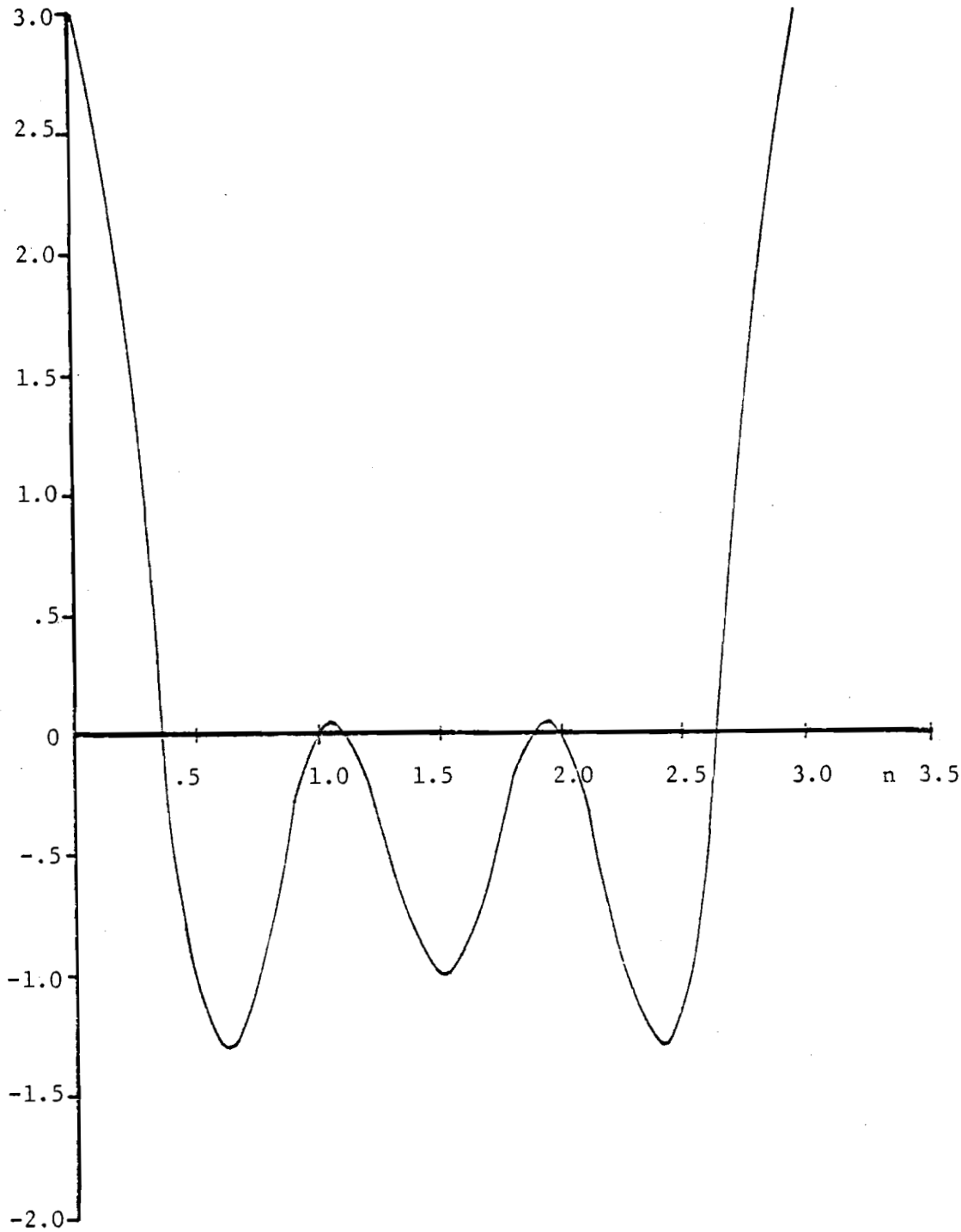

Figure 50. Harmonic Coefficients, Three Blades

C. Coupled Rotor-Tower Instability - Blade Lag/Tower Sway

Up to now the tower has been visualized as infinitely stiff, allowing for the effects of the rotor and blades to be assessed independently. In actuality, long slender towers can have low enough bending stiffness to affect the rotor motion and loads.[32] The formulation and solution of such problems must deal with coupled tower deflections and rotor deflections, and include the effects of tower mass, damping and stiffness as well as blade mass, damping and stiffness. Recent work by Thresher and Smith has identified possible "whirl mode" instabilities on wind generators with soft tower restraint.[33]

A classical dynamic stability analysis dealt with a disk rotor mounted in bearings of unequal flexibility (Foote, et al: 1943);[34] the case of flexible helicopter rotor blades in flexible supports was investigated later (Coleman, Feingold: 1958);[35] the present formulation of rotor blade lead-lag motion coupled with tower sway (lateral motion) has been done by Sheu and Dugundji (1977) following the classical methods (see References 36 and 37). This section follows the Sheu formulation and solution; results and stability boundaries are obtained for two and three-bladed rotors.

The following figure shows the pole tower deflected to the side, and the ith blade at azimuth ψ_i with a lead-lag angle and hinge offset:

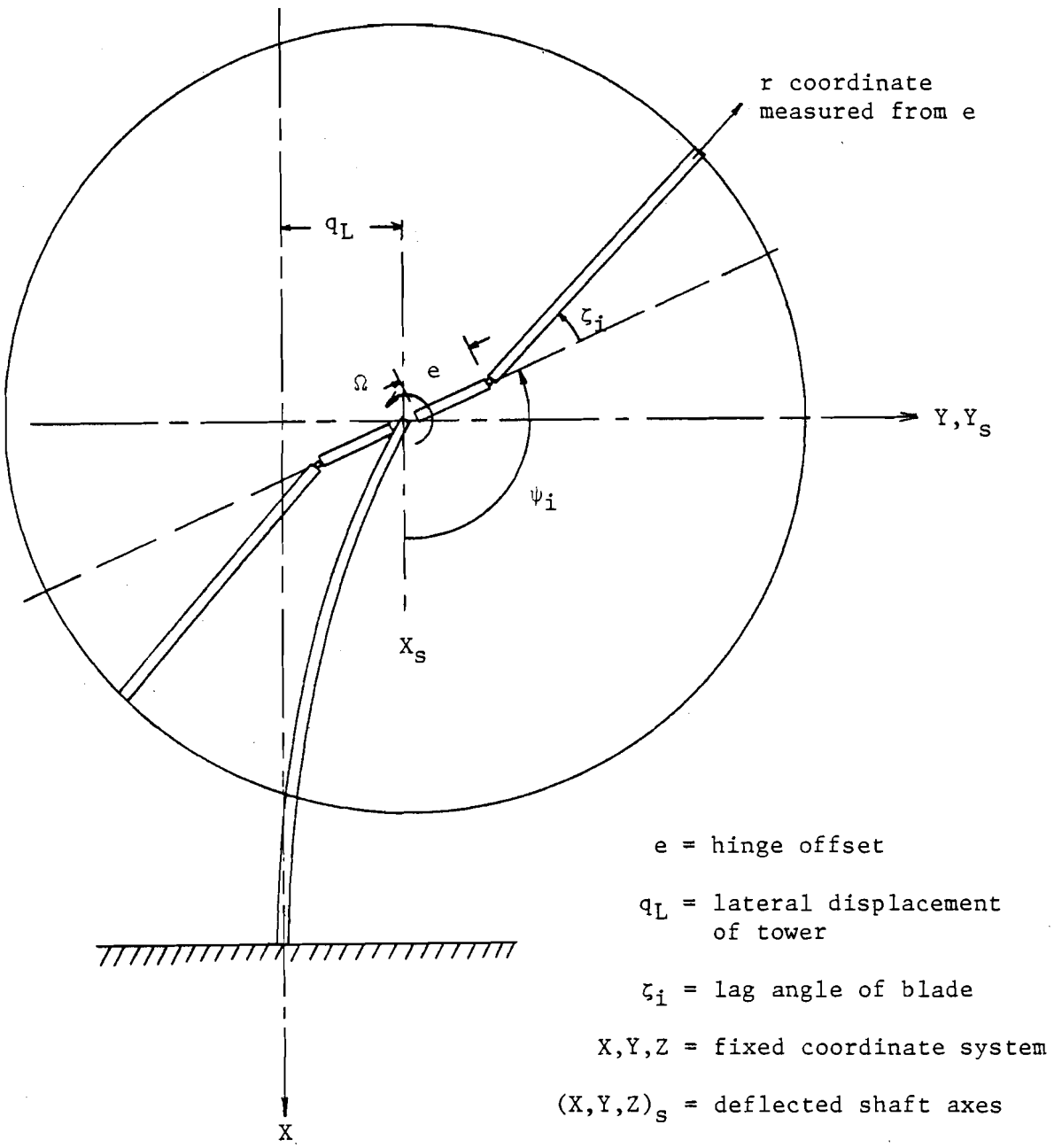

Figure 51. Lateral Deflection of Tower + Blade Lead-Lag

The velocities of a point (x,y) on the blade are derived from the polar coordinate expression:

$$x = e \cos \psi_i + r \cos (\psi_i + \zeta_i)$$

$$y = q_L + e \sin \psi_i + r \sin (\psi_i + \zeta_i) \qquad \text{(V-26)}$$

$$\dot{x} = - e\,\Omega \sin \psi_i - (\Omega + \dot{\zeta}_i)\, r \sin (\psi_i + \zeta_i)$$

$$\dot{y} = \dot{q}_L + e\,\Omega \cos \psi_i + (\Omega + \dot{\zeta}_i)\, r \cos (\psi_i + \zeta_i) \qquad \text{(V-27)}$$

In anticipation of using Lagrange's equation, the kinetic energy for the blades and tower is found:

$$T_{b_i} = \begin{matrix}\text{kinetic energy} \\ \text{of } i^{\underline{th}} \text{ blade}\end{matrix} = \int_m \frac{1}{2} [\dot{x}^2 + \dot{y}^2]\, dm$$

$$\boxed{\begin{aligned} T_b &= \sum_{i=1}^{N} T_{b_i} = \sum_{i=1}^{N} \int_m \frac{1}{2} [\dot{x}^2 + \dot{y}^2]\, dm \\ T_t &= \frac{1}{2} M_{TL}\, \dot{q}_L^2 \end{aligned}} \qquad \text{(V-28)}$$

Kinetic Energy of System

where:

T_b = total KE of N blades

T_t = KE of tower

M_{TL} = tower mass (corresponding to q_L)

m = mass of each blade

The total elastic potential energy of the tower and blade is the sum of the stiffnesses times their deflections squared, viz.:

$$\boxed{U = \frac{1}{2} K_L\, q_L^2 + \sum_{i=1}^{N} \frac{1}{2} K_\zeta\, \zeta_i^2} \qquad \text{(V-29)}$$

Potential Energy of System

where:

K_L = lateral tower stiffness

K_ζ = blade lead-lag stiffness

To include effects of gravity and damping, we must write the incremental work $\delta W = F\delta s$:

$$\boxed{\begin{aligned} \delta W &= \sum_{i=1}^{N} \int_m g\ \delta x\ dm - C_L\ \dot{q}_L\ \delta q_L - \sum_{i=1}^{N} C_\zeta\ \dot{\zeta}_i\ \delta\zeta_i \\ \delta W &= -\ g\ \left[\int_m r\ dm\right] \sum_{i=1}^{N} \sin\ (\psi_i + \zeta_i)\ \delta\zeta_i \\ &\quad -\ C_L\ \dot{q}_L\ \delta\ q_L - \sum_{i=1}^{N} L_\zeta\ \zeta_i\ \delta\zeta_i \end{aligned}} \qquad \text{(V-30)}$$

Incremental Work ($F\delta s$)

where:

δx = incremental distance over which gravity acts

C_L = tower lateral damping coefficient

C_ζ = blade lead-lag damping

The mass integrals are:

$$m = \int_m dm = \text{mass of blade}$$

$$S = \int_m r\ dm = \text{first mass moment about lag hinge}$$

$$I = \int_m r^2\ dm = \text{blade mass moment of inertia}$$

The final expression for the total kinetic energy and incremental work is then:

$$\begin{aligned} T = \frac{1}{2} M_{TL}\ \dot{q}_L^{\ 2} + \sum_{i=1}^{N} \Big[&\frac{1}{2} m\ \dot{q}_L^{\ 2} + \frac{1}{2} m\ e^2\Omega^2 + \frac{1}{2} I\ (\Omega + \zeta_i)^2 \\ &+ Se\ \Omega(\Omega + \zeta_i)\ \cos\ \zeta_i + m\ \dot{q}_L\ e\Omega\ \cos\ \psi_i \\ &+ S\dot{q}_L\ (\Omega + \zeta_i)\ \cos\ (\psi_i + \zeta_i)\Big] \end{aligned} \qquad \text{(V-31)}$$

$$\delta W = - g\, S \sum_{i=1}^{N} \sin\,(\psi_i + \zeta_i)\ \delta\zeta_i - C_L\, \dot{q}_L\ \delta q_L - \sum_{i=1}^{N} C_\zeta\, \dot{\zeta}_i\ \delta\zeta_i$$

$$= \Sigma\, Q_n\ \delta q_n \qquad q_n = q_L,\ \zeta_1,\ \zeta_2,\ \zeta_3,\ \ldots \tag{V-32}$$

Now Lagrange's equation is used:

$$\frac{d}{dt}\left(\frac{\partial T}{\partial \dot{q}_n}\right) - \frac{\partial T}{\partial q_n} + \frac{\partial u}{\partial q_n} = Q_n \tag{V-33}$$

q_n = generalized coordinate

$= q_L,\ \zeta_1,\ \zeta_2,\ \zeta_3,\ \ldots\ \zeta_N$

After differentiation, neglecting higher order terms, and using small angle assumption on ζ, the linear equations of motion in terms of q_L and ζ are found:

$$(M_{TL} + Nm)\ddot{q}_L + C_L\, \dot{q}_L + K_L\, q_L + S\, \frac{d^2}{dt^2} \sum_{i=1}^{N} (\zeta_i \cos\, \psi_i) = 0 \tag{V-34}$$

total lateral mass — tower lateral damping — tower spring force — sum of components of lag angles

$$S\ddot{q}_L \cos\, \psi_i + I\ddot{\zeta}_i + C_\zeta \dot{\zeta} + [S\Omega^2 e + K_\zeta + g\, S \cos\, \psi_i]\zeta_i = - g\, S \sin\, \psi_i$$

tower coupling term — blade lag damping — blade lag stiffness — gravity forcing function

$(i = 1, 2, \ldots, N)$ (V-35)

The simple equations of motion illustrate the lag angle-mass coupling in V-34, the tower equation; and the tower lateral acceleration coupling in V-35, the blade equation. Mechanical damping can be added in either the tower, C_L, or the blades, C_ζ. And the blade lead-lag stiffness is the same as before (Chapter II) being increased by hinge

offset and affected by the periodic spring due to gravity. Expression V-35 yields N equations, one for each blade.

In the solution to follow, hinge offset and gravity are set to zero. The method of multiblade coordinates is used, wherein new coordinates are introduced, representing the lead-lag motion as a harmonic series:

$$\zeta_i = \zeta_o + \zeta_A(-1)^i + a_1 \sin \psi_i + b_1 \cos \psi_i + a_2 \sin 2\psi_i + b_2 \cos 2\psi_i + \ldots \quad (i = 1, 2, \ldots, N) \qquad \text{(V-36)}$$

This series is identical to the series introduced in Chapter III to evaluate blade deflections:

$$\zeta_i = \zeta_o + \zeta_{1s} \sin \psi_1 + \zeta_{1c} \cos \psi_1 + \ldots$$

With $N \geq 3$, only the first N terms of the series are retained. The ζ_A term occurs only in even-bladed rotors; and is used to replace the last two terms of the truncated series. The physical meaning of V-36 is as before, with the addition of ζ_A for four bladed rotors:

$$\zeta_o = \frac{1}{N} \sum_{i=1}^{N} \zeta_i = \text{collective lag angle (constant for each blade)}$$

$$\zeta_A = \frac{1}{N} \sum_{i=1}^{N} \zeta_i(-1)^i = \text{differential collective lag angle (occurs only for even bladed rotors; e.g., 4, 6, 8 blades. For a 4-blade rotor it represents a departure from the usual 90° phase between adjacent blades).}$$

$$\left.\begin{aligned} a_1 &= \frac{2}{N} \sum_{i=1}^{N} \zeta_i \sin \psi_i \\ b_1 &= \frac{2}{N} \sum_{i=1}^{N} \zeta_i \cos \psi_i \end{aligned}\right\} = \text{first order cyclic lagging}$$

$$\left.\begin{aligned} a_2 &= \frac{2}{N}\sum_{i=1}^{N} \zeta_i \sin 2\psi_i \\ b_2 &= \frac{2}{N}\sum_{i=1}^{N} \zeta_i \cos 2\psi_i \end{aligned}\right\} = \text{second order cyclic lagging (usually neglected)} \qquad \text{(V-37)}$$

The blade summation formulas (V-16) are again used:

$$\begin{aligned} \sum_{i=1}^{N} \begin{Bmatrix}\sin\\ \cos\end{Bmatrix} (n\psi_i) &= 0 \qquad n \text{ not a multiple of } N \\ &= N \begin{Bmatrix}\sin\\ \cos\end{Bmatrix} (n\psi) \quad n = \text{integer multiple of } N, \\ &\qquad\qquad n = SN,\ s = 1, 2, \ldots \end{aligned} \qquad \text{(V-16)}$$

Using the above relations, the periodic coefficients in the equations of motion (V-34, V-35) can always be eliminated for $N \geq 3$. For a two-bladed rotor, and for the cases including gravity, the periodic coefficients do not vanish, and another solution method must be used (Floquet Transition Matrix Method; see References 38 and 39).

For the three bladed rotor, we have:

$$\begin{aligned} q_L &= a_o(t) \\ \zeta_i &= \zeta_o(t) + a_1(t) \sin \psi_i + b_1(t) \cos \psi_i \end{aligned} \qquad \text{(V-38)}$$

Substitution in the equations of motion gives the system of coupled equations for a three-bladed rotor:

$$\begin{aligned} &M_L \ddot{a}_o + C_L \dot{a}_o + K_L a_o + \frac{3}{2} S\ddot{b}_1 = 0 \qquad (M_L = M_{TL} + 3m) \\ &I\ddot{a}_1 + C_\zeta \dot{a}_1 + (K_\zeta - I\Omega^2)\, a_1 - 2\Omega\, I\dot{b}_1 - \Omega\, C_\zeta b_1 = 0 \\ &S\ddot{a}_o + I\ddot{b}_1 + C_\zeta \dot{b}_1 + (K_\zeta - I\Omega^2)\, b_1 + 2\Omega\, I\dot{a}_1 + \Omega\, C_\zeta a_1 = 0 \\ &I\ddot{\zeta}_o + C_\zeta \dot{\zeta}_o + K_\zeta \zeta_o = 0 \end{aligned} \qquad \text{(V-39)}$$

The last equation is uncoupled, and is therefore unnecessary for the stability solution. This equation is the simple lead-lag equation

derived in Chapter II; again, the damping term C_ζ, must be added mechanical damping, because there is no aerodynamic damping in lead-lag without drag. This is the reason why inplane motion, and the possible inplane instabilities, are so significant for rotors.

The first three equations of V-39 are non-dimensionalized, and time derivatives are replaced by azimuth derivatives, $(d/dt) = \Omega(d/d\psi)$:

$$\frac{a_o''}{R} + \frac{C_L}{M_L}\frac{a_o'}{(R\Omega)} + \frac{K_L}{M_L}\frac{a_o}{(R\Omega^2)} + \frac{3S}{2M_L R} b_1'' = 0$$

$$a_1'' + \frac{C_\zeta}{I\Omega} a_1' + \left(\frac{K_\zeta}{I\Omega^2} - 1\right) a_1 - 2b_1' - \frac{C_\zeta}{I\Omega} b_1 = 0$$

$$\frac{S}{I} a_o'' + 2a_1' + \frac{C_\zeta}{I\Omega} a_1 + b_1'' + \frac{C_\zeta}{I\Omega} b_1' + \left(\frac{K_\zeta}{I\Omega^2} - 1\right) b_1 = 0 \qquad \text{(V-40)}$$

The column vectors are defined as:

$$\{\bar{q}\} = \{\frac{a_o}{R} \quad a_1 \quad b_1\}$$

$$\{\bar{q}\}' = \{\frac{a_o'}{R} \quad a_1' \quad b_1'\}$$

$$\{\bar{q}\}'' = \{\frac{a_o''}{R} \quad a_1'' \quad b_1''\} \qquad \text{(V-41)}$$

And the matrix form is simply:[12]

$$[M]\ \{\bar{q}''\} + [B]\ \{\bar{q}'\} + [K]\ \{\bar{q}\} = 0 \qquad \text{(V-42)}$$

where $[M]$ = mass matrix

$[B]$ = damping matrix

$[K]$ = stiffness matrix

This gives the values of the matrices:

$$[M] = \begin{bmatrix} 1 & 0 & \frac{3S}{2M_L R} \\ 0 & 1 & 0 \\ \frac{RS}{I} & 0 & 1 \end{bmatrix} = \text{mass matrix} \qquad \text{(V-43)}$$

$$[B] = \begin{bmatrix} \frac{C_L}{M_L \Omega} & 0 & 0 \\ 0 & \frac{C_\zeta}{I\Omega} & -2 \\ 0 & 2 & \frac{C_\zeta}{I\Omega} \end{bmatrix} = \text{damping matrix} \qquad \text{(V-44)}$$

$$[K] = \begin{bmatrix} \frac{K_L}{M_L \Omega^2} & 0 & 0 \\ 0 & (\frac{K_\zeta}{I\Omega^2} - 1) & -\frac{C_\zeta}{I\Omega} \\ 0 & \frac{C_\zeta}{I\Omega} & (\frac{K_\zeta}{I\Omega^2} - 1) \end{bmatrix} = \text{stiffness matrix} \qquad \text{(V-45)}$$

It is illustrative to point out that the terms in the damping and stiffness matrices can easily be related to the damping coefficient (ω_ζ) and natural frequency (ξ_ζ) of the isolated (and uncoupled) blade lead-lag oscillator:

$$\zeta'' + 2\xi_\zeta \left(\frac{\omega_\zeta}{\Omega}\right) \zeta' + \left(\frac{\omega_\zeta}{\Omega}\right)^2 \zeta = 0 \qquad \text{Classical Form} \qquad \text{(V-46)}$$

Or:

$$\zeta'' + \left(\frac{C_\zeta}{I\Omega}\right) \zeta' + \left(\frac{K_\zeta}{I\Omega^2}\right) \zeta = 0 \qquad \text{Present Form} \qquad \text{(V-47)}$$

In terms of the damping ratios and natural frequencies the stiffness and damping matrices are simply:

$$[B] = \begin{bmatrix} 2\xi_L(\frac{\omega_L}{\Omega}) & 0 & 0 \\ 0 & 2\xi_\zeta(\frac{\omega_\zeta}{\Omega}) & -2 \\ 0 & 2 & 2\xi_\zeta(\frac{\omega_\zeta}{\Omega}) \end{bmatrix} \tag{V-48}$$

$$[K] = \begin{bmatrix} (\frac{\omega_L}{\Omega})^2 & 0 & 0 \\ 0 & (\frac{\omega_\zeta}{\Omega})^2-1 & -2\xi_\zeta(\frac{\omega_\zeta}{\Omega}) \\ 0 & 2\xi_\zeta(\frac{\omega_\zeta}{\Omega}) & (\frac{\omega_\zeta}{\Omega})^2-1 \end{bmatrix} \tag{V-49}$$

Knowing the tower natural frequency (ω_L), blade lead-lag natural frequency (ω_ζ), the damping (ξ_L, ξ_ζ), the blade radius, the blade first mass moment (S), and masses of the system, the matrices of the system are known: V-43, V-48, and V-49. Solutions of harmonic form are assumed to find the eigenvalues, $p = \alpha + i\omega$:

$$X = \underline{\overline{X}}\, e^{p\psi i} = \underline{\overline{X}}\, e^{(\alpha + i\omega)t} \tag{V-50}$$

Instability exists when the damping term α is positive, and the deflection grows without limit at frequency ω.

The solution of a set of three, coupled, second order, linear differential equations is straightforward, and is most easily handled by computer methods. Analytically we have:

$$(a_1x''+a_2x'+a_3x) + (b_1y''+b_2y'+b_3y) + (c_1z''+c_2z'+c_3z) = 0$$

$$(a_4x''+a_5x'+a_6x) + (b_4y''+b_5y'+b_6y) + (c_4z''+c_5z'+c_6z) = 0$$

$$(a_7x''+a_8x'+a_9x) + (b_7y''+b_8y'+b_9y) + (c_7z''+c_8z'+c_9z) = 0 \tag{V-51}$$

Substitution of V-50 gives:

$$(a_1p^2+a_2p+a_3)\underline{\overline{X}} + (b_1p^2+b_2p+b_3)\underline{\overline{Y}} + (c_1p^2+c_2p+c_3)\underline{\overline{Z}} = 0$$

$$(a_4p^2+a_5p+a_6)\underline{\overline{X}} + (b_4p^2+b_5p+b_6)\underline{\overline{Y}} + (c_4p^2+c_5p+c_6)\underline{\overline{Z}} = 0$$

$$(a_7p^2+a_8p+a_9)\underline{\overline{X}} + (b_7p^2+b_8p+b_9)\underline{\overline{Y}} + (c_7p^2+c_8p+c_9)\underline{\overline{Z}} = 0 \qquad \text{(V-52)}$$

The characteristic equation is found by setting the determinant of the coefficients (of $\underline{\overline{X}}$, $\underline{\overline{Y}}$, and $\underline{\overline{Z}}$) to zero; a sixth order polynomial results, yielding six roots which in general are three pairs of complex conjugates.

The results are plotted in Figures 52 through 57 from Reference 36. In the first five graphs the uncoupled natural frequency of the tower (divided by the uncoupled natural frequency of the blades) is set to 0.2, 0.5, 0.924, 2.0, and 5.0 (this constitutes a large range of stiffness ratio). The tower and blade damping (ξ_L and ξ_ζ) are set to zero in these plots.

Three modes (or frequencies) of the system result for the original lead-lag coefficients a_o, a_1 and b_1, respectively. The abscissas are non-dimensional rotor speed (Ω/ω_ζ), and the ordinates are the natural frequencies of the solution, again non-dimensionalized by blade natural frequency (ω/ω_ζ). Mode three begins near 1.0 and increases rapidly with increasing rotor speed; the mode is always stable. Mode two begins at 1.0, but falls rapidly to zero at $\Omega/\omega_\zeta = 1$; then it rises and passes through an unstable range. Mode one (collective) is very nearly horizontal, and also becomes unstable with mode two.

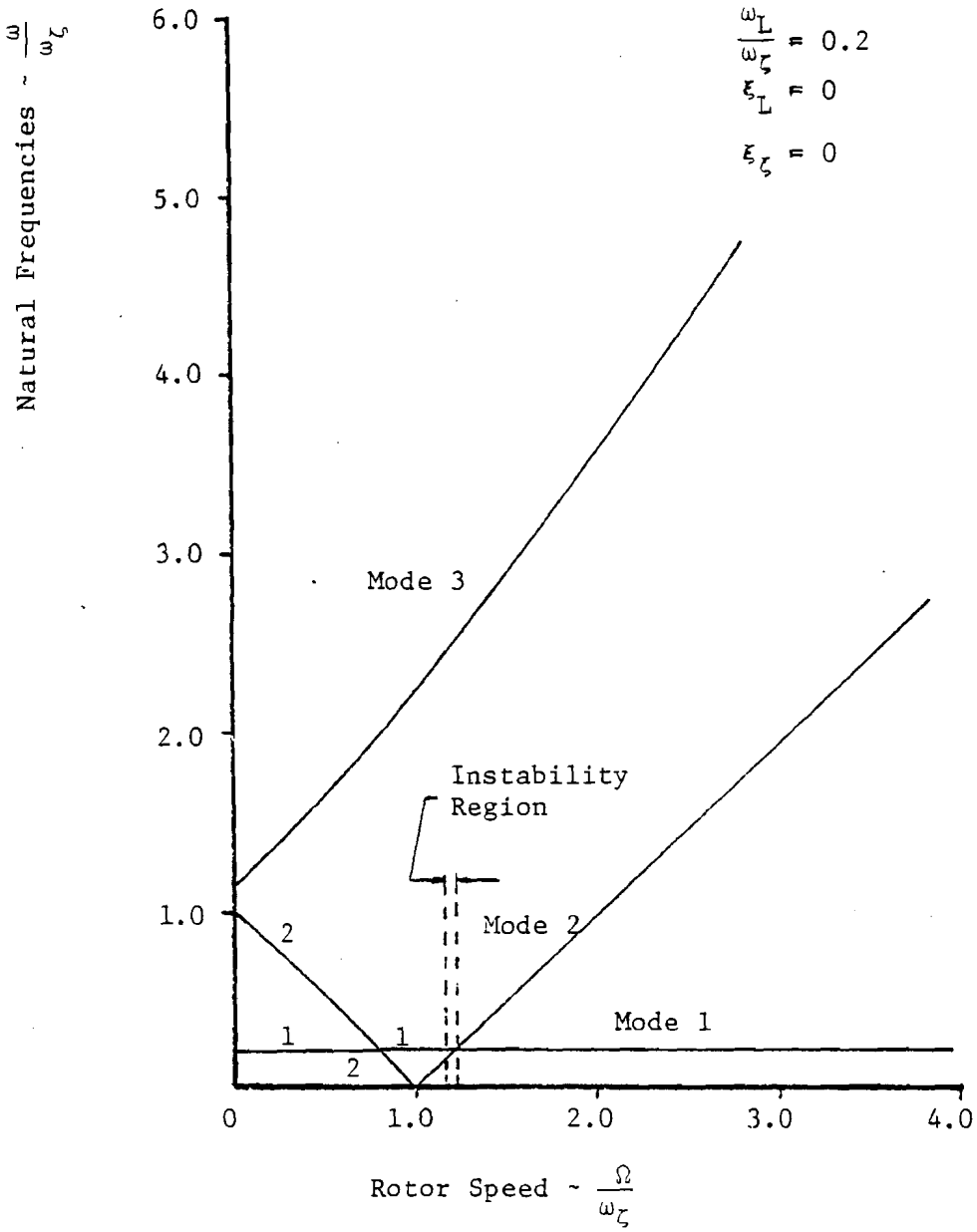

Figure 52. Blade Lag/Tower Sway Frequencies (Reference 36)

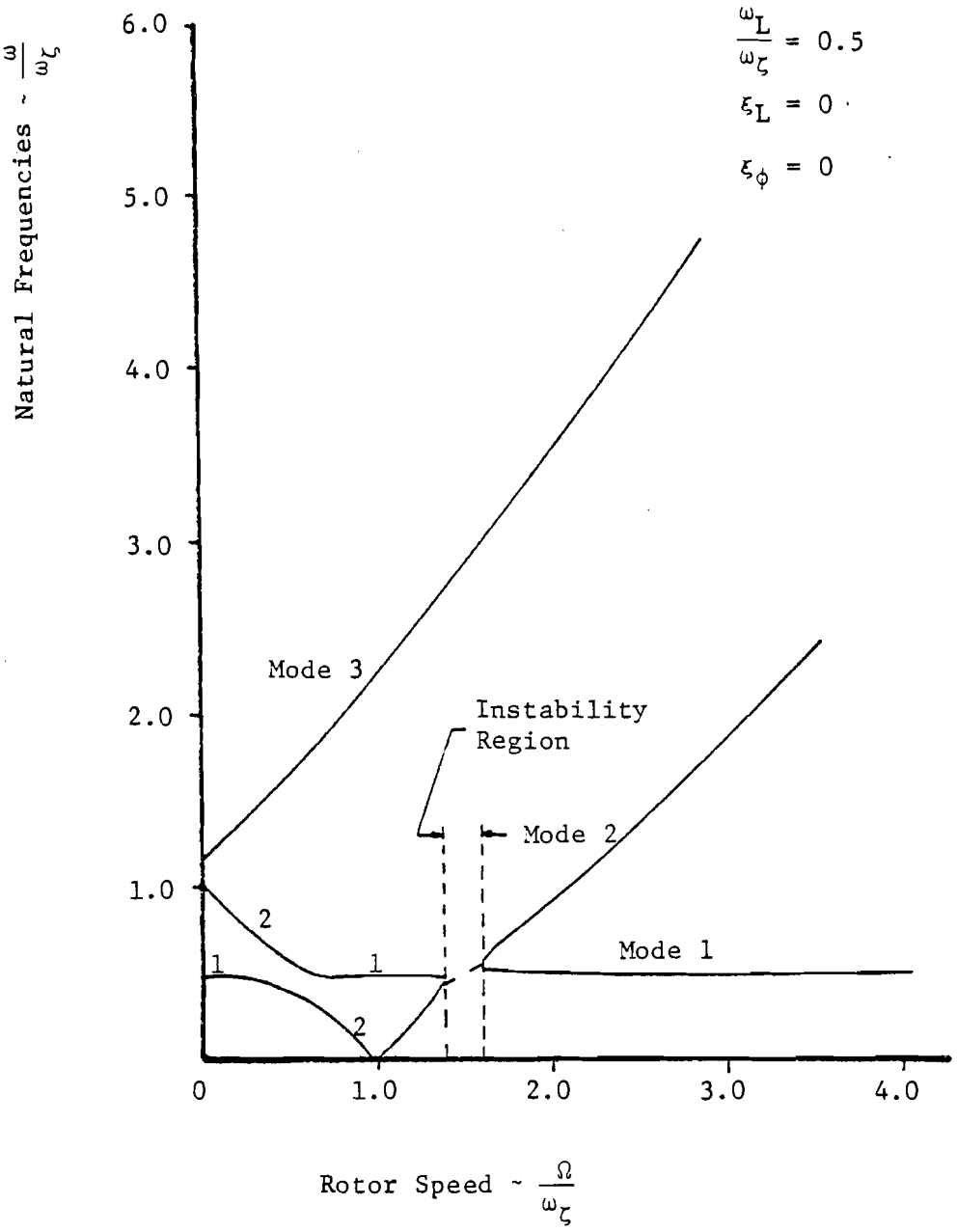

Figure 53. Blade Lag/Tower Sway Frequencies (continued)

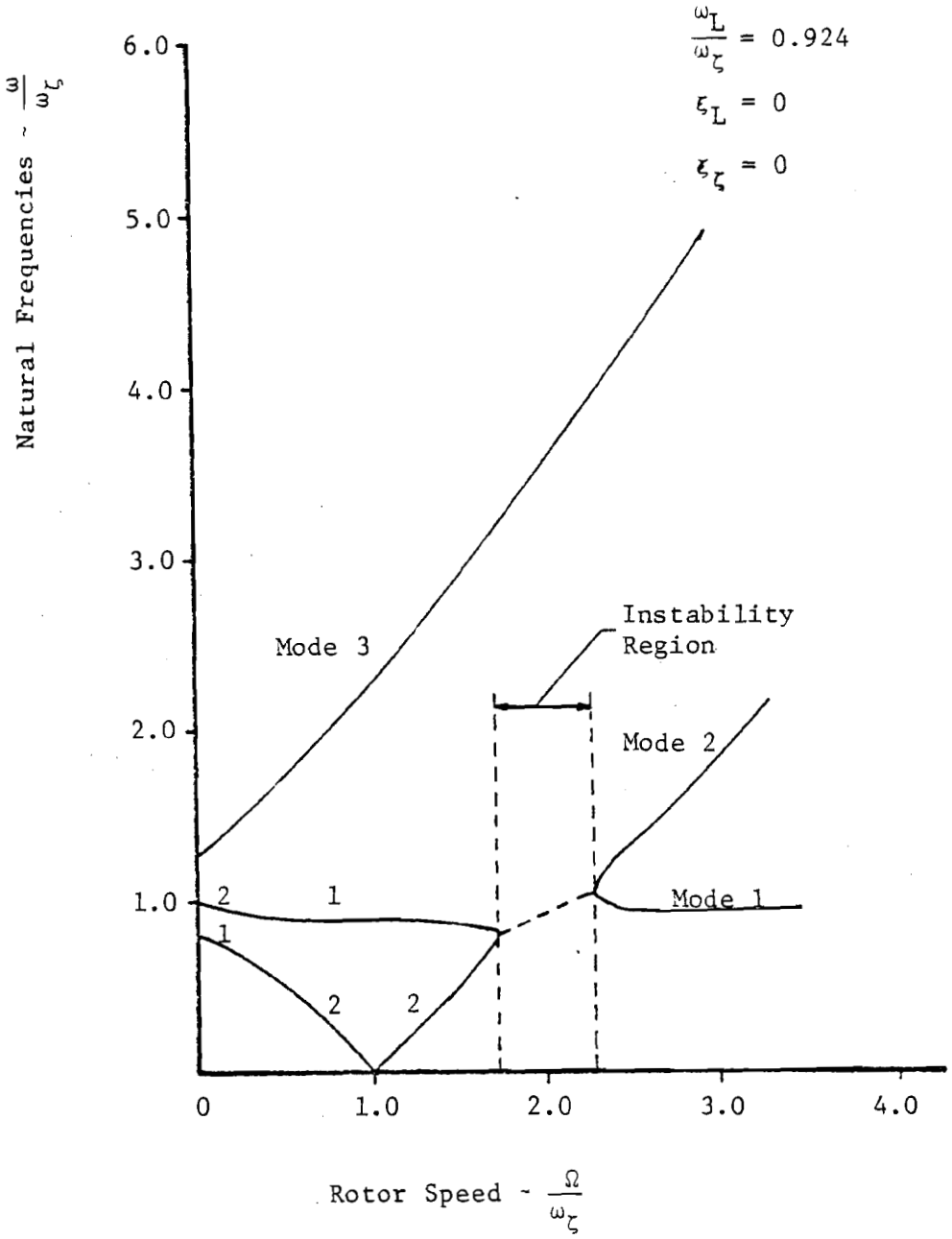

Figure 54. Blade Lag/Tower Sway Frequencies (continued)

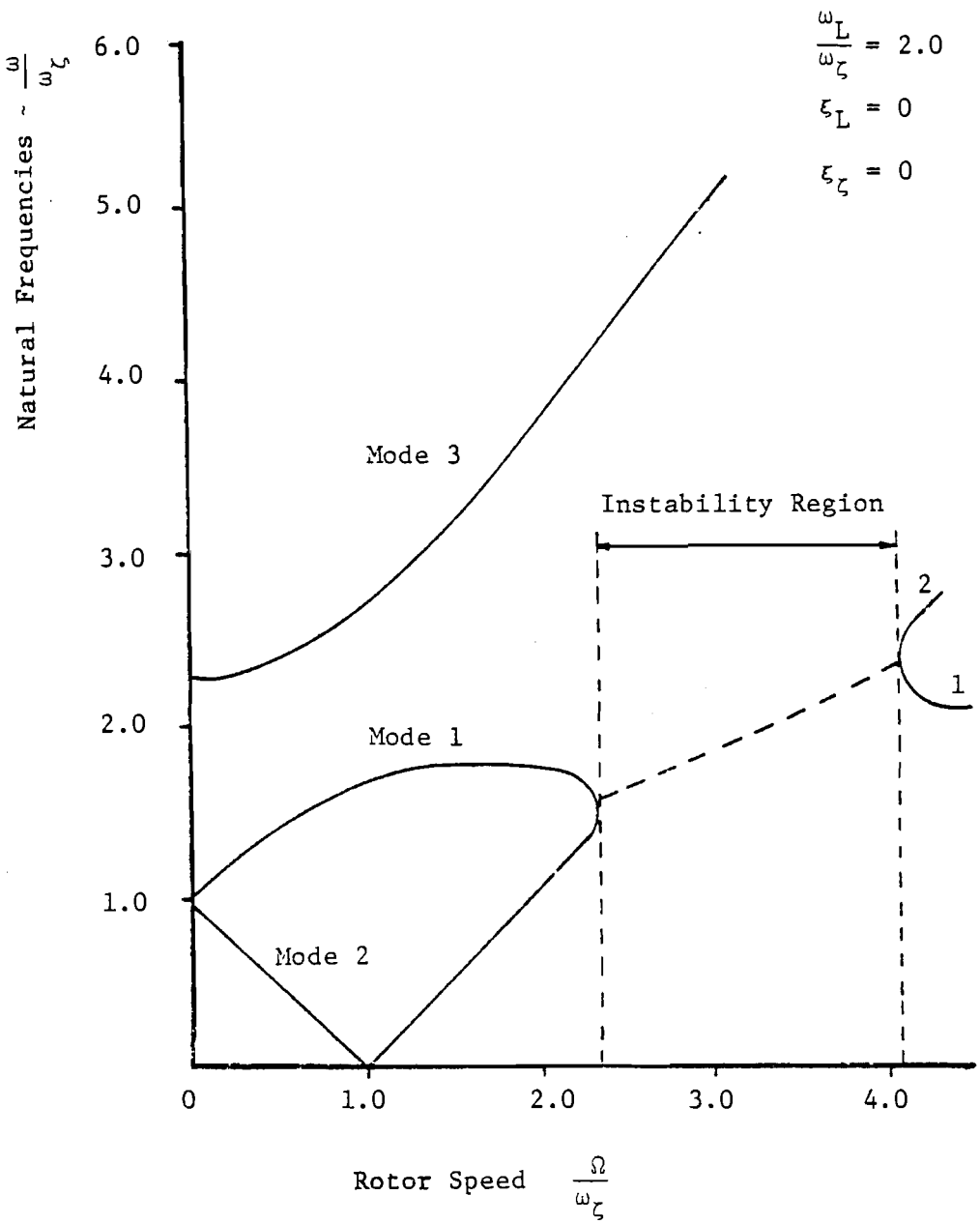

Figure 55. Blade Lag/Tower Sway Frequencies (continued)

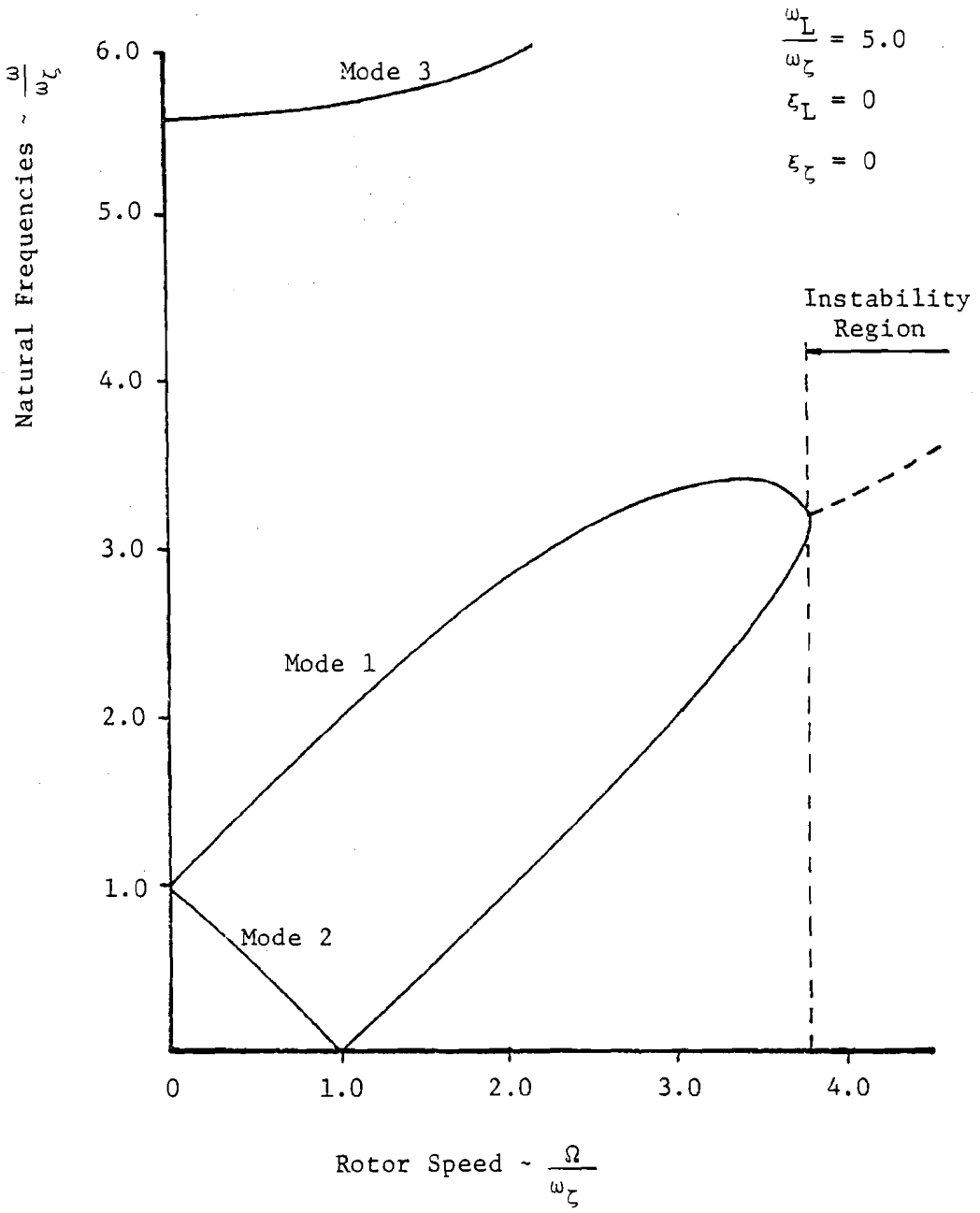

Figure 56. Blade Lag/Tower Sway Frequencies (continued)

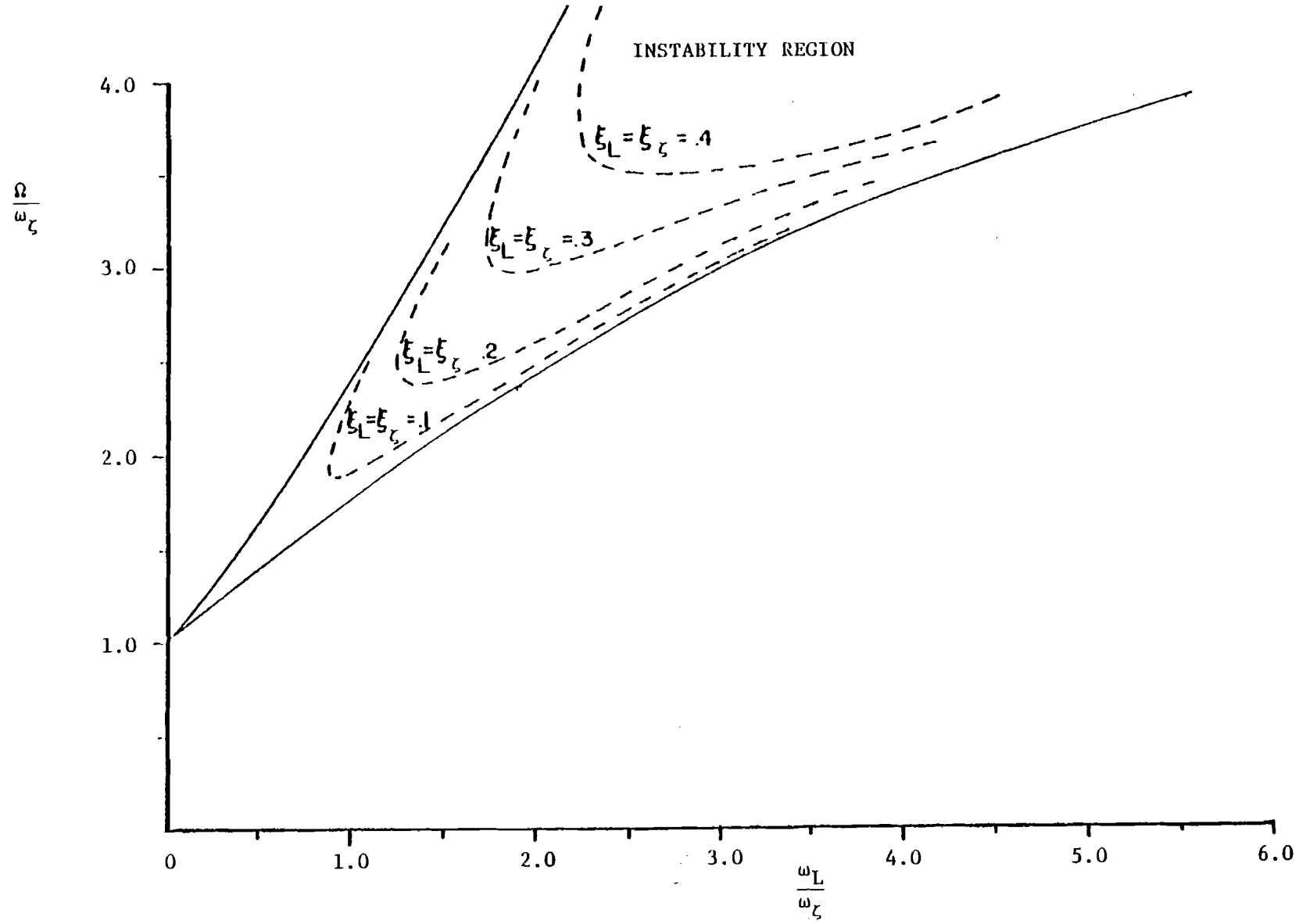

Figure 57. Blade Lag/Tower Sway Instability Region (Reference 36)

The instability region is more easily seen in Figure 57. Here damping has been added to the blades and tower; this causes a dramatic reduction in the region of instability. For instance: with no damping, the system is unstable at $\Omega/\omega_\zeta = 2.0$ for towers of about the same stiffness as the blades; the lead-lag angles would increase without limit, destructively. Adding a slight amount of damping to the blades and to the tower makes the system stable at that point, pushing the region of instability up to higher rotor speeds and slightly higher tower stiffness. Physically this result dictates a high lead-lag frequency (i.e., no lag hinge) for soft towers (ω_L/ω_ζ low). For an articulated blade with a lag frequency less than the rotor speed, this result determines the damping which must be added to the lag hinge to avoid the instability.

This instability -- the coupling of lateral motion of the mast to inplane motion of the blades -- is called "ground resonance" for helicopters because it historically has occurred with soft-masted ships while the wheels are on the ground (thus adding lateral ground reaction forces).

Solving the three-bladed system using the other numerical method (Floquet Transition Matrix) is necessary when the gravity effect is included (the equations then have periodic coefficients). Sheu found the gravity effect to be negligible, since the pendulum frequency of the blade ($\omega_{pendulum} = \frac{\sqrt{gS}}{I}$) is much lower than the uncoupled blade frequency. However, the effect of tower flexibility and motion on the Mathieu's instability described in Chapter II, is yet to be assessed.

The case of a two-bladed rotor was also solved by Sheu, by using the Floquet Method, including gravity effect. More solution modes result because higher harmonics are taken into account in the Fourier series (i.e., sin $2\Omega t$, cos $2\Omega t$, sin $3\Omega t$, and cos $3\Omega t$). For the single ratio of tower to blade frequency he considered (ω_L/ω_ζ = .924), the instability region is roughly the same as for the above three-bladed rotor. Actually, small additional regions of instability crop up for each additional set of higher harmonic terms considered, but these new regions vanish for even a small amount of damping. Again, the gravity effect was negligible.

D. Coupled Rotor-Tower Instability - Tower Pitching and Blades Flapping

A more complex dynamic situation exists for the tower pitching motion. In this motion the tower bending is coupled with the blades in flapping; there are two distinct motions, as represented in Figure 59 -- axial translation and rotorplane pitching. It is certainly more convenient to separate these two motions and search for independent solutions for instability boundaries. One justification for this step is to notice that the two motions (degrees of freedom) roughly correspond to solutions to the simpler problem of an elastic pole plus the nacelle mass.[40] That is, looking at Figure 59, a nacelle with distributed mass atop a flexible tower has two pitching modes. One mode, Case 1, has mostly tower bending and little nacelle pitching; the other, Case 2, has mostly nacelle pitching and little tower bending. Of course, the degree of coupling between these two extremes depends on the moment of inertia

of the nacelle, and the stiffness of attachment to the pole. When the blade dynamics are also included, the problem is complex; therefore, the two degrees of freedom will be separated here, and solutions are presented to the independent coupled motions.

Case 1 motion, the axial translation mode, will be studied first. The simplest dynamic model to represent this mode is a coupled spring-mass system:

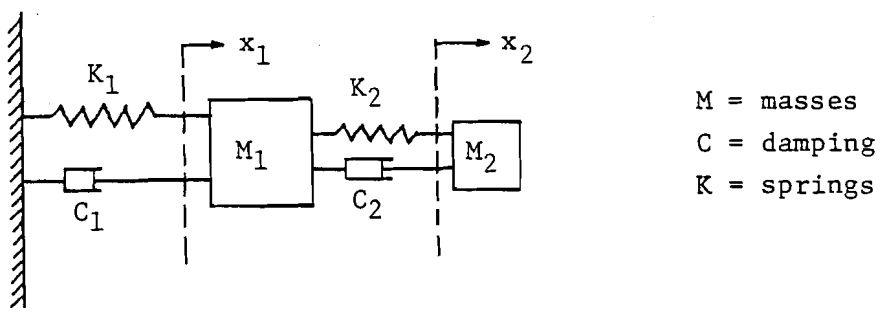

Figure 58. Coupled Spring-Mass System

Equations of motion for this system are:

$$m_1\ddot{x}_1 + C_1\dot{x}_1 + K_1x_1 - C_2(\dot{x}_2-\dot{x}_1) - K_2(x_2-x_1) = 0$$

$$m_2\ddot{x}_2 + C_2(\dot{x}_2-\dot{x}_1) + K_2(x_2-x_1) = 0 \qquad \text{(V-53)}$$

Substituting $x_1 = A_1e^{pt}$ and $x_2 = A_2e^{pt}$ gives the characteristic equation:

$$\begin{bmatrix} m_1p^2 + (C_1+C_2)p + (K_1+K_2) & -(C_2p+K_2) \\ -(C_2p+K_2) & (m_2p^2+C_2p+K_2) \end{bmatrix} \begin{Bmatrix} A_1 \\ A_2 \end{Bmatrix} = 0$$

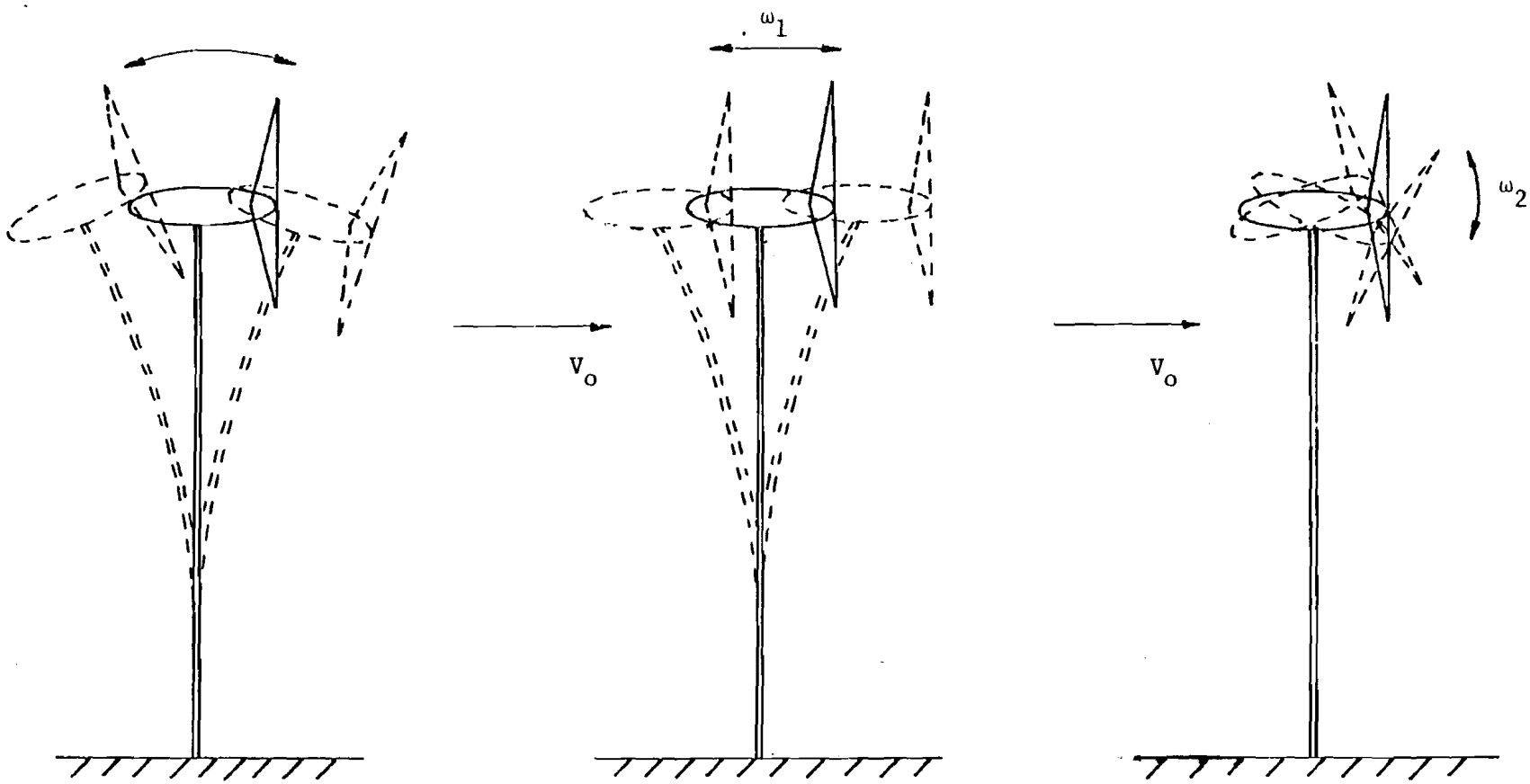

Tower Pitching
Plus Blades in Flapping

Mostly Tower Bending
(Axial Translation)

Mostly Nacelle Pitching
(Nacelle Rotation)

Figure 59. Coupled Rotor-Tower Motion

$$\boxed{\begin{aligned}&[m_1m_2]p^4 + [C_1m_2 + C_2\ (m_1+m_2)]p^3 + [K_1m_2 + K_2\ (m_1+m_2)]p^2 \\ &\quad + [K_1C_2 + K_2C_1]p + K_1K_2 = 0\end{aligned}} \qquad \text{(V-54)}$$

Characteristic Equation of Coupled Spring-Mass System

The roots of this equation give the natural frequencies of the damped, transient motion of the coupled spring-mass system. There will be two pairs of complex conjugates for each set of parameters, (m_i, C_i, K_i).

In this idealization, the m_1 system represents the isolated tower plus nacelle mass, with its own generalized mass and natural frequency. The m_2 system represents the rotating rotor blade, with its own separate characteristics.

The simple second order oscillator equations are:

$$\ddot{x} + \frac{C}{m}\dot{x} + \frac{K}{m}x = 0 \qquad \text{for simple spring mass} \qquad \text{(V-55)}$$

or:

$$\ddot{x} + 2\xi\ \omega_o\ \dot{x} + \omega_o^2\ x = 0 \qquad \text{in general} \qquad \text{(V-56)}$$

where: ξ = damping ratio

ω_o = natural frequency of motion

The characteristic equation can now be written in terms of the general quantities ξ and ω_o (damping ratio and natural frequency). The spring-mass equation V-54 can be rewritten as:

$$p^4 + [\frac{C_1}{m_1} + \frac{C_2}{m_2}\ (1 + \frac{m_2}{m_1})]p^3 + [\frac{K_1}{m_1} + \frac{K_2}{m_2}\ (1 + \frac{m_2}{m_1})]p^2$$

$$+ [(\frac{K_1}{m_1})\ (\frac{C_2}{m_2}) + (\frac{K_2}{m_2})\ (\frac{C_1}{m_1})]p + (\frac{K_1}{m_1})\ (\frac{K_2}{m_2}) = 0$$

This gives the general form of the characteristic equation:

$$\boxed{\begin{aligned} & p^4 + [2\ \xi_T\ \omega_T + 2\ \xi_B\ \omega_B\ (1 + \frac{I_b}{I_T})]\ p^3 \\ & + [\omega_T{}^2 + \omega_B{}^2\ (1 + \frac{I_b}{I_T})]\ p^2 \\ & + [2\ \omega_T\ \omega_B\ (\xi_B\ \omega_T + \xi_T\ \omega_B)]\ p \\ & + \omega_T{}^2\ \omega_B{}^2 = 0 \end{aligned}} \qquad \text{(V-57)}$$

where: I_T = mass moment of inertia of the tower including the nacelle (as a point mass)

I_b = blade moment of inertia

ω_T = natural frequency in bending of the tower and nacelle mass

ω_B = natural frequency of rotating blade

$2\xi_T\omega_T$ = tower damping = $\frac{C_T}{I_T}$

The flapping equation from Chapter III (with no gravity or crosswind) is:

$$\ddot{\beta} + \frac{\gamma\Omega}{8}\ \dot{\beta} + [\Omega^2(1+\varepsilon) + \frac{K_B}{I_b}]\ \beta = 0$$

This gives the blade damping ratio and frequency:

$$2\ \xi_B\ \omega_B = \frac{\gamma}{8}\ \Omega$$

$$\omega_B{}^2 = \Omega^2[1+\varepsilon + \frac{K_B}{I_b\Omega^2}] \qquad \text{(V-58)}$$

Thus, the characteristic equation can be reduced to:

$$\boxed{\begin{aligned} & p^4 + \left[\frac{C_T}{I_T} + \frac{\gamma\Omega}{8}\left(1 + \frac{I_b}{I_T}\right)\right] p^3 \\ & \quad + \left[\omega_T{}^2 + \Omega^2 \left(1 + \frac{I_b}{I_T}\right) \left(1+\varepsilon + \frac{K_B}{I_b\Omega^2}\right)\right] p^2 \\ & \quad + \left[\frac{\gamma\Omega}{8}\,\omega_T{}^2 + \Omega^2\left(\frac{C_T}{I_T}\right) \left(1+\varepsilon + \frac{K_B}{I_b\Omega^2}\right)\right] p \\ & \quad + \omega_T{}^2\,\Omega^2 \left[1+\varepsilon + \frac{K_B}{I_b\Omega^2}\right] = 0 \end{aligned}} \qquad \text{(V-59)}$$

This equation is the characteristic equation of the rotating blade-tower system; with all the input quantities known, the natural motion and damping can be found from the usual complex root form: $p = \alpha \pm i\omega$. For illustration and computation here, equation V-59 is non-dimensionalized with ω_T, the tower frequency, and damping is omitted. Blade natural frequency is written as ω_B, and the characteristic equation becomes:

$$\boxed{\frac{p^4}{\omega_T{}^4} + \left[1 + \left(\frac{\omega_B}{\omega_T}\right)^2 \left(1 + \frac{I_b}{I_T}\right)\right] \frac{p^2}{\omega_T{}^2} + \left(\frac{\omega_B}{\omega_T}\right)^2 = 0} \qquad \text{(V-60)}$$

Blade-Tower Equation, No Damping

The results are plotted in Figure 60. Blade frequency, divided by tower frequency, is along the abscissa. Characteristic frequency, divided by tower frequency, is along the ordinate. As the mass ratio decreases ($I_B/I_T << 1.0$) the mass effect diminishes rapidly. Wind generators usually have massive towers so I_B/I_T is very small. Hence, the effect of blade mass (or I_B) on this frequency is small; however, the effect of increased blade mass or I_B is also to decrease blade

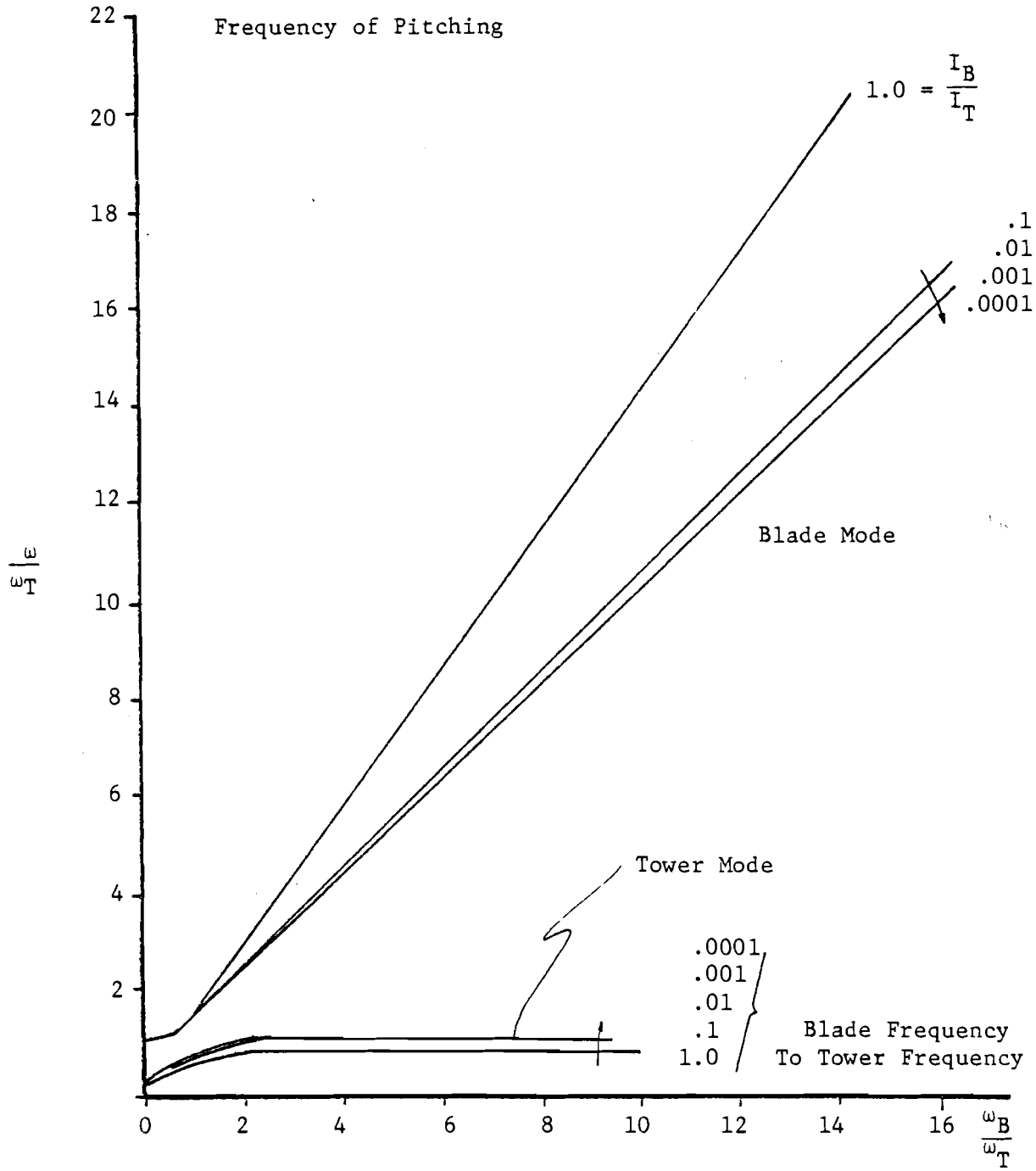

Figure 60. Frequencies of Pitching Motion:
Axial Translation Mode (No Damping)

frequency ω_B, thus moving back along the abscissa. So, the designer must keep in mind the effects of increased I_B on blade frequency.

Also, the plot shows the rapid uncoupling of the modes as blade frequency gets larger than tower frequency. The upper mode represents the blade vibrating along $(\frac{\omega}{\omega_T} \approx \frac{\omega_B}{\omega_T})$, and the lower mode represents the tower alone $(\frac{\omega}{\omega_T} \approx 1.0)$. The curve does point out the "softening" effect of the vibrating blade on the tower when the natural frequencies are close $(\omega_B \approx \omega_T)$. Also, for "subharmonic" blades, that is, blades with frequencies less than the tower frequency, the combined motion is highly coupled, and the frequencies are not well separated. For a soft blade like above, the blade frequency will also vary due to rotation, Ω, so the tower pitching motion will have a range of frequencies denoted by the range of travel of $\frac{\omega_B}{\omega_T}$ along the abscissa. Certainly, wise design and common sense would cause one to separate the tower frequency from the blade frequencies to avoid these problems.

In lead-lag motion, the blades have little damping, so the "damping-free" curves are sufficient for guidance. But in flapping motion, there is substantial aerodynamic damping, which can affect the frequencies of motion. Certainly for this simple axial translation model, or the coupled spring-mass system, there are no self-excited oscillations or instabilities, and the design problem consists of pinning down the frequencies of the coupled motion and adding damping if it appears lightly damped.

Blade damping enters by way of the Lock number, γ, the ratio of aerodynamic forces to inertial forces. No tower damping exists in this

model; should the resulting roots indicate poor damping (i.e., $\alpha \simeq 0$), dampers could be added to the tower guy wires or incorporated in the elastic pole. For a constant value of $I_B/I_T = .01$, a number of cases were calculated for low blade damping; $\gamma = 4$. The results are shown in Figure 61.

The graph shows the no damping curve and another curve for $\gamma = 4$, and for various values of rotational speed Ω (since both Ω and γ appear in the damping terms). It can be seen that the frequencies of the blade mode are changed a slight amount by damping (increased); the tower mode is virtually unchanged. The oscillation of the blade actually vanishes for large damping (large γ, or large Ω), e.g., the blade motion is over critically damped. Again, around the point $\frac{\omega_B}{\omega_T} = 1$, the modes coalesce, and damping and frequency play a significant role. Blade damping around this region affects tower motion by decreasing tower frequency, ($\omega_T \simeq .953$), and damping tower motion slightly. Below $\frac{\omega_B}{\omega_T} < 1$, good damping exists for both modes. The results of this indicate no problem to a designer from this mode, except for the large variation in frequencies around the point $\omega_B/\omega_T \simeq 1$. Thus, there is nothing to indicate a problem in going to a "soft" tower, i.e., one with a frequency substantially less than blade or rotational frequencies. Of course, it may be difficult to design a tower that is both strong in bending (to resist rotor thrust) and having a low (subcritical) frequency in bending.

Going on, Case 2 motion is nacelle pitching atop a steady tower, as depicted in Figure 59. This motion is solved by modelling the dynamics of a pitching, rotating rotor, looking for instabilities and

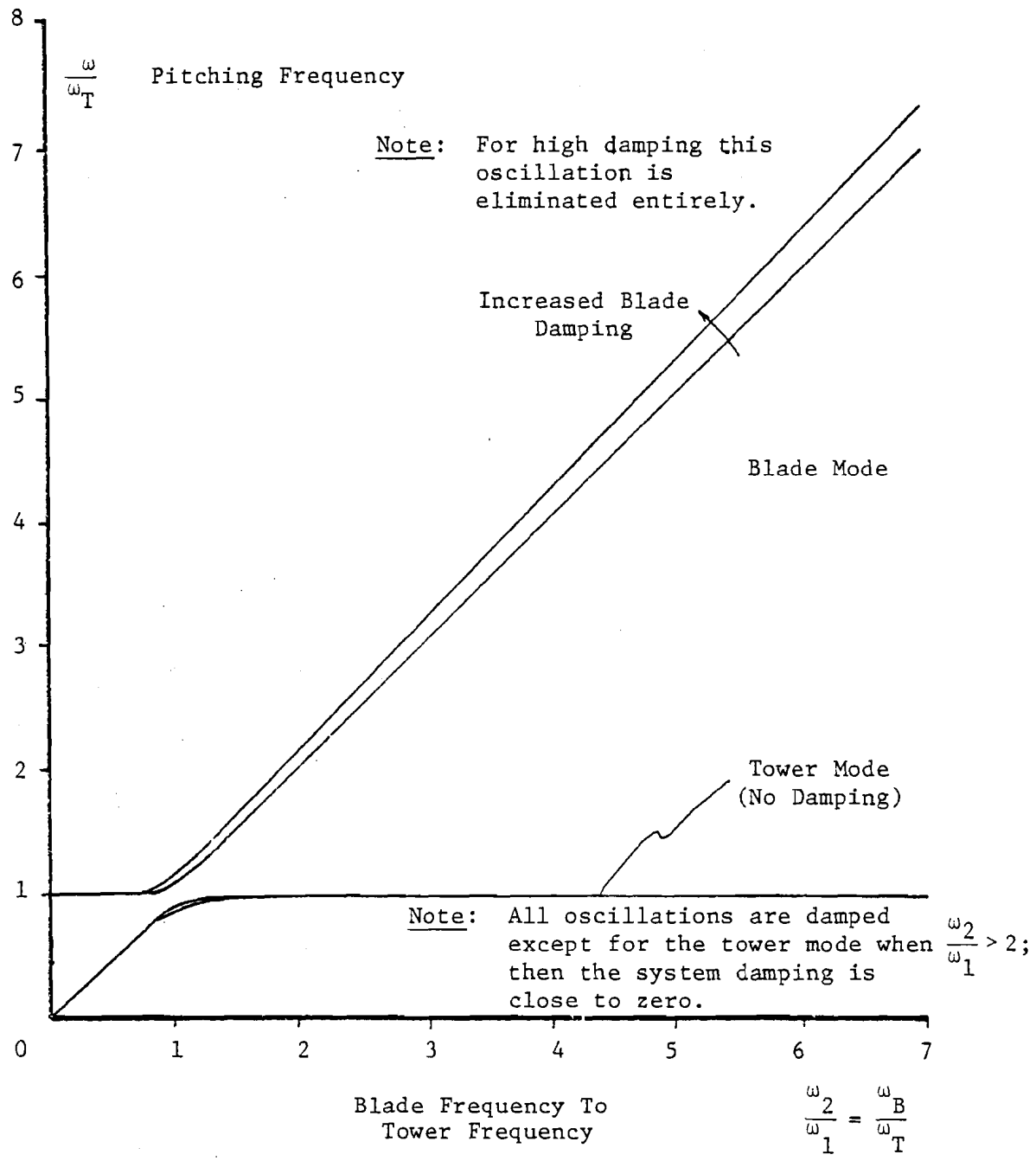

Figure 61. Frequencies of Pitching Motion ($\frac{I_b}{I_T} = 0.01$, $\gamma = 4$)

depicting the motion response. The tower-nacelle system is not included in the model, except as an understood "mechanism" to provide a pitch oscillation of the rotor hub. The designer's problem is to assess the stiffness of attachment of the nacelle to the pole tower; a "soft" attachment will yield a low hub pitching frequency, and a "hard" attachment will yield a high frequency. The Case 2 solution here solves the dynamic response of the rotor to this input hub frequency.

From Chapter II, the flapping equation is:

$$\boxed{\ddot{\beta} + \Omega^2 \left(1+\varepsilon + \frac{K_B}{I_b \Omega^2}\right) \beta = \frac{M_A}{I_b}} \tag{V-61}$$

[Note: where M_A represents all aerodynamic forces.]

For a hub pitching at an angular velocity Q, the blade angular velocities in the XYZ (blade) system are the same as for a yaw rate q, displaced by $\pi/2$ in azimuth (see Equation II-37); that is, the angular velocity is in the vertical plane (Q) rather than the horizontal plane (q):

$$\omega_x = Q \sin \psi \cos \beta + \Omega \sin \beta$$

$$\omega_y = Q \cos \psi - \dot{\beta}$$

$$\omega_z = - Q \sin \psi \sin \beta + \Omega \cos \beta \tag{V-62}$$

The dynamic equation is again derived by using the Euler equations; this time Q is not constant:

$$\ddot{\beta} + \Omega^2 \left[1+\varepsilon + \frac{K_B}{I_b \Omega^2}\right] \beta = \frac{M_A}{I_b} - \underbrace{2\Omega Q(1+\varepsilon) \sin \psi}_{\text{gyroscopic inertia moment}} + \underbrace{\dot{Q}(1+\varepsilon) \cos \psi}_{\text{pitching acceleration term}} \tag{V-63}$$

Including aerodynamic terms, and dropping the hinge offset ε, gives the flapping equation due to a pitching oscillation $\hat{Q} = \frac{Q}{\Omega}$:

$$\boxed{\frac{d^2\beta}{d\psi^2} + \frac{\gamma}{8}\frac{d\beta}{d\psi} + \left(1 + \frac{K_B}{I_b\Omega^2}\right)\beta = \frac{\gamma}{8}\hat{Q}\cos\psi - 2\hat{Q}\sin\psi + \frac{d\hat{Q}}{d\psi}\cos\psi} \quad \text{(V-64)}$$

Blade Flapping Due to Hub Pitching Rate $\hat{Q}$

For a periodic input $\hat{Q} = \hat{Q}(\psi)$, the flapping solution is also periodic:

$$\beta(\psi) = \beta_o(\psi) - \beta_{1c}(\psi)\cos\psi - \beta_{1s}(\psi)\sin\psi \quad \text{(V-65)}$$

Now the coefficients of the harmonic series are not constant as they were in Chapter III, but represent periodic functions, solutions to a coupled set of differential equations.[12] Strictly speaking, the flapping solution V-65 should include many harmonics in the series. The coefficients of course will depend on the input parameters (Equation V-64) and the numbers of terms taken in the series. For simplicity here, only the first order terms are retained.

Equation V-65 is substituted in the equation of motion V-64, and like harmonic coefficients are equated as before (i.e., $\cos\psi$, $\sin\psi$, etc.). A system of two coupled equations results:

$$\boxed{\begin{aligned} -a_1'' - \frac{\gamma}{8}a_1' - \left(\frac{K_B}{I_b\Omega^2}\right)a_1 - 2b_1' - \frac{\gamma}{8}b_1 &= \frac{\gamma}{8}\left(\frac{Q_o}{\Omega}\right)\sin\omega_p + \left(\frac{Q_o}{\Omega}\right)\nu\cos\omega_p \\ 2a_1' + \frac{\gamma}{8}a_1 - b_1'' - \frac{\gamma}{8}b_1' - \left(\frac{K_B}{I_b\Omega^2}\right)b_1 &= -2\left(\frac{Q_o}{\Omega}\right)\sin\omega_p \end{aligned}} \quad \text{(V-66)}$$

Coupled Flapping Due to Hub Pitching: $Q \sin \nu\Omega$

$$\beta_{1c} \simeq -\frac{16}{\gamma}\hat{Q} + [(\frac{16}{\gamma})^2 - 1]\frac{d\hat{Q}}{d\psi}$$

$$\beta_{1s} \simeq -\hat{Q} + (\frac{24}{\gamma})\frac{d\hat{Q}}{d\psi} \qquad \text{(V-70)}$$

Periodic Solution when $\nu < 0.10$ (Sissingh and Zbrozek)

For $\hat{Q} = (Q_o/\Omega)\sin\nu\Omega$, and ν very small, the second terms above are small compared to the first terms; i.e., they get multiplied by ν by differentiating. The first terms are the same as in Chapter III, for the rotor plane tilting due to a <u>constant</u> yaw rate. Therefore, the dynamic solution is approximated by the quasi-steady solution when the tower frequency is 10% or less than the rotational frequency. For higher tower frequencies (i.e., higher hub pitching frequencies), Equation V-70 does not hold. The tower frequency of interest here is the nacelle pitching via an elastic attachment at the pole top; in most wind turbines this attachment is stiff, giving a high pitching frequency. Thus, the approximate solution described above is not applicable to stiffly-attached rotors, and must be limited to wind turbines with softly attached nacelles.

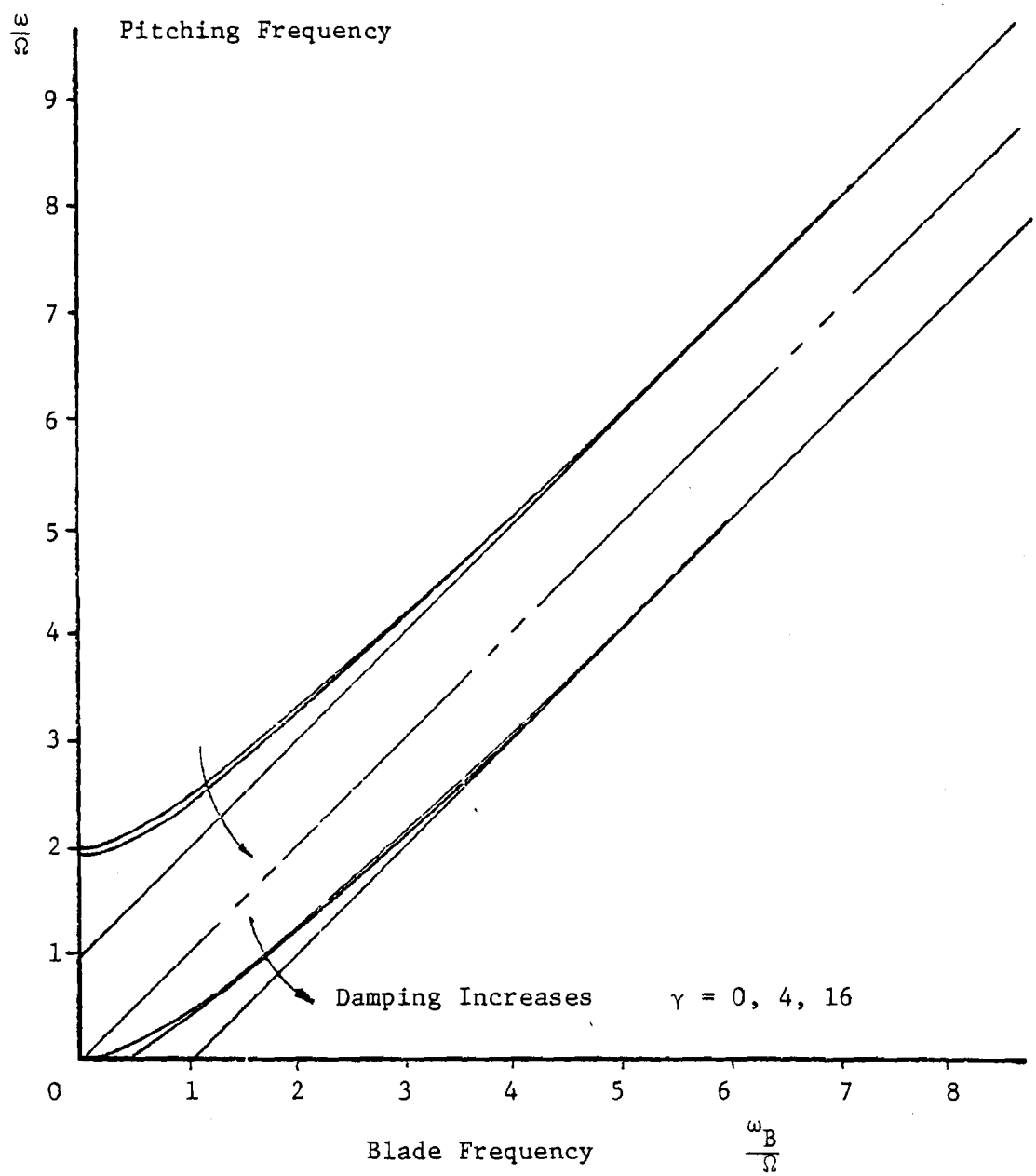

Figure 62. Blade Pitching Frequency
Versus Blade Natural Frequency

The results are shown in Figure 62. Three pairs of curves are shown, for three values of Lock number: $\gamma = 0$ (no blade damping), $\gamma = 4$ (light damping), $\gamma = 16$ (heavy damping). The abscissa is non-dimensional rotor blade frequency and the ordinate is the frequency of coupled flapping.

Two distinct, well-separated roots are seen: the familiar $(\omega + 1)$ and $(\omega - 1)$ frequencies which appear when a rotating frequency is simply transformed to the non-rotating tower system. At large values of blade frequency (stiff cantilevered blade) the blade damping does not affect the frequencies, and the tower sees the familiar $(\omega_B \pm 1)$ roots. However, as blade frequency approaches 1.0 (articulated blade), the roots are "stiffened" slightly. That is, the frequencies which the hub sees on an articulated blade $(\omega_B/\Omega = 1)$, are a little higher than 2.0 and 0 (i.e., in flapping resonance). The difference is greatly dependent on Lock number γ. No self-excited oscillations occur, and this transient motion is well-damped for all roots.

Another part of this motion is the forced response, or the particular solution to the differential equations V-66. The case of an articulated rotor $(\omega_B/\Omega = 1)$ has been solved by Sissingh and Zbrozek, for sinusoidal $Q(\psi)$.[41] A harmonic series was assumed, and a solution matrix was formed by equating harmonic coefficients. For slow pitching frequencies, i.e., pitch frequency to rotational frequency is $\leq 10\%$, the coefficients can be approximated by:

where:

$$\hat{Q} = \frac{Q_o}{\Omega} \sin \nu\Omega = \frac{Q_o}{\Omega} \sin \omega_p$$

ν = ratio of hub pitching angular velocity to = $\frac{\omega_p}{\Omega}$

Q_o = hub pitching amplitude

$a_1 = \beta_{1c}$

$b_1 = \beta_{1s}$

To search for response, we assume general solutions of the form:

$$a_1 = A\ e^{ip\psi} = A\ e^{(\alpha + i\omega)\ t}$$

$$b_1 = B\ e^{ip\psi} = B\ e^{(\alpha + i\omega)\ t} \qquad \text{(V-67)}$$

This gives the homogeneous solution matrix (right-hand side = 0):

$$[p^2 + \frac{\gamma}{8} p + \frac{K_B}{I_b\Omega^2}]\ A + [2p + \frac{\gamma}{8}]\ B = 0$$

$$[-2p - \frac{\gamma}{8}]\ A + [p^2 + \frac{\gamma}{8} p + \frac{K_B}{I_b\Omega^2}]\ B = 0 \qquad \text{(V-68)}$$

And the characteristic equation is then:

$$\boxed{p^4 + \frac{\gamma}{4} p^3 + [(\frac{\gamma}{8})^2 + \frac{2K_B}{I_b\Omega^2} + 4]\ p^2 + \frac{\gamma}{4}\ [2 + \frac{K_B}{I_b\Omega^2}]\ p + [(\frac{\gamma}{8})^2 + (\frac{K_B}{I_b\Omega^2})^2] = 0} \qquad \text{(V-69)}$$

Again, the roots of this equation represent the time constants and frequencies of the rotor system to a hub pitching freedom of motion. The solution roots denote the transient response, which is the place to look for self-excited instabilities.

CHAPTER VI

ROTOR AEROELASTIC INSTABILITIES

The rotor blades have been viewed up to now largely as having predominantly uncoupled degrees of freedom. Including the coupling between the degrees of freedom yields sets of non-simple equations to depict the coupling "modes." The choice of which particular coupling effects to study, has depended on observed instabilities and unexplained vibration in helicopter rotors.[42] However, the study of the entire coupled situation, freedom in flapping, lead-lag, and torsion as well as hub flexibility, is currently receiving a great amount of analytical and computational effort by rotary wing dynamicists (see References 43, 44, 45, and 46). Historically, only the important coupling effects were studied; now it is in vogue to write the whole generalized rotor model, and search for instabilities depicted by the equations, but possibly having no observed experimental occurrence. These general solutions are also quite difficult to interpret.

For wind turbine blades, the aeroelastic terms are different in many ways from helicopter values. A significant difference is the increased planform area and twist of most wind generators; another is the usual aft chordwise location of the blade mass axis. The "global" solution may point out dynamic pitfalls which will have to be avoided in wind turbines, but at present, much can be learned from test results and observations. An important difference between analytical work on

helicopters and wind turbines is the continually changing frequency and torque in operation for wind turbines. This added complexity needs to be studied via the global solution approach.

This chapter describes the four most important aeroelastic instabilities observed and successfully explained via theory for helicopter rotors (Bramwell, 1977; Loewy, 1969).[9,42] The results serve to provide a "feel" for similar aerodynamically-induced situations on wind turbine rotors, but are not directly applicable to most wind generators. The wind turbine environment is very different; thus non-constant forcing functions, search for new hypotheses, and across-the-board damping (rather than discrete frequency fixes like vibration absorbers, etc.) will become more important to wind generator aeroelasticians.

A. Flap-Lag Instability

Flap-lag instability is an unstable oscillation of single rotor blades, consisting of a coupling of flapping motion with lead-lag motion. It is caused by the coupling of the inplane Coriolis moment caused by flapping velocity ($\dot{\beta}$), and modification of the flapping centrifugal moment by the difference in inplane blade velocity ($\dot{\zeta}$). The instability has been observed on articulated and hingeless rotors, and can be predicted from the blade flapping and lead-lag equations of motion. The complete derivation can be found in References 47 and 48.

The additional terms in the equations already derived in Chapter III are inertial terms and aerodynamic terms. The new inertial term in the flapping equation is the additional Coriolis term ($2I_b\Omega\beta\dot{\zeta}$) due to

lead-lag oscillation. It is the most significant term derived from using the new instantaneous inplane velocity of $(\Omega + \dot{\zeta})$ rather than the assumed constant Ω. The lead-lag equation of motion contains the Coriolis moment $(-2I_b\Omega\beta\dot{\beta})$ already derived in Chapter II. The aerodynamic moments are also coupled; the tangential velocity at the blade element is now written:

$$U_T = (\Omega + \dot{\zeta})r \qquad \text{(VI-1)}$$

rather than:

$$U_T = \Omega r \quad \text{(Chapter II)}$$

If the flapping and lead-lag mass moments of inertia are equal (I_b), the coupled equations of motion are:

FLAPPING:
$$\frac{d^2\beta}{d\psi^2} + \frac{\gamma}{8}\frac{d\beta}{d\psi} + \left(\frac{\omega_\beta}{\Omega}\right)^2\beta + C_{\dot{\zeta}}\frac{d\zeta}{d} = 0 \qquad \text{(VI-2)}$$

LEAD-LAG:
$$F_{\dot{\beta}}\frac{d\beta}{d\psi} + \frac{d^2\zeta}{d\psi^2} + F_{\dot{\zeta}}\frac{d\zeta}{d\psi} + \left(\frac{\omega_\zeta}{\Omega}\right)^2\zeta = 0 \qquad \text{(VI-3)}$$

Flapping and Lead-Lag Coupling by Coriolis Moments

where:

$C_{\dot{\zeta}}$ = coupling coefficient due to coning angle $= 2\beta_o - \frac{\gamma}{8}\left[2\theta - \frac{4}{3}\frac{v_i}{\Omega R}\right]$

$F_{\dot{\beta}}$ = inplane Coriolis moment term coefficient $= \frac{\gamma}{8}\left[\theta - \frac{8}{3}\frac{v_i}{\Omega R}\right] - 2\beta_o$

$F_{\dot{\zeta}}$ = damping term including artificial inplane damping K_ζ $= \frac{\gamma}{8}\left[K_{\dot{\zeta}} + \frac{2C_D}{a} + \frac{4}{3}\theta\frac{v_i}{\Omega R}\right]$ (VI-4)

The characteristic equation of this matrix yields a quartic stability criterion:

$$[\lambda^2 + \frac{\gamma}{8}\lambda + (\frac{\omega_\beta}{\Omega})^2]\,[\lambda^2 + F_{\dot\zeta}\lambda + (\frac{\omega_\zeta}{\Omega})^2] - C_{\dot\zeta}F_{\dot\beta}\lambda^2 = 0 \qquad \text{(VI-5)}$$

or

$$\lambda^4 + B\lambda^3 + C\lambda^2 + D\lambda + E = 0 \qquad \text{(VI-6)}$$

where:

$$B = \frac{\gamma}{8} + F_{\dot\zeta}$$

$$C = (\frac{\omega_\beta}{\Omega})^2 + (\frac{\omega_\zeta}{\Omega})^2 + \frac{\gamma}{8}F_{\dot\zeta} - C_{\dot\zeta}F_{\dot\beta}$$

$$D = \frac{\gamma}{8}(\frac{\omega_\zeta}{\Omega})^2 + F_{\dot\zeta}(\frac{\omega_\beta}{\Omega})^2$$

$$E = (\frac{\omega_\beta}{\Omega})^2(\frac{\omega_\zeta}{\Omega})^2 \qquad \text{(VI-7)}$$

And the neutral stability boundary is given by:

$$[\theta - \frac{4}{3}\frac{v_i}{\Omega R}]^2 = \frac{(\frac{\omega_\beta}{\Omega})^2}{2(\frac{\omega_\beta^2}{\Omega^2} - 1)(2 - \frac{\omega_\beta^2}{\Omega^2})}\left\{\frac{2C_D}{a} + K_{\dot\zeta} + \frac{64\,\alpha\,\{(\frac{\omega_\beta}{\Omega})^2 - (\frac{\omega_\zeta}{\Omega})^2\}}{\gamma^2(1+\alpha)\,\{(\frac{\omega_\beta}{\Omega})^2 + \alpha\,(\frac{\omega_\zeta}{\Omega})^2\}}\right\} \qquad \text{(VI-8)}$$

and:

$$\alpha = K_{\dot\zeta} + 2\frac{C_D}{a} + \frac{4}{3}\theta\frac{v_i}{\Omega R}$$

The instability will occur only if:

$$1 \le (\frac{\omega_\beta}{\Omega})^2 < 2 \qquad \text{or} \qquad \Omega \le \omega_\beta \le \Omega\sqrt{2} \qquad \text{(VI-9)}$$

This is a normal range of flapping frequencies for helicopter rotors. Small wind generators have much higher natural frequencies, but large wind generators, or rotors with flapping hinges, have ω_β's close to Ω, as VI-9.

Results for $K_\zeta = 0$ (no mechanical damping) are shown in Figure 63 from Reference 47. For the instability to occur at all, flapping frequency ω_β must be close to lead-lag frequency, ω_ζ, in value. As pitch angle θ is increased the region of instability grows in size, but stays roughly centered on the $\omega_\beta = \omega_\zeta$ locus. The addition of lag damping can be expected to reduce these boundaries considerably.

This instability has not been seen on helicopter main rotors, but has been observed on tail rotors, where lead-lag frequencies are higher and a large range of pitch is used. The resulting lead-lag frequency of a tail rotor can be close to the flapping frequency, thus allowing the instability mechanism to appear. Wind generators usually will have "supercritical" lag frequencies, i.e., frequencies higher than the shaft speed. This instability, therefore, may be seen more often with wind generators, especially at high thrust levels and high pitch angles. This condition is most likely to occur when the windmill rotor enters the turbulent wake state, or has suddenly lost its shaft power and been allowed to overspeed. It should be a straightforward design fix to add inplane damping to a case like this, but the instability may become quite destructive if unheeded since the aerodynamic inplane damping is nil.

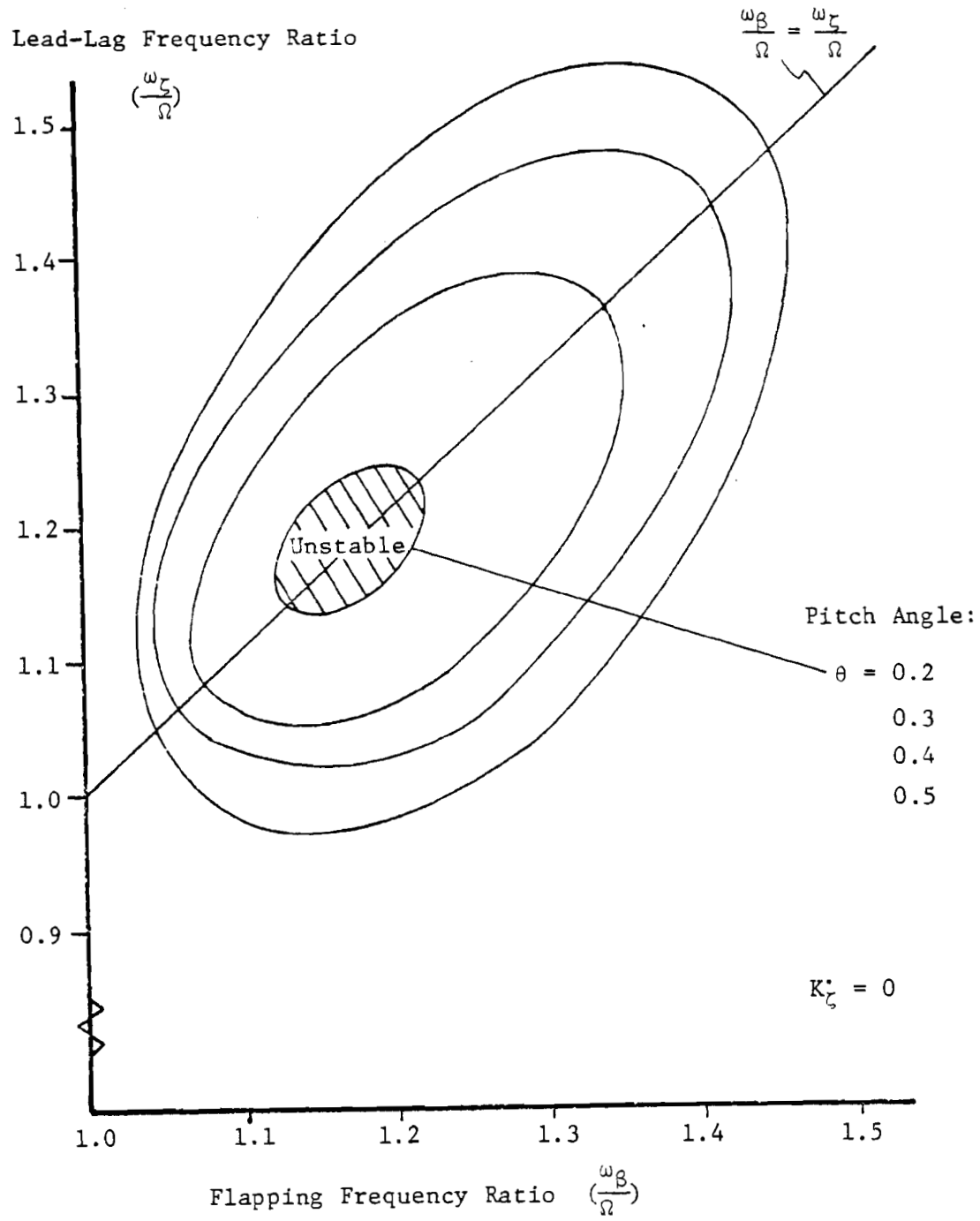

Figure 63. Stability Boundaries for Coupled Flap-Lag Motion

B. Pitch-Lag Instability

Structural torsional coupling (twisting of the blade due to bending), or pitch change due to a programed tilt of the lead-lag hinge, can introduce other coupling terms leading to instability (References 42, 49, and 50). Employing "matched stiffness" in the bending of a hingeless rotor is useful in avoiding this type of coupling. Briefly, a blade under aerodynamic loading will deflect in lead-lag as well as in flapping. The resulting offset of the aerodynamic axis (locus of action of all aerodynamic forces) will cause torsional moments at the blade root. Also, the blade, by virtue of its airfoil shape, will not have equal stiffness inplane and in flapping (i.e., $EI_x \neq EI_y$). The induced torque at the root will be zero, however, if the two root stiffnesses are equal; this is called "matched stiffness" and is simply a design attempt to reduce unwanted pitch changes. The usual practice of the industry is to make the blade root attachment softer than the actual blade by using a "dog bone" element.[9] The flapping frequency is determined largely by centrifugal forces, and the lead-lag frequency by blade structure and root attachment. Thus the induced torsional moment can be zeroed by judicious design. This approach may be useful for wind turbines if the bending deflections of blades become large enough to cause unwanted pitch changes. This is most likely for fiberglass (glass reinforced plastic) or wood blades which have shown high deflections in practice, but they also have the potential for variable design stiffness.

In general, the torsional deflection can be written (Reference 49):

$$\theta(\psi) = \zeta(\psi)\ \beta(\psi)\ \frac{1 - (\frac{\omega_\beta}{\Omega})^2 + (\frac{\omega_\zeta}{\Omega})^2}{(\frac{\omega_\theta}{\Omega})^2}\ \frac{I_\beta}{I_\theta} \tag{VI-10}$$

From this equation, the torsional deflection can be made to be zero, no matter what the instantaneous flapping or lagging angles are, by requiring:

$$1 - (\frac{\omega_\beta}{\Omega})^2 + (\frac{\omega_\zeta}{\Omega})^2 = 0 \tag{VI-11}$$

Thus coupled blade twist can be largely eliminated by suitable choice of lag frequency (i.e., choice of root lag stiffness via the "dog bone" element).

Now the torsional coupling terms of the above expression can be calculated and then added to the two coupled equations of the last section (VI-4, VI-5). This will modify the stability criterion developed before. The new approximate criterion is from Reference 50:

$$\boxed{F_\zeta^{\bullet} + \frac{2K_\zeta}{1 - (\frac{\beta_o}{\theta_o})K_\beta}\ \frac{\beta_o^2}{\theta_o}\ \Omega I_\zeta > 0} \tag{VI-12}$$

Stability Criterion, Hingeless Blade (Pei)

The quantities K_β and K_ζ are coefficients derived from the torsional deflection equation:

$$\Delta\theta = \frac{1 - (\frac{\omega_\beta}{\Omega})^2 + (\frac{\omega_\zeta}{\Omega})^2}{(\frac{\omega_\theta}{\Omega})^2}\ \frac{I_\beta}{I_\theta}\ \beta_o\zeta + \zeta_o\beta \tag{VI-13}$$

and:

$$\Delta\theta = K_\beta\beta + K_\zeta\zeta \tag{VI-14}$$

where:

I_β = flapping mass moment of inertia

I_θ = torsional mass moment of inertia

β_o = coning or equilibrium flapping angle

θ_o = equilibrium pitch angle

For articulated blades (hinged) the criterion is:

$$\boxed{F_{\dot{\zeta}} + \frac{2 \tan \alpha_2}{1 - (\frac{\beta_o}{\theta_o}) \tan \delta_3} \frac{\beta_o^2}{\theta_o} \Omega I_\zeta > 0} \qquad \text{(VI-15)}$$

Stability Criterion, Hinged Blades

where:

α_2 = lag hinge tilt, to cause pitch change due to lagging $= \Delta\theta/\zeta$

δ_3 = flapping hinge tilt, to cause pitch change due to flapping $= \Delta\theta/\beta$

θ_o = equilibrium pitch angle

The stability follows roughly the results of the previous section. Torsional coupling is not likely to get you into trouble unless the bending stiffnesses are very different (VI-12) or the coning angle is very high (VI-15). Each case must be checked on its own.

C. Pitch-Flap Flutter

The classical torsional flutter of aircraft wings appears in a rotor blade as an instability combining torsional oscillation destructively with flapping oscillation. The mechanism is that as the blade flaps, twisting moments arise due to inertial moments (due to mass axis

offset) and aerodynamic moments (due to aerodynamic offset). The resultant twisting of the blade further affects the flapping moments.

The coupled equations are not derived here. For a straight, untwisted, uniform blade the two equations (feathering and flapping) are:

$$\theta'' + \frac{1}{32}\frac{\gamma c^2}{R^2}\frac{I_b}{I_f}\theta' + \left(\frac{\omega_\theta}{\Omega}\right)^2\theta - \frac{3}{2}\left(\frac{Y_I}{R}\right)\frac{I_b}{I_f}[\beta''+\beta] + \frac{1}{32}\frac{c^2}{R^2}\gamma\frac{I_b}{I_f}\beta = 0 \qquad \text{(VI-16)}$$

$$\beta'' + \frac{\gamma}{8}C(K)\beta' + \left(\frac{\omega_\beta}{\Omega}\right)^2\beta + \frac{I_R}{I_b}[\theta''+\theta] - \frac{\gamma}{8}C(K)\theta = 0 \qquad \text{(VI-17)}$$

Flutter Equations

where:

$$I_R = -\int_0^R Y_I\, r\, dm = -Y_I\frac{M_b R}{2} = \text{mass axis offset inertia term } (Y_I \text{ positive aft of elastic axis})$$

The above expressions are easily derived from the simple feathering equation III-66 and the flapping equation III-6 neglecting gravity, crosswind, yaw and products of inertia. Unsteady aerodynamic affects can be included in the factor C(K). The inertia terms, β'' and θ'' are here included in the coupling (they are usually neglected if the flutter mechanism is not being studied). The torsional coupling term in the flapping equation and the last mass coupling term in the torsional equation are small and hence are neglected. The final equations are then:

$$\theta'' + \frac{\gamma}{32}\frac{I_b}{I_f}\left(\frac{c}{R}\right)^2\theta' + \left(\frac{\omega_\theta}{\Omega}\right)^2 - \frac{3}{2}\left(\frac{Y_I}{R}\right)\frac{I_b}{I_f}[\beta''+\beta] = 0 \qquad \text{(VI-18)}$$

$$\beta'' + \frac{\gamma}{8} C(K)\beta' + \left(\frac{\omega_\beta}{\Omega}\right)^2 - \frac{\gamma}{8} C(K)\theta = 0 \qquad \text{(VI-19)}$$

The characteristic equation is thus a quartic:

$$\lambda^4 + A\lambda^3 + B\lambda^2 + C\lambda + D = 0$$

$$A = \frac{\gamma}{8} C(K) + \frac{I_b}{4I_f}\left(\frac{c}{R}\right)^2$$

$$B = \left(\frac{\omega_\theta}{\Omega}\right)^2 + \left(\frac{\omega_\beta}{\Omega}\right)^2 - \frac{3}{16}\gamma\left(\frac{Y_I}{R}\right)\frac{I_b}{I_f} C(K) + \frac{\gamma^2}{252}\frac{I_b}{I_f}\left(\frac{c}{R}\right)^2 C(K)$$

$$C = \frac{\gamma}{8}\left(\frac{\omega_\theta}{\Omega}\right)^2 C(K) + \frac{1}{4}\frac{I_b}{I_f}\left(\frac{c}{R}\right)^2$$

$$D = \left(\frac{\omega_\theta}{\Omega}\right)^2\left(\frac{\omega_\beta}{\Omega}\right)^2 - \frac{3}{16}\gamma\left(\frac{Y_I}{R}\right)\frac{I_b}{I_f} C(K) \qquad \text{(VI-20)}$$

Characteristic Equation - Classical Flutter of Uniform Blade

The constants in the above equation contain the frequency information in the form of natural frequencies in flapping (ω_β) and torsion (ω_θ); the torsional frequency may be the natural frequency of the pitch change system if the blade is stiff in torsion. Also, the mass axis offset from the elastic axis (Y_I measured positive aft) and the mass moments of inertia (I_f, I_b) are important variables. The above equation will give conservative answers for a twisted tapered blade; a uniform blade was assumed.

Divergence of the blade in torsion will occur when the last term is equal to zero. The mechanism of divergence is that if the c.g. position is located sufficiently aft of the elastic axis, the resulting nose up moment due to centrifugal force is greater than the torsional structural restoring moment; the blade simply twists off in torsion. This is a

likely occurrence only with very soft blades in torsion, or control system misdesign, combined with an aft center of mass ("unbalanced" blade). The divergence criterion is:

$$\boxed{\left(\frac{\omega_\theta}{\Omega}\right)^2 = \frac{3}{16}\,\gamma\,\frac{I_b}{I_f}\,C(K)\,\left(\frac{Y_I}{R}\right)\,\left(\frac{\Omega}{\omega_\beta}\right)^2} \qquad \text{(IV-21)}$$

Divergence Boundary

C(K) is a measure of the "unsteadiness" of the aerodynamic forces;[53] for no unsteady aerodynamic effect C(K) = 1. For a rotor with a strong, viscous wake C(K) ≠ 1. For preliminary analysis C(K) is always taken as unity, and for wind turbines the effect of returning vorticity in the wake can probably be neglected (the bound vorticity is only a fraction of usual helicopter values and the wake is rapidly expanding).

The flutter mechanism is simply an oscillatory combination of the two torsional moments, which has negative damping. The flutter boundary is also found from the characteristic equation. A value of flutter frequency, ω, is assumed, and the real and imaginary parts of the root are found and set to zero. The resulting torsional frequency and mass axis offset for flutter are found to be:

$$\omega_\theta^{\,2} = \omega^2 + \frac{3}{16}\,\frac{(\omega^2-1)}{C(K)}\,c^2\,\left(\frac{I_b}{I_f}\right) \qquad \text{(VI-22)}$$

$$\frac{Y_I}{C} = \frac{4}{3}\,\frac{1}{\gamma}\,\left(\frac{c}{R}\right)\,\frac{1}{C(K)}\,\omega^2 - \left(\frac{\omega_\beta}{\Omega}\right)^2 + \frac{\gamma^2\,\omega^2\,C(K)}{64\,(\omega^2-1)} \qquad \text{(VI-23)}$$

Flutter Boundary

For a particular set of parameters, the boundaries can be found; a typical set is seen in Figure 64. The curve beginning at the origin

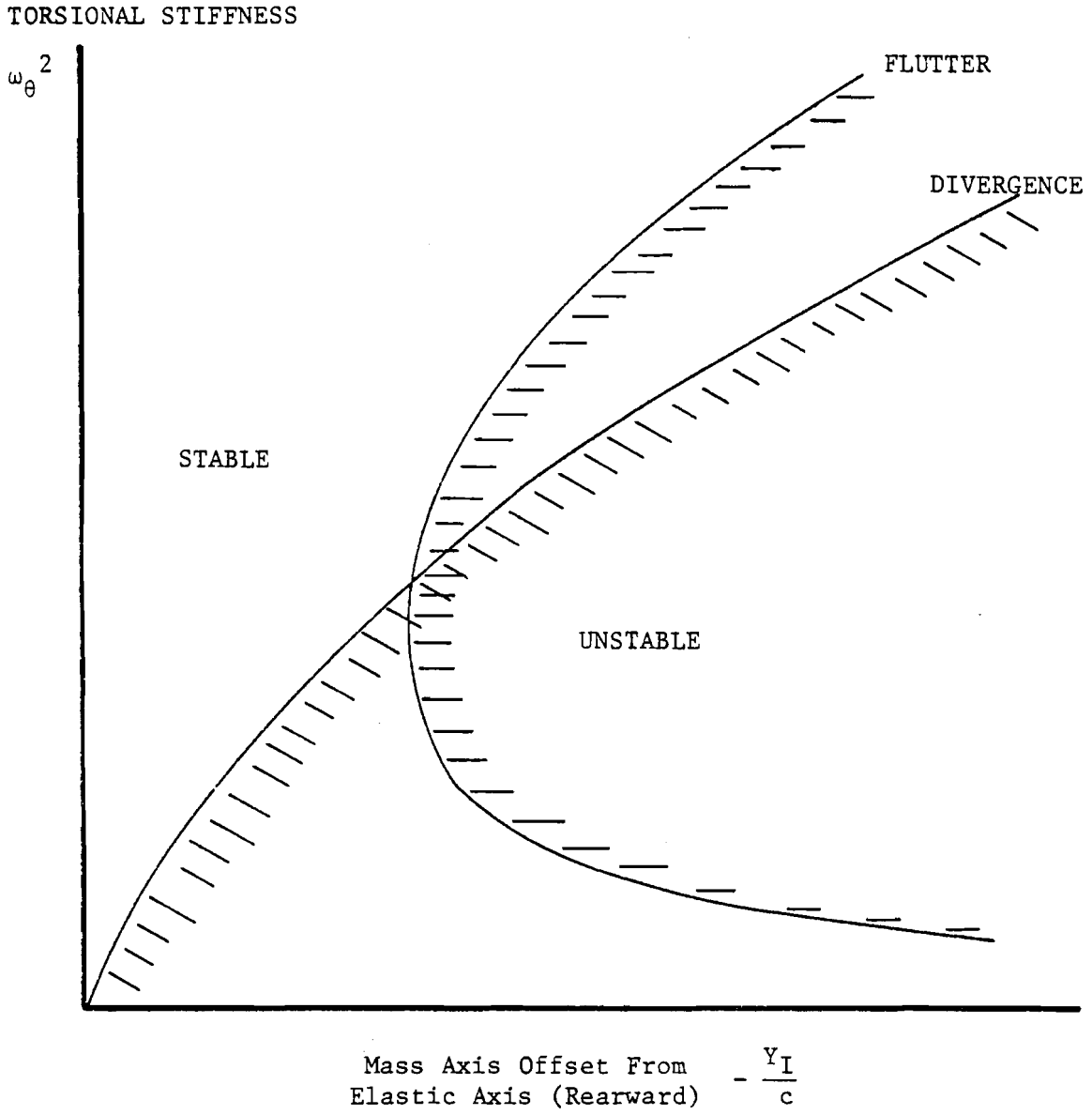

Figure 64. Stability Boundaries - Classical Flutter and Divergence

is the divergence boundary; values to the left are stable, to the right, unstable. For a particular value of torsional stiffness on the ordinate (usually corresponding to control system stiffness) the boundary gives the maximum allowable rearward position of the mass axis. For a mass axis ahead of the elastic axis (negative Y_I) divergence never could occur. Likewise, the flutter boundary is shown; minimum flutter speed corresponds to the left-most value of Y_I. As torsional stiffness increases, divergence becomes less of a problem, and flutter is the torsional design criterion. In general, hingeless blades are less stable in flutter than hinged blades, and heavy blades are less stable than light ones. The possible flutter of large wind turbine blades is a much greater possibility than for rotors since the masses are larger and the centrifugal stiffening is much less (lower rotational speed). Small wind generators would not be expected to flutter unless a failure in the control system drastically reduced the torsional root stiffness. Therefore, mass balancing of small wind generator blades is not worthwhile, but large blades may need it, especially if the flapping natural frequency is much higher than Ω.

D. Stall Flutter

Stall flutter is a phenomenon observed on highly loaded helicopter rotors in forward flight (References 54 and 55). The angle of attack on the blade varies considerably as it travels around one revolution. The analogous case for wind generators is for a large blockage due to tower obstruction, causing the airfoils to be stalled when they pass

through the tower wake. Large towers or framework assemblies of wind generators with many structural wake obstructions may cause stall flutter.

The mechanism lies in the aerodynamics of a pitching airfoil. Briefly, the pitching moment developed on an airfoil lags the pitching frequency. At certain values of pitching frequency at large angles of attack, the aerodynamic damping may become negative, leading to a limit cycle type of oscillation excited by aerodynamic phenomena alone. If the structural torsional restoring moment is low (low torsional stiffness) this limit cycle may become destructive. In any case, it leads to high oscillatory control loads during the limit cycle occurrence.

For particular airfoils, with specific pitching moment characteristics operated at various values of frequency and high angle of attack, the aerodynamic torsional damping can be estimated.[55] The difference between theory and experimental results is still great, however, even though the physical mechanism is known. The most profitable method for wind generators will be to avoid large obstructions leading to stalling at high frequencies, and to employ airfoils which have poor dynamic stall characteristics.

CHAPTER VII

BLADE STRUCTURAL ANALYSIS

The blades designed and built for the University of Massachusetts Wind Furnace are of spar-stiffened hollow shell construction, using glass fiber reinforced epoxy (GRP) as the structural material (References 1, 2, 3, and 4). This chapter describes the structural analysis of composite shell blades with arbitrary steady loading.

The strength and stiffness parameters of an arbitrarily twisted and tapered composite shell blade are developed in the first section. The computer program which mechanizes this analysis was written by E. Van Dusen,[4] and was updated and refined for this application; it can be found in Appendix II.

Expressions for the stresses and deflections of the shell beam under prescribed arbitrary loading are developed in the second section using input parameters developed in the first section. The stress-deflection program was also written by Dr. Van Dusen, and subsequently applied to the wind generator blade;[4] it can be found in Appendix III.

The third section develops expressions for the calculation of blade natural frequencies in bending and torsion; this analysis uses the stiffness, geometric and mass parameters provided by the analysis of Section A. A computer program for this is listed in Appendix IV. The fourth section describes methods of extension of the theory to include twisted blades.

The last section, Section E, provides the link between the static strength-stiffness solutions of this chapter, to the dynamic idealization of the blade. Rationale, assumptions, and analyses are provided which describe the simplified uncoupled blade dynamics in terms of the parameters developed from geometry, mass, stiffness, and natural frequency. In the rotor blade literature, this idealization is called the "hinge offset - spring" model.

A. Section and Stiffness Analysis for Arbitrary Shell Beam

The computer program is listed in Appendix II; the geometric, elasticity, and stress derivation can be followed in Theory and Analysis of Flight Structures by R. M. Rivello,[56] or in any thorough strength of materials text. A sample calculation for a simple beam is also given.

The shell beam (University of Massachusetts Wind Furnace blade) is shown in Figure 66. The XYZ axis system rotates with the blade; X-axis is spanwise, Y-axis in the plane of rotation, and Z-axis along the axis of rotation. A typical cross-section appears as follows; the X'Y' axis system is written for each blade section with origin at the nose and X' along the chord line:

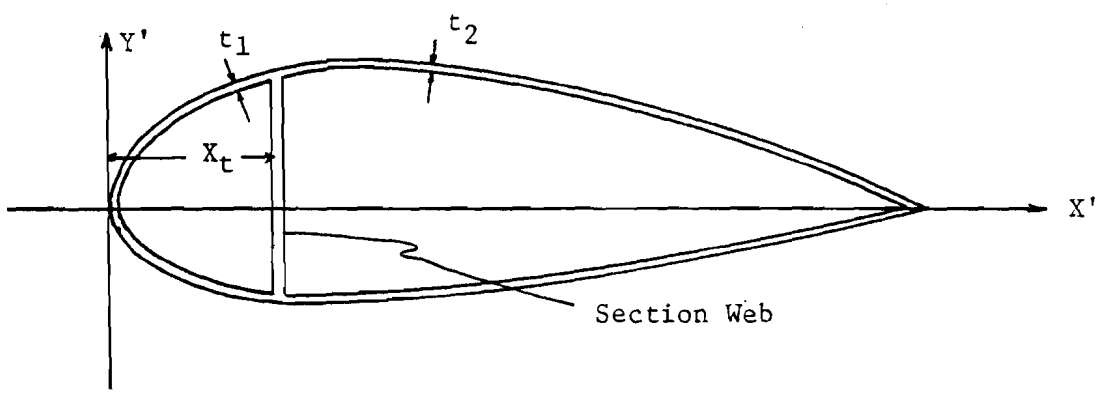

Figure 65. Blade Cross Section

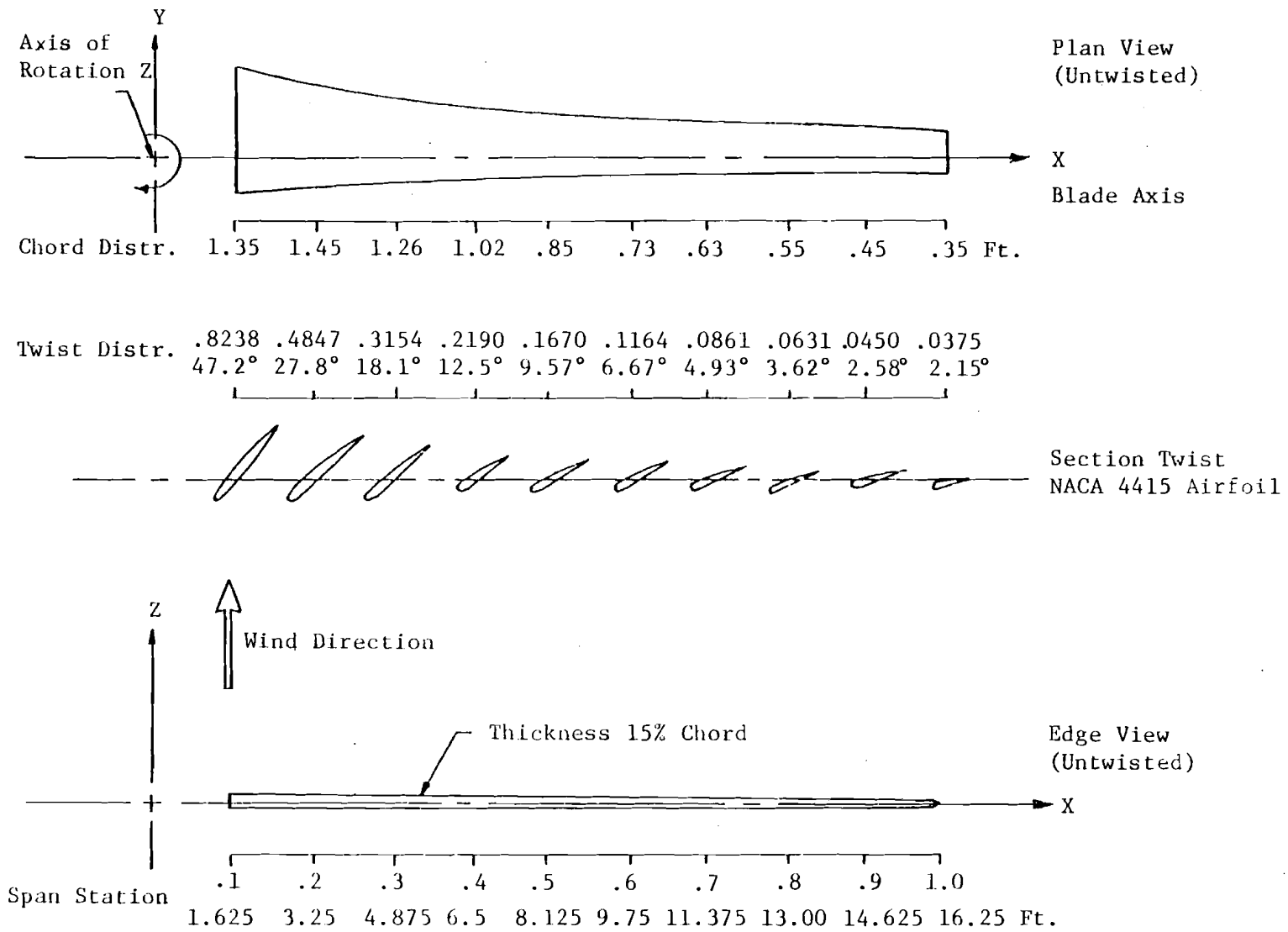

Figure 66. Composite Blade Design - University of Massachusetts Wind Furnace

The skin (which is a continuous laminate) has an integral D-spar in the nose, and a transverse web at the spar termination, X_t. The skin-spar combination is the principal bending structure and is composed of varying types and characteristic laminates (see Figures 20 and 21). For simplicity, the spar laminate thickness is weighted to have an effective modulus equal to the modulus of the skin laminate. For example, the skin laminate could be several layers of high quality balanced weave glass cloth, having a Young's modulus (E) of 2.2×10^6 psi; and the spar contain primarily uni-directional cloth, with a spanwise modulus of 4.4×10^6 psi, as shown:

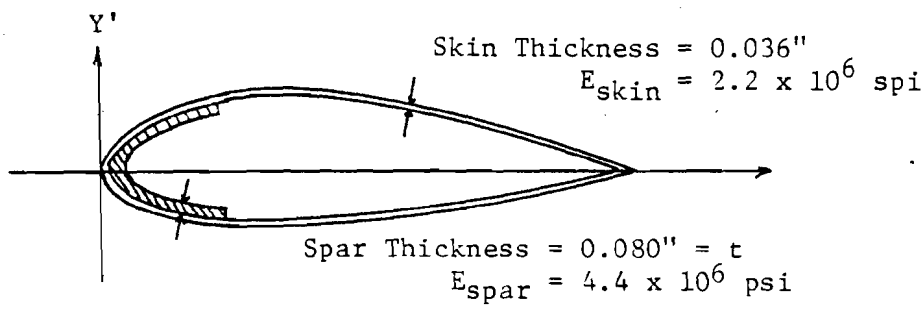

Figure 67. Actual Laminate

The equivalent cross section is modulus-weighted to the skin value, and new spar thickness calculated to yield equivalent EI:

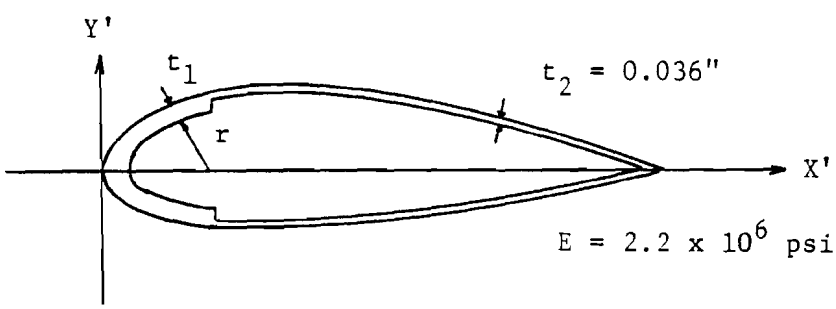

Figure 68. Weighted Laminate

We have:

$$\text{differential EI} = \delta(EI) = E_{spar}\,[r^4 - (r-t)^4]$$

$$= E_{skin}\,[r^4 - (r-t^*)^4] \qquad \text{(VII-1)}$$

For $t \ll r$ = radius from centroid, the differential stiffness is:

$$\delta(EI) = E_{spar}\, r_o^3\,(4t) = E_{skin}\, r_o^3\,(4t^*)$$

This gives the simple formula:

$$\boxed{t^* = \left(\frac{E}{E_1}\right)t} \qquad \text{(VII-2)}$$

with t = unweighted spar thickness

E = original modulus of D-spar laminate

t^* = weighted spar thickness

E_1 = reference modulus

This is actually a special case of the general theory for shells, which uses (Reference 56, p. 348 ff.):

$$t^* \int_{Z_{o_{lower}}}^{Z_{o_{upper}}} dZ_o^* = \int_{Z_{o_\ell}}^{Z_{o_u}} \frac{E(Z_o)}{E_1}\, dZ_o \qquad \text{(VII-3)}$$

with $E(Z_o)$ = shell modulus which varies with thickness Z_o

E_1 = reference modulus

t^*, Z^* = modulus-weighted quantities

For the present example this gives a weighted spar thickness of:

$$t^* = \left(\frac{4.4}{2.2}\right)(0.08) = 0.16 \text{ inches}$$

The geometry of the airfoil at each span station is simply a scaled value from a standard set of offsets (X,Y points) from an airfoil reference. The program fits a second order curve through each set of

three given offsets, divides the curve into differential segments, and chooses the correct modulus-weighted thickness. The program then calculates the differential areas, first moment of the area, and second moment of the area about the X and Y axes. The skin-spar area, moments of inertia, and centroid are found simply as:

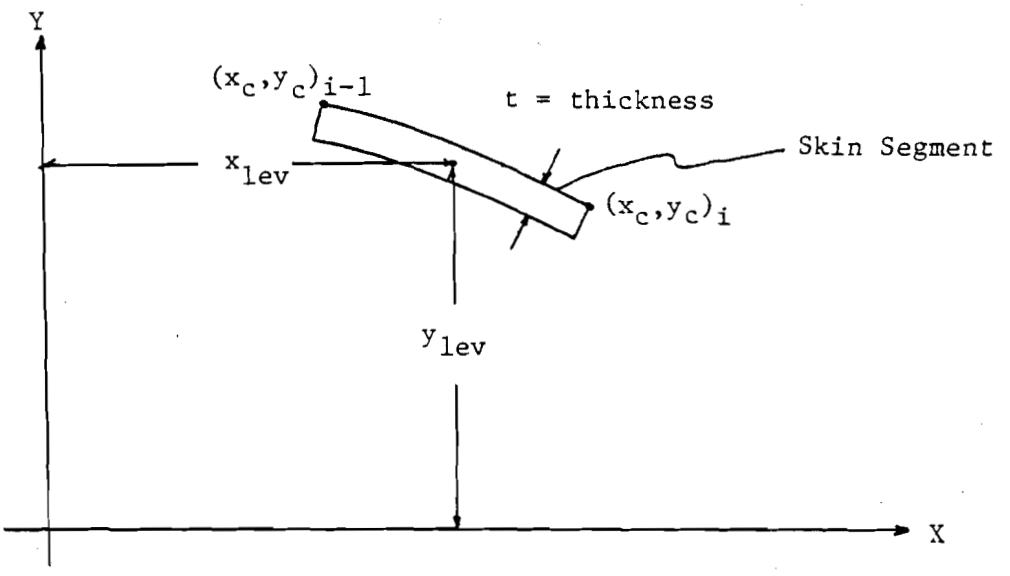

Figure 69. Differential Segment Geometry

$$A_T = \text{total area} = \int dA = \Sigma\, dA$$

$$M_x = \text{1st moment of the area about x-axis} = \int y\, dA = \Sigma\, y_{lev}\, dA$$

$$M_y = \text{1st moment of the area about y-axis} = \int x\, dA = \Sigma\, x_{lev}\, dA$$

$$I_x = \text{moment of inertia about x-axis} = \iint y^2\, dA = \Sigma\, y^2_{lev}\, dA$$

$$I_y = \text{moment of inertia about y-axis} = \iint x^2\, dA = \Sigma\, x^2_{lev}\, dA$$

$$I_{xy} = \text{product of inertia} = \iint xy\, dA = \Sigma\, x_{lev}\, y_{lev}\, dA \qquad \text{(VII-4)}$$

The centroid and section stiffness of the skin-spar are then simply:

$$\bar{x}_c = \frac{M_y}{A} \quad ; \qquad \bar{y}_c = \frac{M_x}{A}$$

$$EI_x = E_{skin} \iint y^2_{lev}\, dA$$

$$EI_y = E_{skin} \iint x^2_{lev}\, dA \qquad \text{(VII-5)}$$

The spar web is now added as a structural addition, using a simple rectangular cross section and values referenced to the centroid to simplify the calculation. This method is quite convenient for adding additional webs or spar structure to the beam.

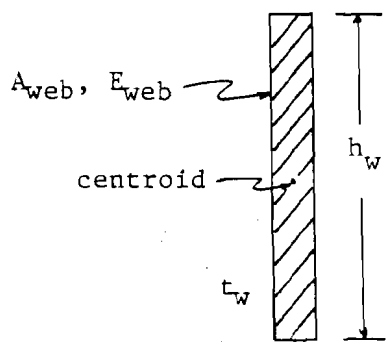

$A_w = ht$

$I_{xw} = th^3$

$I_{yw} = ht^3$

$I_{xyw} = 0$

X_w, Y_w centroid

Figure 70. Simple Spar Web

The values for the total composite section are then:

Total area = $A_{total} = A_s + A_{web}$

$$\bar{x} = \text{x-centroid} = \frac{[EM_y]_{skin} + [EM_y]_{web}}{EA_{total}}$$

$$\bar{y} = \text{y-centroid} = \frac{[EM_x]_{skin} + [EM_x]_{web}}{EA_{total}} \qquad \text{(VII-6)}$$

The section stiffnesses are found for the total structure by applying the parallel axis theorem in sequence (s subscript refers to the skin-spar, w refers to the added web, t refers to the total structure):

$$EI_{xt} = E_s I_{xs} + E_w I_{xw} - E_s A_s \left[\bar{y}_s^{\,2} - (\bar{y}_s - y_t)^2\right] + E_w A_w \left[y_w - \bar{y}_t\right]^2$$

$$EI_{yt} = E_s I_{ys} + E_w I_{yw} - E_s A_s \left[\bar{x}_s^{\,2} - (\bar{x}_s - \bar{x}_t)^2\right] + E_w A_w \left[x_w - \bar{x}_t\right]^2$$

$$EI_{xyt} = E_s I_{xys} + E_w I_{xyw} - E_s A_s \left[\bar{x}_s \bar{y}_s - (\bar{x}_s - \bar{x}_t)(\bar{y}_s - \bar{y}_t)\right]$$

$$+ E_w A_w \left[x_w - \bar{x}_t\right]\left[y_w - \bar{y}_t\right] \qquad \text{(VII-7)}$$

The principal axes of inertia are found from a Mohr's circle representation:

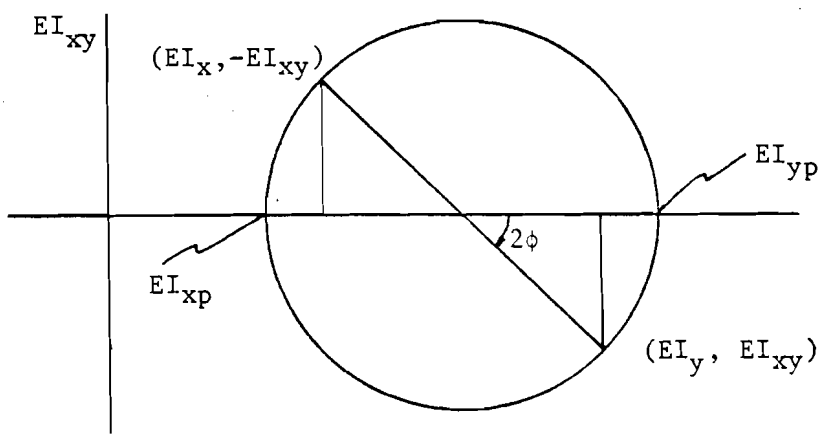

Figure 71. Mohr's Circle

This gives:

$$EI_{xp} = \frac{EI_y + EI_x}{2} - \left[\frac{EI_y - EI_x}{2}\right] \frac{1}{\cos 2\phi}$$

$$EI_{yp} = \frac{EI_y + EI_x}{2} + \left[\frac{EI_y - EI_x}{2}\right] \frac{1}{\cos 2\phi}$$

$$\phi = \begin{matrix}\text{principal}\\ \text{axis angle}\end{matrix} = \frac{1}{2} \arctan \left[\frac{2\, EI_{xy}}{EI_y - EI_x}\right] \qquad \text{(VII-8)}$$

The principal radius of gyration is:

$$r_x = \sqrt{\frac{I_x}{A}} \quad ; \qquad r_y = \sqrt{\frac{I_y}{A}} \tag{VII-9}$$

And the polar moment of inertia is:

$$J = I_x + I_y \tag{VII-10}$$

The torsional centroid is calculated using the torsional moduli of the skin and the web, and the first moments of area:

$$\bar{x}_t = \begin{matrix}\text{x coordinate of} \\ \text{torsional centroid}\end{matrix} = \frac{G_s\ M_{ys} + G_w\ M_{yw}}{G_s\ A_{total}}$$

$$\bar{y}_t = \begin{matrix}\text{y coordinate of} \\ \text{torsional centroid}\end{matrix} = \frac{G_s\ M_{xs} + G_w\ M_{xw}}{G_s\ A_{total}} \tag{VII-11}$$

Using the parallel axis theorem again, the torsional stiffness is (s = skin-spar, w = web, t = torsional):

$$\begin{aligned} GJ &= G[I_x+I_y] \\ &= G_s\ I_{xs} + G_w\ I_{xw} - G_sA_s\ [\bar{y}_s^{\,2} - (\bar{y}_s-\bar{y}_t)^2] \\ &\qquad + G_wA_w\ [y_w-\bar{y}_t] \\ &\quad + G_s\ I_{ys} + G_w\ I_{yw} - G_sA_s\ [\bar{x}_s^{\,2} - (\bar{x}_s-\bar{x}_t)^2] \\ &\qquad + G_wA_w\ [x_w-\bar{x}_t] \end{aligned} \tag{VII-12}$$

The EI program (Appendix II) then lists a data file for the stress-deflection program. It has calculated for each spanwise section of the blade (usually 10):

(a) A_{total}, total cross sectional area

(b) EA_{total}, reference EA

(c) I_x, I_y, I_{xy} moments of inertia in section axes

(d) EI_x, EI_y, EI_{xy} section stiffness

(e) EI_{xp}, EI_{yp} principal axes stiffness

(f) ϕ angle to principal axes from section axes

(g) GJ torsional stiffness

(h) $\bar{x}$, $\bar{y}$ bending centroid of section

(i) $\bar{x}_t$, $\bar{y}_t$ torsional centroid of section

The EI program requires for input:

(a) The number of stations to be calculated (10)

(b) Young's modulus of skin and for spar web (E)

(c) Torsional modulus of skin and spar web (G)

(d) Offsets which describe the reference airfoil shape

(e) Chord length for each section

(f) Modulus-weighted skin thickness (skin + spar) (t_1)

(g) Skin thickness (skin alone) (t_2)

(h) Position of spar web (x_t)

(i) Spar web information (A_w, I_x, I_y, I_{xy}, $\bar{x}_w$, $\bar{y}_w$)

A sample result can be seen in Appendix II; it is plotted in Figure 23.

B. Stresses and Deflections for Arbitrary Shell Beam

Given the EI, GJ, and principal axes information for each section of the blade, the stress program (Appendix III) now uses the geometric blade axis location and twist angles for each section. For the blades of interest in the Wind Furnace Program, the airfoil quarter chord was chosen for the blade axis, to allow a simple representation of airloads and aerodynamic pitching moment, which are referenced to the aerodynamic

center. And for the NACA 4415 airfoil used, the aerodynamic center is very close to the quarter chord for reasonable operating angles of attack.[6] The twist angles are referenced to the plane of rotation; the largest twist by far is for the root section. Then the applied steady loading, which consists of steady airloading (flapping and lead-lag forces), torsion (aerodynamic pitching moment), and centrifugal forces, are all referenced to the blade axis or quarter chord. With the beam now expressed by a locus of centroids and a distribution of EI's, and GJ's, and with the applied loading referenced to a given axis system (i.e., the quarter chords), the stress and deflection can be calculated.

The approximate theory (Bernoulli-Euler) for bending and extension of slender beams is used rather than the more exact theory of elasticity (see References 57 and 58). Normals to the centroidal axis remain normal and unchanged in length as the beam deforms. Stresses in the transverse direction are neglected, and plane sections remain plane. This gives a uniaxial stress-strain relationship, and satisfies equilibrium in that the stress resultants are in equilibrium with the applied forces. The beam is cantilevered at the root. If hinged blades are used, the appropriate root boundary condition must be satisfied, and reflected in the applied beam loading.

Figure 72 shows a blade section; the y-z plane is a cross section plane, the x-axis is spanwise, the z-axis is along the axis of rotation in the wind direction, and the y-axis is parallel to plane of rotation (lagging).

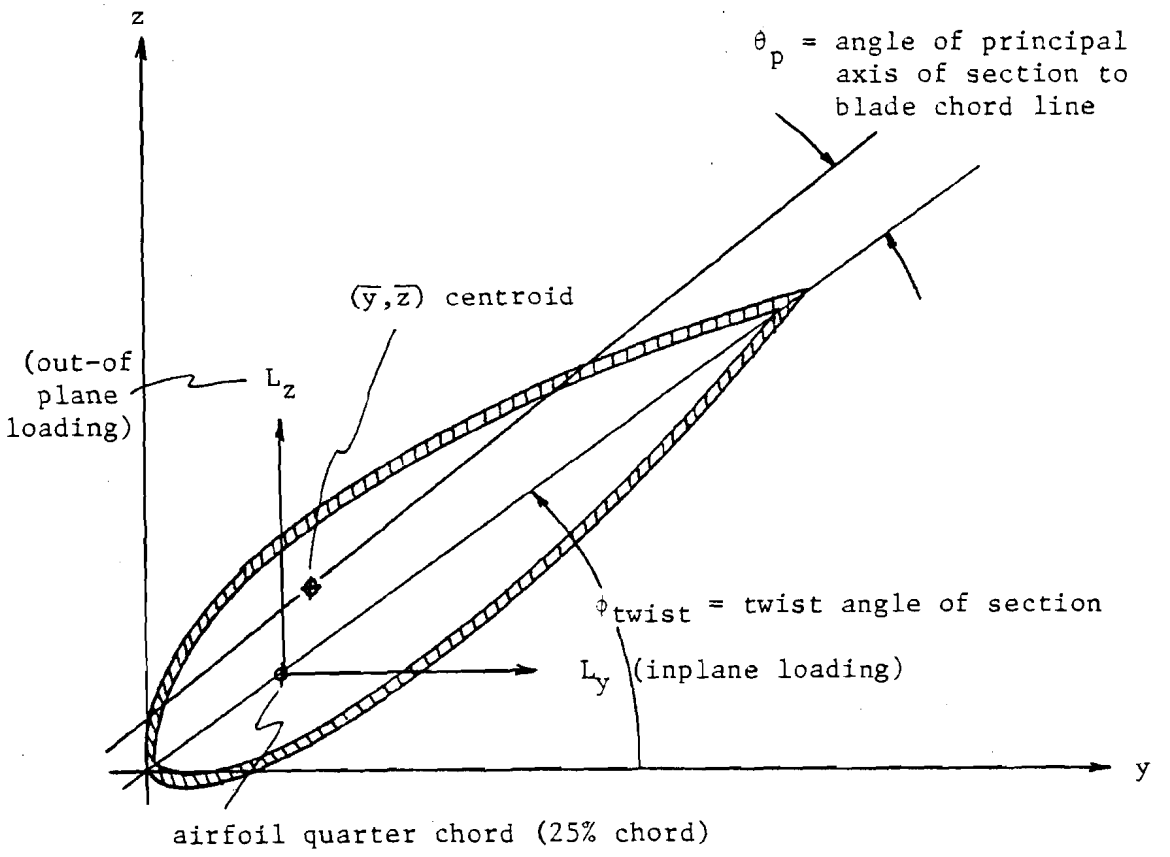

Figure 72. Blade Cross Section

The twist angle of the blade section (φ_t) and the principle axis angle of the section (θ_p) are shown. The two airloadings, L_y and L_z, are shown; they are expressed in units of lb./ft. along the span. Then the beam shear and bending moments can be written:

$$V_y = \text{inplane shear} = \int_{\text{beam}} L_y \, dx$$

$$V_z = \text{flapping shear} = \int_{\text{beam}} L_z \, dx \qquad \text{(VII-13)}$$

$$M_y = \text{inplane moment} = \int_{\text{beam}} V_y \, dx$$

$$M_z = \text{flapping moment} = \int_{\text{beam}} V_z \, dx \qquad \text{(VII-14)}$$

The resulting loads, (L), shears (V), and moments (M) can be shown vectorially as follows (moments use the right hand rule convention):

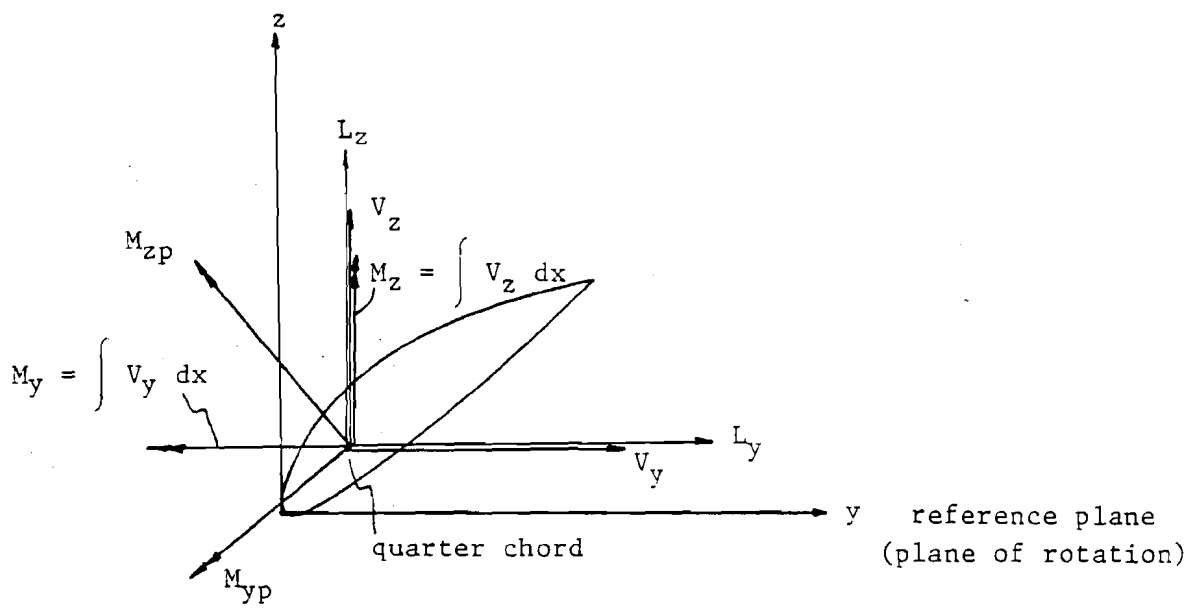

Figure 73. Loading Convention

With the angle to the principal axis written $\phi = \phi_t + \theta_p$, the bending moments can be resolved to the section principal axes, y_p, z_p:

$$M_{y_p} = M_y \cos \phi - M_z \sin \phi$$

$$M_{z_p} = M_z \cos \phi + M_y \sin \phi \qquad \text{(VII-15)}$$

The <u>neutral axis</u> of the section defines the line which separates tension from compression and is therefore also dependent on applied

load. The neutral axis angle (from the reference plane) can be written as:

$$\phi_{na} = \tan^{-1} \left[\frac{M_{py}/EI_{yp}}{M_{pz}/EI_{zp}}\right] + \phi_t \qquad \text{(VII-16)}$$

The calculation of shell stresses proceeds as follows; Figure 74 shows an arbitrary cross section of an unsymmetric shell subjected to pure bending (Reference 57, p. 240):

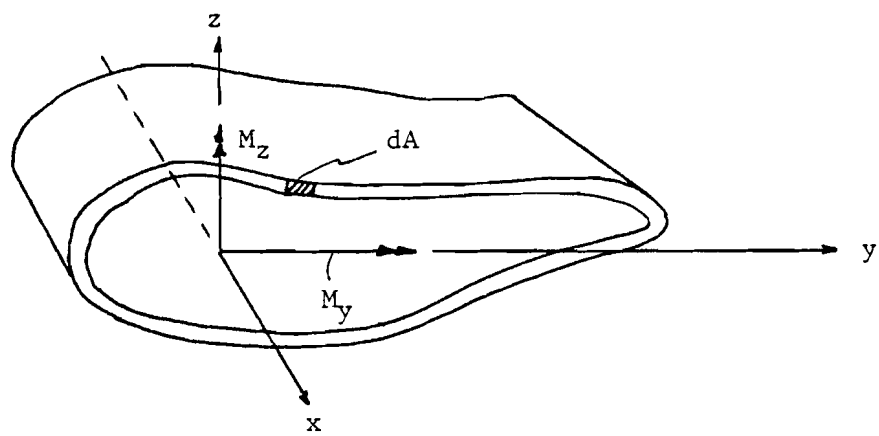

Figure 74. Arbitrary Cross Section

The generalized flexure formula from beam theory gives the stress due to bending:

$$\sigma = \frac{[M_z I_y + M_y I_{yz}]\, y + [-M_y I_z - M_z I_{yz}]\, z}{I_y I_z - I_{yz}^2} \qquad \text{(VII-17)}$$

For the special case of y and z along principal axes, and the bending taking place only about the z-axis, we have $I_{yz} = M_y = 0$, and the above expression reduces to the simple result:

$$\sigma = \frac{M_z y}{I_z}\ , \text{ alternatively } \sigma = \frac{M_y z}{I_y} \qquad \text{(VII-18)}$$

The program takes designated points on the shell surface, which are input in terms of the standard airfoil curve; they are simply scaled to match each desired section. Then expression VII-18 is used to calculate the stress due to bending in the orthogonal planes in the principal axes: the moments (M's), and I's (in Exp. VII-18) are referred to the principal axes, and the y and z quantities are simply the distances to the fiber in question from the neutral axis calculated above. The axial stress due to centrifugal tension is added to the stress due to bending to get the total stress.

$$\sigma_{total} = \frac{M_z y_c}{I_z} + \frac{M_y z_c}{I_y} + \frac{T}{A} \qquad \text{(VII-19)}$$

The above expression is simple because the stress is calculated on the principal axes, and the EI's have already been calculated to a reference modulus. The more general form for the axial stress in a composite beam is from Reference 56:

$$\sigma_{xx} = \frac{E}{E_1}\left\{\frac{P^*}{A^*} - \frac{M_z{}^*I_{yy}{}^* - M_y{}^*I_{yz}{}^*}{I_{yy}{}^*I_{zz}{}^* - (I_{yz}{}^*)^2}\, y - \frac{M_y{}^*I_{zz}{}^* - M_z{}^*I_{yz}{}^*}{I_{yy}{}^*I_{zz}{}^* - (I_{yz}{}^*)^2}\, z\right\} \qquad \text{(VII-20)}$$

where:

σ_{xx} = axial stress along beam axis

P^*/A^* = stress due to pure axial load

E_1 = reference modulus ($=E_{skin}$)

* refers to the modulus weighted quantities:

$$A^* = \int_A dA^* = \int_A \frac{E}{E_1}\, dA$$

$$I_{yy}{}^* = \int_A z^2 dA^*, \quad I_{zz}{}^* = \int_A y^2 dA^*, \text{ etc.}$$

The torsional deflection of the beam can also be found by using approximate theory. Figure 75 shows an arbitrary cross section of the shell beam, the beam is now idealized as a thin-walled tube with constant thickness t. The shear flow is the (constant) shear stress times the thickness.

$$q = \begin{matrix}\text{shear}\\ \text{flow}\end{matrix} = \tau t = \text{constant for a thin-walled tube} \qquad \text{(VII-21)}$$

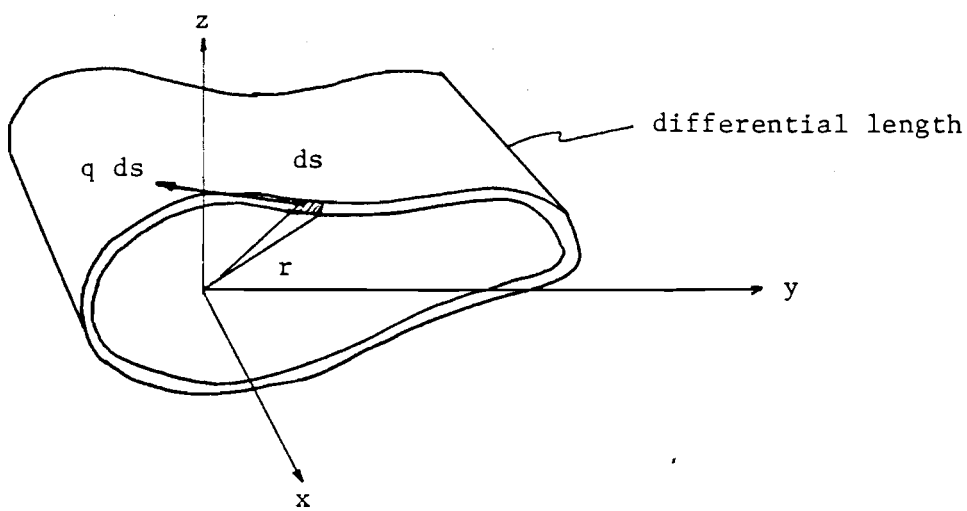

Figure 75. Arbitrary Cross Section

The twisting moment is found from Figure 75:

$$T = \begin{matrix}\text{twisting}\\ \text{moment}\end{matrix} = q \oint r\, ds$$

$$= ZAq \quad \text{with A the area inside the tube wall centerline per unit length} \qquad \text{(VII-22)}$$

Then the angle of twist per unit length of the section is:

$$\theta = \begin{matrix}\text{angle of}\\ \text{twist}\end{matrix} = \frac{T}{4A^2G} \oint \frac{ds}{t} \qquad \text{(VII-23)}$$

with:

T = twisting moment per unit length

G = torsional modulus

t = thickness

A = cross sectional area

For a rectangular tube (see Figure 76), the above expression is:

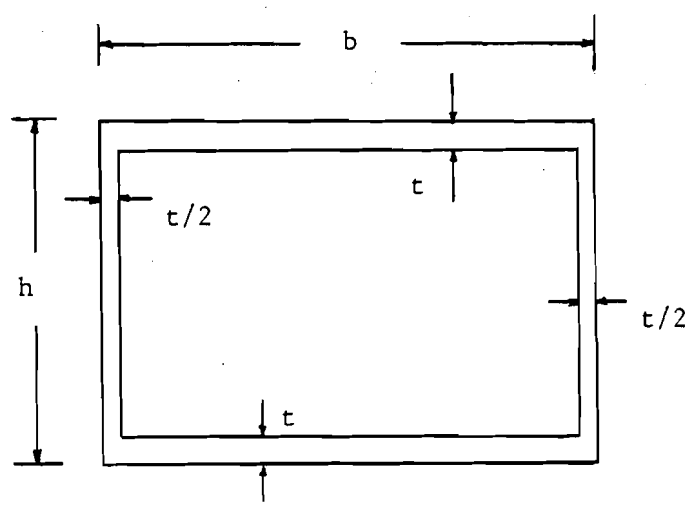

Figure 76. Rectangular Tube Example

$$\theta = \begin{matrix}\text{angle of} \\ \text{twist} \\ \text{per unit} \\ \text{length}\end{matrix} = \frac{T}{4b^2h^2G}\left[\frac{2b}{t} + \frac{2h}{t/2}\right] = \frac{T}{G}\left[\frac{(2b+4h)}{4b^2h^2t}\right] \qquad \text{(VII-24)}$$

However, the airfoil cross section is a complex non-symmetrical shape; Exp. VII-23 for a thin-walled airfoil could be written as:

$$\theta = \frac{T}{4A^2G} \oint_{\text{airfoil}} \frac{ds}{t}$$

Past experience with torsion of tubes has shown that this expression is less and less accurate as the actual cross sectional curve differs from a circle.[59] Empirical results have indicated a larger deflection than predicted by Exp. VII-23;[60] this is most likely due to slight buckling of the non-circular wall section. Hence, empirical factors have been developed. For this analysis, a correction factor of 2.0 was chosen.

For this case, the twist per unit length is approximated by:

$$\theta \approx 2.0 \left(\frac{T}{GJ}\right) \tag{VII-25}$$

The total torsional deflection is then the sum, integrated from the fixed end:

$$\Theta = \begin{matrix}\text{total angle}\\ \text{of twist}\end{matrix} = \int_0^x \theta dx \tag{VII-26}$$

The bending deflection of the beam is obtained by integrating the applied moment; small deflections are not assumed. Since deflections are desired in the reference axis system (rotor plane), the moments are transformed from principal axes to the xyz system:

$$\left(\frac{M}{EI}\right)_y = \left(\frac{M}{EI}\right)_{yp} \cos\phi - \left(\frac{M}{EI}\right)_{zp} \sin\phi$$

$$\left(\frac{M}{EI}\right)_z = \left(\frac{M}{EI}\right)_{yp} \sin\phi + \left(\frac{M}{EI}\right)_{zp} \cos\phi \tag{VII-27}$$

And they are numerically integrated to obtain the deflections in the y (lead-lag) and z (flapping) directions:

$$\frac{d^2y}{dx^2} = \left(\frac{M}{EI}\right)_y$$

$$\frac{d^2z}{dx^2} = \left(\frac{M}{EI}\right)_z \tag{VII-28}$$

A sample result follows the program in Appendix III; the blade deflection is plotted in Figure 24.

This simple structural model allows an assessment of principal bending stresses in the composite blade for prescribed steady loading. Of course, the actual loading will be a combination of steady and dynamic airloading and inertial loading. The design process requires a range of expected loads: steady loads, maximum gravity loads, cross-wind and yaw loads, estimated dynamic loads for operation near a structural resonance, and other maximum transient loadings (i.e., gusts, ice, impact, etc.). The stresses and deflections can be calculated in a quasi-steady way by knowing the time history of a transient load. For design purposes, though, it is often sufficient to prescribe maximum expected loading combinations, and soloe for the "steady" stress and deflections for each set; thus the blade will be designed to keep reactions within allowable stress and deflection limits.

Another limitation is a buckling constraint. The buckling criteria must be applied to the maximum bending condition for the design of interest to keep within allowable limits. Of course, no buckling theory is accurate, especially for a highly twisted, tapered composite such as this, so empirical testing must be the final analysis.

C. Blade Frequency of Vibration Analysis--Myklestad Method

This method of solution for frequencies of vibration was originated by Holzer (1921) for the purpose of finding natural torsional frequencies of crankshafts,[61] and then modified by Myklestad (1944) for bending

vibrations of variable stiffness beams.[62] Later propeller work included the effect of rotation, simply called centrifugal stiffening (References 63 and 64). The method derived here can be followed in more detail in Reference 63. A unique method for including direct flight testing data into the free body diagram representation, to increase accuracy and establish in-flight resonance was developed by Ashley (Reference 65).

The continuous blade (beam) is represented by a number of discrete segments; analytically, the partial differential equation for bending is replaced by a set of simultaneous ordinary differential equations (one for each segment). Additionally, the free body diagrams for each segment are simple to analyze, and lead to a direct physical knowledge of the vibrating beam. The number of segments chosen can vary from just a few, to get quick estimates for simple beams by hand, to very many, which by computer methods can yield accurate frequencies for complex beams. This method is the standard for companies involved in the design of rotor or propeller blades.[11]

The deflected blade, rotating about axis Z, is shown in Figure 77. The blade is segmented into arbitrary lengths and the mass of each length is equally divided into lumped masses at either end. The elastic properties (EI or GJ) are assumed constant over the beam element.

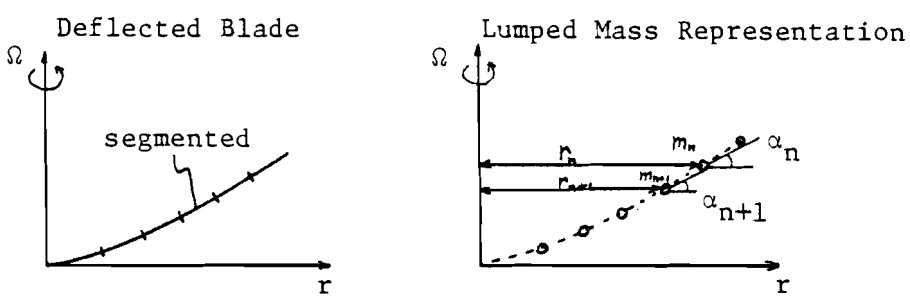

Figure 77. Deflected Blade

The free body diagram for the $n^{\underline{th}}$ element is:

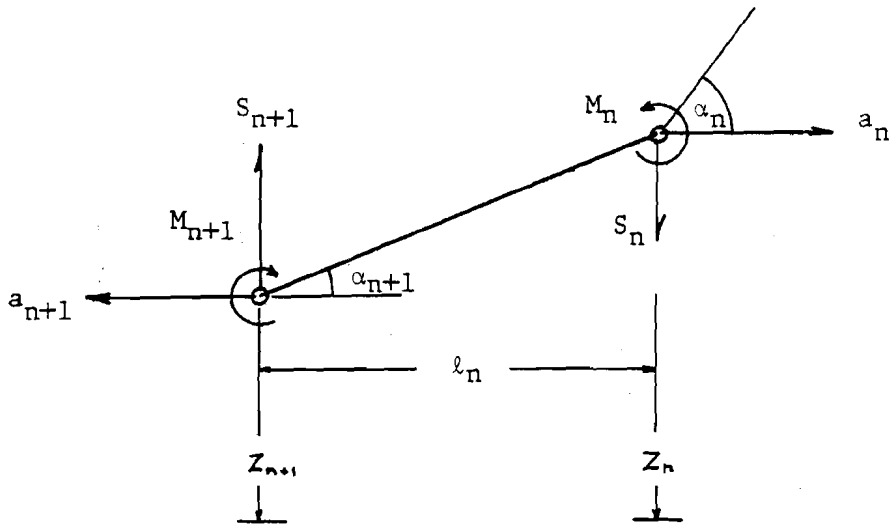

Figure 78. Free Body Diagram

where:

m_n = $n^{\underline{th}}$ lumped mass

α_n = $n^{\underline{th}}$ slope

a_n = $n^{\underline{th}}$ tension (centrifugal force)

M_n = $n^{\underline{th}}$ bending moment

ℓ_n = $n^{\underline{th}}$ segment length

S_n = $n^{\underline{th}}$ shear

Z_n = $n^{\underline{th}}$ bending deflection

The partial differential equation of bending of the continuous beam is fourth order; therefore, four coefficients are needed to express unit load effects due to an applied moment and an applied force. The unit load and moment coefficients are derived from a simple cantilever with a unit end load, F, or a unit moment, M:

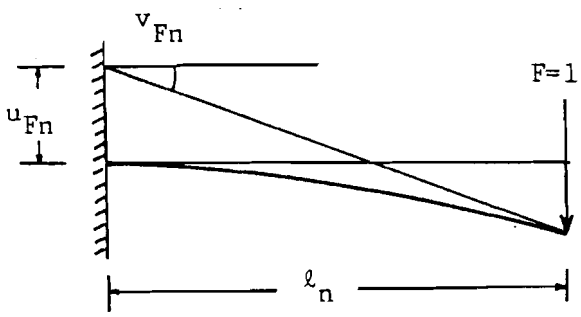

Unit Load Diagram

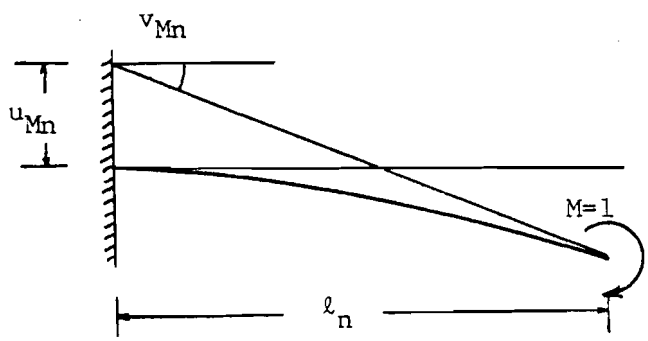

Unit Moment Diagram

Figure 79. Unit Load Diagram, Unit Moment Diagram

The resulting coefficients are:

$$u_{Fn} = \text{deflection due to unit force} = \frac{\ell_n^{\,3}}{6(EI)_n}$$

$$v_{Fn} = \text{slope due to unit force} = \frac{\ell_n^{\,2}}{2(EI)_n}$$

$$u_{Mn} = \text{deflection due to unit moment} = \frac{\ell_n^{\,2}}{2(EI)_n}$$

$$v_{Mn} = \text{slope due to unit moment} = \frac{\ell_n}{(EI)_n} \qquad \text{(VII-29)}$$

Note: The above coefficients are sometimes written in non-unit form as:[11]

$$u_{Fn} = u_F = \frac{F\ell^3}{6EI}$$

$$v_{Fn} = \theta_F = \frac{F\ell^2}{2EI}$$

$$u_{Mn} = u_M = \frac{M\ell^2}{2EI}$$

$$v_{Mn} = \theta_M = \frac{M\ell}{EI} \qquad \text{(VII-30)}$$

Also, the Maxwell Reciprocal Relationship is easily seen in VII-29 above: "The u due to the M = θ due to the F."

Now the segmented blade, rotating at frequency Ω, is assumed to vibrate at frequency ω. An additional inertial force $M_{n+1}\ \omega^2\ z_{n+1}$ is added to the free body diagram above. Force and moment equilibrium then yield:

Tension:	$a_{n+1} = a_n + m_{n+1}\ \Omega^2\ r_{n+1}$	(VII-31)
Shear:	$S_{n+1} = S_n + m_{n+1}\ \omega^2\ z_{n+1}$	(VII-32)
Moment:	$M_{n+1} = M_n - S_n\ \ell_n + a_n\ (z_n - z_{n+1})$	(VII-33)
Slope:	$\alpha_{n+1} = \alpha_n\ (1 + a_n\ v_{Fn}) - S_n\ v_{Fn} + M_n\ v_{Mn}$	(VII-34)
Displacement:	$z_{n+1} = z_n - (\ell_n + u_{Fn}\ a_n)\ \alpha_n + u_{Fn}\ S_n - u_{Mn}\ M_n$	(VII-35)

The tension at the $n^{\underline{th}}$ segment can be rewritten as a sum of tensions:

$$a_n = \sum_{i=1}^{n} m_i\ \Omega^2\ r_i \qquad \text{(VII-36)}$$

And the deflection can be substituted into the moment expression to give:

$$M_{n+1} = M_n\ (1 + u_{Mn}\ a_n) - S_n\ (\ell_n + u_{Fn}\ a_n) + \alpha_n\ a_n\ (\ell_n + u_{Fn}\ a_n) \qquad \text{(VII-37)}$$

These recurrence formulas could be solved by successive substitution, working from the tip of the blade to the root. Shear, moment, slope, and deflection would be calculated for each segment, and resultant distributions would be known. There is a problem in solution, however. The boundary conditions at the tip (station 1) are not determinate; for a free tip, the shear, moment, slope and deflection are:

S_1 = shear at tip = $m_1 \omega^2$

M_1 = moment at tip = 0

α_1 = slope at tip = ϕ

$z_1 = 1.0$ (VII-38)

The usual requirement of shear being zero at the tip no longer holds since the mass of a segment is now concentrated at the tip; thus S constitutes an average value. To continue with the solution, the slope can be assumed to be an arbitrary angle, ϕ, and the deflection a unit quantity. These are purely arbitrary conditions for the present. If a ϕ happens to be known corresponding to some unknown frequency ω, the value could be introduced into the recurrence formulas, and the resulting conditions at the root of the blade could be found. Obviously, for the trial ω to be the correct frequency, the slope at the root and the deflection must correspond to the appropriate root boundary condition; viz:

<u>Cantilevered</u>:

Slope at root = deflection at root = 0 (VII-39)

<u>Hinged</u>:

Moment at root = deflection at root = 0 (VII-40)

Thus the solution method involves iteration on variable ω until appropriate root conditions are calculated; by hand, a plot of successive root deflections with trial ω can be plotted to help find the roots:

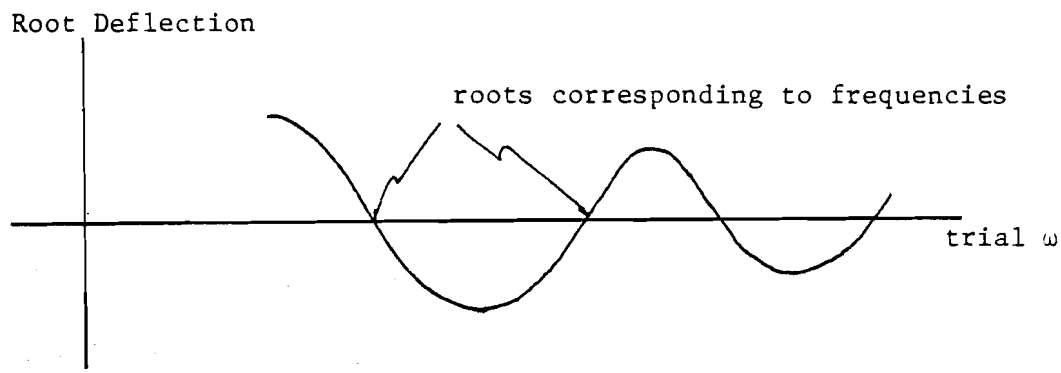

Figure 80. Iterative Graphical Solution

The method can be applied to systematic computation by making judicious new definitions and substitutions, as follows.

The load and moment coefficients, and centrifugal forces can be combined via the definitions:

$$\boxed{\begin{aligned} A_n &= 1 + v_{Fn}\, a_n \\ B_n &= 1 + u_{Mn}\, a_n \\ C_n &= \ell_n + u_{Fn}\, a_n \\ D_n &= C_n\, a_n = (\ell_n + u_{Fn}\, a_n)\, a_n \end{aligned}} \qquad \text{(VII-41)}$$

Myklestad Definitions

A set of assumed linear functions is substituted in the remaining set of four recurrence formulas for shear, moment, slope and deflection. The assumed slope at the tip, ϕ, is carried as the independent variable, and the assumed amplitude coefficients are called the G's and H's:

Shear:	$S_n = - G_{\phi n}\ \phi + G_n$
Moment:	$M_n = H_{\phi n}\ \phi - H_n$
Slope:	$\alpha_n = h_{\phi n}\ \phi - h_n$
Deflection:	$z_n = - g_{\phi n}\ \phi + g_n$

(VII-42)

Myklestad Amplitude Coefficients

Substituting these linear functions into the original recurrence formulas and equating coefficients, yields simple recurrence formulas for the amplitude coefficients now suitable for systematic computation.

$$G_{\phi(n+1)} = G_{\phi n} + M_{(n+1)}\ \omega^2\ g_{\phi(n+1)}$$

$$G_{(n+1)} = G_n + M_{(n+1)}\ \omega^2\ g_{(n+1)} \qquad \text{(VII-43)}$$

$$H_{\phi(n+1)} = B_n\ H_{\phi n} + D_n\ h_{\phi n} + C_n\ G_{\phi n}$$

$$H_{(n+1)} = B_n\ H_n + D_n\ h_n + C_n\ G_n \qquad \text{(VII-44)}$$

$$h_{\phi(n+1)} = A_n\ h_{\phi n} + v_{Mn}\ H_{\phi n} + v_{Fn}\ G_{\phi n}$$

$$h_{(n+1)} = A_n\ h_n + v_{Mn}\ H_n + v_{Fn}\ G_n \qquad \text{(VII-45)}$$

$$g_{\phi(n+1)} = g_{\phi n} + C_n\ h_{\phi n} + u_{Mn}\ H_{\phi n} + u_{Fn}\ G_{\phi n}$$

$$g_{(n+1)} = g_n + C_n\ h_n + u_{Mn}\ H_n + u_{Fn}\ G_n \qquad \text{(VII-46)}$$

For the free tip case, the initial values are in VII-38:

$$S_1 = M_1\ \omega^2 \qquad M_1 = 0 \qquad \alpha_1 = \phi \qquad z_1 = 1.0$$

This yields the initial values of the amplitude coefficients:

$$G_{\phi 1} = 0 \qquad G_1 = M_1\ \omega^2$$

$$H_{\phi 1} = 0 \qquad H_1 = 0$$

$$h_{\phi 1} = 1.0 \qquad h_1 = 0$$

$$g_{\phi 1} = 0 \qquad g_1 = 1.0 \qquad \text{(VII-47)}$$

The cantilever root (or base) then gives the condition (from deflection = 0):

$$\phi = \frac{g_{base}}{g_{\phi base}} \qquad \text{(VII-48)}$$

And the base slope is then:

$$\alpha_{base} = h_{\phi base}\,\phi - h_{base} \qquad \text{(VII-49)}$$

This root slope constitutes the remainder; when it is zero, the trial value of ω^2 was a correct frequency, and the computation can then proceed to the next frequency of the beam.

In general, this iterative method will give as many roots (frequencies) as there are lumped masses. The corresponding shear, moment, and deflection mode shapes are found for each root by simple substitution in the recurrence formulas VII-43 to VII-46. For most blade work mentioned in this paper, the lowest or fundamental, frequency and mode are most important. This analysis method can be used for the two bending directions (i.e., flapping and lead-lag), and for the torsional frequency. The computer program is listed in Appendix IV.

D. Extension To Twisted Blades

The work of this paper has assumed largely that the two bending modes of the blade are uncoupled. In effect, this is asking for zero twist in the blade, because a twisted beam, as shown in Sections A and B, has twisting of the principal axes of bending (and torsional) stiffness. Various finite element methods have been developed, and are in use, for the analysis of twisted propeller and turbine blades. These approaches are in general time consuming and complicated. This section

mentions two rather physical approaches to the extension of the uncoupled theory developed here, to the coupled, twisted vibration case.

The first approach was developed by Ormiston and Miller (References 47 and 8); it allows a simple analytic extension to the existing equations which contain hinge offsets and hinge springs for first mode modelling. This method assumes the two bending vibration directions are still orthogonal, but are now inclined to the rotor plane by an angle, which can be due to pitch angle or twist angle.

Figure 81 shows a view of the idealized hinge offset-spring blade, showing the end view of the blade. The first view shows the two hinge springs, K_β and K_ζ, and the two bending moments, M_β and M_ζ, with no inclination. The second view contains an inclination α to the plane of rotation.

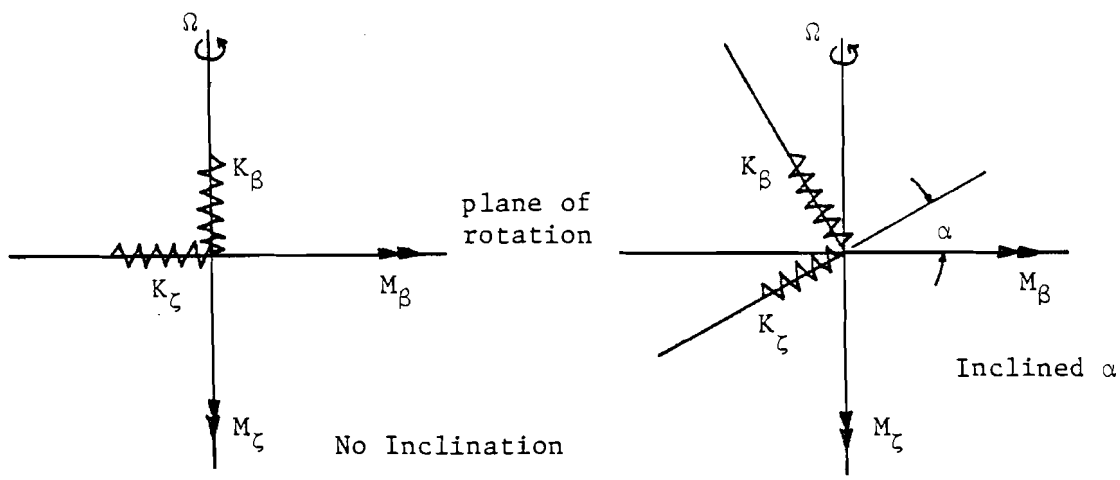

Figure 81. Elastic Coupling at the Root Due to Twist

where:

K_β = flapping spring equivalent

K_ζ = lead-lag spring equivalent

α = inclination angle at root

M_β = flapping bending moment

M_ζ = lead-lag bending moment

Now the simple coordinate transformation is done to relate the bending moments, hinge springs, and inclination α in the second view:

$$\begin{Bmatrix} M_\beta \\ M_\zeta \end{Bmatrix} = \begin{bmatrix} \cos\alpha & -\sin\alpha \\ \sin\alpha & \cos\alpha \end{bmatrix} \begin{Bmatrix} K_\beta\beta \\ K_\zeta\zeta \end{Bmatrix}$$

$$\boxed{\begin{aligned} M_\beta &= K_\beta\beta\cos\alpha - K_\zeta\zeta\sin\alpha \\ M_\zeta &= K_\beta\beta\sin\alpha + K_\zeta\zeta\cos\alpha \end{aligned}} \qquad \text{(VII-50)}$$

With the inclination equal to zero, the bending moments reduce to the original case:

$$M_\beta = K_\beta\beta$$

$$M_\zeta = K_\zeta\zeta$$

This method is a direct, quick way of re-entering an analysis of a particular blade in order to assess the added effects of inclination (or twist) angle.

Another method uses a computer approach, and is in wide use in industry to accomplish what the above method does analytically. This formulation can be followed in Reference 25; this example does not include the effects of rotational speed Ω, but is a direct extension of the Myklestad table approach.[63]

For the segmented beam of Section C, the free body diagram contained motion in only one plane. Now there is motion in two planes (flapping and lead-lag) at frequency ω. The vibration now takes place in both planes, so there will be eight equations instead of the usual four (VII-32 to VII-35):

SHEAR:

$$S_{z,n+1} = S_{x,n} + m_n \omega^2 z_n \qquad \text{(VII-51)}$$

$$S_{y,n+1} = S_{y,n} + m_n \omega^2 y_n \qquad \text{(VII-52)}$$

MOMENT:

$$M_{z,n+1} = M_{z,n} + S_{z,n+1} \ell_n \qquad \text{(VII-53)}$$

$$M_{y,n+1} = M_{y,n} + S_{y,n+1} \ell_n \qquad \text{(VII-54)}$$

SLOPE:

$$Z'_{n+1} = Z'_n + \frac{\ell_n}{E[I_{zn}I_{yn}-I_{zyn}^2]} \; I_{yn}(M_{z,n+1} - \frac{S_{z,n+1}\ \ell_n}{2} + I_{zyn}(M_{y,n+1} - \frac{S_{z,n+1}\ \ell_n}{2}) \qquad \text{(VII-55)}$$

$$Y'_{n+1} = Y'_n + \frac{\ell_n}{E[I_{zn}I_{yn}-I_{zyn}^2]} \; I_{zn}(M_{y,n+1} - \frac{S_{y,n+1}\ \ell_n}{2} + I_{zyn}(M_{z,n+1} - \frac{S_{z,n+1}\ \ell_n}{2}) \qquad \text{(VII-56)}$$

DEFLECTION:

$$Z_{n+1} = Z_n + Z'_n \ell_n + \frac{\ell_n^{\,2}}{E[I_{zn}I_{yn}-I_{zyn}^2]} \; I_{yn}(M_{z,n+1} - \frac{2}{3} S_{z,n+1} \ell_n) + I_{zyn}(M_{y,n+1} - \frac{2}{3} S_{y,n+1} \ell_n) \qquad \text{(VII-57)}$$

$$Y_{n+1} = Y_n + Y'_n \ell_n + \frac{\ell_n^{\,2}}{E[I_{zn}I_{yn}-I_{zyn}^2]} \; I_{zn}(M_{y,n+1} - \frac{2}{3} S_{y,n+1} \ell_n) + I_{zyn}(M_{z,n+1} - \frac{2}{3} S_{z,n+1} \ell_n) \qquad \text{(VII-58)}$$

In this formulation tension could be included as one additional equation (as in VII-36), and the additional force terms which appear in the force equations like before.

Den Hartog suggests this approach start at the root of the blade, with deflections and slopes all equal to zero (cantilever).[25] The calculation begins with an assumed frequency ω^2, and dummy values M_{yo}, S_{zo}, S_{yo} (two shears and one moment) at the root. The calculation proceeds with the dummy values carried along, to the free end of the blade, where boundary conditions dictate moments and shears to be zero. S_{zo}, S_{yo}, and M_{yo} can be solved, and the value of the fourth end condition will not be zero. This constitutes the remainder value, as ϕ did in the earlier case. The computation simply proceeds as before until all end conditions are satisfied. A coupled bending frequency and mode shape will be found, and the next one can be initiated on the program. This method is also capable of including torsional coupling, provided the slopes and deflections are written correctly in the free body diagram of the blade segment. Also, it should be possible to include the effects of centrifugal stiffening (Ω), and to reduce the complicated recurrence formulas VII-51 to VII-54, to amplitude coefficients as Myklestad has done for the uncoupled case.

E. Dynamic Blade Model

The vibration of a tapered, twisted cantilever is a complex phenomenon. A classic method of solution may involve a description of assumed orthogonal, uncoupled, bending and torsional mode shapes, a

force equilibrium using the boundary conditions, and resulting combined mode shapes and frequencies. The EI and mass taper of the beam define the bending mode shapes, and the torsional stiffness and mass distributions define the torsional mode shapes. The elastic axis - mass axis offset yields inertial coupling between modes, and the geometric twist produces structural, or EI, coupling between bending modes. The usual engineering approach to this problem is to use finite element representations of each structural element, in sufficient detail to use the elasticity equations. Such a program yields combined mode shapes and frequencies to a high order. One drawback to this method is the uncertainty of modulus and damping for most composites, and the resulting sensitivity of the finite element program to errors. Thus, these programs, in industry, are continually refined and updated with test results from actual blades.[22] It has been argued with some reason, in the study of helicopter blades, that such programs are unnecessary in preliminary design since the aerodynamic environment of such blades is so complex. It is very difficult to represent the unsteady, or higher order aerodynamic forces; therefore, it may seem unimportant to represent the vibrating beam to any great degree of complexity. Hence, a first order or first mode representation of the blade, can be considered practical in preliminary vibration design. The first bending mode is the one with the lowest natural frequency of motion, and with the largest tip deflections. This mode provides the greatest range of possibility of transfer of energy from an external forcing function.

The blade model to be used considers only the first bending mode, uncoupled from other bending or torsion. The complex tapered beam is

represented by a simple hinged, cantilevered beam with a spring at the hinge, viz:

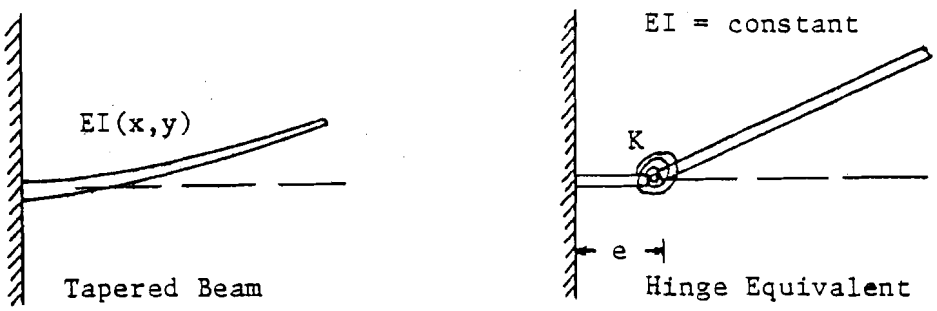

Figure 82. First Bending Mode

The equivalent beam is uniform in cross section and mass, and has a hinge at offset e and a hinge spring of value K. The equivalent beam has the same mass as the original beam, but the blade mass moment of inertia, I_b, is not the same by virtue of the mass center being more outboard on the equivalent beam. [Note: This has the effect of biasing the inertial forces towards higher absolute values, and is conservative in the design approach; this bias is larger for blades with mass centers more and more inboard from mid span.]

The tapered beam has a fundamental bending frequency in a "soft" direction (i.e., flapping, flapwise, out-of-plane, etc.) and another frequency in a "hard" direction (i.e., edgewise, lead-lag, chordwise, inplane, etc.). The dynamic model thus has a hinge equivalent for flapping (K_β, e_β) and another for lead-lag (K_ζ, e_ζ). The original beam will yield a slightly higher frequency of vibration when rotated as a blade, due to centrifugal stiffening. The degree of stiffening depends

on the mass distribution and the rotational speed Ω. For the present, we consider the beam to be representable by two already known bending frequencies: a non-rotating frequency ω_N, and a rotating frequency ω_R at a specific value of Ω. These two frequencies are important; the usual method of solution is to model the blade with a series of connected lumped masses and springs, and do a Myklestad table analysis for the non-rotating case and a Myklestad-Prohl table analysis for the rotating case. Such a frequency calculation is listed in Appendix IV and is described in the previous section. Another, more direct, method is to build a blade and test it to get these frequencies. Experimentally-derived frequencies are always more credible than predicted ones.

Once the two frequencies are known, vibration analysis of the equivalent blade is straightforward. The blade mass moment of inertia for a uniform blade hinged at the root is:

$$I_b = \int_o^R r^2 \, dm = \frac{MR^2}{3} \, [\text{slug}\cdot\text{ft}^2] \text{ or } [\text{ft}\cdot\text{lb}\cdot\text{sec}^2] \qquad \text{(VII-50)}$$

where:

R = radius

M = mass of blade

For the same blade with non-dimensional hinge offset e the integration starts at the hinge:

$$I_b = \int_o^{R(1-e)} r^2 \, dm = \frac{MR^2}{3} \, [1-e]^3 \qquad \text{(VII-51)}$$

The non-rotating frequency of this blade is simply:

$$\omega_N = \sqrt{\frac{K_\beta}{I_b}} \qquad \text{(VII-52)}$$

The rotating frequency will be higher due to centrifugal force "stiffening" the blade; the frequency for the uniform blade hinged at the root is:

$$\omega_R^2 = \omega_N^2 + \Omega^2 \qquad \text{(VII-53)}$$

The hinge offset blade has somewhat different geometry:

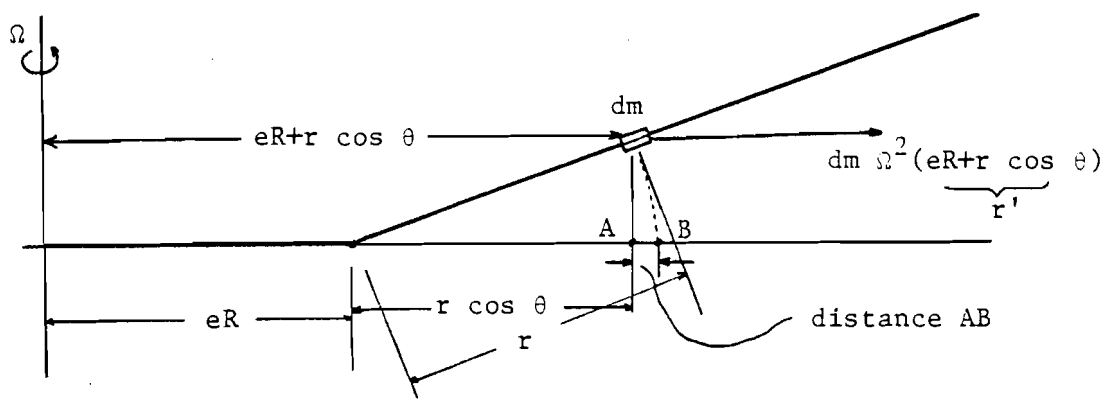

Figure 83. Hinge Offset Blade

The distance over which the centrifugal force acts on mass element dm is AB:

$$AB = [r - r\cos\theta] \approx r\left(\frac{\theta^2}{2}\right)$$

The potential energy of mass dm is the work done, or the force time the distance:

$$\Delta PE = (\Omega^2\, r'\, dm) \cdot \left(r\,\frac{\theta^2}{2}\right)$$

And the total potential energy is the integral over the vibrating blade:

$$PE = \int_0^{R(1-e)} \Delta PE = \int_0^{R(1-e)} r'\,\Omega^2\left(\frac{r\theta^2}{2}\right) dm$$

$$PE = \frac{1}{4}\,\Omega^2\,\theta^2\,MR^2\,e(1-e)^2 + \frac{1}{2}\,\Omega^2\,\theta^2\,I_b \qquad \text{(VII-54)}$$

If the vibration is at frequency ω, the kinetic energy of mass dm is:

$$\Delta KE = \frac{1}{2}\, dm \cdot v^2 = \frac{1}{2}\, dm\ (AB)^2\ \omega^2 = \frac{1}{2}\, dm\ \theta^2\ r^2\ \omega^2$$

And:

$$KE = \int_0^{R(1-e)} \Delta KE = \frac{1}{2}\, \theta^2\ \omega^2\ I_b \qquad \text{(VII-55)}$$

Now we can equate KE and PE to obtain ω:

$$\left(\frac{\omega}{\Omega}\right)^2 = 1 + \frac{1}{2}\,\frac{MR^2}{I_b}\, e(1-e)^2 \qquad \text{(VII-56)}$$

But for the equivalent blade $I_b = \frac{MR^2}{3}\,(1-e)^3$, which gives:

$$\left(\frac{\omega}{\Omega}\right)^2 = 1 + \frac{3}{2}\,\frac{e}{1-e} \qquad \text{(VII-57)}$$

So the complete rotating frequency of the hinge offset blade is then:

$$\omega_R^2 = \omega_N^2 + \Omega^2$$

$$\boxed{\omega_R^2 = \omega_N^2 + \Omega^2\ \left[1 + \frac{3}{2}\,\frac{e}{1-e}\right]} \qquad \text{(VII-58)}$$

Rotating Natural Frequency of Hinge Offset Blade

This expression reduces to the familiar VII-53 form for zero hinge offset.

Figure 84 shows natural frequency curves for various values of hinge offset e. By virtue of the squared terms in VII-58 all the curves are quadratic. With no hinge offset the curve is simply VII-53, and the effect of increasing offset is to increase the rotating frequencies more and more with increasing Ω.

Now we have a method to represent a complicated tapered EI beam by a simple hinge equivalent beam with hinge offset e and hinge spring K. The equivalent beam has the same <u>non-rotating</u> natural frequency as the

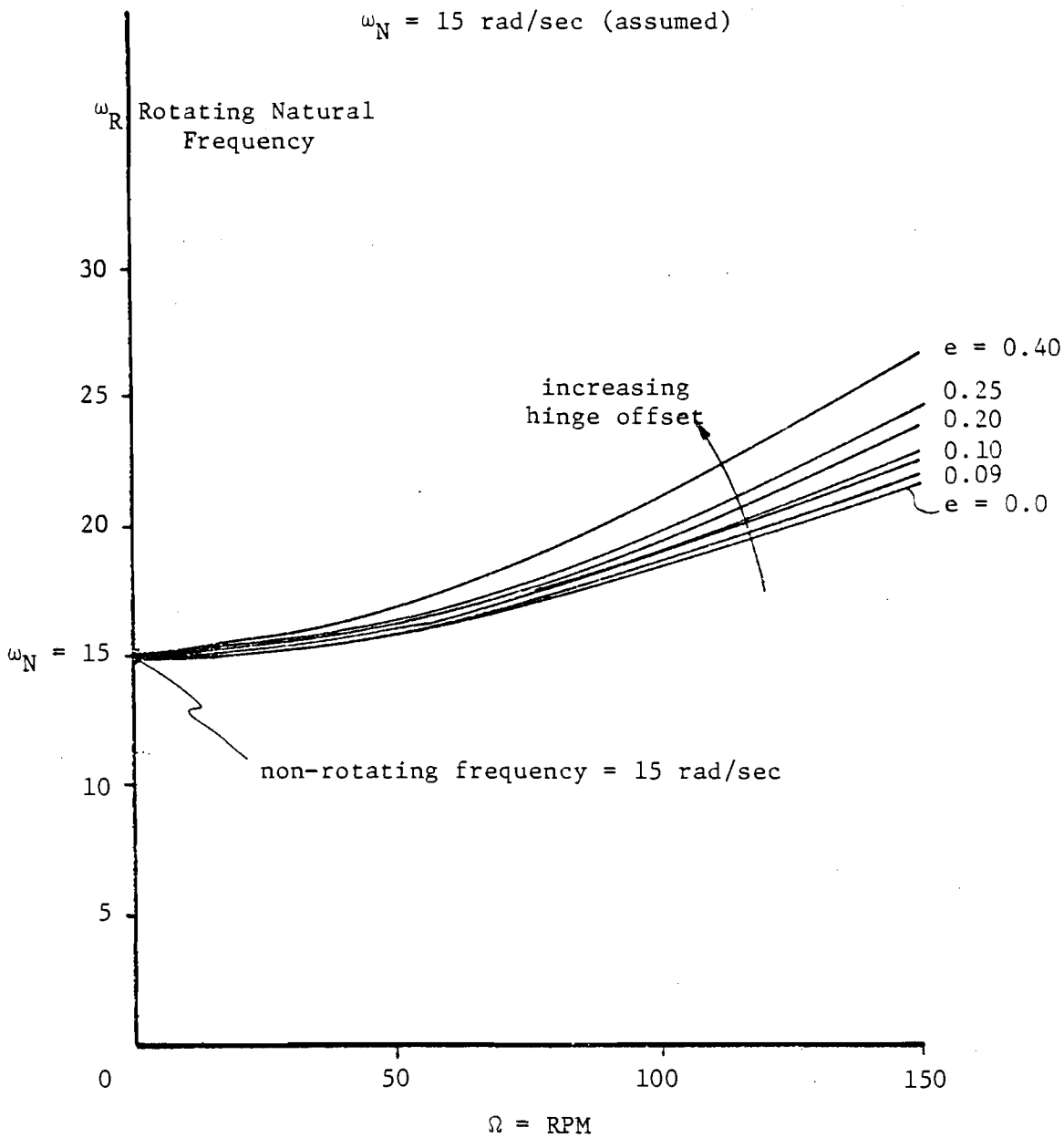

Figure 84. Rotating Natural Frequencies of Various Equivalent Blades

original beam, and has the same rotating natural frequency, calculated at some operational Ω. The equivalence relations are VII-52 and VII-58:

$$\boxed{\begin{aligned} \omega_R^2 &= \omega_N^2 + \Omega^2 \left[1 + \frac{3}{2}\frac{e}{1-e}\right] \\ \omega_N^2 &= \frac{K_\beta}{I_b}\ ; \qquad I_b = \frac{MR^2}{3}\left[1-e\right]^3 \end{aligned}} \qquad \text{(VII-59)}$$

Beam Equivalence Relations

With:

ω_R = rotating frequency of original beam

ω_N = non-rotating frequency of original beam

I_b = mass moment of inertia

e = nondimensional hinge offset

K_β = hinge spring

The design procedure is to solve the first expression for e, given ω_R and ω_N from experiment. Then I_b is computed for the equivalent beam, and K can be found from the second expression.

The equations are solved for a specific value of Ω, so strictly speaking the equivalence is only good for that frequency. However, other studies have shown that the "stiffening" factor in VII-58, $[1 + \frac{3}{2}\frac{e}{1-e}]$, represents a particular mode shape "coefficient" in the more general equation:[25]

$$\omega_R^2 = \omega_N^2 + a\Omega^2 \qquad \text{(VII-60)}$$

These mode shapes are geometric orthogonal modes as illustrated in Figure 85; the values of the stiffening coefficients, a, are also shown. These are the normal modes of the beam; the example modes are calculated for a non-rotating, uniform blade with:[9]

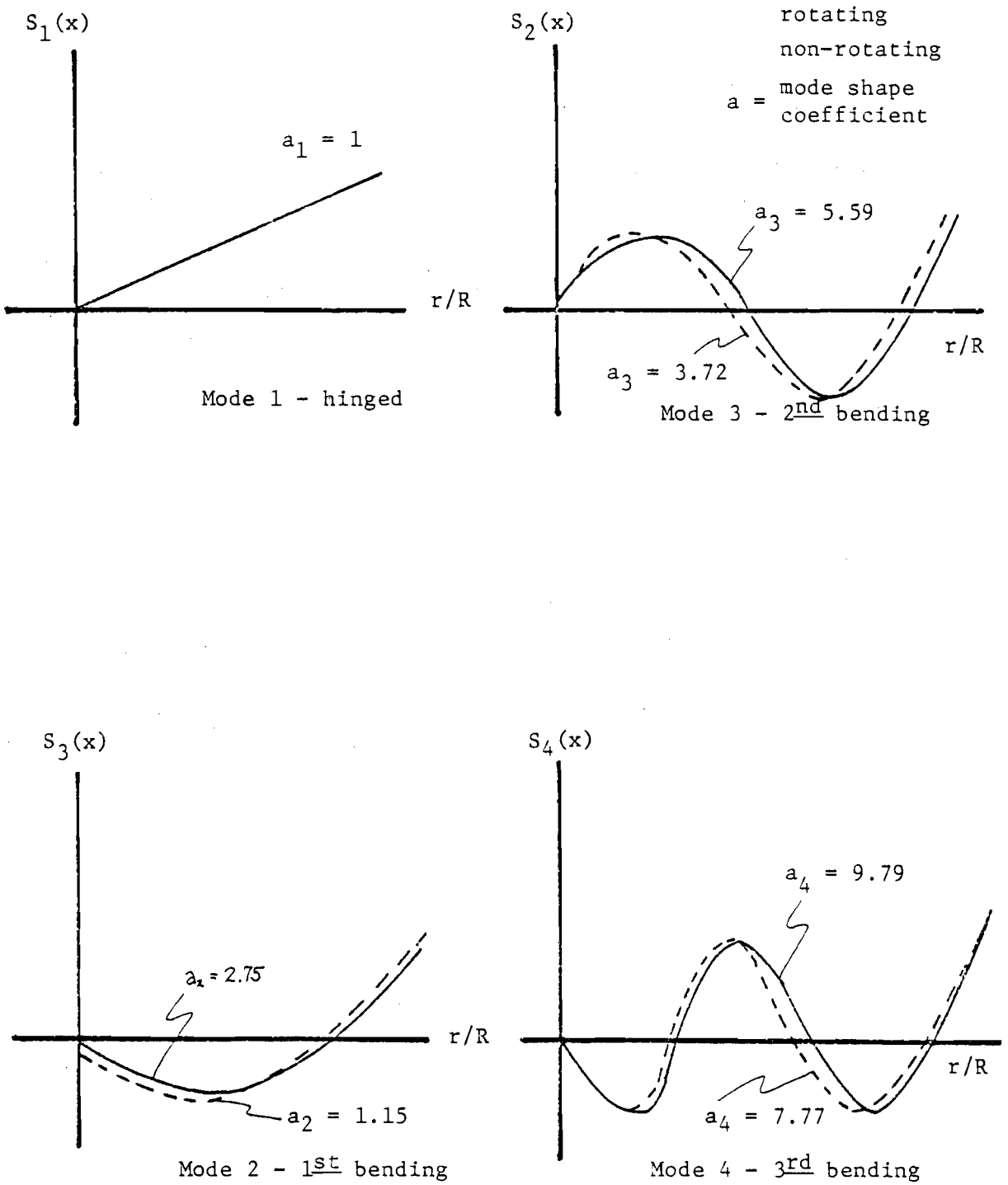

Figure 85. Uniform Blade Normal Modes (Reference 9)

$$k^2 = \frac{EI}{m\Omega^2 R^4} = \text{constant} = 0.0055$$

The modes represent analytical solutions to the following equation, and are specific for the above mass and stiffness distribution:

$$\frac{\partial^2 \phi_n}{\partial \psi^2} + a_n^{\ 2}\ \phi_n = \frac{1}{\Omega^2 R^2 f(n)} \int_o^1 \frac{\partial F}{\partial x}\ S_n(x)\ dx$$

However, for the rotating case there are no closed form solutions, and the mode equation becomes:

$$k^2\ \frac{d^4 Z}{dX^4} - \frac{1}{2}\ \frac{d}{dx}\ [(1-x^2)]\frac{dZ}{dx} - a_n^{\ 2}\ Z = 0$$

For the above case, or $k^2 = .0055$, rotating blade shapes were calculated, and the results can be seen in Figure 85. The mode shapes change very little under rotating conditions. Therefore, it is a normal engineering assumption to use the non-rotating mode shape to approximate the rotating mode. And since we are only interested in fundamental (first) mode shapes and frequencies, it is correct to assume that factor a in Exp. VII-60 remains constant over the entire Ω range. This gives a direct equivalence between the original blade and the equivalent blade, valid over the entire dynamic range of interest $0 \leq \Omega \leq \Omega_{max}$.

The limits of this equivalence model are really not determined, but the approach is useful for blade motions and fundamental frequencies. The model gets progressively worse for higher and higher frequencies. But this approach has been used extensively and routinely on hingeless helicopter rotors to calculate flapping motion and hub moments.[9]

As an example, consider the blade of the NASA Mod-0 WTG (see References 28, 29, and 30). The fundamental flap frequency is ω_N = 100 cycles/min. = 10.472 rad/sec. At a rotational speed Ω = 50 RPM, the rotating flap frequency is ω_R = 115 cycles/min. = 12.043 rad/sec. Also:

$R = 62.5$ ft.

$\Omega = 50$ RPM $= 5.236$ rad/sec.

NASA Mod-0 Blade

$M = 61.53$ slugs

$\omega_N = 10.472$ rad/sec.

$\omega_R = 12.043$ rad/sec.

Solving VII-59:

$$1 + \frac{3}{2}\left(\frac{e}{1-e}\right) = \frac{\omega_R^2 - \omega_N^2}{\Omega^2} = \frac{(12.043)^2 - (10.472)^2}{(5.236)^2}$$

$\boxed{e = 0.1620}$ equivalent hinge offset

Then I_b for the equivalent blade can be calculated:

$$I_b = \frac{MR^2}{3}\,[1-e]^3 = 47{,}142 \text{ slug}\cdot\text{ft.}^2$$

And finally, the equivalent hinge spring is:

$$\boxed{K_\beta = \omega_N^2\, I_b = 5.171 \times 10^6 \left[\frac{\text{ft-lb}}{\text{radian}}\right]}$$

And the Mod-0 dynamic model is:

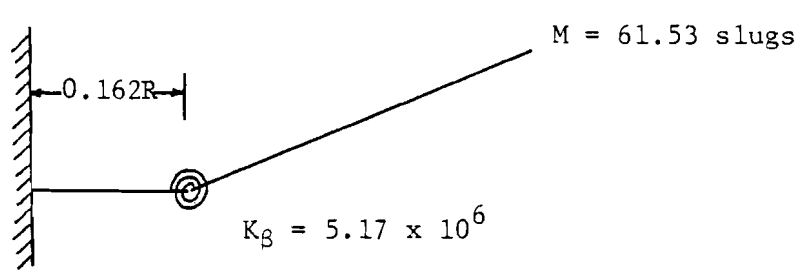

Figure 86. NASA Mod-0 Dynamic Blade Model

CHAPTER VIII

CONCLUSION

A. State of the Art for Design of Wind Turbine Generators

To design a wind turbine generator is a routine engineering task; all the characteristics, parameters, and physical effects of the rotor behavior on the structure, and vice versa, are known. The characteristics of the subsystems and their operational limits, hence requirements, can be predicted and designed. Tradeoffs can be made, and optimum configurations can be chosen to deliver maximum power, productivity, or energy for minimum cost. The barriers to the use of wind turbines are not engineering ones, but social and political ones. And the crucial issue, unlike the early days of the airplane or automobile, is cost. It remains no secret to build and operate a successful wind turbine; the problem, an engineering one now, is to do it cheaply.

The study of wind turbine dynamics, an example being this dissertation, does not automatically make wind power an attractive industry. However, we must understand the pitfalls and problems we are likely to encounter in operating a wind turbine; we have to do the calculations and studies necessary to predict the instabilities and failure modes in order to reduce the risk and keep the cost of the system low. On the other hand, we cannot do unnecessary calculations or build over-sophisticated systems for their own sake--that also is not cost effective. Again, the "soft path" approach in engineering systems

means a fundamental shift in our thinking, re-emphasizing cost in our studies and re-injecting "elegant simplicity" in our designs.

This dissertation has covered the dynamics and vibration of the most significant (and potentially catastrophic) part of any wind turbine system, the rotor. Using the programs listed in the Appendices as the simple tools they are, and using the simple models developed in the equations of motion, one can predict the loads and deflections of the blades. The significant mechanical and aeroelastic instabilities which may occur can also be predicted (Chapters V and VI), and other qualitative cases of instability have been discussed and can give food for thought. Chapter VII has shown how to analyze a complex shell composite blade to reasonable accuracy, and to model this blade as a dynamic member. This dissertation should provide a learning experience for designers unfamiliar with flexible rotors, and should also offer a comprehensive reference source to designers actively engaged in wind turbine preliminary analysis and testing.

A convenient reference listing is in Appendix V; references are grouped into sections and the entries have been chosen for their relevance and clarity. Valuable information is found in the so-called "backyard experiment" literature; ten years from now our own "sophisticated" machines will appear backward and archaic to us--we can't afford to overlook any potential source of information, results or enlightenment. The last two sections of this chapter suggest further work to be done to enhance the state-of-the-art, and outline suggested methods for initiating the wind turbine design process.

B. Needed Work

This paper has dealt with a high aspect ratio (slender) wind turbine rotor operating at constant rotational speed (Ω). Equilibrium values for the loads and deflections have been found. Unfortunately, no wind turbine ever operates at equilibrium conditions for very long, unless in a wind tunnel. Our machines are constantly being accelerated or decelerated, pitch is constantly changing, and load lagging. The most important analytical work remaining to be done is the true dynamic study of wind turbine systems, including random frequency and amplitude forcing from the wind function. One direct way to study these effects is to assume the system proceeds from equilibrium to equilibrium continuously; this is called the quasi-steady assumption. A particular set of inertias, masses, natural frequencies and coupling terms can be derived from formulations in this dissertation. All the mass, stiffness, spring, and control parameters can be found for a particular machine of interest. Then the response of the system can be determined by linearizing the equations (stability derivative approach) or by repetitive computation (computer approach). This type of study is absolutely crucial in a final design process.

The other significant area which needs time and effort is testing. There are some test data already in the literature. But we have precious little with which to verify and update our theories. As in the helicopter industry, we put great significance on test results and use them continuously to refine and update our formulations. An example of poorly understood phenomena peculiar to wind turbines is the "upwind

yaw stability" occurrence (References 66 and 67); this effect is not predicted by simple theory but may be a viscous effect attributable to skewed wake, hence predictable by a more sophisticated wake-modelling program. The first step, though, is to test the occurrence and define its limits.

Testing wind turbines also includes the assessment of productivity and end use energy quality and availability. These results affect the cost effectiveness of our machines and will ultimately determine where and how wind generators are used in the commercial market place.

C. Formalized Design Process

A process, or series of jobs, to formalize the design of wind turbine is described here. No good system can be done with analytical solutions alone, or with testing alone. Both avenues must be used, and must reinforce each other. The starting point can be as narrow as the defined operational limits, or can be as broad as simply the end product desired. We start with an assumed set of requirements that define the end product and the environment and some general guidelines for performance along the lines of safety, reliability and system life.

Five separate but interdependent studies are used. The whole process is cyclic, with analytical and test work methodically developing results until the performance of the candidate system can be compared to the given requirements. New iterations and modifications can be made to increase the performance or reduce the cost.

The study of system performance must come first. Parametric studies which model the input and output of each of a series of candidate subsystems will yield combinations which are favorable and worthy of further analysis. There always exists too broad a list of candidates to do detailed studies of each. One method for doing system performance can be seen in Figure 87. The performance of the rotor, at the top, can be reasonably predicted with momentum theory or strip theory (Appendix I). Experimental studies will continually modify such a program so confidence is increased.

A rotor performance study will also give steady-state loads (on the blades, shaft, and tower). The generator subsystem has its own "static" performance, as shown, and the torque loads produced by the rotor must be related to generator torque and excitation. Finally, a "static" system model, for performance, is developed. This model may be one of many to offer comparison and optimization, or it may be a detailed look at specifically different generators, step-up gears, etc., to pick the best.

This model could be extended via the quasi-static assumption to give a dynamic model dependent on wind forcing functions. This "stability" model can show valuable trends between candidate systems and lead to philosophy of design and control system verification. The dynamic model "juggles" the performance variables, e.g., RPM, wind speed, excitation, rotor diameter, tip speed ratio, etc., to find the proper control system. This can also identify required control logic (e.g., for overspeed) and ratios of variables which are unstable (e.g., stalling the rotor). This dissertation has not been concerned with

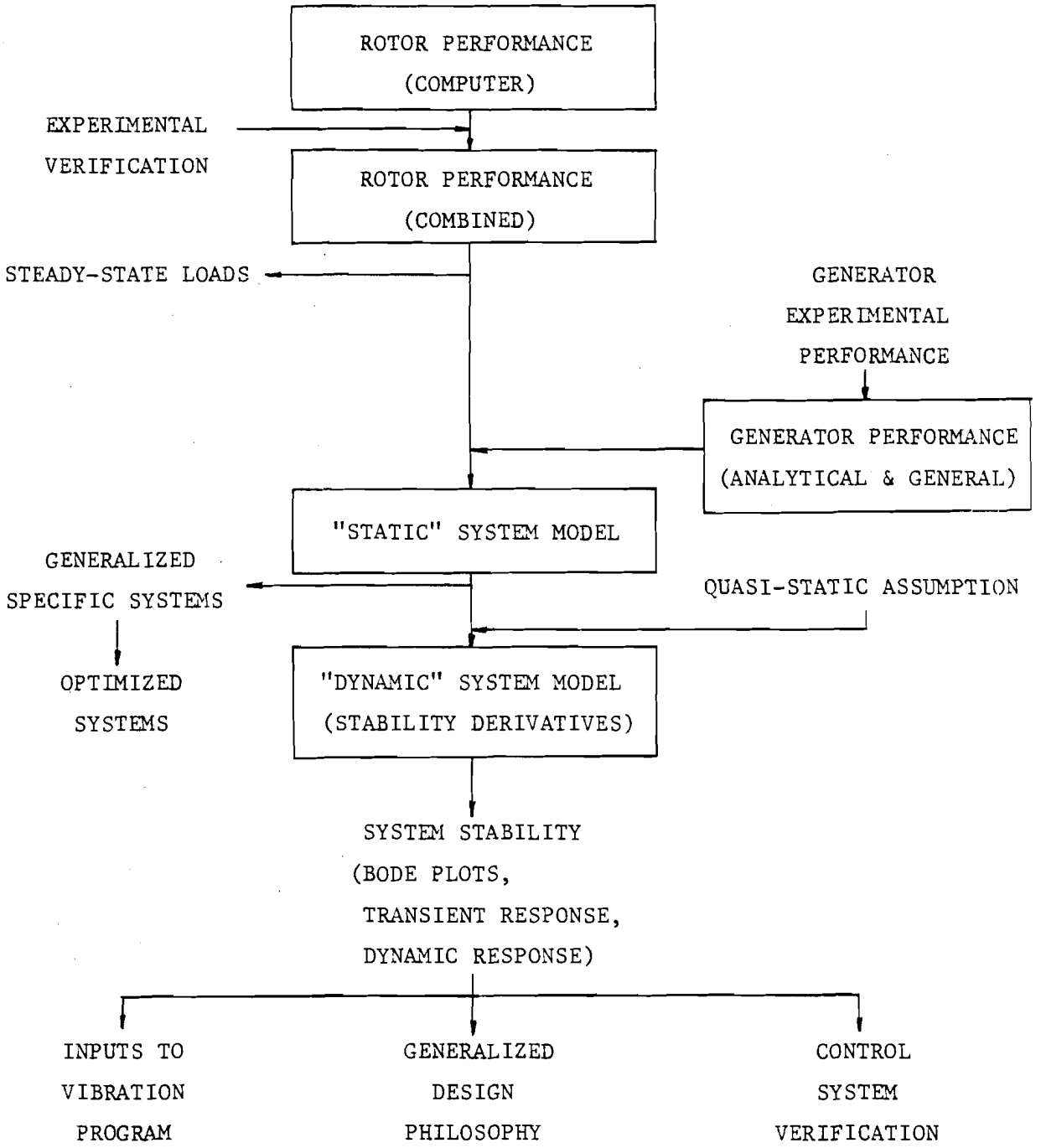

Figure 87. System Performance

performance and productivity studies since the subject is well covered in the literature due to its primary significance.

Next, the blades must be studied in a detailed way; the blade structure and its response must be determined. The performing geometry, and the assumed weights and stiffnesses of various candidate materials, will determine the blade strength and flexibility via the EI program (Appendix II). Now the loadings can be introduced to calculate stresses and deflections. First the steady loads are used, and then the dynamic loads (airloading, inertial, gravitational, etc.) are used. The structural response of the blade will be found, and the stresses and deflections may or may not be acceptable. Additionally, the natural frequency of the blade can be found via the program in Appendix IV. This will give the dynamicist a chance to see if the vibrating blades are at the wrong frequency, or if an instability may be present. It is his job to look for hazard signs which will necessarily change the blade design of the other path. The vibration model will also provide additional vibratory loads to be included in the stress-deflection analysis, along with the others.

Now the blade dynamics study, the most significant input to this process, can be done. The rotor is now a specific arrangement of structural pieces, with detailed geometries. The analytical blade equations of motion are coupled; the steady state loading will give starting values of loads and deflections, and the aerodynamic functions can now be introduced in complexity. The dynamic blade model describes a complete rotor system and provides for time-varying forcing. This

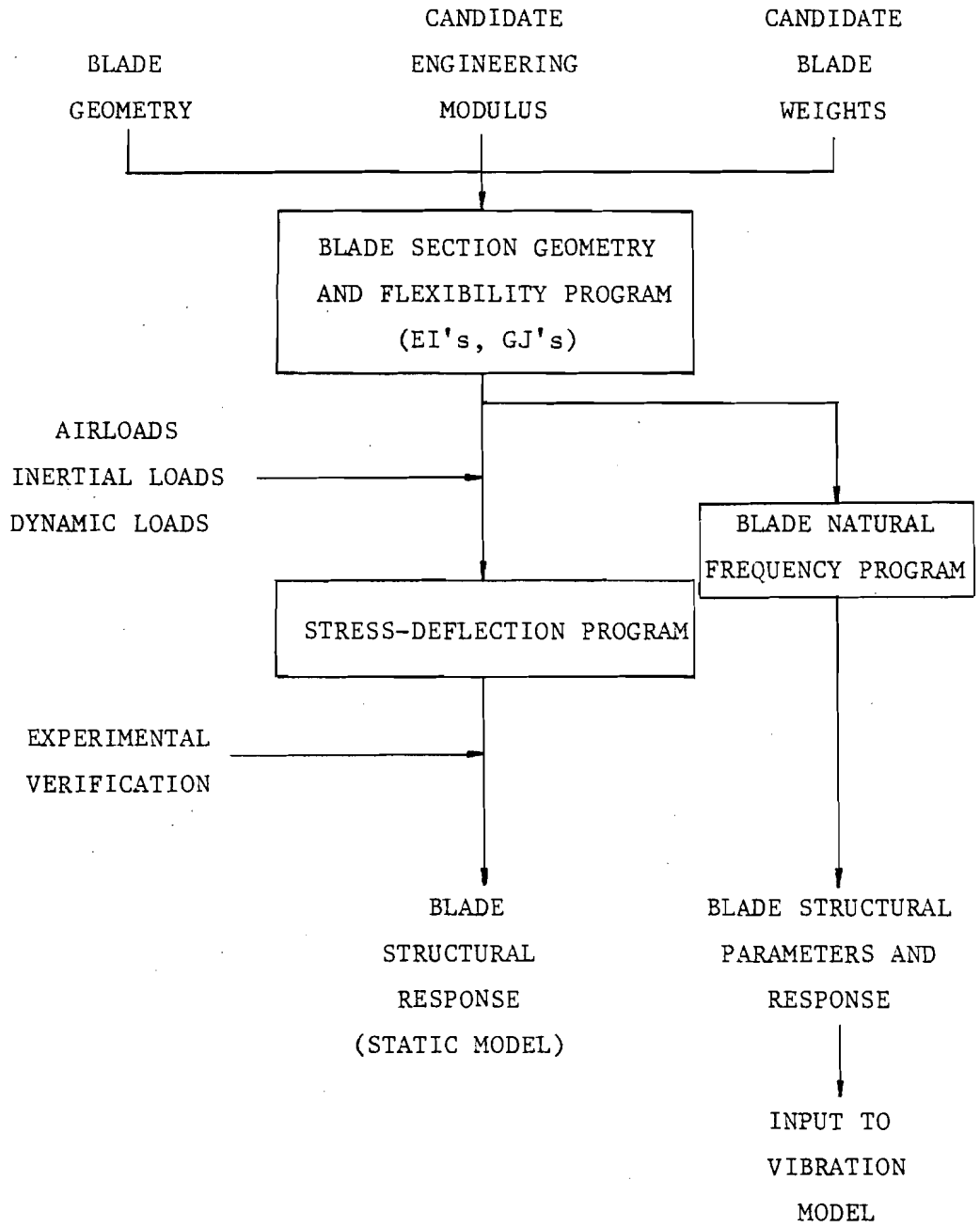

Figure 88. Blade Structure

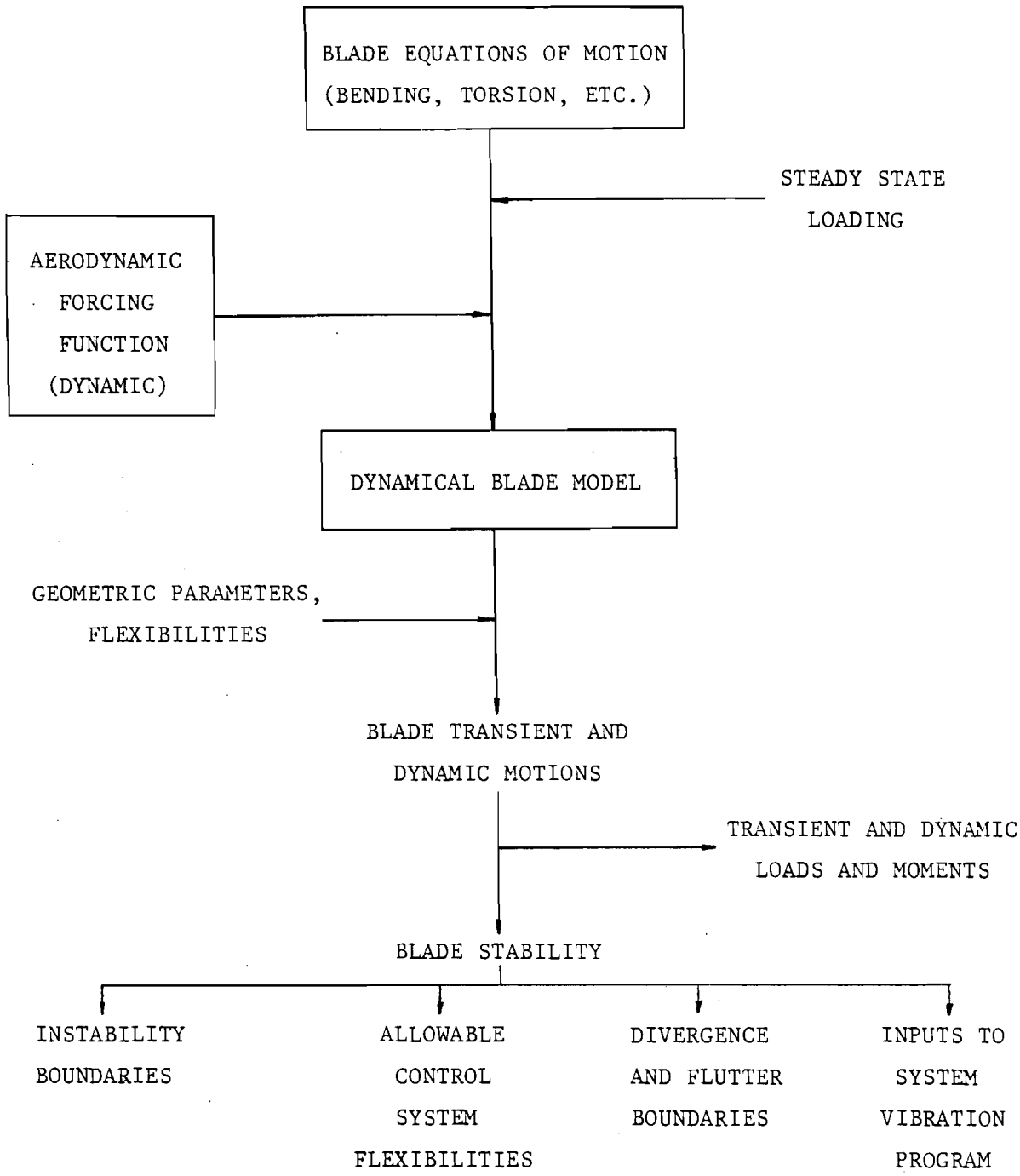

Figure 89. Blade Dynamics

model could be as complex as a set of coupled integro-differential equations to be solved only with finite difference techniques, to a simplified set of equations as done in this dissertation. This model yields the blade motions, time-varying deflections and loads. This in turn generates stability of the rotor system (Chapter VI), and the transient and dynamic loads on the rest of the system (Chapter V). This set of results is the major subject of this dissertation; the various developments in Chapter III give the blade deflections and motions, and Chapter IV gives blade and hub loads. Control system flexibilities, hub design (cantilevered, teetering, or articulated), and nacelle moments of inertia have been included.

The tower response and vibration program is shown in Figure 90. The tower static model is analogous to the static blade model and the tower vibration model to the blade vibration model, giving natural frequencies and motions for design criteria. This paper has not dealt with the tower detailed design, instead describing the tower as a set of masses, moments of inertia, and with a natural frequency in bending (Chapters I and V).

Finally, the various studies can be brought together in an overall system vibration model. The blade dynamics, system performance dynamics, and wind dynamics can all be thought of as a forcing function for the blade vibration model. The tower model is also an input. This, for the final candidate design, will be the method used to find all the predicted loads and deflections, and along with test data, will provide the needed vibration design knowledge.

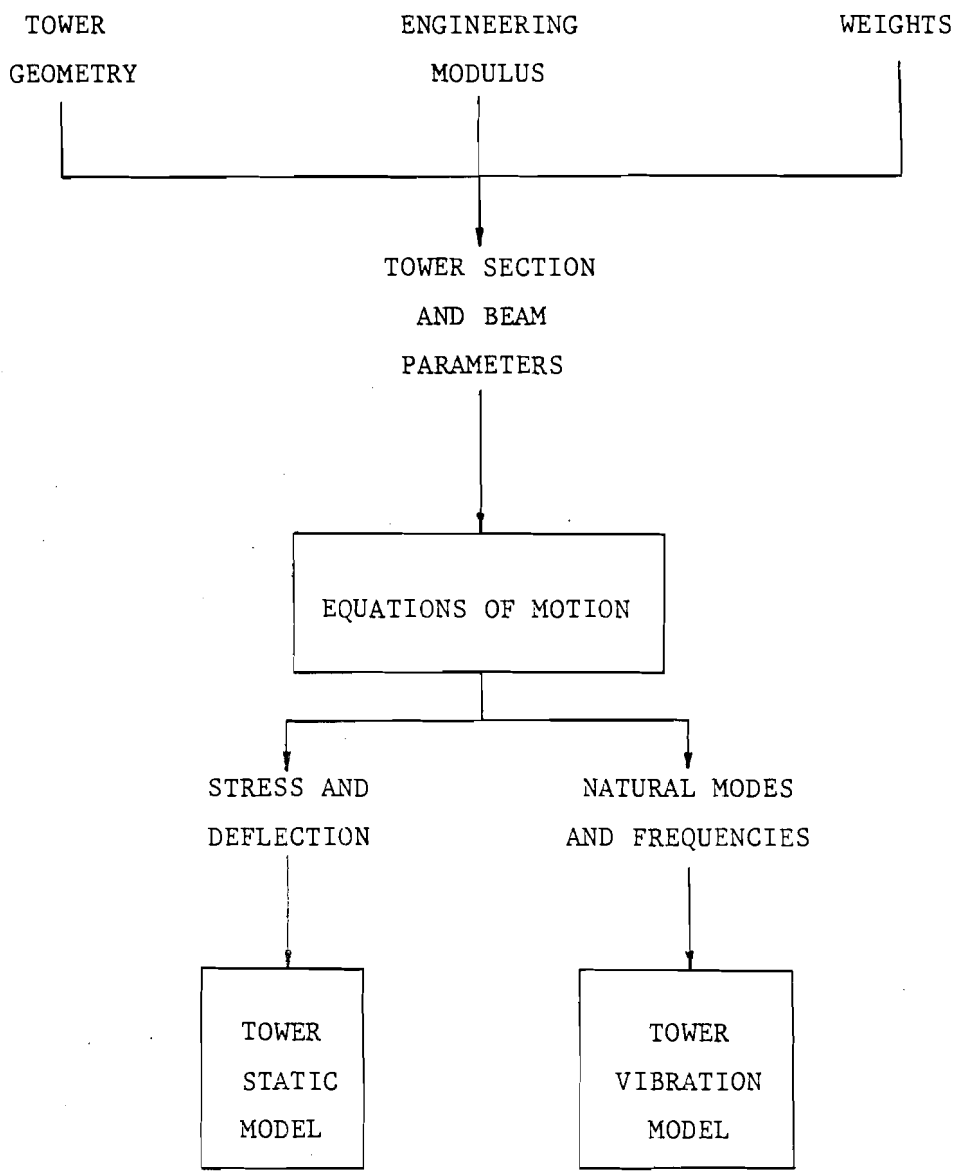

Figure 90. Tower Response and Vibration

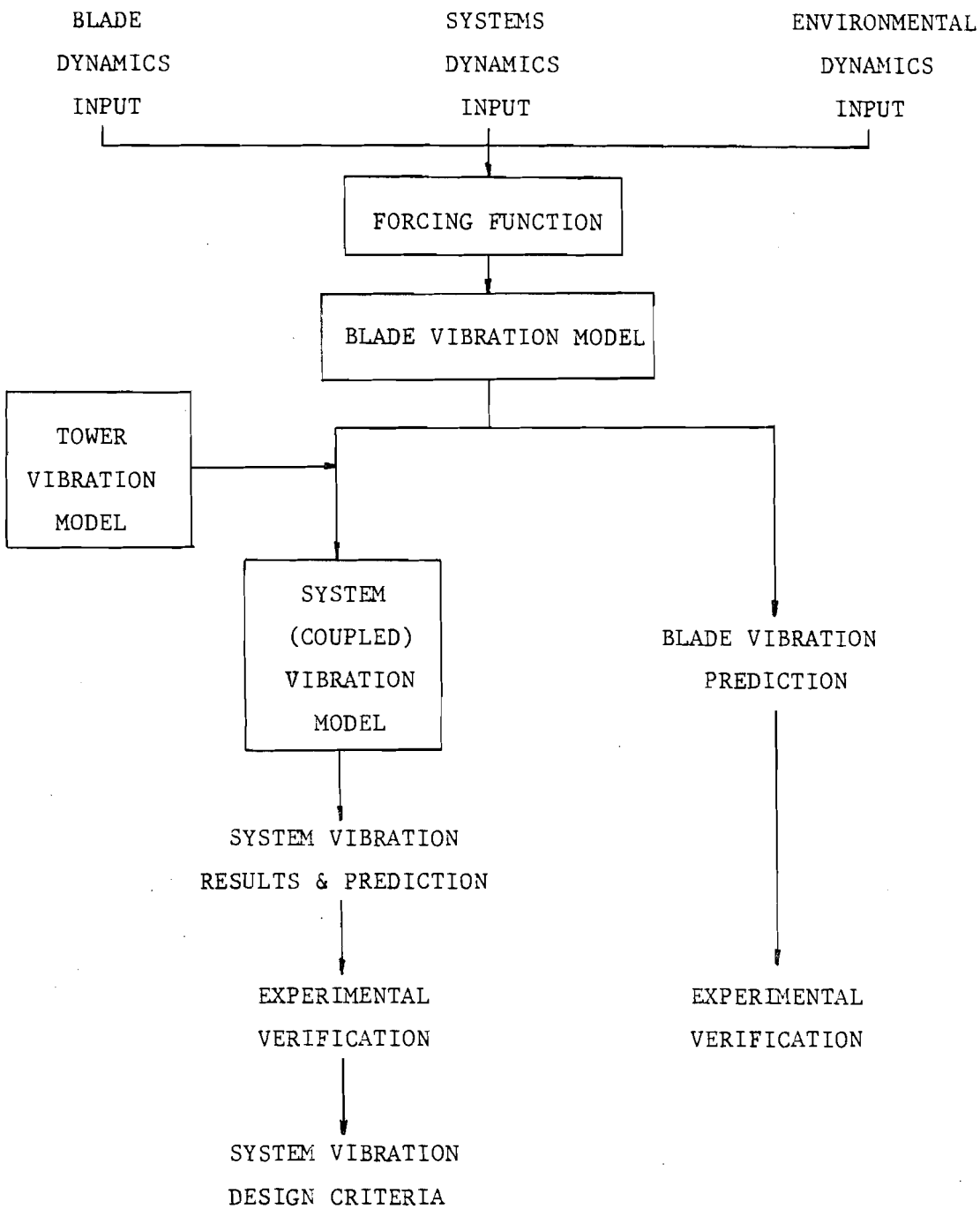

Figure 91. System Vibration Model

REFERENCES

[1]Heronemus, W. E., Principal Investigator, "Investigation of the Feasibility of Using Windpower for Space Heating in Colder Climates," Phase II Final Report, D.O.E. Report ERDA/2365-77/2, Energy Alternatives Program, University of Massachusetts, UM-WF-PR-77-2, Amherst, Massachusetts, September, 1977.

[2]Heronemus, W. E., Editor, "The Working Drawings and Bills of Material for Wind Furnace I as Installed at Solar Habitat I, Orchard Hill, University of Massachusetts, Amherst," Energy Alternatives Program, UM-WF-TR-77-10, Amherst, Massachusetts, September, 1977.

[3]Cromack, D. E., Heronemus, W. E., and J. G. McGowan, "Design and Operational Aspects of a 25 KW Wind Turbine Generator for Residential Heating Applications," presented at 12th Intersociety Energy Conversion Engineering Conference, Washington, D. C., August 28 - September 2, 1977.

[4]Heronemus, W. E., Principal Investigator, "Investigation of the Feasibility of Using Windpower for Space Heating in Colder Climates," Third Quarterly Progress Report Covering the Final Design and Manufacturing Phase, N.S.F. Grant AER 75-00603, Report NSF/RANN/AER-75-00603/PR/75/3, Energy Alternatives Program, University of Massachusetts, UM-WF-PR-75-3, December, 1975.

[5]Chilcott, R. E., "The Design, Development and Testing of a Low Cost, 10 Hp. Windmill Prime Mover," Brace Research Institute No. MT. 7, McGill University, Canada, July, 1969.

[6]Abbott, I. H., and A. E. VonDoenhoff, Theory of Wing Sections, McGraw-Hill Book Company, New York, 1949.

[7]Perkins, F. W., and D. E. Cromack, "Wind Turbine Blade Stress Analysis and Natural Frequencies," Energy Alternatives Program, UM-WF-TR-78-8, University of Massachusetts, Amherst, Massachusetts, August, 1978.

[8]Miller, R. H., "Wind Energy Conversion - Progress Report to July 15, 1975," Appendix D: "Notes on Aeroelastic Stability," N.S.F. Grant AER 75-00826, Massachusetts Institute of Technology, Cambridge, Massachusetts, August, 1975.

[9]Bramwell, A. R. S., Helicopter Dynamics, John Wiley, New York, 1976.

[10]Halfman, R. L., Dynamics: Particles, Rigid Bodies, and Systems, Addison-Wesley Publishing Company, Inc., Reading, Massachusetts, 1962.

[11]Crossley, F. R. E., Mechanical Vibrations, Class Notes, Mechanical Engineering Department, University of Massachusetts, June, 1976.

[12]Hildebrandt, F. B., Advanced Calculus for Applications, Prentice Hall, Inc., Englewood Cliffs, New Jersey, 15th printing, 1962.

[13]Jenney, D. M., "Helicopter Principles," Lectures given at the Naval Test Pilot School, Sikorsky Aircraft, Stratford, Connecticut, 1968.

[14]Ham, N. D., V/STOL Aerodynamics and Dynamics, Class Notes, Courses 16.50 and 16.51, Massachusetts Institute of Technology, Department of Aeronautics and Astronautics, Cambridge, Massachusetts, 1968.

[15]Ormiston, R. A., "Dynamic Response of Wind Turbine Rotor Systems," Preprint S-993, 31st Annual Forum of the American Helicopter Society, Washington, D. C., May, 1975.

[16]Miller, R. H., "Rotor Blade Harmonic Airloading," Preprint 62-82, Institute of Aeronautical Sciences 30th Annual Meeting, New York, January, 1962.

[17]Wolkovitch, J., and J. A. Hoffman, "MOSTAB-Flight Characteristics of Airplanes and Helicopters," Mechanics Research, Inc., Technical Note 581-1, Los Angeles, December, 1969.

[18]Gessow, A., and G. C. Myers, Jr., Aerodynamics of the Helicopter, Frederick Ungar Publishing Company, New York, 3rd printing, 1952.

[19]Clegg, P., Energy for the Home, Garden Way Publishing, Charlotte, Vermont, 1975.

[20]Saunders, G. H., Dynamics of Helicopter Flight, John Wiley, New York, 1974.

[21]anon., "Development of an 8 KW. Wind Turbine Generator," D.O.E. Request for Proposals No. PF 64086F, Federal Wind Energy Program, Rocky Flats Test Center, Golden, Colorado, 28 March 1977.

[22]Jarosch, Stepan, "Fatigue Properties and Test Procedures of GRP Plastic Rotor Blades," presented at American Helicopter Society 25th Annual Forum, Washington, D. C., May, 1969.

[23]Glauert, H., "Windmills and Fans," Division L, Part XI, Aerodynamic Theory, W. F. Durand, ed., Springer Publishing, Berlin, 1935.

[24]Dommasch, D. O., Sherby, Connolly, Airplane Aerodynamics, Pitman Publishing, New York, 1967.

[25]DenHartog, J. P., Mechanical Vibrations, McGraw-Hill Book Company, New York, 4th edition, 1956.

[26]Ormiston, R. A., Technical Chairman, "Rotorcraft Dynamics," Conference on Rotorcraft Dynamics sponsored by Ames Research Center and American Helicopter Society, Moffett Field, California, February 13-15, 1974.

[27]Kolesar, C. E., "Cyclic Pitch Control on a V/STOL Tilt Wing Aircraft," Boeing Vertol Company, Air Force Flight Dynamics Laboratory Report AFFDL-TR-71-91, October, 1971.

[28]Donham, R., Schmidt, and Linscott, "100-KW Hingeless Metal Wind Turbine Blade Design, Analysis, and Fabrication," Preprint S-998, presented at 31st Annual Forum of the American Helicopter Society, Washington, D. C., May, 1975.

[29]Thomas, R., Sholes, and Sholes, "Preliminary Results of the Large Experimental Wind Turbine Phase of the National Wind Energy Program," NASA TM-X-71796, NASA Lewis Research Center, Cleveland, Ohio, October, 1975.

[30]Chamis, C. C., and T. L. Sullivan, "Free Vibrations of the ERDA-NASA 100 KW Wind Turbine," NASA TM-X-71879, NASA Lewis Research Center, Cleveland, Ohio, March, 1976.

[31]Hohenemser, K. H., and S. K. Yin, "Some Applications of the Method of Multiblade Coordinates," Journal of the American Helicopter Society, Volume 17, July, 1972.

[32]Wilson, R. E., et al., "Rigid Body Model for Analysis of Aerogenerator Rotor Dynamics," Preprint S-991, presented at 31st Annual Forum of the American Helicopter Society, Washington, D. C., May, 1975.

[33]Thresher, R. W., and C. E. Smith, "Free Vibration Approximations for Horizontal Axis Wind Turbines," D.O.E. Contract No. EY-76-S-06-2227, Federal Wind Energy Program, Oregon State University, Corvallis, Oregon, July, 1978.

[34]Foote, W. R., Poritsky, H., and J. J. Slade, Jr., "Critical Speeds of a Rotor with Unequal Shaft Flexibilities, Mounted in Bearings of Unequal Flexibility," Journal of Applied Mechanics, Volume 10, No. 2, June, 1943.

[35]Coleman, R. P., and A. M. Feingold, "Theory of Self-Excited Mechanical Oscillations of Helicopter Rotors with Hinged Blades," NACA Report 1351, 1958.

[36]Sheu, D. T., "Effects of Tower Motion on the Dynamic Response of Windmill Rotor," S.M. Thesis, Department of Aeronautics and Astronautics, Massachusetts Institute of Technology, February, 1977.

[37]Dugundji, J., "Some Dynamic Problems of Rotating Windmill Systems," NASA CP-2001, presented at 13th Annual Meeting of the Society of Engineering Science, Advances in Engineering Science, Hampton, Virginia, November, 1976.

[38]Hall, W. E., Jr., "Application of Floquet Theory to the Analysis of Rotary-Wing VTOL Stability," USAARC Contract NAS-2 5143, Department of Aeronautics and Astronautics, Stanford University, Stanford, California, February, 1970.

[39]Hammond, C. E., "An Application of Floquet Theory to Prediction of Mechanical Instability," Journal of the American Helicopter Society, Volume 19, No. 4, October, 1974.

[40]White, M. P., "Dynamics of New England Wind Furnace," Appendix XI to Fourth Quarterly Progress Report Covering the Final Manufacturing and Construction Phase, "Investigation of the Feasibility of Using Wind-power for Space Heating in Colder Climates," W. E. Heronemus, Principal Investigator, N.S.F. Grant AER 75-00603, Report NSF/RANN/AER-75-00603/PR/76/1, Energy Alternatives Program, University of Massachusetts, UM-WF-TR-76-9, April, 1976.

[41]Sissingh, G. J., "Investigations on Automatic Stabilization of the Helicopter," Royal Aircraft Establishment Report Aero. 2277, 1948.

[42]Loewy, R. G., "Review of Rotary-Wing V/STOL Dynamic and Aeroelastic Problems," American Institute of Aeronautics and Astronautics Paper No. 69-202, February 19, 1969.

[43]Miller, R. H., and C. W. Ellis, "Helicopter Blade Vibration and Flutter," Journal of the American Helicopter Society, July, 1956.

[44]Friedmann, P., and Tong, "Dynamic Nonlinear Elastic Stability of Helicopter Rotor Blades in Hoves and in Forward Flight," NASA CR-114485, Massachusetts Institute of Technology, M.I.T. ASRL 166-3, May, 1972.

[45]Lemnios, A. Z., "The Aeroelastic Behavior of Rotary Wings in Forward Flight," Ph.D. Dissertation, University of Connecticut, Storrs, Connecticut, June, 1967.

[46]Houbolt, J. C., and G. W. Brooks, "Differential Equations of Motion for Combined Flapwise Bending, Chordwise Bending and Torsion of Twisted Non-Uniform Rotor Blades," NACA Report 1346, 1958.

[47]Ormiston, R. A., and D. H. Hodges, "Linear Flap-Lag Dynamics of Hingeless Helicopter Rotor Blades in Hover," Journal of the American Helicopter Society, Volume 17, No. 2, April, 1972.

[48]Hohenemser, K. H., "Hingeless Rotorcraft Flight Dynamics," AGARDograph 197, 1974.

[49]Hansford, R. E., and I. A. Simons, "Torsion-Flap-Lag Coupling on Helicopter Rotor Blades," Journal of the American Helicopter Society, October, 1973.

[50]Pei, C. C., "Pitch-Lag Instability of Helicopter Rotor Blades," Journal of the American Helicopter Society, July, 1958.

[51]Shapiro, J., Principles of Helicopter Engineering, McGraw-Hill, New York, 1955.

[52]Stammers, C. W., "The Flutter of a Helicopter Rotor Blade in Forward Flight," Aeronautical Quarterly, February, 1970.

[53]Miller, R. H., "Unsteady Airloads on Helicopter Rotor Blades," Journal of the Royal Aeronautical Society, Volume 68, No. 640, April, 1964.

[54]Carta, F. O., "An Analysis of the Stall Flutter Instability of Helicopter Rotor Blades," Journal of the American Helicopter Society, October, 1967.

[55]Ham, N. D., and M. I. Young, "Torsional Oscillations of Rotor Blades Due to Stall," Journal of Aircraft, May, 1966.

[56]Rivello, R. M., Theory and Analysis of Flight Structures, McGraw-Hill Book Company, New York, 1969.

[57]Nash, W. A., Strength of Materials: Theory and Problems, 2nd edition, Schaum's Outline Series, McGraw-Hill Book Company, New York, 1972.

[58]Timoshenko, S. P., and J. N. Goodier, Theory of Elasticity, 3rd edition, McGraw-Hill Book Company, New York, 1970.

[59]DenHartog, J. P., Strength of Materials, McGraw-Hill Book Company, New York, 1948.

[60]Marks, L. S., Editor (1916 to 1951), and T. Baumeister, Editor, Standard Handbook for Mechanical Engineers, 7th edition, McGraw-Hill Book Company, New York, 1967.

[61]Holzer, H., Die Berechnung der Drehschivingungen, Springer Verlag, Berlin, 1921.

[62]Myklestad, N. O., "A New Method for Calculating Natural Modes of Uncoupled Bending Vibration of Airplane Wings and Other Types of Beams," Journal of Aeronautical Sciences, April, 1944.

[63]Myklestad, N. O., Fundamentals of Vibration Analysis, McGraw-Hill Book Company, 1956.

[64]Prohl, M. A., "A General Method for Calculating Critical Speeds of Flexible Rotors," ASME Transaction A-142, September, 1945.

[65]Bisplinghoff, R. L., Ashley, H., and R. L. Halfman, Aeroelasticity, Addison Wesley Publishing Company, Inc., Reading, Massachusetts, 1955.

[66]Stoddard, F., Perkins, F., and D. Cromack, "Wind Tunnel Tests for Fixed-Pitch Start-Up and Yaw Characteristics," University of Massachusetts Energy Alternatives Program, Technical Report UM-WT-TR-78-1, June, 1978.

[67]Hohenemser, K. H., "Some Alternative Dynamic Design Configurations for Large Horizontal Axis Wind Energy Conversion Systems," presented at the Wind Turbine Structural Dynamics Workshop, NASA Conference Publication 2034, D.O.E. Publication CONF-771148, NASA Lewis Research Center, Cleveland, Ohio, November 15-17, 1977.

APPENDIX I

COMPUTER PROGRAM: AERODYNAMIC STRIP THEORY, LOADS AND MOMENTS FOR PERFORMANCE

The strip theory program, WMLPER, is written in Fortran and is listed in this appendix. The method of summing two-dimensional airfoil contributions to assess rotor performance is well documented in the literature; see Reference 24 (Dommasch, 1967) and Wilson and Lissaman (1975, 1977) in the bibliography. This strip theory assumes a horizontal axis rotor running at constant speed (Ω) in a constant free stream (V_o). The blade airfoil is NACA 4415 throughout. A tip loss is accounted for, and the blade contributions are summed over the rotor.

The sample run in this appendix used a blade geometry given by the following file. The first line denotes the blade twist (radians) and the second the blade chord (feet):

$$\left\{\begin{array}{l} 0.3473,0.2740,0.1981,0.1274,0.0771,0.0471,0.0265,0.0115,0.0027,0.0000 \\ 2.019,\ 1.793,\ 1.639,\ 1.345,\ 1.099,\ 0.948,\ 0.837,\ 0.750,\ 0.685,\ 0.602 \end{array}\right\}$$

This input file is compiled as TAPE 1 in the program. The program then queries the user for the following information:

$$\left\{\begin{array}{l} \text{blade radius (feet), number of blades, blade tip pitch (degrees)} \\ \text{rotor RPM, wind speed (MPH), air density} \end{array}\right\}$$

The example given here used:

$$\left\{\begin{array}{lll} 20.0, & 3.0, & 0.0 \\ 145.0, & 26.0, & 0.0023769 \end{array}\right\}$$

The output lists the aerodynamic and force data for each of the ten blade sections, as shown in the following blade element:

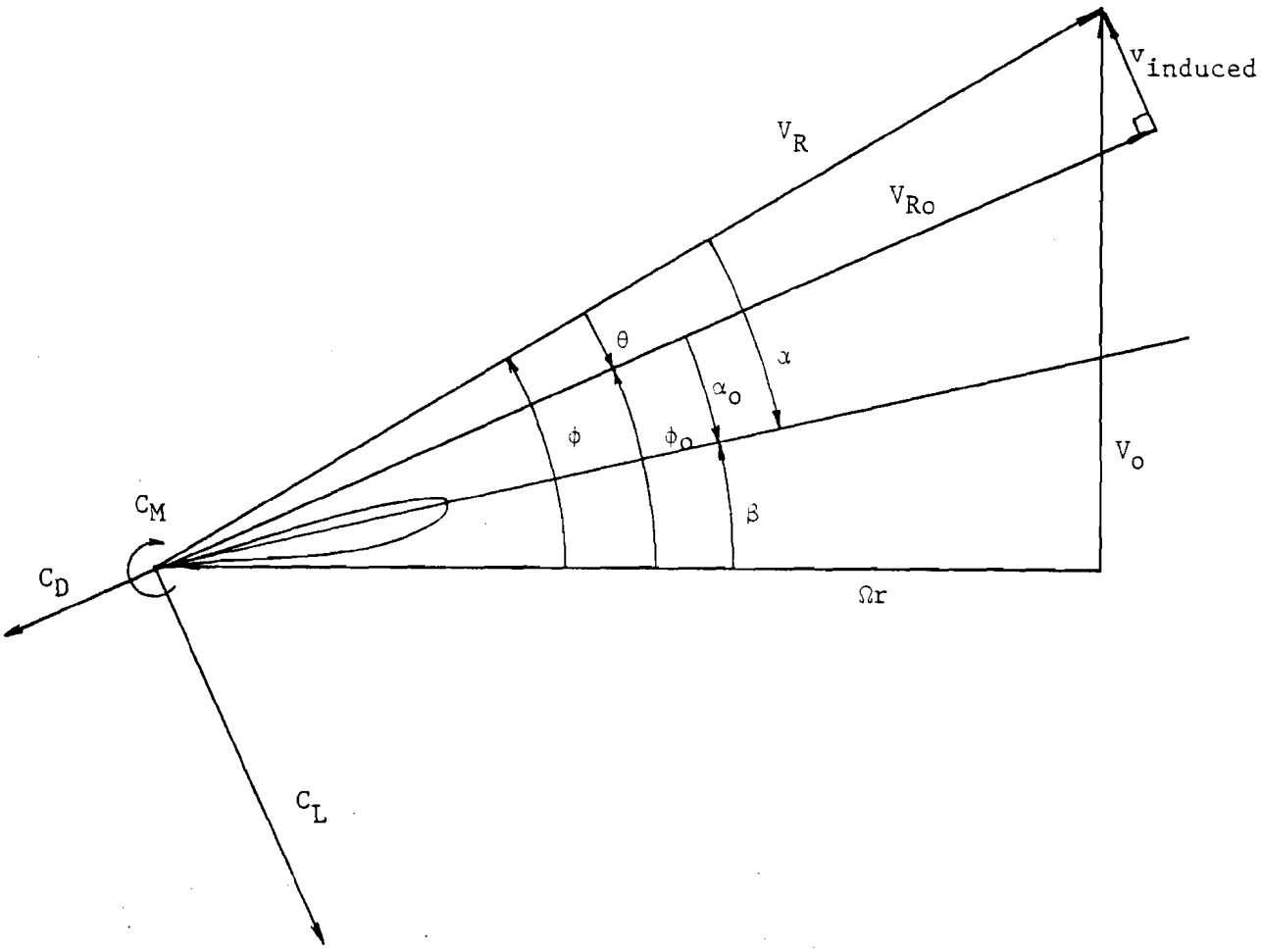

The program then integrates along the blade to calculate rotor thrust (T,lb.), shaft torque (Q, ft.-lb.), shaft horsepower, disc loading, torque coefficient, power coefficient, pitching moment, and blade bending moment.

```
10 PROGRAM WNDMILL (INPUT,TAPE1, TAPE2, TAPE3, OUTPUT)
20 DIMENSION BETA1(10),BETA(10),CB(10),DTR(10),DM(10),DMR(10)
30 DIMENSION TLAMBDA(10),QLAMBDA(10),DT(10),DQ(10),DQR(10),R(10)
40 40 FORMAT(3X,F6.2,F4.1,F7.4)
42 42 FORMAT(3X,F5.1,F5.1,F9.7)
45 45 FORMAT(3X,10F6.4,3X,10F6.3)
50 READ (1,45) (BETA1(N),N=1,10)
55 READ (1,45) (CB(N),N=1,10)
60 READ, RAD,B,PITCH
65 READ, RPM,SPEED,RHO
66 REWIND 1
67 REWIND 2
68 REWIND 3
70 70 FORMAT(*THIS PROGRAM CALCULATES WINDMILL PERFORMANCE USING STRIP THEORY*)
75 PRINT 70
80 ALPHAO=0.01
85 VINF=SPEED*(88./60.)
90 ADVRAT=(RPM*.1047*RAD)/VINF
95 APX(A,B)=A*(ALPHAO+B)
100 OMEGA=2.0*3.14159*RPM/60.0
105 S=3.1415926*(RAD**2.0)
110 SCREW=(VINF)/((RPM/60.)*2.0*RAD)
115 RE=RHO*VINF*ADVRAT*0.591/.00000037452
118 BETAO=PITCH*((2.0*3.141592654)/360.)
120 DELTR=RAD/10.0
125 125 FORMAT(/,/,12X,*TIP SPEED RATIO=*,F6.2)
130 130 FORMAT(12X,*WIND SPEED=*,F6.2)
135 135 FORMAT(12X,*RPM=*,F6.2)
140 140 FORMAT(12X,*OMEGA=*,F6.3)
145 145 FORMAT(12X,*PITCH=*,F6.2)
147 147 FORMAT(12X,*REYNOLD'S NO.=*,E12.6,/,/,/,/)
150 PRINT 125,ADVRAT
151 PRINT 130,SPEED
152 PRINT 135,RPM
153 PRINT 140,OMEGA
154 PRINT 145,PITCH
155 PRINT 147,RE
200 DO 210 N=1,10
205 BETA(N)=BETA1(N)+BETAO
210 210 CONTINUE
215 DO 780 N=1,10
217 R(N)=FLOAT(N)*DELTR
218 BETAWK=BETA(10)
219 IF(BETAWK.LE.0.035)  BETAWK=0.035
220 DO 680 I=1,1000
230 PHI=ATAN2(VINF,(OMEGA*R(N)))
240 THETA=PHI-BETA(N)-ALPHAO
250 VR=SQRT((VINF**2.0)+(OMEGA*R(N))**2.0)
260 VRO=VR*COS(THETA)
270 270 IF(ALPHAO.LT.-1.5708) ALPHAO=-1.5708
275 275 IF(ALPHAO.GT.-1.4312)  GO TO 285
280 CL=APX(-1.4733,1.5708) $ CD=0.178 $ CM=APX(-.1364,-1.8151)
281 GO TO 480
285 285 IF(ALPHAO.GT.-1.3439)  GO TO 295
290 CL=APX(-1.4733,1.5708) $ CD=APX(-.7162,-1.0472) $ CM=APX(-.1364,-1.8151)
291 GO TO 480
295 295 IF(ALPHAO.GT.-1.1432)  GO TO 305
300 CL=APX(-1.4733,1.5708) $ CD=APX(-.7162,-1.0472) $ CM=APX(-.3508,.1571)
301 GO TO 480
305 305 IF(ALPHAO.GT.-.8727)   GO TO 315
310 CL=APX(-.6945,2.0944) $ CD=APX(-1.6454,.1920) $ CM=APX(-.3508,.1571)
311 GO TO 480
315 315 IF(ALPHAO.GT.-.6807)   GO TO 325
320 CL=-.810   $           CD=APX(-1.6454,.1920) $ CM=APX(-.3508,.1571)
321 GO TO 480
325 325 IF(ALPHAO.GT.-.3665)   GO TO 335
330 CL=APX(.7003,-.4887) $ CD=APX(-1.6454,.1920) $ CM=APX(-.3508,.1571)
331 GO TO 480
```

```
335 335 IF(ALPHAO.GT.-.3142)   GO TO 345
340 CL=APX(-3.0156,.5760) $ CD=APX(-.6875,-.0349) $ CM=0.0
341 GO TO 480
345 345 IF(ALPHAO.GT.-.2740)  GO TO 355
350 CL=APX(-3.0156,.5760) $ CD=APX(-.6875,-.0349) $ CM=APX(-.7162,.3142)
351 GO TO 480
355 355 IF(ALPHAO.GT.-.2199)   GO TO 365
360 CL=-.880 $ CD=APX(-2.2918,.1745) $ CM=APX(-.7162,.3142)
361 GO TO 480
365 365 IF(ALPHAO.GT.-.1745)   GO TO 375
370 CL=APX(5.8981,.0698) $ CD=APX(-1.1459,.1396) $ CM=APX(-.7162,.3142)
371 GO TO 480
375 375 IF(ALPHAO.GT.-.1571)   GO TO 385
380 CL=APX(5.8981,.0698) $ CD=APX(-1.1459,.1396) $ CM=APX(.0409,-2.4435)
381 GO TO 480
385 385 IF(ALPHAO.GT.0.1274)   GO TO 395
390 CL=APX(5.8981,.0698) $ CD=0.025             $ CM=APX(.04093,-2.4435)
391 GO TO 480
395 395 IF(ALPHAO.GT.0.1745)   GO TO 405
400 CL=APX(3.0971,.2478) $ CD=0.030             $ CM=APX(.4093,-.3665)
401 GO TO 480
405 405 IF(ALPHAO.GT.0.1990)   GO TO 415
410 CL=APX(3.0971,.2478) $ CD=APX(2.7026,-.1623) $ CM=APX(.4093,-.3665)
411 GO TO 480
415 415 IF(ALPHAO.GT.0.2443)   GO TO 425
420 CL=1.400              $ CD=APX(2.7026,-.1623) $ CM=APX(-.08188,.576)
421 GO TO 480
425 425 IF(ALPHAO.GT.0.3142)   GO TO 435
430 CL=APX(-2.2596,-.8639) $ CD=APX(.9241,0.0) $ CM=APX(-.08188,.576)
431 GO TO 480
435 435 IF(ALPHAO.GT.0.3665)    GO TO 445
440 CL=APX(-.5278,-2.6704) $ CD=APX(1.6711,-.1396) $ CM=APX(-.08188,.576)
441 GO TO 480
445 445 IF(ALPHAO.GT.0.9599)   GO TO 455
450 CL=APX(-.5278,-2.6704) $ CD=APX(1.6711,-.1396) $ CM=APX(-.3508,-.1571)
451 GO TO 480
455 455 IF(ALPHAO.GT.1.3439)   GO TO 465
460 CL=APX(-1.4733,-1.5708) $ CD=APX(1.0418,.3578) $ CM=APX(-.3508,-.1571)
461 GO TO 480
465 465 CONTINUE
470 CL=APX(-1.4733,-1.5708) $ CD=0.178            $ CM=APX(-.1364,1.8151)
471 GO TO 480
480 480 CONTINUE
483,  STATEMENTS 485 AND 505 CONTAIN INPUT INFORMATION
485 IF(N.EQ.10) R(N)=19.
490 FF=B*((R(N)/RAD)-1.)/(2.*SIN(BETAWK))
495 WK=(2.0/3.1415926)*ACOS(EXP(FF))
500 PHIO=PHI-THETA
505 IF(N.EQ.10) R(N)=20.
506,  ABSOLUTE VALUE TAKEN TO MAKE A CONVERGENCE INTERVAL FROM BOTH SIDES
510 IF(ABS(PHIO)-0.01) 515,515,600
515 515 CONTINUE
520 AA=B*CB(N)*RAD*5.8981/(8.*3.1415926*WK*COS(PHI)*R(N)*R(N))
525 BB=TAN(PHI)+AA
530 CC=AA*(PHI-BETA(N))
535 DETER=BB**2.-4.*CC
538 THETA=BB/2.+0.5*SQRT(ABS(DETER))
540 VIND=VR*SIN(THETA)
545 PHIO=PHI-THETA
560 VRO=SQRT(VR**2.-VIND**2.)
565 ALPHA=PHI-BETA(N)
570 ALPHAO=ALPHA-THETA
575 CL=APX(5.8981,.0698)  $  CD=0.025    $  CM=APX(.04093,-2.4435)
595 GO TO 685
600 600 CONTINUE
```

```
610 610 VIND=CL*VRO*B*CB(N)/(8.0*3.14159*R(N)*WK*SIN(PHIO))
615 615 SPUR=VIND/VRO
620 THETA=ATAN(SPUR)
625 625 CONTINUE
630 ALPHA1=ALPHAO
640 ALPHAO=PHI-THETA-BETA(N)
645 ALPHA=ALPHAO+THETA
650 DELTA=ABS(ALPHAO-ALPHA1)
660 IF(DELTA-.00001) 685,685,670
670 670 IF(I.EQ.1000) PRINT 675,DELTA
675 675 FORMAT(*NO ALPHA CONVERGENCE*,5X,*DELTA=*,E12.6,/)
680 680 CONTINUE
685 685 CONTINUE
690 690 FORMAT(2X,*N=*,I3,10X,*R=*,F6.3,9X,*I=*,I3,10X,*WK=*,F7.5,/)
692 692 FORMAT(2X,*PHI=*,F6.4,4X,*ALPHA=*,F6.4,4X,*VR=*,
693+ F12.6,4X,*THETA=*,F6.4)
694 694 FORMAT(2X,*PHIO=*,F6.4,3X,*ALPHAO=*,F6.4,3X,*VRO=*,
695+ F12.6,3X,*VIND=*,F12.6,/)
696 696 FORMAT(4X,*CL=*,F8.4,8X,*CD=*,F8.4,8X,*CM=*,F8.4,/)
700 700 FORMAT(4X,*DT/DR=*,F9.4,4X,*DQ/DR=*,F9.4,4X,*DM/DR=*,F8.4)
705 705 FORMAT(4X,*DELTAT=*,F8.2,4X,*DELTAQ/R=*,F6.2,4X,*DELTAM=*,F8.4,/,/)
710 PRINT 690,N,R(N),I,WK
711 PRINT 692,PHI,ALPHA,VR,THETA
712 PRINT 694,PHIO,ALPHAO,VRO,VIND
713 PRINT 696,CL,CD,CM
730 TLAMBDA(N)=(CL*COS(PHIO)+CD*SIN(PHIO))/(COS(PHI)**2.0)
740 QLAMBDA(N)=(CL*SIN(PHIO)-CD*COS(PHIO))/(COS(PHI)**2.0)
750 DT(N)=(RHO/2.0)*(OMEGA**2.0)*TLAMBDA(N)*CB(N)*B*(R(N)**2.0)
755 DTR(N)=DT(N)*DELTR/B
760 DQ(N)=(RHO/2.0)*(OMEGA**2.0)*QLAMBDA(N)*CB(N)*B*(R(N)**3.0)
765 DQR(N)=DQ(N)*DELTR/R(N)/B
770 DM(N)=(RHO/2.)*VRO**2.*CB(N)**2.0*CM
773 DMR(N)=DM(N)*DELTR
775 PRINT 700,DT(N),DQ(N),DM(N)
778 PRINT 705,DTR(N),DQR(N),DMR(N)
780 780 CONTINUE
783 BMT=0.0
784 BMQ=0.0
785 DO 794 N=1,10
790 BMT=BMT+DTR(N)*R(N)
792 BMQ=BMQ+DQR(N)*R(N)
794 794 CONTINUE
796 BM=SQRT(ABS(BMT)**2.0+ABS(BMQ)**2.0)
800 T=((DELTR)/3.0)*(DT(10)+4.0*(DT(1)+DT(3)+DT(5)+
801+ DT(7)+DT(9))+2.0*(DT(2)+DT(4)+DT(6)+DT(8)))
810 Q=((DELTR)/3.0)*(DQ(10)+4.0*(DQ(1)+DQ(3)+DQ(5)+
811+ DQ(7)+DQ(9))+2.0*(DQ(2)+DQ(4)+DQ(6)+DQ(8)))
815 XM=((DELTR)/3.)*(DM(10)+4.*(DM(1)+DM(3)+DM(5)+DM(7)+DM(9))
816+ +2.0*(DM(2)+DM(4)+DM(6)+DM(8)))
820 CT=T/(RHO*((RPM/60.)**2.0)*((2.0*RAD)**4.0))
830 CQ=Q/(RHO*((RPM/60.)**2.0)*((2.0*RAD)**5.0))
840 CP=2.0*3.14159*CQ
850 P=CP*RHO*((RPM/60.)**3.)*((2.*RAD)**5.0)
852 CPB=P/(0.5*RHO*S*(VINF**3.))
853 CQB=Q/(0.5*RHO*S*RAD*(VINF**2.0))
855 HP=P/550.
860 DL=T/S
869 869 FORMAT(*INTEGRATION ALONG THE BLADE GIVES*)
870 870 FORMAT(/,/,/,4X,*T=*,F12.6,8X,*Q=*,F12.6,8X,*HP=*,
871+ F12.6)
875 875 FORMAT(4X,*DL=*,F12.8,7X,*CQ=*,F12.8,7X,*CP=*,
876+ F12.8)
878 878 FORMAT(4X,*PITCHING MOMENT=*,F10.4,5X,*BENDING MOMENT=*,F12.4)
889 PRINT 869
890 PRINT 870,T,Q,HP
891 PRINT 875,DL,CQB,CPB
892 PRINT 878,XM,BM
900 END
```

```
THIS PROGRAM CALCULATES WINDMILL PERFORMANCE USING STRIP THEORY

          TIP SPEED RATIO=  7.96
          WIND SPEED= 26.00
          RPM=145.00
          OMEGA=15.184
          PITCH=  0.
          REYNOLD'S NO.= .113885E+07


N=  1          R= 2.000          I= 22          WK=1.00000

PHI= .8983    ALPHA= .5510    VR=   48.748428    THETA= .2447
PHIO= .6535   ALPHAO= .3062   VRO=   47.296015   VIND=   11.811316

  CL=  1.2601        CD=   .2830        CM=  -.0722

  DT/DR=  20.0569    DQ/DR=  18.5244    DM/DR=  -.7828
  DELTAT=   13.37    DELTAQ/R=  6.17    DELTAM= -1.5657


N=  2          R= 4.000          I=  5          WK=1.00000

PHI= .5606    ALPHA= .2866    VR=   71.715993    THETA= .1579
PHIO= .4028   ALPHAO= .1288   VRO=   70.824045   VIND=   11.275384

  CL=  1.1662        CD=   .0300        CM=  -.0973

  DT/DR=  35.6628    DQ/DR=  56.4877    DM/DR= -1.8649
  DELTAT=   23.78    DELTAQ/R=  9.41    DELTAM= -3.7298


N=  3          R= 6.000          I=  9          WK=1.00000

PHI= .3964    ALPHA= .1983    VR=   98.764743    THETA= .1079
PHIO= .2895   ALPHAO= .0904   VRO=   98.190656   VIND=   10.633761

  CL=   .9451        CD=   .0250        CM=  -.0963

  DT/DR=  52.0479    DQ/DR=  83.7718    DM/DR= -2.9645
  DELTAT=   34.70    DELTAQ/R=  9.31    DELTAM= -5.9291


N=  4          R= 8.000          I=  4          WK=1.00000

PHI= .3042    ALPHA= .1768    VR=  127.319603    THETA= .0874
PHIO= .2168   ALPHAO= .0894   VRO=  126.833821   VIND=   11.110883

  CL=   .9389        CD=   .0250        CM=  -.0964

  DT/DR=  71.6983    DQ/DR= 110.4164    DM/DR= -3.3324
  DELTAT=   47.80    DELTAQ/R=  9.20    DELTAM= -6.6649


N=  5          R=10.000          I=  3          WK=1.00000

PHI= .2460    ALPHA= .1689    VR=  156.558630    THETA= .0743
PHIO= .1717   ALPHAO= .0946   VRO=  156.126506   VIND=   11.623584

  CL=   .9698        CD=   .0250        CM=  -.0961

  DT/DR=  92.1834    DQ/DR= 135.5144    DM/DR= -3.3638
  DELTAT=   61.46    DELTAQ/R=  9.03    DELTAM= -6.7276
```

```
N=  6          R=12.000          I=  2          WK=1.00000

PHI= .2063    ALPHA= .1592    VR=  186.159728    THETA= .0647
PHIO= .1416   ALPHAO= .0945   VRO=  185.770790   VIND=   12.028323

  CL=   .9693        CD=   .0250        CM=  -.0961

  DT/DR= 112.8197    DQ/DR= 157.5676    DM/DR= -3.5438
  DELTAT=   75.21    DELTAQ/R=  8.75    DELTAM= -7.0876

N=  7          R=14.000          I=  4          WK=1.00000

PHI= .1775    ALPHA= .1510    VR=  215.974073    THETA= .0573
PHIO= .1202   ALPHAO= .0937   VRO=  215.619217   VIND=   12.375827

  CL=   .9641        CD=   .0250        CM=  -.0962

  DT/DR= 133.6522    DQ/DR= 176.8554    DM/DR= -3.7229
  DELTAT=   89.10    DELTAQ/R=  8.42    DELTAM= -7.4459

N=  8          R=16.000          I=  4          WK= .99988

PHI= .1557    ALPHA= .1442    VR=  245.924119    THETA= .0515
PHIO= .1042   ALPHAO= .0927   VRO=  245.597799   VIND=   12.665731

  CL=   .9583        CD=   .0250        CM=  -.0962

  DT/DR= 154.5502    DQ/DR= 193.4834    DM/DR= -3.8799
  DELTAT=  103.03    DELTAQ/R=  8.06    DELTAM= -7.7597

N=  9          R=18.000          I=  5          WK= .99125

PHI= .1386    ALPHA= .1360    VR=  275.965687    THETA= .0469
PHIO= .0918   ALPHAO= .0892   VRO=  275.662940   VIND=   12.924522

  CL=   .9377        CD=   .0250        CM=  -.0964

  DT/DR= 174.0961    DQ/DR= 204.3708    DM/DR= -4.0834
  DELTAT=  116.06    DELTAQ/R=  7.57    DELTAM= -8.1669

N= 10          R=20.000          I=  6          WK= .92517

PHI= .1249    ALPHA= .1249    VR=  306.071830    THETA= .0423
PHIO= .0826   ALPHAO= .0826   VRO=  305.798421   VIND=   12.935059

  CL=   .8991        CD=   .0250        CM=  -.0966

  DT/DR= 180.5841    DQ/DR= 198.2831    DM/DR= -3.8918
  DELTAT=  120.39    DELTAQ/R=  6.61    DELTAM= -7.7837

INTEGRATION ALONG THE BLADE GIVES


  T= 1878.794817        Q= 2473.560597        HP=   68.289844
  DL=  1.49509744       CQ=   .05694981       CP=   .45353805
  PITCHING MOMENT=  -59.2027     BENDING MOMENT=   9663.5255
END.
```

APPENDIX II

COMPUTER PROGRAM: EI, GJ OF ARBITRARY SHELL BEAM

The EI program equations are described in Chapter VII. The program is listed on the following pages with a sample input file and corresponding output. The input file is compiled as TAPE 60 in the program, and is listed in this appendix as file NEWBL. The input and output information is fully described in comment lines in the program listing. The input file represents the final geometry and laminates used in the University of Massachusetts Wind Furnace.

```
10 PROGRAM STATNS (INPUT,TAPE1,TAPE2,TAPE60,TAPE62,OUTPUT)
15,  THIS PROGRAM FITS PARABOLIC SEGMENTS THROUGH EACH GROUP OF THREE
16,  POINTS; THE I OF THE SKIN IS CALCULATED BY DIVIDING THE GROUP INTO
17,  DIV STRAIGHT LINE SEGMENTS OF ROUGHLY EQUAL SIZE
20 DIMENSION XC(40),YC(40),R(4),XX(33),YY(33),ST1(10),ST2(10),ST3(10)
30 DIMENSION ST4(10),ST5(10),ST6(10),ST7(10)
40 COMMON X(33),Y(33)
50 INTEGER STA,IST,NPT,I,J,DIV,ID,KC,JC,IC,J1
55,  READ THE NUMBER OF STATIONS, E SKIN, E LONGITUDINAL, NO. OF
56,  DIVISIONS PER OFFSET FOR NUMERICAL INTEGRATION, G SKIN, G LONG
60 READ(60,601) STA,ES,EL,DIV,GS,GL
70 ES=ES*10**6  $  EL=EL*10**6  $  GS=GS*10**6  $  GL=GL*10**6
80 PRINT 602, STA,ES,EL,DIV,GS,GL
85, READ NUMBER OF POINTS
90 READ(60,605) NPT
92,  READ SECTION COORDINATES - X..., Y... - X-AXIS IS CHORD LINE
95 READ(60,610) (X(I),I=1,NPT)
100 READ(60,610) (Y(I),I=1,NPT)
105 DO 111 I=1,NPT
110 XX(I)=X(I)    $    YY(I)=Y(I)
111 111 CONTINUE
115 DO 570 IST=1,STA
117, READ THE SCALE FACTOR FOR SIMILAR SECTIONS, NOSE THICKNESS (THK1),
118, AFT THICKNESS (THK2), AND X COORD OF CHANGE
120 READ(60,622) SCALE,THK1,THK2,XTHK
125 DO 131 I=1,NPT
130 X(I)=SCALE*XX(I)    $   Y(I)=SCALE*YY(I)
131 131 CONTINUE
135 PRINT 615, IST,THK1,THK2,XTHK
140 PRINT 612, (X(I),I=1,NPT)
145 PRINT 612, (Y(I),I=1,NPT)
150 TXSM=0   $   TYSM=0
155 TXSI=0    $   TYSI=0
160 TXYSI=0   $   TAREA=0
165 J1=NPT-2
170 DO 340 J=1,J1,2
172, CALCULATION OF SKIN MOMENT OF INERTIA AND CENTROID FROM CHORD LINE
175 CALL LCOE(COE1,COE2,COE3,J)
178, SELECTION OF DIVISIONS BY DIVIDING A STRAIGHT LINE BETWEEN POINTS
179, INTO EQUAL SEGMENTS
180 DX1=(X(J+1)-X(J))/DIV
185 DX2=(X(J+2)-X(J+1))/DIV
190 I5=DIV+1
195 DO 210 ID=1,I5
200 XC(ID)=X(J)+(ID-1)*DX1
205 XC(ID+DIV)=X(J+1)+(ID-1)*DX2
210 210 CONTINUE
215 I3=2*DIV+1
220 DO 230 ID=1,I3
225 YC(ID)=COE1*XC(ID)**2+COE2*XC(ID)+COE3
230 230 CONTINUE
235 TA=0  $  XSM=0  $  YSM=0  $  XSI=0  $  YSI=0  $  XYSI=0
238,  CORRECT FOR SHELL THICKNESS; OUTER SKIN GEOMETRY IS GIVEN;
239,  XLEV, YLEV ARE COORDINATES OF MIDPOINT OF DAREA
240 DO 305 ID=2,I3
242 XLV=(XC(ID-1)+XC(ID))/2.
244 YLV=(YC(ID-1)+YC(ID))/2.
246 THK=THK1
248 IF(XLV.GT.XTHK) THK=THK2
250 DYC=YC(ID)-YC(ID-1)
252 DXC=XC(ID)-XC(ID-1)
254 HYP=SQRT(DYC**2+DXC**2)
256 DX=THK*DYC/(2.*HYP)
258 DY=THK*DXC/(2.*HYP)
260 XLEV=XLV+DX
262 YLEV=YLV-DY
265 DAREA=THK*HYP
```

```
269, TOTAL AREA
270 TA=TA+DAREA
274, FIRST MOMENT ABOUT X-AXIS
275 XSM=XSM+YLEV*DAREA
279, FIRST MOMENT ABOUT Y-AXIS
280 YSM=YSM+XLEV*DAREA
284, X MOMENT OF INERTIA
285 XSI=XSI+DAREA*(YLEV**2)
289, Y MOMENT OF INERTIA
290 YSI=YSI+DAREA*(XLEV**2)
299, PRODUCT OF INERTIA
300 XYSI=XYSI+DAREA*XLEV*YLEV
305 305 CONTINUE
310 TAREA=TAREA+TA
315 TXSM=TXSM+XSM
320 TYSM=TYSM+YSM
325 TXSI=TXSI+XSI
330 TYSI=TYSI+YSI
335 TXYSI=TXYSI+XYSI
340 340 CONTINUE
345 SXB=TYSM/TAREA
350 SYB=TXSM/TAREA
355 EXSI=TXSI*ES
360 EYSI=TYSI*ES
365, READ SPAR INFORMATION - CROSS-SECTIONAL AREA(AL),IX, IY, IXY, ALL
366, ABOUT SPAR CENTROID, XL, YL
370 READ(60,620) AL,XLI,YLI,XYLI,XL,YL
375 PRINT 625, AL,XLI,YLI,XYLI,XL,YL
380 XLM=AL*YL
385 YLM=AL*XL
390 EXLI=EL*XLI
395 EYLI=EL*YLI
398, CALCULATION OF CENTROID AND EI FOR TOTAL COMPOSITE STRUCTURE
400 EA=ES*TAREA+EL*AL
410 XB=(ES*TYSM+EL*YLM)/EA
415 YB=(ES*TXSM+EL*XLM)/EA
420, FIND EIX, EIY, EIXY FOR TOTAL STRUCTURE BY USING THE PARALLEL AXIS
421, THEOREM IN SEQUENCE
425 EXI=EXSI+EXLI-ES*TAREA*(SYB**2-(SYB-YB)**2)
426+ +EL*AL*((YL-YB)**2)
430 EYI=EYSI+EYLI-ES*TAREA*(SXB**2-(SXB-XB)**2)
431+ +EL*AL*((XL-XB)**2)
435 EXYI=XYSI*ES+XYLI*EL-ES*TAREA*(SXB*SYB-(SXB-XB)*(SYB-YB))
436+ +AL*EL*(XL-XB)*(YL-YB)
438. FIND PRINCIPAL AXES OF INERTIA BY USING MOHR'S CIRCLE
440 SUM=(EXI+EYI)/2.
445 DIF=(EYI-EXI)/2.
450 PP=ATAN(EXYI/DIF)
455 PHI=PP/2.
457 RAD=DIF/COS(PP)
459, PRINCIPAL EIX AND EIY
460 PXI=SUM-RAD
465 PYI=SUM+RAD
469, PRINCIPAL RADIUS OF GYRATION
470 PRX=SQRT(PXI/EA)
475 PRY=SQRT(PYI/EA)
480 PRINT 630, XB,YB,TAREA,PHI,PXI,PYI,PRX,PRY,EA
```

```
490 ST1(IST)=PXI
495 ST2(IST)=PYI
500 ST3(IST)=EA
505 ST4(IST)=-PHI
510, POLAR MOMENT OF INERTIA = J = IX + IY
511, IF GSKIN AND ESKIN ARE DIFFERENT THE TORSIONAL CENTROID WILL DIFFER
512, FROM THE BENDING CENTROID
520 GA=GS*TAREA+GL*AL
525 XBT=(GS*TYSM+GL*YLM)/GA
530 YBT=(GS*TXSM+GL*XLM)/GA
540 GJ=GS*TXSI+GL*XLI-GS*TAREA*(SYB*SYB-(SYB-YBT)**2)
541+ +GL*AL*(YL-YBT)*(YL-YBT)+GS*TYSI+GL*YLI
542+ -GS*TAREA*(SXB*SXB-(SXB-XBT)**2)+GL*AL*(XL-YBT)*(XL-XBT)
550 PRINT 640, XBT,YBT,GJ
555 ST5(IST)=GJ
560 ST6(IST)=-XBT
565 ST7(IST)=-YBT
570 570 CONTINUE
601 601 FORMAT(5X,I2,2F6.2,I2,2F6.2)
602 602 FORMAT(10H NO STA = ,I2,9X,9HE SKIN = ,E11.2,9X,10HE LONG. = ,
603+ E11.2,5X,10HNO. DIV = ,I2,/,5H GS =,E12.3,5X,5H GL =,E12.3,/,/)
605 605 FORMAT(5X,I2)
610 610 FORMAT(5X,9F6.4,/,5X,8F6.4,/,5X,8F6.4,/,5X,8F6.4)
612 612 FORMAT(5X,9F8.4,/,3(5X,8F8.4,/,))
615 615 FORMAT( 20H OFFSETS FOR STATION,I2,5X,8H THK1 = ,F6.4,5X,
616+ 8H THK2 = ,F6.4,5X,8H XTHK = ,F7.3)
620 620 FORMAT(5X,6F6.3)
622 622 FORMAT(5X,4F6.3)
625 625 FORMAT(31H SPAR DATA - AL,IX,IY,IXY,XL,YL,/,6(3X,F8.3),/)
630 630 FORMAT(40H POSITION OF CENTROID FROM BASE LINE X =,F8.2,
631+ 5H  Y =,F8.2,/,10H SKIN AREA,F10.4,/,24H ANGLE OF PRINCIPAL AXES,
632+ F6.2,7H EIX = ,E10.4,8H  EIY = ,E10.4,7H  RX = ,F6.2,7H  RY = ,
633+ F6.2,/,6H EA = ,E10.4,/,/)
640 640 FORMAT(36H POSITION OF TORSIONAL CENTROID  X =,F8.2,
641+ 5H  Y =,F8.2,5X,5H GJ =,E12.5,/,/,/)
645 645 FORMAT(5E10.3,/,5E10.3)
646 646 FORMAT(10F8.5)
649, PREPARE A FILE OF DATA FOR THE STRESS/DEFLECTION PROGRAM
650 WRITE(62,645) ST3
655 WRITE(62,645) ST1
660 WRITE(62,645) ST2
665 WRITE(62,645) ST5
670 WRITE(62,646) ST6
675 WRITE(62,646) ST7
680 WRITE(62,646) ST4
685 REWIND 1   $   REWIND 2  $  REWIND 60  $  REWIND 62
690 END
700 SUBROUTINE LCOE(CO1,CO2,CO3,J)
702, THIS ROUTINE FITS A 2ND ORDER CURVE THROUGH EACH SET OF THREE
703, POINTS, X THE ABSCISSA AND Y THE ORDINATE, VIZ:
704, Y =  CO1 * X**2 + CO2 * X + CO3   (THE PARABOLIC AXIS IS VERTICAL)
705 COMMON X(33),Y(33)
710 C1N=X(J)*(Y(J+2)-Y(J+1))+X(J+1)*(Y(J)-Y(J+2))+X(J+2)*
711+ (Y(J+1)-Y(J))
715 C2N=(X(J)**2)*(Y(J+1)-Y(J+2))+(X(J+1)**2)*(Y(J+2)-Y(J))
716+ +(X(J+2)**2)*(Y(J)-Y(J+1))
720 C3N=(X(J)**2)*(X(J+1)*Y(J+2)-X(J+2)*Y(J+1))+(X(J+1)**2)*
721+ (X(J+2)*Y(J)-X(J)*Y(J+2))+(X(J+2)**2)*(X(J)*Y(J+1)-X(J+1)
722+ *Y(J))
725 DET=X(J)*((X(J+2)**2)-(X(J+1)**2))+X(J+1)*((X(J)**2)-(X(J+2)
726+ **2))+X(J+2)*((X(J+1)**2)-(X(J)**2))
730 CO1=C1N/DET
735 CO2=C2N/DET
740 CO3=C3N/DET
787 RETURN
790 END
```

```
FILE   NEWBL

10    10  2.20  4.40 8  0.50  0.30
20    33
30     .0000 .0125 .0250 .0500 .0750 .1000 .1500 .2000 .2500
32     .3500 .5000 .6000 .7000 .8000 .9000 .95001.0000
34     .9500 .9000 .8000 .7000 .6000 .5000 .3500 .2500
36     .2000 .1500 .1000 .0750 .0500 .0250 .0125 .0000
40     .0000 .0307 .0417 .0574 .0691 .0784 .0927 .1025 .1092
42     .1135 .1053 .0930 .0763 .0555 .0308 .0167 .0000
44    -.0179-.0248-.0327-.0371-.0398-.0418-.0414-.0398
46    -.0340-.0272-.0214-.0155-.0103-.0057-.0036 .0000
70     2.000  0.08  0.08  0.86
75     0.000 0.000 0.000 0.000 0.000 0.000
80     5.376  0.08  0.08  2.31
85     0.000 0.000 0.000 0.000 0.000 0.000
90     6.600  0.08  0.08  2.84
95     0.000 0.000 0.000 0.000 0.000 0.000
100    7.572  0.08  0.08  3.26
105    0.120 0.035 0.019 0.000 3.670 0.290
110    8.736  0.11  0.08  3.76
115    0.121 0.056 0.025 0.000 4.230 0.340
120   10.200  0.11  0.08  4.39
125    0.162 0.102 0.035 0.000 4.650 0.400
130   12.240  0.11  0.08  5.26
135    0.200 0.173 0.053 0.000 5.330 0.480
140   15.072  0.11  0.08  6.48
145    0.240 0.272 0.084 0.000 6.360 0.590
150   17.460  0.11  0.08  7.51
155    0.251 0.288 0.116 0.000 7.430 0.690
160   16.236  0.11  0.08  6.98
165    0.246 0.281 0.100 0.000 6.880 0.640
```

```
  FILE   BEEMEIS

NO STA = 10          E SKIN =      .22E+07          E LONG. =      .44E+07      NO. DIV =  8
GS =     .500E+06      GL =     .300E+06


OFFSETS FOR STATION 1       THK1 =  .0800       THK2 =  .0800       XTHK =     .860
      0.        .0250   .0500   .1000   .1500   .2000   .3000   .4000   .5000
       .7000  1.0000  1.2000  1.4000  1.6000  1.8000  1.9000  2.0000
      1.9000  1.8000  1.6000  1.4000  1.2000  1.0000   .7000   .5000
       .4000   .3000   .2000   .1500   .1000   .0500   .0250  0.

      0.        .0614   .0834   .1148   .1382   .1568   .1854   .2050   .2184
       .2270   .2106   .1860   .1526   .1110   .0616   .0334  0.
     -.0358  -.0496  -.0654  -.0742  -.0796  -.0836  -.0828  -.0796
     -.0620  -.0544  -.0428  -.0310  -.0206  -.0114  -.0072  0.

SPAR DATA - AL,IX,IY,IXY,XL,YL
     0.         0.         0.         0.         0.         0.

POSITION OF CENTROID FROM BASE LINE X =      .99  Y =      .05
SKIN AREA      .3293
ANGLE OF PRINCIPAL AXES  -.14 EIX =  .5394E+03  EIY =  .2490E+06  RX =     .03  RY =     .59
EA =  .7244E+06


POSITION OF TORSIONAL CENTROID  X =      .99  Y =      .05      GJ =  .56724E+05


OFFSETS FOR STATION 2       THK1 =  .0800       THK2 =  .0800       XTHK =   2.310
      0.        .0672   .1344   .2688   .4032   .5376   .8064  1.0752  1.3440
      1.8816  2.6880  3.2256  3.7632  4.3008  4.8384  5.1072  5.3760
      5.1072  4.8384  4.3008  3.7632  3.2256  2.6880  1.8816  1.3440
      1.0752   .8064   .5376   .4032   .2688   .1344   .0672  0.

      0.        .1650   .2242   .3086   .3715   .4215   .4984   .5510   .5871
       .6102   .5661   .5000   .4102   .2984   .1656   .0898  0.
     -.0962  -.1333  -.1758  -.1994  -.2140  -.2247  -.2226  -.2140
     -.1828  -.1462  -.1150  -.0833  -.0554  -.0306  -.0194  0.

SPAR DATA - AL,IX,IY,IXY,XL,YL
     0.         0.         0.         0.         0.         0.

POSITION OF CENTROID FROM BASE LINE X =     2.65  Y =      .13
SKIN AREA      .8851
ANGLE OF PRINCIPAL AXES  -.14 EIX =  .6837E+05  EIY =  .4912E+07  RX =     .19  RY =    1.59
EA =  .1947E+07


POSITION OF TORSIONAL CENTROID  X =     2.65  Y =      .13      GJ =  .11319E+07


OFFSETS FOR STATION 3       THK1 =  .0800       THK2 =  .0800       XTHK =   2.840
      0.        .0825   .1650   .3300   .4950   .6600   .9900  1.3200  1.6500
      2.3100  3.3000  3.9600  4.6200  5.2800  5.9400  6.2700  6.6000
      6.2700  5.9400  5.2800  4.6200  3.9600  3.3000  2.3100  1.6500
      1.3200   .9900   .6600   .4950   .3300   .1650   .0825  0.

      0.        .2026   .2752   .3788   .4561   .5174   .6118   .6765   .7207
       .7491   .6950   .6138   .5036   .3663   .2033   .1102  0.
     -.1181  -.1637  -.2158  -.2449  -.2627  -.2759  -.2732  -.2627
     -.2244  -.1795  -.1412  -.1023  -.0680  -.0376  -.0238  0.

SPAR DATA - AL,IX,IY,IXY,XL,YL
     0.         0.         0.         0.         0.         0.

POSITION OF CENTROID FROM BASE LINE X =     3.26  Y =      .16
SKIN AREA     1.0866
ANGLE OF PRINCIPAL AXES  -.14 EIX =  .1402E+06  EIY =  .9104E+07  RX =     .24  RY =    1.95
EA =  .2390E+07


POSITION OF TORSIONAL CENTROID  X =     3.26  Y =      .16      GJ =  .21009E+07
```

```
OFFSETS FOR STATION 4       THK1 =  .0800       THK2 =  .0800       XTHK =   3.260
      0.        .0946   .1893   .3786   .5679   .7572  1.1358  1.5144  1.8930
      2.6502  3.7860  4.5432  5.3004  6.0576  6.8148  7.1934  7.5720
      7.1934  6.8148  6.0576  5.3004  4.5432  3.7860  2.6502  1.8930
      1.5144  1.1358   .7572   .5679   .3786   .1893   .0946  0.

      0.        .2325   .3158   .4346   .5232   .5936   .7019   .7761   .8269
       .8594   .7973   .7042   .5777   .4202   .2332   .1265  0.
      -.1355  -.1878  -.2476  -.2909  -.3014  -.3165  -.3135  -.3014
      -.2574  -.2060  -.1620  -.1174  -.0780  -.0432  -.0273  0.

SPAR DATA - AL,IX,IY,IXY,XL,YL
      .120       .035       .019       0.         3.670       .290

POSITION OF CENTROID FROM BASE LINE X =    3.73  Y =     .20
SKIN AREA    1.2466
ANGLE OF PRINCIPAL AXES  -.14 EIX =  .3807E+06  EIY =  .1385E+08  RX =    .34  RY =   2.06
EA =  .3271E+07

POSITION OF TORSIONAL CENTROID  X =    3.73  Y =     .18      GJ =  .31950E+07


OFFSETS FOR STATION 5       THK1 =  .1100       THK2 =  .0800       XTHK =   3.760
      0.        .1092   .2184   .4368   .6552   .8736  1.3104  1.7472  2.1840
      3.0576  4.3680  5.2416  6.1152  6.9888  7.8624  8.2992  8.7360
      8.2992  7.8624  6.9888  6.1152  5.2416  4.3680  3.0576  2.1840
      1.7472  1.3104   .8736   .6552   .4368   .2184   .1092  0.

      0.        .2682   .3643   .5014   .6037   .6849   .8098   .8954   .9540
       .9915   .9199   .8124   .6666   .4848   .2691   .1459  0.
      -.1564  -.2167  -.2857  -.3241  -.3477  -.3652  -.3617  -.3477
      -.2970  -.2376  -.1870  -.1354  -.0900  -.0498  -.0314  0.

SPAR DATA - AL,IX,IY,IXY,XL,YL
      .121       .056       .025       0.         4.230       .340

POSITION OF CENTROID FROM BASE LINE X =    3.99  Y =     .23
SKIN AREA    1.6718
ANGLE OF PRINCIPAL AXES  -.13 EIX =  .7012E+06  EIY =  .2471E+08  RX =    .41  RY =   2.42
EA =  .4210E+07

POSITION OF TORSIONAL CENTROID  X =    3.97  Y =     .22      GJ =  .57122E+07


OFFSETS FOR STATION 6       THK1 =  .1100       THK2 =  .0800       XTHK =   4.390
      0.        .1275   .2550   .5100   .7650  1.0200  1.5300  2.0400  2.5500
      3.5700  5.1000  6.1200  7.1400  8.1600  9.1800  9.6900 10.2000
      9.6900  9.1800  8.1600  7.1400  6.1200  5.1000  3.5700  2.5500
      2.0400  1.5300  1.0200   .7650   .5100   .2550   .1275  0.

      0.        .3131   .4253   .5855   .7048   .7997   .9455  1.0455  1.1138
      1.1577  1.0741   .9486   .7783   .5661   .3142   .1703  0.
      -.1826  -.2530  -.3335  -.3784  -.4060  -.4264  -.4223  -.4060
      -.3468  -.2774  -.2183  -.1581  -.1051  -.0581  -.0367  0.

SPAR DATA - AL,IX,IY,IXY,XL,YL
      .162       .102       .035       0.         4.650       .400

POSITION OF CENTROID FROM BASE LINE X =    4.63  Y =     .27
SKIN AREA    1.9520
ANGLE OF PRINCIPAL AXES  -.13 EIX =  .1202E+07  EIY =  .3930E+08  RX =    .49  RY =   2.80
EA =  .5007E+07

POSITION OF TORSIONAL CENTROID  X =    4.63  Y =     .26      GJ =  .91078E+07
```

```
OFFSETS FOR STATION 7       THK1 =  .1100       THK2 =  .0800       XTHK =   5.260
      0.        .1530   .3060   .6120   .9180  1.2240  1.8360  2.4480  3.0600
      4.2840  6.1200  7.3440  8.5680  9.7920 11.0160 11.6280 12.2400
     11.6280 11.0160  9.7920  8.5680  7.3440  6.1200  4.2840  3.0600
      2.4480  1.8360  1.2240   .9180   .6120   .3060   .1530  0.

      0.        .3758   .5104   .7026   .8458   .9596  1.1346  1.2546  1.3366
      1.3892  1.2889  1.1383   .9339   .6793   .3770   .2044  0.
      -.2191  -.3036  -.4002  -.4541  -.4872  -.5116  -.5067  -.4872
      -.4162  -.3329  -.2619  -.1897  -.1261  -.0698  -.0441  0.

SPAR DATA - AL,IX,IY,IXY,XL,YL
      .200       .173       .053       0.         5.330       .480

POSITION OF CENTROID FROM BASE LINE X =    5.52  Y =     .33
SKIN AREA    2.3424
ANGLE OF PRINCIPAL AXES  -.13 EIX =  .2116E+07  EIY =  .6799E+08  RX =    .59  RY =   3.36
EA =  .6033E+07

POSITION OF TORSIONAL CENTROID  X =    5.54  Y =     .31      GJ =  .15767E+08


OFFSETS FOR STATION 8       THK1 =  .1100       THK2 =  .0800       XTHK =   6.480
      0.        .1884   .3768   .7536  1.1304  1.5072  2.2608  3.0144  3.7680
      5.2752  7.5360  9.0432 10.5504 12.0576 13.5648 14.3184 15.0720
     14.3184 13.5648 12.0576 10.5504  9.0432  7.5360  5.2752  3.7680
      3.0144  2.2608  1.5072  1.1304   .7536   .3768   .1884  0.

      0.        .4627   .6285   .8651  1.0415  1.1816  1.3972  1.5449  1.6459
      1.7107  1.5871  1.4017  1.1500   .8365   .4642   .2517  0.
      -.2698  -.3738  -.4929  -.5592  -.5999  -.6300  -.6240  -.5999
      -.5124  -.4100  -.3225  -.2336  -.1552  -.0859  -.0543  0.

SPAR DATA - AL,IX,IY,IXY,XL,YL
      .240       .272       .084       0.         6.360       .590

POSITION OF CENTROID FROM BASE LINE X =    6.76  Y =     .40
SKIN AREA    2.8844
ANGLE OF PRINCIPAL AXES  -.13 EIX =  .3830E+07  EIY =  .1271E+09  RX =    .72  RY =   4.14
EA =  .7402E+07

POSITION OF TORSIONAL CENTROID  X =    6.81  Y =     .38      GJ =  .29481E+08


OFFSETS FOR STATION 9       THK1 =  .1100       THK2 =  .0800       XTHK =   7.510
      0.        .2183   .4365   .8730  1.3095  1.7460  2.6190  3.4920  4.3650
      6.1110  8.7300 10.4760 12.2220 13.9680 15.7140 16.5870 17.4600
     16.5870 15.7140 13.9680 12.2220 10.4760  8.7300  6.1110  4.3650
      3.4920  2.6190  1.7460  1.3095   .8730   .4365   .2183  0.

      0.        .5360   .7281  1.0022  1.2065  1.3689  1.6185  1.7397  1.9066
      1.9817  1.8385  1.6238  1.3322   .9690   .5378   .2916  0.
      -.3125  -.4330  -.5709  -.6478  -.6949  -.7298  -.7228  -.6949
      -.5936  -.4749  -.3736  -.2706  -.1798  -.0995  -.0629  0.

SPAR DATA - AL,IX,IY,IXY,XL,YL
      .251       .288       .116       0.         7.430       .690

POSITION OF CENTROID FROM BASE LINE X =    7.85  Y =     .46
SKIN AREA    3.3414
ANGLE OF PRINCIPAL AXES  -.13 EIX =  .5475E+07  EIY =  .1976E+09  RX =    .80  RY =   4.83
EA =  .8455E+07

POSITION OF TORSIONAL CENTROID  X =    7.89  Y =     .44      GJ =  .45827E+08
```

```
OFFSETS FOR STATION10       THK1 =  .1100       THK2 =  .0800       XTHK =   6.980
      0.        .2029    .4059    .8118   1.2177   1.6236   2.4354   3.2472   4.0590
      5.6826   8.1180   9.7416  11.3652  12.9888  14.6124  15.4242  16.2360
     15.4242  14.6124  12.9888  11.3652   9.7416   8.1180   5.6826   4.0590
      3.2472   2.4354   1.6236   1.2177    .8118    .4059    .2029   0.

      0.        .4984    .6770    .9319   1.1219   1.2729   1.5051   1.6642   1.7730
      1.8428   1.7097   1.5099   1.2388    .9011    .5001    .2711   0.
      -.2906   -.4027   -.5309   -.6024   -.6462   -.6787   -.6722   -.6462
      -.5520   -.4416   -.3475   -.2517   -.1672   -.0925   -.0584   0.

SPAR DATA - AL,IX,IY,IXY,XL,YL
      .246        .281        .100        0.          6.880        .640

POSITION OF CENTROID FROM BASE LINE X =     7.29   Y =      .43
SKIN AREA    3.1072
ANGLE OF PRINCIPAL AXES   -.13 EIX =  .4577E+07  EIY =  .1589E+09  RX =     .76  RY =    4.48
EA =  .7918E+07


POSITION OF TORSIONAL CENTROID  X =     7.34   Y =      .41       GJ =  .36850E+08
```

APPENDIX III

COMPUTER PROGRAM: STRESS AND DEFLECTION OF ARBITRARY SHELL BEAM

The stress and deflection equations are described in Chapter VII. The program is listed on the following pages with sample input and output. The input file is compiled as DFTEST3, and represents a 20-foot long rectangular prismatic shell beam. The beam has section dimensions of four and twelve inches, a wall thickness of 0.15 inch, and is made of steel ($E = 30 \times 10^6$). The cross section is inclined to the Y-Z axes by an angle of 30°. The beam is loaded uniformly with 20 lb./in. along the soft principal axis (flapping) and 10 lb./in. along the stiff principle axis (lead-lag). The input and output information is described in the program listing.

```
10 PROGRAM STRESS (INPUT, TAPE1,TAPE2,TAPE60,TAPE61,OUTPUT)
15,  THIS PROGRAM CALCULATES THE STRESS OF A CANTILEVER BEAM FREE AT
16,  STATION 1 SUBJECTED TO A DISTRIBUTED LOAD RESOLVED INTO X, Y, AND
17,  Z COMPONENTS;  X LIES ALONG THE AXIS OF THE BEAM.
18,  FOR A ROTOR, ROTATION IS ABOUT THE NEGATIVE Z-AXIS;  X-AXIS IS IN
19,  THE LAGGING DIRECTION, AND Z-AXIS IS IN THE FLAPPING DIRECTION
20,  THE FREE STREAM WIND IS IN THE POSITIVE Z-DIRECTION
25 REAL CY,LX(10),LY(10),LZ(10),MY(10),MZ(10),MPY(10),MPZ(10),NANG(10)
27 REAL MYE(10),MZE(10),MYP(10),MZP(10)
30 DIMENSION STX(10),EIYP(10),EIZP(10),FX(10),PANG(10),VY(10),VZ(10)
31+ ,SCALE(10),EA(10),Z(6),HEAD(8),Y(6),AANG(10),SXTN(10),SX(10),
32+ TITLE(30),DEFY(10),DEFZ(10),YCB(10),ZCB(10),GJ(10)
35 DIMENSION YCT(10),ZCT(10),PM(10),TANG(10)
40 DATA (TITLE=7HSTA POS,6HX LOAD,6HY LOAD,6HZ LOAD,6HT LOAD,2HEA,
41+ 4HEIYP,4HEIZP,2HGJ,5HSCALE,1HY,1HZ,7HY BCENT,7HZ BCENT,7HTORSION,
42+ 8HTORS DEF,7HTENSION,6HV INPL,7HBM INPL,6HV FLAP,7HBM FLAP,
43+ 6HPR A A,6HSX TEN,5HN A A,7HSX BEND,8HSX TOTAL,6HM/EIYP,6HM/EIZP,
44+ 5HY DEF,5HZ DEF)
50 READ(60,940) NCAL
60 DO 930 IS=1,NCAL
65 READ(60,940) NSTA
70 READ(60,945) ES
75,  LIST STATION POSITION FROM FREE END AND LOAD PER UNIT LENGTH
76,  X-LOAD IS TOWARDS TIP;  Y-LOAD POSITIVE IN LAG DIRECTION;
77,  Z-LOAD POSITIVE IN FLAP DIRECTION; PITCHING MOMENT IS POSITIVE
78,  NOSEDOWN (INCH-LB)
80 READ(60,962) (STX(I),I=1,NSTA)
85 READ(60,962) (LX(I),I=1,NSTA)
90 READ(60,962) (LY(I),I=1,NSTA)
95 READ(60,962) (LZ(I),I=1,NSTA)
97 READ(60,962) (PM(I),I=1,NSTA)
100,  LIST EA, PRINCIPAL EI, GJ, ANGLE SECTION AXES MAKE WITH REFERENCE
101,  PLANE
110 READ(60,950) (EA(I),I=1,NSTA)
115 READ(60,950) (EIYP(I),I=1,NSTA)
120 READ(60,950) (EIZP(I),I=1,NSTA)
125 READ(60,950) (GJ(I),I=1,NSTA)
128,  TWIST ANGLE IS IN DEGREES. POSITIVE COUNTERCLOCKWISE
130 READ(60,965) (TANG(I),I=1,NSTA)
140,  LIST COORDINATES OF POINTS TO BE CALCULATED AND THE COORDINATES OF
141,  THE BENDING CENTROID RELATIVE TO THE AXES OF THE SECTION. AND THE
142,  ANGLE OF ROTATION FROM SECTION AXES TO PRINCIPAL AXES IN RADIANS
150 READ(60,940) NPT
155 READ(60,963)(Y(I),I=1,NPT)
160 READ(60,963)(Z(I),I=1,NPT)
165 READ(60,962)(YCB(I),I=1,NSTA)
170 READ(60,962)(ZCB(I),I=1,NSTA)
175 READ(60,965)(PANG(I),I=1,NSTA)
180 READ(60,962)(SCALE(I),I=1,NSTA)
190,  LIST COORDINATES OF THE TORSIONAL CENTROID
195 READ(60,962)(YCT(I),I=1,NSTA)
200 READ(60,962)(ZCT(I),I=1,NSTA)
205,  HEADING FOR THIS RUN
208 READ(60,968) HEAD
210 PRINT 980, HEAD
220 PRINT 955, (I,I=1,NSTA)
225 PRINT 960, TITLE(1),STX
230 PRINT 960, TITLE(2),LX
235 PRINT 960, TITLE(3),LY
240 PRINT 960, TITLE(4),LZ
245 PRINT 966, TITLE(6),EA
250 PRINT 966, TITLE(7),EIYP
255 PRINT 966, TITLE(8),EIZP
260 PRINT 966, TITLE(9),GJ
265 PRINT 960, TITLE(10),SCALE
270 PRINT 975, (I,I=1,NPT)
275 PRINT 961, TITLE(11),Y
```

```
280 PRINT 961, TITLE(12),Z
285 PRINT 960, TITLE(13),YCB
290 PRINT 960, TITLE(14),ZCB
295 PRINT 955, (I,I=1,NSTA)
300,  CALCULATE TORSION; SECTION TORQUE = L*(0.25 CHORD - Y TORSIONAL
301,  CENTROID) + PITCHING MOMENT;  POSITIVE NOSEDOWN
305,  ENTER CHORD LENGTH USED TO CALCULATE SCALE FACTOR
306,  REMEMBER:  AIRFOIL NOSE IS ORIGIN OF SECTION AXIS SYSTEM FOR
307,  TORSION CALCULATION
310 CHORD=12.0
320 DO 340 I=1,NSTA
322 TANG(I)=TANG(I)/57.29577951
325 AANG(I)=PANG(I)+TANG(I)
330 VY(I)=(-LY(I)*SIN(AANG(I))+LZ(I)*COS(AANG(I)))*(SCALE(I)*0.25
331+ *CHORD)
335 VY(I)=VY(I)+PM(I)
340 340 CONTINUE
360 CALL INTEG(STX,VY,MY,1,NSTA)
370 PRINT 966, TITLE(15),MY
375,  TWIST = TORSION*TORK/GJ;  TORK IS A VALUE FROM HANDBOOKS
380 TORK=2.0
390 DO 405 I=1,NSTA
394,  REVERSE THE INDEX TO PERFORM INTEGRATION STARTING AT ROOT END
395 IR=NSTA+1-I
400 VZ(I)=MY(IR)*TORK/GJ(IR)
405 405 CONTINUE
420 CALL INTEG(STX,VZ,MZ,1,NSTA)
422 MZ(10)=MZ(9)
425 DO 445 I=1,NSTA
430 IR=NSTA+1-I
438,  RENUMBER THE INDEX
440 VZ(I)=MZ(IR)
445 445 CONTINUE
450 PRINT 966, TITLE(16),VZ
455,  CALCULATE BEAM SHEARS AND BENDING MOMENTS IN REFERENCE AXES
456,  BLADE SHEARS AND MOMENTS ARE SUMMED FROM THE FREE END
457,  INPLANE SHEAR (VY) AND MOMENT (MZ) POSITIVE IN LAGGING DIRECTION;
458,  FLAPPING SHEAR (VZ) AND MOMENT (MY) POSITIVE IN FLAPPING DIRECTION
460 CALL INTEG(STX,LX,FX,1,NSTA)
470 CALL INTEG(STX,LY,VY,1,NSTA)
480 CALL INTEG(STX,VY,MZ,1,NSTA)
482 PRINT 966, TITLE(17),FX
484 PRINT 966, TITLE(18),VY
485 PRINT 966, TITLE(19),MZ
490 CALL INTEG(STX,LZ,VZ,1,NSTA)
495 CALL INTEG(STX,VZ,MY,1,NSTA)
498 PRINT 966, TITLE(20),VZ
500 PRINT 966, TITLE(21),MY
505,  PRINCIPAL AXIS ANGLE (AANG) = CHORD TO REFERENCE ANGLE (TANG)
506,  + CHORD TO PRINCIPAL AXIS ANGLE (PANG)
507,  CALCULATE THE STRESS DUE TO AXIAL TENSION
508,  RESOLVE BENDING MOMENT TO PRINCIPAL AXES
509,  FIND NEUTRAL AXIS RELATIVE TO DISC
515 DO 570 I=1,NSTA
530 SXTN(I)=FX(I)*ES/EA(I)
532,  NOTE:  ROTATION OF AXES FROM SECTION COORDS TO PRINC AXES COORDS
533,  IS THROUGH POS ANGLE (COUNTERCLKWISE); THEREFORE XFORMATION MATRIX
534,  IS COS SIN, -SIN COS; REMEMBER MOMENTS ARE IN OPPOSITE SENSE Z=Y
535 MPY(I)=MY(I)*COS(AANG(I))-MZ(I)*SIN(AANG(I))
540 MPZ(I)=MZ(I)*COS(AANG(I))+MY(I)*SIN(AANG(I))
545 IF(MPZ(I)*EIZP(I).EQ.0.) GO TO 560
550 NANG(I)=ATAN(-MPY(I)*EIYP(I)/(MPZ(I)*EIZP(I)))+AANG(I)
555 GO TO 570
560 560 CONTINUE
565 NANG(I)=90.0
570 570 CONTINUE
```

```
580 PRINT 960, TITLE(22),AANG
585 PRINT 960, TITLE(23),SXTN
590 PRINT 960, TITLE(24),NANG
600,  CALCULATE STRESSES DUE TO BENDING
601,  STRESS IS THE SUM OF BENDING IN PLANES OF PRINCIPAL AXES
610 DO 705 K=1,NPT
620 DO 660 J=1,NSTA
630,  TRANSLATE Y,Z TO COORDINATES THROUGH CENTROID
635 YK=Y(K)*SCALE(J)-YCB(J)
640 ZK=Z(K)*SCALE(J)-ZCB(J)
641,  C'S ARE DISTANCES TO STRESSED FIBER FROM PRINCIPAL AXES
645 CY=YK*COS(PANG(J))+ZK*SIN(PANG(J))
650 CZ=ZK*COS(PANG(J))-YK*SIN(PANG(J))
651,  NEGATIVE SIGN DENOTES FIBER IN COMPRESSION
652,  THE FLEXURE FORMULA IS: BEND STRESS = M * C / I
653,  POSITIVE ZP MOMENT IS IN LAGGING DIRECTION (APPROX), AND GIVES
654,  TRAILING EDGE COMPRESSION;  POSITIVE YP MOMENT IS IN FLAPPING
655,  DIRECTION (APPROX), AND GIVES UPPER SURFACE COMPRESSION
659 SX(J)=-MPY(J)*CZ*ES/EIYP(J)-MPZ(J)*CY*ES/EIZP(J)
660 660 CONTINUE
670 PRINT 964, TITLE(25),K,SX
680 DO 690 J=1,NSTA
685 SX(J)=SX(J)+SXTN(J)
690 690 CONTINUE
700 PRINT 964, TITLE(26),K,SX
705 705 CONTINUE
710,  BENDING DEFLECTION
711,  DEFINE CURVE M/EI IN REVERSE ORDER TO INTEGRATE FROM FIXED END
715 DO 736 I=1,NSTA
720 IR=NSTA+1-I
725 LX(IR)=STX(NSTA)-STX(I)
728 MYP(I)=MPY(I)/EIYP(I)
729 MZP(I)=MPZ(I)/EIZP(I)
730 MY(IR)=MPY(I)*COS(-AANG(I))/EIYP(I)-MPZ(I)*SIN(-AANG(I))/EIZP(I)
735 MZ(IR)=MPZ(I)*COS(-AANG(I))/EIZP(I)+MPY(I)*SIN(-AANG(I))/EIYP(I)
736 736 CONTINUE
738,  REVERSE THE ORDER
740 DO 748 I=1,NSTA
742 IR=NSTA+1-I
744 MYE(I)=MY(IR)
746 MZE(I)=MZ(IR)
748 748 CONTINUE
750 PRINT 964, TITLE(27),MYP
751 PRINT 964, TITLE(28),MZP
755,  FIND DEFLECTION BY INTEGRATION:  D2Y/DX2 = M/EI
756,  WHERE LY = DY/DX AND LZ = DZ/DX
760 LY(1)=0.0  $  LZ(1)=0.0
765 DEFY(1)=0.0  $  DEFZ(1)=0.0
770 I6=NSTA-1
775 DO 885 JJ=1,I6,2
780 J=JJ
785 IF(J.EQ.I6) J=J-1
790 CALL LCOE(C1,C2,C3,J,LX,MZ)
795 CALL LCOE(D1,D2,D3,J,LX,MY)
800 IF(JJ.EQ.I6) J=J+1
805 C4=LY(J)-C1*LX(J)**3/3-C2*LX(J)**2/2-C3*LX(J)
810 D4=LZ(J)-D1*LX(J)**3/3-D2*LX(J)**2/2-D3*LX(J)
815 C5=DEFY(J)-C1*LX(J)**4/12-C2*LX(J)**3/6-C3*LX(J)**2/2-C4*LX(J)
820 D5=DEFZ(J)-D1*LX(J)**4/12-D2*LX(J)**3/6-D3*LX(J)**2/2-D4*LX(J)
825 K=J+1
830 LY(K)=C1*LX(K)**3/3+C2*LX(K)**2/2+C3*LX(K)+C4
835 LZ(K)=D1*LX(K)**3/3+D2*LX(K)**2/2+D3*LX(K)+D4
840 DEFY(K)=C1*LX(K)**4/12+C2*LX(K)**3/6+C3*LX(K)**2/2+C4*LX(K)+C5
845 DEFZ(K)=D1*LX(K)**4/12+D2*LX(K)**3/6+D3*LX(K)**2/2+D4*LX(K)+D5
850 IF(JJ.EQ.I6) GO TO 885
855 K=J+2
```

```
860 LY(K)=C1*LX(K)**3/3+C2*LX(K)**2/2+C3*LX(K)+C4
865 LZ(K)=D1*LX(K)**3/3+D2*LX(K)**2/2+D3*LX(K)+D4
870 DEFY(K)=C1*LX(K)**4/12+C2*LX(K)**3/6+C3*LX(K)**2/2+C4*LX(K)+C5
875 DEFZ(K)=D1*LX(K)**4/12+D2*LX(K)**3/6+D3*LX(K)**2/2+D4*LX(K)+D5
885 885 CONTINUE
890,  REVERSE ORDER
895 DO 915 I=1,NSTA
900 IR=NSTA+1-I
905 VY(IR)=DEFY(I)
910 VZ(IR)=DEFZ(I)
915 915 CONTINUE
920 PRINT 960, TITLE(29),VY
925 PRINT 960, TITLE(30),VZ
930 930 CONTINUE
940 940 FORMAT(5X,I3)
945 945 FORMAT(5X,E10.0)
950 950 FORMAT(5X,5E10.5,/,5X,5E10.5)
955 955 FORMAT(8H STATION,10(10X,I2))
960 960 FORMAT(1H ,A8,3X,10F12.2)
961 961 FORMAT(1H ,A8,3X,6F12.2)
962 962 FORMAT(5X,8F8.2,/,5X,2F8.2)
963 963 FORMAT(5X,6F8.2)
964 964 FORMAT(1H ,A8,1X,I2,10E12.4)
965 965 FORMAT(5X,8F8.4,/,5X,2F8.4)
966 966 FORMAT(1H ,A8,3X,10E12.4)
968 968 FORMAT(5X,8A8)
970 970 FORMAT(1H1)
975 975 FORMAT(15H STRESS OFFSETS,3X,10(I2,10X))
980 980 FORMAT(1H ,8A8,/,/)
985 REWIND 1  $  REWIND 2  $  REWIND 60  $  REWIND 61
990 END
1000 SUBROUTINE INTEG(X,Y,XS,IS,IE)
1005,  THIS ROUTINE INTEGRATES THE AREA UNDER A CURVE OF HEIGHT Y AND
1006,  SPACING X BY FITTING A SECOND ORDER EQUATION THROUGH THE POINTS
1007,  XI IS THE AREA OF EACH SEGMENT, AND XS IS THE SUM UP TO THAT
1008,  POINT. IT STARTS AT X(IS) AND STOPS AT X(IE)
1015 DIMENSION X(12),Y(12),XI(12),XS(12)
1018 XI(1)=0.0  $  XS(1)=0.0
1020 I2=IS+1
1025 DO 1070 JJ=I2,IE,2
1030 J=JJ
1035 IF(JJ.EQ.IE) J=J-1
1040 CALL LCOE(CO1,CO2,CO3,J-1,X,Y)
1043 K=J+1
1050 XI(K)=CO1*(X(K)**3-X(J)**3)/3.+CO2*(X(K)**2-X(J)**2)/2.+CO3
1051+ *(X(K)-X(J))
1055 IF(JJ.EQ.IE) GO TO 1070
1060 K=J-1
1065 XI(J)=CO1*(X(J)**3-X(K)**3)/3.+CO2*(X(J)**2-X(K)**2)/2.+CO3
1066+ *(X(J)-X(K))
1070 1070 CONTINUE
1075 XS(IS+1)=XI(IS+1)
1080 IF(IS.LT.IE-1) GO TO 1087
1085 GO TO 1110
1087 1087 CONTINUE
1090 I5=IS+2
1095 DO 1105 J=I5,IE
1100 XS(J)=XI(J)+XS(J-1)
1105 1105 CONTINUE
1110 1110 CONTINUE
1115 RETURN
1120 END
```

```
1150 SUBROUTINE LCOE(CO1,CO2,CO3,J,X,Y)
1155,  THIS ROUTINE FITS A 2ND ORDER CURVE THROUGH EACH SET OF THREE
1156,  POINTS, X THE ABSCISSA AND Y THE ORDINATE, VIZ:
1157,  Y = CO1 * X**2 +CO2 * X + CO3  (THE PARABOLIC AXIS IS VERTICAL)
1160 DIMENSION X(12),Y(12)
1165 CO1=0.0  $  CO2=0.0  $  CO3=0.0
1170 C1N=X(J)*(Y(J+2)-Y(J+1))+X(J+1)*(Y(J)-Y(J+2))+X(J+2)*
1171+ (Y(J+1)-Y(J))
1175 C2N=(X(J)**2)*(Y(J+1)-Y(J+2))+(X(J+1)**2)*(Y(J+2)-Y(J))
1176+ +(X(J+2)**2)*(Y(J)-Y(J+1))
1180 C3N=(X(J)**2)*(X(J+1)*Y(J+2)-X(J+2)*Y(J+1))+(X(J+1)**2)*
1181+ (X(J+2)*Y(J)-X(J)*Y(J+2))+(X(J+2)**2)*(X(J)*Y(J+1)-X(J+1)
1182+ *Y(J))
1185 DET=X(J)*((X(J+2)**2)-(X(J+1)**2))+X(J+1)*((X(J)**2)-(X(J+2)
1186+ **2))+X(J+2)*((X(J+1)**2)-(X(J)**2))
1190 CO1=C1N/DET
1195 CO2=C2N/DET
1200 CO3=C3N/DET
1205 RETURN
1210 END
```

```
FILE   DFTEST3

10   001
20   010
30      30.E+06
40     000.00  024.00  048.00  072.00  096.00  120.00  144.00  168.00
42     192.00  240.00
45      00.00   00.00   00.00   00.00   00.00   00.00   00.00   00.00
47      00.00   00.00
50     -21.21  -21.21  -21.21  -21.21  -21.21  -21.21  -21.21  -21.21
52     -21.21  -21.21
55      07.07   07.07   07.07   07.07   07.07   07.07   07.07   07.07
57      07.07   07.07
58      00.00   00.00   00.00   00.00   00.00   00.00   00.00   00.00
59      00.00   00.00
60   .14400E+09.14400E+09.14400E+09.14400E+09.14400E+09
62   .14400E+09.14400E+09.14400E+09.14400E+09.14400E+09
70   .52490E+09.52490E+09.52490E+09.52490E+09.52490E+09
72   .52490E+09.52490E+09.52490E+09.52490E+09.52490E+09
80   .27243E+10.27243E+10.27243E+10.27243E+10.27243E+10
82   .27243E+10.27243E+10.27243E+10.27243E+10.27243E+10
90   .12239E+10.12239E+10.12239E+10.12239E+10.12239E+10
92   .12239E+10.12239E+10.12239E+10.12239E+10.12239E+10
100   15.0000 15.0000 15.0000 15.0000 15.0000 15.0000 15.0000 15.0000
102   15.0000 15.0000
110  006
120     00.00   -2.00   03.20   08.39   09.39   10.39
130     00.00   03.46   06.46   09.46   07.73   06.00
140     04.20   04.20   04.20   04.20   04.20   04.20   04.20   04.20
142     04.20   04.20
150     04.73   04.73   04.73   04.73   04.73   04.73   04.73   04.73
152     04.73   04.73
160     .5236   .5236   .5236   .5236   .5236   .5236   .5236   .5236
162     .5236   .5236
170     01.00   01.00   01.00   01.00   01.00   01.00   01.00   01.00
172     01.00   01.00
190     04.20   04.20   04.20   04.20   04.20   04.20   04.20   04.20
192     04.20   04.20
195     04.73   04.73   04.73   04.73   04.73   04.73   04.73   04.73
197     04.73   04.73
200  TEST 1
```

TEST 1

STATION	1	2	3	4	5	6	7	8	9	10
STA POS	0.	24.00	48.00	72.00	96.00	120.00	144.00	168.00	192.00	240.00
X LOAD	0.	0.	0.	0.	0.	0.	0.	0.	0.	0.
Y LOAD	-21.21	-21.21	-21.21	-21.21	-21.21	-21.21	-21.21	-21.21	-21.21	21.21
Z LOAD	7.07	7.07	7.07	7.07	7.07	7.07	7.07	7.07	7.07	7.07
EA	.1440E109	.1440E109	.1440E109	.1440E109	.1440E109	.1440E109	.1440E109	.1440E109	.1440E109	.1440E109
EIYP	.5249E109	.5249E109	.5249E109	.5249E109	.5249E109	.5249E109	.5249E109	.5249E109	.5249E109	.5249E109
EIZP	.2724E110	.2724E110	.2724E110	.2724E110	.2724E110	.2724E110	.2724E110	.2724E110	.2724E110	.2724E110
GJ	.1224E110	.1224E110	.1224E110	.1224E110	.1224E110	.1224E110	.1224E110	.1224E110	.1224E110	.1224E110
SCALE	1.00	1.00	1.00	1.00	1.00	1.00	1.00	1.00	1.00	1.00

STRESS OFFSETS	1	2	3	4	5	6
Y	0.	-2.00	3.20	8.39	9.39	10.39
Z	0.	3.46	6.46	9.46	7.73	6.00

Y BEND	4.20	4.20	4.20	4.20	4.20	4.20	4.20	4.20	4.20	4.20
Z BEND	4.73	4.73	4.73	4.73	4.73	4.73	4.73	4.73	4.73	4.73
STATION	1	2	3	4	5	6	7	8	9	10
TORSION	0.	.1440E104	.2880E104	.4319E104	.5759E104	.7199E104	.8639E104	.1008E105	.1152E105	.1440E105
TORS DEF	.2202E-02	.2202E-02	.2118E-02	.1976E-02	.1779E-02	.1525E-02	.1214E-02	.8470E-03	.4941E-03	0.
BENDING	0.	0.	0.	0.	0.	0.	0.	0.	0.	0.
V INCL	0.	-.5090E103	-.1018E104	-.1527E104	-.2036E104	-.2545E104	-.3054E104	-.3563E104	-.4072E104	-.5090E104
DN INCL	0.	-.6108E104	-.2443E105	-.5498E105	-.9774E105	-.1527E106	.2199E106	-.2993E106	-.3909E106	-.6108E106
V LEAF	0.	.1697E103	.3394E103	.5090E103	.6787E103	.8484E103	.1018E104	.1188E104	.1357E104	.1697E104
DN LEAF	0.	.2036E104	.8145E104	.1833E105	.3258E105	.5090E105	.7330E105	.9977E105	.1303E106	.2036E106
FR A A	.79	.79	.79	.79	.79	.79	.79	.79	.79	.79
SX TEN	0.	0.	0.	0.	0.	0.	0.	0.	0.	0.
N A A	90.00	1.15	1.15	1.15	1.15	1.15	1.15	1.15	1.15	1.15
SX BEND 1	0.	.4660E103	.1067E104	.4201E104	.7468E104	.1167E105	.1680E105	.2287E105	.2987E105	.4660E105
SX TOTAL 1	0.	.4660E103	.1067E104	.4201E104	.7468E104	.1167E105	.1680E105	.2287E105	.2987E105	.4660E105
SX BEND 2	0.	-.8400E103	-.3395E104	-.7639E104	-.1358E105	-.2122E105	-.3056E105	-.4159E105	-.5432E105	-.8400E105
SX TOTAL 2	0.	-.8400E103	-.3395E104	-.7639E104	-.1358E105	-.2122E105	-.3056E105	-.4159E105	-.5432E105	-.8400E105
SX BEND 3	0.	-.6570E103	-.2631E104	-.5920E104	-.1052E105	-.1644E105	-.2368E105	-.3223E105	-.4210E105	-.6570E105
SX TOTAL 3	0.	-.6570E103	-.2631E104	-.5920E104	-.1052E105	-.1644E105	-.2368E105	-.3223E105	-.4210E105	-.6570E105
SX BEND 4	0.	-.4687E103	-.1875E104	-.4218E104	-.7499E104	-.1172E105	-.1687E105	-.2297E105	-.3000E105	-.4687E105
SX TOTAL 4	0.	-.4687E103	-.1875E104	-.4218E104	-.7499E104	-.1172E105	-.1687E105	-.2297E105	-.3000E105	-.4687E105
SX BEND 5	0.	.1891E103	.7563E103	.1702E104	.3025E104	.4727E104	.6807E104	.9265E104	.1210E105	.1891E105
SX TOTAL 5	0.	.1891E103	.7563E103	.1702E104	.3025E104	.4727E104	.6807E104	.9265E104	.1210E105	.1891E105
SX BEND 6	0.	.8460E103	.3380E104	.7629E104	.1355E105	.2117E105	.3049E105	.4150E105	.5420E105	.8460E105
SX TOTAL 6	0.	.8460E103	.3380E104	.7629E104	.1355E105	.2117E105	.3049E105	.4150E105	.5420E105	.8460E105
N/ELYP	0.	.1097E-04	.4309E-04	.9705E-04	.1755E-03	.2743E-03	.3950E-03	.5376E-03	.7022E-03	.1097E-02
N/ELZP	0.	-.1057E-05	-.4220E-05	.9513E-05	.1691E-04	-.2643E-04	-.3805E-04	-.5179E-04	-.6765E-04	-.1057E-03
Y DEF	8.17	-7.94	-7.32	6.40	-5.29	-4.08	2.87	1.76	-.85	0.
Z DEF	6.73	6.54	6.03	5.28	4.36	3.37	2.37	1.45	.70	0.

END.

APPENDIX IV

COMPUTER PROGRAM: BLADE FREQUENCY OF VIBRATION ANALYSIS

The Myklestad table frequency analysis is described in Chapter VII; the Fortran program is listed on the following pages.

```
10  PROGRAM VIBRATE (INPUT,TAPE1,TAPE2, OUTPUT)
15,  THIS PROGRAM FINDS THE NATURAL FREQUENCIES IN BENDING OF A CANTI-
16,  LEVER BEAM BY THE MYKLESTAD METHOD
17,  THE BEAM IS FIXED AT STATION 10, THE BEAM IS DIVIDED INTO DISCRETE
18,  LUMPED MASSES, AND THE BEAM ROTATES AT FREQUENCY OMEGA ABOUT THE
19,  FIXED END
20  DIMENSION  EL(10),RM(10),EI(10),UF(10),VF(10),UM(10),VM(10),EM(10)
25  DIMENSION ELRC(10),ELR(10),EMR(10),FCR(10),FC(10)
30  DIMENSION A(10), B(10), C(10), D(10)
35  DIMENSION BGP(10),BHP(10),HP(10),GP(10),BG(10),BH(10),H(10),G(10),DEF(10)
50 50  FORMAT(3X,10F6.4,3X,10F6.4,3X,I5,3X,F6.2)
55 55  FORMAT(3X,10F6.4)
57,  READ LENGTH, RUNNING MASS, AND EI'S, BEGINNING AT THE TIP
60  READ (1,50) (EI(N),N=1,NSTA)
65  READ (1,50) (RM(N),N=1,NSTA)
70 READ(1,) NSTA,RAD
75  READ (2,55) (EI(N),N=1,NSTA)
80  READ, RPM
85  REWIND 1      $   REWIND 2
90 90 FORMAT(*FREQUENCIES AND MODES OF BENDING VIBRATION OF A ROTATING LUMPED
91C  MASS BEAM*)
95  PRINT 90
100 100  FORMAT(/,/,/,/,12X,*LENGTH =*,F6.2)
105 105  FORMAT(12X,*RPM =*,F6.2,/,/,/,/)
107  PRINT 100, RAD
109  PRINT 105, RPM
110 110  FORMAT(5H MODE,6X,9HFREQUENCY,5X,5H(TIP),11X,7HSTATION,22X,6H(ROOT))
112 112  FORMAT(8X,12HRAD/SEC  RPM,3X,10I5)
114  PRINT 110
116  PRINT 112, (N)(N=1,10)
120  OMEGA2=(RPM*2.*3.1415926/60.)**2.
123,  CALCULATE THE INFLUENCE VALUES FROM L'S AND EI'S
125  DO 145 N=1,NSTA
130  UF(N)=(EL(N)**3.)/(6.*EI(N))
135  VF(N)=(EL(N)**2.)/(2.*EI(N))
137  UM(N)=VF(N)
140  VM(N)=EL(N)/EI(N)
145 145  CONTINUE
150  EM(0)=0.0  $  ELRC(0)=0.0   $  RM(0)=0.0   $  EL(0)=0.0   $   A(0)=0.0
151  J=0
152,  CALCULATE THE LUMPED MASSES
155 DO 165 N=1,NSTA
160  EM(N)=(RM(N-1)*EL(N-1)/2.)+(RM(N)*EL(N)/2.)
165 165 CONTINUE
170,  CALCULATE THE TENSION DUE TO CENTRIFUGALFORCE, STARTING AT THE ROOT END
172  ELR(0)=0.0  $  EMR(0)=0.0   $  FCR(0)=0.0
175 DO 195 N=1,NSTA
180  NR=NSTA+1-N
185  ELR(NR)=EL(N)
190  EMR(NR)=EM(N)
195 195  CONTINUE
200 DO 215 NR=1,NSTA
205  ELRC(NR)=ELRC(NR-10+ELR(NR)
210  FCR(NR)=EMR(NR)*OMEGA2*(ELRC(NR)**2.)+FCR(NR-1)
215 215  CONTINUE
220,  RENUMBER THE INDEX
225 DO 240 NR=1,NSTA
230 N=NSTA+1-NR
235  FC(N)=FCR(NR)
240 240  CONTINUE
245,  CALCULATE THE NUMERICAL COEFFICIENTS IN THE ASSUMED LINEAR FUNCTIONS:
246,  SHEAR = (-) BGP * PHI  +  BG , ETC.
250 DO 300 N=1,NSTA
260  A(N)=1.+VF(N)*FC(N)
270  B(N)=1.+UM(N)*FC(N)
280  C(N)=EL(N)+UF(N)*FC(N)
290  D(N)=C(N)*FC(N)
300 300  CONTINUE
```

```
305,  SET THE INITIAL VALUE OF THE ITERATION FREQUENCY(SQUARED), WSQ
306,  1 RAD/SEC FREQUENCY = 6.28 SECOND PERIOD
310  WSQ=1.0
312,  ENTER THE COARSE ITERATION LOOP ON FREQUENCY (SQUARED)
314 314  CONTINUE
315 DO 580 I=1,1000
320,  SET INITIAL VALUES OF AMPLITUDE COEFFICIENTS AT THE TIP, DUE TO
321,  FREE BOUNDARY CONDITION
325  BGP(1)=0.0
327  BHP(1)=0.0
329  HP(1)=1.0
331  GP(1)=0.0
333  BG(1)=EM(1)*WSQ
335  BH(1)=0.0
337  H(1)=0.0
339  G(1)=1.0
345,  CALCULATE VALUES OF AMPLITUDE COEFFICIENTS FOR EACH STATION
350  DO 450 N=1,NSTA-1
360  G(N+1)=G(N)+C(N)*H(N)+UM(N)*BH(N)+UF(N)*BG(N)
370  GP(N+1)=GP(N)+C(N)*HP(N)+UM(N)*BHP(N)+UF(N)*BGP(N)
380  H(N+1)=A(N)*H(N)+VM(N)*BH(N)+VF(N)*BG(N)
390  HP(N+1)=A(N)*HP(N)+VM(N)*BHP(N)+VF(N)*BGP(N)
400  BH(N+1)=B(N)*BH(N)+D(N)*H(N)+C(N)*BG(N)
410  BHP(N+1)+B(N)*BHP(N)+D(N)*HP(N)+C(N)*BGP(N)
420  BG(N+1)=BG(N)+EM(N+1)*G(N+1)*WSQ
430  BGP(N+1)+BGP(N)+EM(N+1)*GP(N+1)*WSQ
450 450  CONTINUE
460,  CALCULATE TIP SLOPE FROM B.C. AT ROOT
465  PHI=G(10)/GP(10)
470,  FIND RESULTING SLOPE AT ROOT FROM OTHER B.C. (THIS GIVES THE
471,  REMAINDER FOR THE ITERATION)
475  ALPHA=(HP(10)*PHI)-H(10)
480,  FINE CONVERGENCE
485 IF(ALPHA-.00001) 600,600,490
490 490  CONTINUE
500,  COARSE CONVERGENCE
505  IF(ALPHA-0.10) 510,510,530
510 510  CONTINUE
515  WSQ=WSQ+0.0001
520  GO TO 570
530 530  WSQ=WSQ+1.0
535 535  CONTINUE
540,  NO CONVERGENCE?
545  IF(I.GE.1000) 550,550,570
550 550  FORMAT(*NO CONVERGENCE*)
560  PRIN T 550
565  GO TO 730
570 570  CONTINUE
580 580  CONTINUE
600 600  CONTINUE
605,  FIND MODE SHAPE FOR SOLUTION FREQUENCY
610  DO 625 N=1,NSTA
620  DEF(N)=-GP(N)*PHI+G(N)
625 625  CONTINUE
630  FREQ=SQRT(WSQ)
640  J=J+1
650 650  FORMAT(1X,I3,3X,F6.2,3X,F6.2,2X,10F5.2,/)
660  FREQ1=FREQ*60./(2.*3.1415926)
670  PRINT 650, J,FREQ,FREQ1,(DEF(N),N=1,10)
680,  LOOK FOR HIGHER FREQUENCIES
690  IF(J-NSTA) 700,700,730
700 700  CONTINUE
710  WSQ=WSQ+1.
720  GO TO 314
730 730  CONTINUE
740 740  CONTINUE
750  END
```

APPENDIX V

BIBLIOGRAPHY

A. Energy Strategy - The Big Picture

Commoner, Barry, The Poverty of Power, Alfred A. Knopf, New York, 1976.

Commoner, Barry, Science and Survival, Viking, New York, 1963.

Donovan, P., and W. Woodward, Editors, "Solar Energy as a National Energy Resource," NSF/NASA Solar Energy Panel Proceedings, University of Maryland, College Park, Maryland, December, 1972.

Hannon, Bruce, "Energy, Labor, and the Conserver Society," Technology Review, March-April, 1977.

Lovins, Amory B., Soft Energy Paths - Toward a Durable Peace, Ballinger Publishing Company, Cambridge, Massachusetts, 1977.

Lovins, Amory B., World Energy Strategies - Facts, Issues, and Opinions, Ballinger Publishing Company, Cambridge, Massachusetts, 1975.

Lovins, A. B., and J. H. Price, Non-Nuclear Futures - The Case From Ethical Energy Strategy, Ballinger Publishing Company, Cambridge, Massachusetts, 1975.

Steadman, Philip, Energy, Environment and Building, Cambridge Urban and Architectural Studies, Cambridge University Press, Academy of Natural Sciences of Philadelphia, 1975.

B. Wind Power - Historical

Drees, Jan M., "Blade Twist, Droop Snoot, Forward Spars," Vertiflite, September-October, 1976.

Eldridge, Frank R., Wind Machines, The Mitre Corp., McLean, Virginia, MTR-6971; NSF-RA-N-75-051, October, 1975.

Putnam, Palmer C., Power From The Wind, Van Nostrand Reinhold Co., 1948.

Torrey, Volta, Wind-Catchers--American Windmills of Yesterday and Tomorrow, Stephen Greene Press, Brattleboro, Vermont, 1976.

C. "Backyard Inventors" and Appropriate Technology

Clark, Peter, Natural Energy Workbook, #1 and #2, Visual Purple, Berkeley, California, 1974, 1976.

Clegg, Peter, New Low Cost Sources of Energy for the Home, Garden Way Publishing, Charlotte, Vermont, 1975.

Clews, Henry, "Electric Power from the Wind," Solar Wind Company, E. Holden, Maine, 1974.

Dennis, Landt, Catch the Wind, Four Winds Press, New York, 1976.

deRopp, Robert, Eco-Tech: The Whole Earther's Guide to the Alternate Society, Delta Books, Bell Pub. Co., Inc., New York, 1975.

Evans, Michael, Wind Power Digest-Wind Access Catalog, Wind Power Digest, Fall 1977, No. 10, 54468 CR 31, Bristol, Indiana.

Hackleman, Michael A., Wind and Windspinners, Peace Press, Culver City, California, 1974.

_____, Handbook of Homemade Power, Mother Earth News publication, Bantam Press, New York, 1974.

McGuigan, Dermot, Harnessing the Wind for Home Energy, Garden Way Pub., Charlotte, Vermont, 1978.

Merrill, R., et al., Energy Primer, Portola Institute, Menlo Park, California, 1974.

Noll, E. M., Wind/Solar Energy for Radiocommunications and Low Power Electronic/Electric Applications, Bobbs-Merrill Co., Inc., Indianapolis, 1975.

Park, Jack, Simplified Wind Power Systems for Experimenters, Helion, Sylmar, California, 1975.

Sullivan, George, Wind Power For Your Home, Cornerstone Library, New York, 1978.

D. Engineering Materials

Bowman, J. C., "Prediction of Fatigue Life in Random Vibration Environments," Air Force Conference on Fatigue and Materials, AFFDL TR 70-144; 1969.

_____, Composite Materials, AGARD Conference #63, AGARD CP-63-71, April, 1970.

Jarosch, Stepan, "Fatigue Properties and Test Procedures on GRP Plastic Rotor Blades," Amer. Hel. Society Forum, Washington, D.C., May, 1969.

Hutter, Ulrich, "Load Bearing Aircraft Components Made of Fiberglass-Reinforced Plastics," Luftfahrttechn, Vol. 6, No. 2, 1960.

Hutter, Ulrich, "Highly Stressed Lightweight Components Made of Fiberglass Reinforced Plastics," Kunststoffe, Vol. 50, No. 6, 1960.

Hutter, Ulrich, "Glass Fiber Reinforced Plastics as a Structural Material for the Aircraft Industry," Society of the Plastics Industries, Inc., Technical and Management Conference, Section 13-A, Chicago, 1961.

King, R. D., "Sailplane Wing Constructed of Foam Core and Polyester Fiberglass Skin," AIAA Paper No. 74-258, Washington, D.C., January, 1974.

E. Texts

Bisplinghoff, R. L., Ashley, H., and R. L. Halfman, Aeroelasticity, Addison-Wesley Publishing Company, Inc., Reading, Massachusetts, 1955.

Bramwell, A. R. S., Helicopter Dynamics, Wiley and Sons, New York, 1976.

Champly, R., Wind Motors--Theory, Construction, Assembly and Use in Drawing Water and Generating Electricity, Dunod Pub. Paris, 1933, NASA Tech. Translation F-16201, April, 1975.

Clark, Wilson, Energy For Survival, Doubleday, New York, 1975.

DenHartog, J. P., Mechanical Vibrations, Fourth Edition, McGraw-Hill Book Company, New York, 1956.

Dommasch, Sherby, Connolly, Airplane Aerodynamics, Pitman, New York, 1967.

Fateyev, Y. M., Wind Engines and Installations, Moscow, 1948, NASA Tech. Translation F-16170, 1974.

Gessow, A., and A. C. Myers, Jr., Aerodynamics of the Helicopter, Third Printing, Ungar Pub. Co., New York, 1952.

Golding, E. W., The Generation of Electricity by Wind Power, Philosophical Library, New York, 1955.

James, M. L., Smith G. M., and J. C. Wolford, Applied Numerical Methods for Digital Computation, Second Edition, IEP, Dun-Donnelley Pub., New York, 1976.

McCormick, B. W., Aerodynamics of V/STOL Flight, Academic Press, New York, 1967.

Myklestad, N. O., Fundamentals of Vibration Analysis, McGraw-Hill Book Company, New York, 1956.

Nelson, W. C., Aircraft Propeller Principles, Wiley and Sons, New York, 1944.

Saunders, G. H., Dynamics of Helicopter Flight, John Wiley and Sons, New York, 1975.

Shefter, Ya. I., Wind Powered Machines, Moscow, 1972, NASA Tech. Translation F-15149, 1974.

F. Foreign Studies

Fateyev, Y. M., Wind Power Installations--Present Conditions and Possible Lines of Development, Moscow, 1959, NASA TT-F-16204, 1974.

Honnef, H., "High Wind Power Plants," Berlin, 1939, NASA TT-F-15444, 1974.

Hutter, Ulrich, "The Development of Wind Power Installations for Electric Power Generation in Germany," NASA TT-F-15050, 1973.

Juchem, P., "Present Status of Honnef Wind Power Plants," West Germany, 1955, NASA TT-F-15355, 1974.

Juul, J., "SEAS Examination of Windpower in 1952," Copenhagen, 1953, NASA TT-F-15439, 1974.

Lenner, Ludwig, "Parallel Operation of a Synchronous Generator and an Infinitely High Powered Network when Driven by a Honnef-Gross Wind Turbine," Berlin, 1948, NASA TT-F-15302, 1974.

Pfluger, V. A., "Calculation of Large Dimension Wind Wheels," Ph.D. Dissertation, Hannover Technical College, Germany, 1941.

Sabinin, G. A., "Theory of Stabilized High Speed Wind Wheels," Central Institute of Aerohydrodynamics, Office of Scientific Information, Moscow, BNTN TsAGI Publications, 1953.

Sauer, T., "Wind Power Plants in Russia," Moscow, 1937, NASA TT-F-15331 1974.

Sektorov, V. R., "Using the Energy of the Wind for Electrification," U.S.S.R., 1953, NASA TT-F-15307, 1974.

Sembera, F., "Prospects for the Utilization of Wind Energy in Czechoslovakia," 1949, NASA TT-F-15305, 1974.

Shenfer, K. I., and A. A. Ivanov, "Lines of Development of Rural Wind Power Plants," U.S.S.R., 1941, NASA TT-F-15513, 1974.

Soedergard, Bengt, "Analysis of the Possible Use of Wind Power in Sweden," Sweden, 1973, NASA TT-F-15441, 1974.

Stein, Dimitri, "Importance and Progress of Wind Power Utilization in Denmark," Copenhagen, 1942, NASA TT-F-15353, 1974.

Witte, H., "Economy and Practical Applications of Large Wind Driven Power Plants," Berlin, 1938, NASA TT-F-15308, 1974.

G. Systems Studies

Carter, B. C., "The Vibration of Airscrew Blades with Particular Reference to Their Response to Harmonic Torque Impulses in the Drive," British Aeronautical Research Council Reports and Memoranda (ARC R & M) No. 1758, July 6, 1936.

Cromack, D. E., Heronemus, W. E., and J. G. McGowan, "Design and Operational Aspects of a 25 KW Wind Turbine Generator for Residential Heating Applications," presented at 12th Intersociety Energy Conversion Engineering Conference, Washington, D.C., August 28, 1977.

Dambolena, I. G., "A Planning Methodology for the Analysis and Design of Wind Power Systems," Ph.D. Dissertation, Department of Industrial Engineering, Univ. of Massachusetts, Amherst, Massachusetts, June, 1974.

Harner, K., "High Power Wind Energy Conversion Systems--A Control Challenge," presented at American Wind Energy Association Annual Conference, Warren, Vermont, November, 1976.

Heronemus, W. E., "Power From Offshore Winds," Dept. of Civil Engr., University of Massachusetts, Amherst, Massachusetts, 1972.

Hutter, Ulrich, "Contributions to the Creation of Basic Design Concepts for Wind Power Plants," Ph.D. Dissertation, Technische Hochschule, Vienna, Austria, May, 1942, NASA TT-F-15822, 1974.

Hutter, Ulrich, "Influence of Wind Frequency on Rotational Speed Adjustments of Windmill Generators," Germany, 1948, NASA TT-F-15184, 1974.

Kloss, Max, "The Direct Driving of Synchronous Generators by Large Scale Wind Electric Power Generation Plants in Parallel with a Synchronous Network," Germany, 1942, NASA TT-F-15301, 1974.

Martini, C., "The Measurement of Large Wind Energy Generators," Austria, 1939, NASA TT-F-15433, 1974.

Meier, R. C., "Concept Selection and Analysis of Large Wind Generator Systems," presented at 31st Annual Forum, Amer. Hel. Society, Washington, D.C., May, 1975.

_____, "New York University - Final Report on the Wind Turbine," NYU Research Report PB25370, Office of Production, Research and Development, War Production Board, New York, 1946.

Obermeier, John L., "Wind Electric Power Generation in Montana," M.S. Thesis, Montana State University, March 1976.

Rosen, A., Deabler, H., and E. Hall, "Economic Viability of Large Wind Generator Rotors," 10th Intersociety Energy Conference, Washington, D.C., 1975.

Sullivan, T., Miller, and D. Spera, "Drive Train Normal Modes Analysis for ERDA/NASA 100 KW WTG," presented at Structural Dynamics Workshop, NASA TM-73718, Lewis Research Center, Cleveland, November, 1977.

Walker, J. G., "Utilization of Random Power with Particular Reference to Small Scale Wind Power Plants," Vol. 7, United Nations Conference on New Sources of Energy, Rome, 1961.

H. Rotor Aerodynamics and Performance

Carlson and Hilzinger, "Analysis and Correlation of Helicopter Rotor Blade Response in a Variable Inflow Environment," USAAVLABS TR 65-51, September, 1965.

Critzos, C. C., Heyson, H. H., and R. W. Boswinkle, "Aerodynamic Characteristics of NACA 0012 Airfoil Sections at Angles of Attack from 0 to 180 ; NACA TN-3361, January, 1955.

Glauert, H., "Windmills and Fans," Division L, Part XI, Aerodynamic Theory, Durand, W. F., editor, Springer Pub. Co., Berlin, 1935.

Humes, T. M., "The Calculation of Unsteady Airloads Acting on Wind Turbine Blades," S. M. Thesis, Mass. Inst. of Tech., September, 1976.

Hutter, Ulrich, "Aerodynamic Layout of Wing Blades of Wind Turbines with High Tip Speed Ratios," Vol. 7, United Nations Conference on New Sources of Energy, Rome, 1961.

Hutter, Ulrich, "Optimum Design Concept for Windelectric Generators," Workshop on Adv. Wind Energy Systems, Stockholm, August 29, 1974.

Kroms, A., "Wind Generating Stations Under Joint Operational Conditions," Zurich, 1954, NASA TT-F-15637, 1974.

Liiva, Jan, "Unsteady Aerodynamics and Stall Effects on Helicopter Rotor Blade Airfoil Sections," Journal of Aircraft, Vol. 6, No. 1, January, 1969.

Prouty, R. W., "A State of the Art Survey of Two-Dimensional Airfoil Data," Journal of the Amer. Hel. Society, Vol. 20, No. 4, October, 1975.

Rohrbach, C., and R. Worobel, "Performance Characteristics of Aerodynamically Optimum Turbines for Wind Energy Generators," presented at 31st Annual Forum, Amer. Hel. Society, Washington, D.C., May, 1975.

Stoddard, F. S., "Momentum Theory and Flow States for Windmills," Wind Technology Journal, Vol. 1, No. 1, Spring, 1977.

Walker, S. N., "Performance and Optimum Design Analysis/Computation for Propeller Type Wind Turbines," Ph.D. Dissertation, Oregon State Univ., Corvallis, Oregon, May, 1976.

Wilson, R. E., and P. B. S. Ussaman, "Applied Aerodynamics of Wind Power Machines," Oregon State University, NTIS PB 238594, July, 1974.

Wilson, R. E., Ussaman, P. B. S., and S. Walker, "Aerodynamic Performance of Wind Turbines," Oregon State University, June, 1976.

I. Experimentation and Testing

Brown, C. A. C., "Windmills for the Generation of Electricity," Inst. for Research in Agricultural Engr., Oxford, England, January, 1933.

Butterfield, C. B., Jr., "Design of Hub and Pitching System for Wind Furnace I," M.S. Thesis, University of Massachusetts, Amherst, Massachusetts, June, 1977.

Chamis, C. C., and T. L. Sullivan, "Free Vibrations of the ERDA-NASA 100 KW Wind Turbine," NASA TMX-71879, March, 1976.

Chilcott, R. E., "The Design, Development and Testing of a Low Cost, 10 HP Windmill Prime Mover," Brace Research Institute, No. MT. 7, 2nd edition, June, 1970.

Clausnizer, G., "Various Relationships Between Wind Speed and Power Output of a Wind Power Plant," Volume 7, United Nations Conference on New Sources of Energy, Rome, 1961.

Donham, Schmidt, and Linscott, "100-KW Hingeless Metal Wind Turbine Blade Design, Analysis, and Fabrication," presented at 31st Annual Forum, Amer. Hel. Society, Washington, D. C., May, 1975.

Glasgow, and Linscott, "Early Operational Experience on the ERDA/NASA 100 KW Wind Turbine," NASA TM X-71601, September, 1976.

Heronemus, W. E., Principal Investigator, "Investigation of the Feasibility of Using Windpower for Space Heating in Colder Climates," Phase II Final Report, Energy Alternatives Program, University of Massachusetts, DOE ERDA/2365-77/2, UC-60, UM-WF-PR-77-2, Amherst, Massachusetts, June, 1977.

Heronemus, W. E., et al., "The Working Drawings and Bills of Material for Wind Furnace I as Installed at Soalr Habitat I, Orchard Hill," Energy Alternatives Program, University of Massachusetts, UM-WF-TR-77-10, Amherst, Massachusetts, September, 1977.

Hutter, Ulrich, "Measurement of Three-Dimensional Stress States with Embedded Strain Gages in Glass/Resin Structures," Kunstoffe, Vol. 53, No. 11, 1963.

Hutter, Ulrich, "Operating Experience Gained with a 100-KW Wind Power Plant," NASA TT-F-15068, August, 1973.

Jayadev, T. S., "Novel Electric Generation Schemes for Wind Energy Systems," Quarterly Report, 1 June - 31 August 1975, NSF-RANN Contract, also IECEC Record, 1975.

Kloss, M.,"Problems in the Electrical Equipment of Wind Power Plants," Germany, 1947, NASA TT-F-15312, 1974.

Mackenthun, Werner, "Neuwerk Windmill Power Generation Plant," Frankfurt, 1951, NASA TT-F-15306, 1974.

Meyer, Hans, Principal Investigator, "Instrumentation, Testing and Analysis of Rotor Hub," Windworks Contract, NSF Program Solicitation No. 74-11, Mukwonago, Wisconsin, July, 1974.

Morrison, J. G., "Development of Method for Measurement of Strains in Blades of Wind mill Rotors," British Electrical and Allied Industries Research Association (ERA), TR C/T117, Surrey, England, 1956.

Rosseler, G., "Wind Power Supply for the Decimeter Range Directional Radio Site at Schoeneberg (Eifel) and the Experience Gained," Germany, 1959, NASA TT-F-15337, 1974.

Seidel, G. R., "Small Wind Electrical Installations for Export," West Germany, 1949, NASA TT-F-15350, 1974.

Smidth, F. L., "Instructions for the FLS Aeromotor, Denmark, NASA TT-F-16138, January, 1975.

Stoddard, F. S., and M. Edds, "Wind Tunnel Test Program of a 200-Watt, 12-Volt Wind Generator System," Energy Alternatives Program, University of Massachusetts, Univ. Mass.-WF-TR-76-10, Amherst, Massachusetts, April, 1976.

Stoddard, F. S., Perkins, F. P., and D. Cromack, "Wind Tunnel Tests for Fixed Pitch Start-Up and Yaw Characteristics," Energy Alternatives Program, University of Massachusetts, UM-WF-TR-78-1, Req. No. 825418/YGH8848, NASA Lewis Res. Center, June, 1978.

Tryon, H. B., and T. Richards, "Installation and Initial Operations of a 4100 Watt Wind Turbine," NASA Lewis Research Center, NASA TM-X-71831, Cleveland, Ohio, December, 1975.

Van Holten, T., "Performance Analysis of a Windmill with Increased Power Output Due to Tipvane Induced Diffusion of the Airstream," Technische Hogeschool, Delft, Nederland, November, 1974.

Voight, T., "Principles of Steel Construction Engineering in the Building and Operation of Wind Driven Power Plants," Copenhagen, 1954, NASA TT-F-14872, 1973.

J. Rotor Dynamics and Aeroelasticity

Amer, K. B., and J. R. Neff, "Vertical Plane Pendulum Absorbers for Minimizing Helicopter Vibratory Loads," Journal of the Amer. Hel. Society (JAHS), Vol. 19, No. 4, October, 1974.

Chopra, Inderjet, "Nonlinear Dynamic Response of Wind Turbine Rotor," Sc.D. Dissertation, Mass. Inst. of Technology, Dept. of Aero. and Astro, February, 1977.

Coleman, R. P., and A. M. Feingold, "Theory of Self-Excited Mechanical Oscillations of Helicopter Rotors with Hinged Blades," NACA Report 1351, 1958.

Duggal, J. S., "Dynamic Analysis of High Speed Wind Turbine Systems," Brace Res. Institute #MT.9, 1971.

Dugundji, John, "Some Dynamic Problems of Rotating Windmill Systems," Advances in Eng. Science 13th Annual Meeting, Society of Eng. Science, Hampton, Virginia, NASA CP-2001, November, 1976.

Friedman, P., "Aeroelastic Modeling of Large Wind Turbines," JAHS, Vol. 21, No. 4, October, 1976.

Goland, J., and A. A. Perlmutter, "A Comparison of the Calculated and Observed Flutter Characteristics of a Helicopter Rotor Blade," JAHS, April, 1957.

Ham, N. D., "Helicopter Blade Flutter," AGARD Report No. R-607, January, 1973.

Ham, N. D., "Some Recent Research on Airfoil Dynamic Stall with Application to Airfoil Design," Dept. of Aero. and Astro., Mass. Inst. of Technology, MIT-ASRL-TR-165-1, Cambridge, Mass., September, 1971.

Hammond, C. E., "An Application of Floquet Theory to Prediction of Mechanical Instability," JAHS, Vol. 19, No. 4, October, 1974.

Hansford, R. E., and I. A. Simons, "Torsion-Flap-Lag Coupling on Helicopter Rotor Blades," JAHS, Vol. 18, No. 4, October, 1973.

Hohenemser, K. H., "Dynamic Stability of a Helicopter with Hinged Rotor Blades," NACA TM-907, 1939.

Hohenemser, K. H., "Some Alternative Dynamic Design Considerations for Large Horizontal Axis WECS," presented at the NASA-ERDA Structural Dynamics Workshop, NASA Lewis Res. Center, Cleveland, Ohio, November, 1977.

Hohenemser, K. H., and S. K. Yin, "On the Question of Adequate Hingeless Rotor Modeling in Flight Dynamics," presented at 29th Annual Forum, American Helicopter Society, Washington, D.C., May, 1973.

Hohenemser, K. H., and S. K. Yin, "Some Applications of the Method of Multiblade Coordinates," JAHS, Vol. 17, November, 1972.

Houbolt, J. C., and G. W. Brooks, "Differential Equations of Motion for Combined Flapwise Bending, Chordwise Bending, and Torsion, of Twisted, Non-Uniform Rotor Blades," NACA TN-3905, February, 1957.

Huber, Hans B., "Effect of Torsion-Flap-Lag Coupling on Hingeless Rotor Stability," presented at 29th Annual Forum, Amer. Helicopter Society, Washington, D.C., May, 1973.

Johnson, Wayne, "Dynamics of Tilting Proprotor Aircraft in Cruise Flight," NASA TND-7677, May, 1974.

Lemnios, A. Z., "The Aeroelastic Behavior of Rotary Wings in Forward Flight," Ph.D. Dissertation, Univ. of Conn., Storrs, Conn., June, 1967.

Lemnios, A. Z., "Analytical Evaluation of the Controllable Twist Rotor and Dynamic Behavior," Kaman Aerospace Corp., AAMRDL Report 72-16, May, 1972.

Loewy, R. G., "Review of Rotary-Wing V/STOL Dynamic and Aeroelastic Problems," AIAA Paper No. 69-202, February 17, 1969.

Miller, R. H., "Helicopter Control and Stability in Hovering Flight," Journal of Aeronautical Sciences (JAS), Vol. 15, August, 1948.

Miller, R. H., and C. W. Ellis, "Helicopter Blade Vibration and Flutter," JAHS, July, 1956.

Oette, H., "Calculation of the Flapwise Bending, Edgewise Bending, and Torsional Vibrations of Rotor Blades with Coupled Natural Modes and Frequencies," NASA TT-F-16004, November, 1974.

Ormiston, R. A., and D. H. Hodges, "Linear Flap-Lag Dynamics of Hingeless Helicopter Rotor Blades in Hover," JAHS, Vol. 17, No. 2, April, 1972.

Ormiston, R. A., "Rotor Dynamic Considerations for Large Wind Power Generator Systems," NASA-ERDA Conf. on Wind Energy Conversion Systems, Savino, J. M., Editor, NASA-TM-X-69,786, 1973.

Ormiston, R. A., and W. G. Bonsman, "A Study of Stall Induced Flap-Lag Instability of Hingeless Rotors," presented at the 29th Annual Forum, Amer. Hel. Society, Washington, D.C., May, 1973.

Ormiston, R. A., and D. H. Hodges, "Stability of Elastic Bending and Torsion of Uniform Cantilever Rotor Blades in Hover with Variable Structural Coupling," NASA TND-8192, April, 1976.

Ormiston, R. A., Technical Chairman, Rotorcraft Dynamics, Conf. on Rotorcraft Dynamics Sponsored by NASA Ames Research Center and Amer. Hel. Society, Ames Research Center, Moffett Field, Calif., NASA SP-352, February 13-15, 1974.

Peters, D. A., "Flap-Lag Stability of Helicopter Rotor Blades in Forward Flight," JAHS, Vol. 20, No. 4, October, 1975.

Peters, D. A., and K. H. Hohenemser, "Application of the Floquet Transition Matrix to Problems of Lifting Rotor Stability," JAHS, Vol. 16, No. 2, April, 1971.

Reed, Wilmer H., III, "Prop-Rotor Whirl Flutter: A State-of-the-Art Review," presented at Symposium on Noise and Loading of Helicopter, V/STOL Aircraft, Southampton, England, 1965.

Reissner, H., and M. Morduchow, "A Theoretical Study of the Dynamic Properties of Helicopter Blade Systems," NACA TN-1430, 1948.

Sissingh, G. J., and N. A. Kuczynski, "Investigations on the Effect of Blade Torsion on the Dynamics of the Flapping Motion," JAHS, April, 1970.

Smith, C. E., Thresher, R. W., Wilson, R. E., and R. B. MacDuff, "A Rigid Body Model for Analysis of Aerogenerator Rotor Dynamics," presented at 31st Annual Forum, American Helicopter Society, Washington, D.C., May, 1975.

Spera, D. A., and D. C. Janetyke, "Effects of Rotor Location, Coning, and Tilt on Critical Loads in Large Wind Turbines," Wind Technology Journal, Vol. 1, No. 2, Summer, 1977.

Sullivan, T. L., "Simplified Modeling for Wind Turbine Model Analysis Using NASTRAN," presented at NASA-ERDA Structural Dynamics Workshop, NASA Lewis Research Center, Cleveland, Ohio, November, 1977.

Thresher, R. W., and C. E. Smith, "Free Vibration Approximations for Horizontal Axis Wind Turbines," Oregon State University, DOE Contract No. EY-76-S-06-2227, RLO/2227-78/1, Corvallis, Oregon, July, 1978.

Yntema, R. T., "Simplified Procedures and Charts for the Rapid Estimation of Bending Frequencies of Rotating Beams," NACA TN-3459, 1955.